EXPERIMENTAL AND NUMERICAL INVESTIGATION OF FLOW INDUCED VIBRATION IN A HIGH PRESSURE DOUBLE VOLUTE CENTRIFUGAL PUMP

BY

Atia Esmaeil Khalifa

A Dissertation Presented to the

DEANSHIP OF GRADUATE STUDIES

KING FAHD UNIVERSITY OF PETROLEUM & MINERALS

DHAHRAN, SAUDI ARABIA

In Partial Fulfillment of the
Requirements for the Degree of

DOCTOR OF PHILOSOPHY

In

MECHANICAL ENGINEERING

June 2009

DEANSHIP OF GRADUATE STUDIES

This dissertation, written by **Mr. Atia Esmaeil Atia Khalifa** under the direction of his dissertation advisor and approved by his dissertation committee, has been presented to and accepted by the Dean of Graduate Studies, in partial fulfillment of the requirements for the degree of **DOCTOR OF PHILOSOPHY IN MECHANICAL ENGINEERING.**

Dissertation Committee

Dr. Amro Al-Qutub
Dissertation Advisor

Prof. Dr. Hassan M. Badr, **Member**

Dr. Amro Al-Qutub
Chairman, Mechanical Engineering

Prof. Dr. Yehia Khulief, **Member**

Dr. Salam A. Zummo
Dean of Graduate Studies

Prof. Dr. Mohammed F. Zedan, **Member**

Date: 15/7/09

Dr. Rached Ben-Mansour, **Member**

ACKNOWLEDGEMENT

I would like to acknowledge the support of the King Fahd University of Petroleum & Minerals for this research. I wish to extend my profound gratitude to Dr. Amro Al-Qutub, the Chairman of my dissertation committee, for being an excellent advisor who always gives exceptional guidance and response. My highest thanks also go to Dr. Rached Ben Mansour for valuable discussions and tutoring through the years. I also wish to sincerely thank all the other committee members; Dr. Yehia Khulief, Dr. Hassan Badr, and Dr. Mohammed F. Zedan for their helpful comments and reviews.

I wish to extend my appreciation to all the staff members at the department for their assistance and cooperation. I must thank all the engineers and technicians in the labs and workshop where I performed various experiments and analysis. I would like to acknowledge the support provided by Saudi Electricity Company (SEC) regarding experimentation and access to industrial data. Thanks to all my friends and colleagues for their continued encouragement.

Special thanks shall be given to my family. This work could not have been completed without their absolute devotion, steadfast sacrifice and continued prayers and supplications.

TABLE OF CONTENTS

		Page
ACKNOWLEDGEMENT		iii
TABLE OF CONTENTS		iv
LIST OF TABLES		vi
LIST OF FIGURES		vii
ABSTRACT		xiii
ABSTRACT (Arabic)		xiv
CHAPTER 1: INTRODUCTION ----------		1
1.1	Introduction and Literature Review	1
1.2	Research Motivation	16
1.3	Analysis	23
1.4	Objectives	24
1.5	Methodology	25
1.6	Dissertation layout	27
CHAPTER 2: EXPERIMENTAL SETUP ----------		**28**
2.1 Description of the Test Loop		28
2.2 Modeling the Pump Volute and Impeller		35
2.2.1 Modeling the Volute		35
2.2.2 Modeling the Impeller		35
2.3 Impellers Balancing		46
2.4 Experimental Measurements		48
4.2.1 Measurement of Flow Rate		48
2.4.2 Measurement of Pump Total Head		50
2.4.3 Measurement of Pressure Fluctuations		51
2.4.4 Measurement of Brake Power		61
2.4.5 Measurement of Case Vibration		64
2.5 Similitude Analysis		66
CHAPTER 3: EXPERIMENTAL RESULTS ----------		**68**
3.1 Introduction		68

3.2 Effect of Operating Variables on Flow Induced Vibration 70
3.2.1 Effect of Flow Rate 73
3.2.2 Effect of Pump Speed 96
3.3 Effect of the V-Shaped Cut at Impeller Blades Exit 105
3.3.1 Effect of the V-cut on Performance Curves 105
3.3.2 Effect of the V-cut on the pressure distribution 110
3.3.3 Effect of The V-cut on the Pressure Fluctuations 116
3.3.4 Effect of the V-cut on the Pump Vibration 124
3.4 Effect of the Radial Gap on the Flow Induced Vibration 128
3.4.1 Impeller Without V-cut at Blade Exit 132
3.4.2 Impeller with V-Cut at Blade Exit 146

CHAPTER 4: NUMERICAL SIMULATIONS ---------- 160

4.1 Introduction 160
4.2 Generation of Pump Geometry 161
4.3 Numerical Procedure 166
4.3.1 Governing Equations 166
4.3.2 Turbulence Model 167
4.3.4 Sliding Mesh Technique 169
4.3.5 Grid Independence Study 172
4.3.5.1 Mesh Size 172
4.3.5.2 Time Step 175
4.3.6 General Parameters of Simulation Models 175
4.3.7 Boundary Conditions 177
4.3.8 Monitoring Locations 177
4.4 Results of the 2D Numerical Simulations 180
4.4.1 Simulations Results for impeller Without V-cut at Blade Exit 180
4.4.2 Effect of the V-cut 202
4.4.3 Effect of Radial Gap between Impeller and Volute Tongues 214
4.5 Validation of CFD Results 230

CHAPTER 5: CONCLUSION AND RECOMMENDATIONS ------ 249

RERERENCES ---------- 253

APPENDIX ---------- 261

VITAE

LIST OF TABLES

Table		Page
2.1	Coordinates of measuring locations	53
3.1	Similitude and experimental results at best efficiency point, 3540 rpm	72
4.1	Coordinates of monitoring locations	179
4.2	Boundary Conditions for Numerical Simulation: speed 3540 rpm, Without V-cut at blades exit: gap 3.6 mm	181
4-3	Boundary conditions used for simulating the V-cut effect: Experimental boundary conditions	208
4-4	Boundary conditions for 7 mm gap: Without V-cut	220
4-5	Boundary conditions for 7 mm gap: the V-cut effect	221

LIST OF FIGURES

Figure		Page
1-1	Variation of radial unbalance force with pump flow rate for single and double volute pumps	15
1-2	Sketch of the boiler feed pump and its components (provided by SEC)	17
1-3	Dismantle of pump inner casing: upper half (provided by SEC)	18
1-4	Boiler feed pump flow arrangement and typical double volute pump stage design, with tolerances	19
1-5	Boiler feed pump cartridge, provided by SEC	20
1-6	Sample of field vibration records for BFP at SEC power plant	21
2-1	Photograph of the test loop	30
2-2	Single line diagram for the test loop	31
2-3	Perforated screens installed inside the tank	32
2-4	Commercial pump used to test model impeller and volute	33
2-5	Tube bundle flow straightener	34
2-6	Collection of geometrical data for original PFB inner split casing	36
2-7	Modeling pump volute	37
2-8	Volute dimensions: Model pump	38
2-9	Geometrical data collection of BFP impeller using milling machine	40
2-10	Procedure of geometrical data collection of BFP impeller	41
2-11	Generation of impeller geometry using Gambit/Fluent Software	42
2-12	Model impellers: without and with the V-cut at blades exit	43
2-13	Dimensions of the impeller and the shaft extension	44
2-14	Impeller and volute assembly	45
2-15	Impeller dynamic balancing process	47
2-16	Orifice meter: installation and dimensions	49
2-17	Locations of measuring sensors inside the pump	52
2-18	Dimensions of the dynamic pressure transducer and flush installation	54
2-19	Plexiglass cover plate installation and dimensions	55
2-20	Power supply used for static and differential pressure transducers	57
2-21	Static pressure manifold	58

2-22	Dimensions of the static pressure manifold and its fittings	59
2-23	Power supply box for dynamic pressure transducers, DAS and a typical block diagram	60
2-24	Instrumentation wiring diagram	62
2-25	Model pump assembly: measurements of dynamic pressure fluctuation and static pressure distribution	63
2-26	Vibration measurements of pump casing	65
3-1	Performance characteristics of the model pump at 3540 rpm	71
3-2	Effect of flow rate on static pressures at measuring locations	74
3-3	Effect of flow rate on time-averaged static pressure distribution around the impeller at 3540 rpm	75
3-4	Effect of flow rate on pressure uniformity inside the pump	77
3-5	Effect of flow rate on pressure fluctuation at location 3	80-81
3-6	Effect of flow rate on dynamic pressure fluctuation (Peak-to-Peak) and the corresponding FFT at all measuring locations	83
3-7	Effect of operating at maximum flow rate on pressure fluctuations compared to operating at design condition	84
3-8	Comparison of pressure fluctuations at geometrically similar locations 3 and 7	86
3-9	Comparison of pressure fluctuations at consecutive locations 3 and 4	87
3-10	Effect of flow rate on fluctuation and the corresponding FFT Mag. at pump discharge side	89
3-11	Effect of flow rate on fluctuation and the corresponding FFT Mag. at pump suction side	90
3-12	FFT magnitudes measured at the first three blade passing frequencies for location 7	91
3-13	FFT magnitudes measured at the first three blade passing frequencies at suction pipe	92
3-14	Typical Vibration behavior of the pump outer casing: vertical direction (case Q/Qn=0.5 at 3540 rpm)	94
3-15	Comparing pump case vibration with the internal pressure fluctuation and FFT measured at 5xRPM at location 3, at different flow rates	95
3-16	Effect of pump speed on performance curves	98
3-17	Effect of speed on pressure distribution at different flow rates	99
3-18	Effect of speed on pressure fluctuations at different flow rates	100
3-19	Effect of speed/flow rate on FFT magnitude of pressure fluctuations	101
3-20	Effect of speed/flow rate on pressure fluctuation and FFT magnitude at measuring location 3	102

3-21	Effect of speed/flow rate on pressure fluctuation and FFT magnitude at pump discharge side	103
3-22	Effect of speed/flow rate on pressure fluctuation and FFT magnitude at pump suction side	104
3-23	Scaled impeller with V-cut at blades exit	106
3-24	Effect of the V-cut at impeller blades exit on the pump performance at different speeds compared to the case of impeller without V-cut at blade exit	108-109
3-25	Effect of the V-cut on static pressure distribution inside the pump at different flow rates, 3540 rpm	111-113
3-26	Effect of the V-cut on static pressure at location 3 at different flow rates, 3540 rpm	114
3-27	Effect of the V-cut on static pressure in discharge pipe, under different flow rates, 3540 rpm	115
3-28	Effect of the V-cut on static pressure distribution inside the pump at different flow rates, 3540 rpm	117-119
3-29	Effect of the V-cut on the FFT magnitude inside the pump, measured at the 1st BPF (5xRPM) at different flow rates, 3540 rpm	120-122
3-30	Effect of the V-cut on the FFT Magnitude (measured at 1st BPF) in suction and discharge pipes, under different flow rates, 3540 rpm	123
3-31	Vertical vibrations of the pump casing with the V-cut at 3540 rpm	125-126
3-32	Effect of the V-cut on pump vertical vibration at 3540 rpm	127
3-33	Extending the volute vanes to decrease the radial gap	130
3-34	Cutting back the volute vanes to increase the gap	131
3-35	Pump performance at 3540 rpm under different gaps: impeller without V-cu at blade exit	133
3-36	Effect of gap design on head and efficiency at Q=Qn: Without V-cut	134
3-37	Static pressure distribution: max and min gaps compared with the original design at two different flow rates: Without V-cut	136
3-38	Effect of decreasing the gap on pressure fluctuation at different flow rates: Without V-cut	137-138
3-39	Effect of increasing the gap on pressure fluctuation at different flow rates: Without V-cut	139-140
3-40	Effect of gap and flow rate at location 4: Without V-cut	141
3-41	Comparison between pressure distributions at geometrically similar pairs of locations around the impeller for the gaps of 3.6 and 7 mm	144
3-42	Comparison the original gap design and max gap of 7 mm for the case vibration at different flow rates: Without V-cut	145

3-43	Pump performance at 3540 rpm under different gaps: impeller with V-cut at blades exit	147
3-44	Effect of gap design on head and efficiency: With V-cut at blade exit	148
3-45	Static pressure distribution: max and min gaps compared with the original design at three different flow rates: With V-cut	150
3-46	Effect of decreasing the gap on pressure fluctuation at different flow rates: With V-cut at blade exit	151-152
3-47	Effect of increasing the gap on pressure fluctuation at different flow rates: With V-cut at blade exit	153-154
3-48	Effect of different gaps and flow rates at different locations with V-cut at blade exit	155
3-49	Comparison between the original gap design and max gap of 7 mm for the case vibration at different flow rates: With V-cut at blade exit	157
3-50	Effect of the asymmetry of splitters lips (locations of volute tongues)	159
4-1	Generation of 2D impeller blades geometry	162
4-2	Generation of the 2D geometry of volute	163
4-3	Merging the impeller and volute mesh files	164
4-4	Components of a sliding mesh	165
4-5	Depiction of sliding mesh configurations at 6 positions during impeller rotation of 0.0025 second, rotational speed is 3540 rpm	171
4-6	Sections of the four meshes used for the grid-independence study	173
4-7	Location of the interface between impeller blades and volute vanes	174
4-8	Locations of pressure monitoring inside the pump, similar to experimental setup	178
4-9	Contours of static pressure (pa), Q=Qn, without V-cut at exit, gap 3.6 mm	184
4-10	Velocity vectors (m/s), Q=Qn, without V-cut at exit, gap 3.6 mm	185
4-11	Contours of static pressures at different flow rates	186-187
4-12	Velocity vectors close to interaction zone; at different flow rates	188-189
4-13	CFD prediction for H-Q curve	190
4-14	Typical waveform and spectral analysis of the unsteady pressure history at point 3	191
4-15	Waveform and spectral analysis of the pressure signal at the discharge nozzle	192
4-16	Time-averaged pressure distribution inside the pump at different flow rates	194
4-17	Time-averaged pressure at geometrically similar points around the impeller, at different flow rates	196

4-18	Peak-to-peak pressure fluctuations for the monitored locations at different flow rates	197
4-19	Effect of flow rate on unsteady pressure signal at point 3	198-200
4-20	FFT peak magnitude of the 1st BPF at point 3 as a function of flow rate	201
4-21	Unsteady pressure signal at geometrically similar point, Q=Qn	203-204
4-22	Peak-to-peak pressure fluctuations at geometrically similar points around the impeller as a function of flow rate	205
4-23	Simulations of impeller geometries	207
4-24	Effect of V-cut on time-averaged pressure distribution	209-210
4-25	Effect of V-cut on pressure fluctuations at different flow rates	211-212
4-26	Effect of V-cut on pressure fluctuation and FFT magnitude at point 3 at reduced flow rates	213
4-27	Extending the volute tongues to reach a gap of 2 mm	216
4-28	Effect of reducing the gap from 3.6 to 2 mm on time-averaged static pressures at points 3 and 4	217
4-29	Effect of reducing the gap from 3.6 to 2 mm on pressure fluctuations at points 3 and 4	218
4-30	Radial gap of 7 mm without V-cut and with the effect of V-cut	219
4-31	Effect of 7 mm gap on pressure distribution inside the pump compared to the original 3.6 mm gap	222-223
4-32	Effect of 7 mm gap on pressure fluctuations inside the pump compared to the original 3.6 mm gap	224-225
4-33	Gap 7 mm: Effect of V-cut on static pressure inside the pump	226-227
4-34	Gap 7 mm: Effect of V-cut on pressure fluctuations inside the pump	228-229
4-35	Comparison between the CFD prediction of pump head and experimental measurements	232
4-36	Effect of flow rate on time-averaged pressure distribution: experimental vs numerical for impeller without V-cut, gap 3.6 mm	233-234
4-37	Effect of flow rate on pressure fluctuations: experimental vs numerical for impeller without V-cut, gap 3.6 mm	235-236
4-38	Effect of flow rate on time-averaged pressure distribution: experimental vs numerical for impeller with V-cut blade, gap 3.6 mm	237-238

4-39	Effect of flow rate on pressure fluctuations: experimental vs numerical for impeller with V-cut blade, gap 3.6 mm	239-240
4-40	Effect of flow rate on pressure distribution: experimental vs numerical for impeller without V-cut, gap 7 mm	241-242
4-41	Effect of flow rate on pressure fluctuations: experimental vs numerical for impeller without V-cut, gap 7 mm	243-244
4-42	Effect of flow rate on pressure distribution: experimental vs numerical for impeller with V-cut blade, gap 7 mm	245-246
4-43	Effect of flow rate on pressure fluctuations: experimental vs numerical for impeller with V-cut blade, gap 7 mm	247-248

DISSERTATION ABSTRACT

Name: **Atia Esmaeil Khalifa**

Title of Study: **Experimental and Numerical Investigation of Flow Induced Vibration in a High Pressure Double Volute Centrifugal Pump**

Major Field: **Mechanical Engineering**
Date of Degree: **June 2009**

The present work is an experimental and numerical investigation of the flow induced vibration problem at blade passing frequencies of a high-pressure double volute boiler feed pump. The effects of variable operating conditions and different design modifications were studied by model testing to minimize the vibration level. The amplitude and strength of the pressure fluctuation inside the pump depend on the measuring location with respect to the interaction zone at volute tongues. The unsteady pressure fluctuations are very sensitive to the flow rate. Pressure fluctuations are increased at high rotational speeds and at off-design conditions. The original pump has a special V-shaped cut at the exit of impeller blades which reduces the pressure fluctuations up to 45% depending on flow rate and measuring location. It also reduced pump vibration by 20 to 50% depending on flow rate. The selection of the suitable gap between impeller and diffuser vanes for minimum vibration levels was based on experimentation under the expected operating conditions. Smaller gaps are not preferable for the pressure fluctuations inside the pump since they produce higher impeller/volute interaction. Increasing the gap from 2.5 to 5% of the impeller diameter with the V-cut design is considered to be a good and simple solution to minimize vibration levels by about 50% on average for the present pump; at a wide range of flow rates. The improvement in reducing pump vibration due to gap increasing was achieved at the expense of 5% loss in pump head and 1.6% loss in efficiency at the rated pump capacity. Detailed uncertainty analysis indicates that uncertainty limits are: ±1.5% in flow rate, ±1% in head, and ± 2% in efficiency, at best efficiency conditions. The 2D CFD simulation using sliding mesh technique can predict the effect of variable flow rate and pump design on flow field. However, the unsteady pressure fluctuations are location dependent and a 3D model is needed for accurate prediction of the fluctuations amplitudes.

ملخص بحث
درجة الدكتوراه فى الفلسفة

الإسم : **عطيه إسماعيل خليفة**
عنوان الرسالة: **بحث تجريبى و عددى للإهتزاز الناتج عن السريان فى مضخة طرد مركزى عالية الضغط ذات غلاف منقسم**
التخصص: **هندسة ميكانيكية – علوم الموائع و الحرارة**
تاريخ التخرج: **يونيه 2009**

تحتوى الرسالة على دراسة عملية و محاكاة عددية للإهتزازات الناتجة عن السريان داخل مضخة تغذي غلاية محطة توليد كهرباء حيث تمت الدراسة على مضخة أنموذج مصغرة لمعرفة تأثير عوامل التشغيل الديناميكية بالاضافة الى تأثير تغير تصميم المضخة بهدف تقليل تذبذب الضغط داخل المضخة و اهتزازها.
و قد وجد أن تذبذب الضغط داخل المضخة يعتمد على معدل التصرف ة المسافة الفاصلة بين الجزء الدوار و ريش الغلاف الثابتة التى تقسم السريان الى المخرج كما انه يختلف من مكان الى أخر داخل المضخة ويزداد تذبذب الضغط داخل المضخة مع زيادة السرعة و عند معدلات تصرف غير مساوية لأعلى كفاءة.
و قد تم دراسة تصميم الجزء الدوار فى المضخة و الذى يحتوى قطع على شكل V فى نهاية الريش حيث وجد انه يقلل من تذبذب الضغط داخل المضخة و الاهتزاز المقاس على جسم المضخة الخارجى خصوصا عند معدلات التدفق المنخفضة. أثبتت المحاكاة العددية ثنائية الابعاد انها مفيدة جدا فى دراسة تأثير
المتغيرات التشغيلية كمعدل التدفق و السرعة، و كذلك تغيير التصميم على توزيع و تذبذب الضغط داخل المضخة و لكن نحتاج الى تطوير محاكاة ثلاثية الابعاد للحصول على قيم أكثر دقة لتذبذب الضغط داخل المضخة.
توصى الدراسة بزيادة الفراغ الفاصل بين الجزءالدوار و الريش الثابتة ليصل الى 5 % من قطر الجزء الدوار عن طريق قص الريش الثابتة للخلف (إبتداء من مقدمتها) وذلك يخفض من مقدار الاهتزازات و تذبذب الضغط داخل المضخة عند جميع ظروف التشغيل ولكن على حساب انخفاض قدره 1.6 % فى الكفاءة و5% فى الضغط عند معدل تدفق ثابت مناظر لأعلى كفاءة.

CHAPTER 1

INTRODUCTION

1.1 INTRODUCTION AND LITERATURE REVIEW

Flow induced vibration is a common problem in high energy pumps. The source of this problem is commonly the interaction between rotating impeller blades and volute diffusers or tongues (also called Rotor-Stator Interaction). The remedy of this problem is a matter of experimentation and depends on the details of pump design and operating conditions. The trend of increasing the power of large hydraulic pumps with the need of increasing the operating range to allow higher capacities has led to many problems. These problems include a rise in pressures, velocities, material stresses, and extreme off-design operating conditions. As a consequence, the vibration levels have increased and fatigue problems have become more common. This limits the power output of new designs and operating conditions. For these reasons, it is important to identify sources of vibration and how it can be controlled. Rotor-stator interaction in diffuser pumps represents one of the most important excitation sources of vibration in pump components; impeller, shaft, casing as well as attached piping system. Pressure fluctuations inside the pump are mainly due to the interaction of the rotating impeller pressure field with the stationary circumferential pressure field generated by a vaned collection element, either volute tongue(s) or diffuser vanes. Vibration is excited by

these fluctuations especially under off-design operating conditions. Vibration at Blade Passing Frequencies (BPF) usually dominates the spectrum (Note: some times it is written as Vane Passing Frequency, VPF, instead of Blade Passing Frequency; however, we will use BPF through this dissertation). In centrifugal pumps, the impeller blades interfere with the diffuser vanes and produces pressure fluctuations downstream of the impeller. These pressure fluctuations, at critical locations, inside the pump may become as large as the total pressure rise across the pump stage. These fluctuations not only generate noise and vibration that cause unacceptable levels of stress and reduce component life due to fatigue, but also introduce unfavourable characteristics of pump performance even at or near the design point. The pump geometry plays an important role in the severity of the pulsation problem. Stability of the pump performance depends on the volute design, position and shape of volute tongue, vaned diffuser, impeller-volute matching, and impeller-volute gap. Pumps are normally designed to avoid the harmonics with significant amplitudes that coincide with natural frequencies of critical components. This is to avoid rapid fatigue, excessive wear, and catastrophic failure. In condition monitoring, it is very important to know the source of vibration. This allows fast corrections for inadequate practices and faults detection. Many experimental studies have shown that the harmonics with higher amplitudes depend mainly on the number of stationary and moving blades, the distance between stationary and moving blades, and the flow rate.

Despite the long history of literature documenting forces on pump impeller, there are few detailed investigations into the effects of various impeller and volute combinations on these forces with a parallel examination of the hydraulic

performance, Baun et al [1]. The exact force magnitude and hydraulic performance depend on the exact geometrical details of pump design.

When centrifugal pumps operate at partial flow rates, the flow in the suction pipe starts to rotate with the impeller and finally a reverse flow from the impeller towards the suction occurs (inlet eye recirculation). This is evident by abnormal rise of suction pipe wall static pressure, noise, and increasing vibration level. Reverse flow causes some amount of energy losses at partial flow rates and the instability was attributed directly to the occurrence of the reverse flow and pre-rotation, and therefore the pump head becomes unstable; Breugehmans and Sen [2]. The pressure and velocity fluctuations have a direct impact on the mechanical damage of the pump components. Accordingly, the extension of the reverse-free range of a centrifugal pump is of great importance. Instability types are blade wakes, blade to blade fluctuation, pre-rotation, and surge of the total system. Improving the stability of the pump used to be at the expense of the pump performance and results in shifting the best efficiency point for the pump. The design of impeller assumes axial, one-dimensional flow in the suction pipe entering the impeller. Flow rate reduction by closing throttle valve imposes a higher loading on the impeller and the impeller itself becomes a source of reverse flow and pre-rotation. Separation inside the impeller causes the inlet flow pre-rotation. The pump critical flow rate depends on the impeller design. Recirculation is reduced by using inlet straightener and extending the blades into the suction eye of the impeller. Also perpendicular leading edge to the axis of rotation gives the best stability results.

The flow is not uniform around the impeller circumferentially, even at design point, due to the interaction between impeller and volute and the velocity profile at impeller

exit; Guo and Maruta [3]. The pressure fluctuations depend on the flow rates and blade/vane angles. The largest blade pressure fluctuations occur at the trailing edge on the pressure side, but the magnitudes depend greatly on the number of vanes and vane angle. At off-design operating conditions, pressure fluctuations due to impeller-volute interaction occur mainly at blade passing frequency and its higher harmonics. The circumferential unevenness of fluctuations, which causes sidebands in frequency spectra, is dependent on the flow rate and guide vanes and become more significant at lower flow rates. The vibration wave is a traveling wave in the circumferential direction when the resonance is exited by rotor-stator interaction.

Model testing of hydro-machinery has long been used to assess expected prototype unsteady behavior. Stochastic flow induced turbulence and fluid flow acoustic resonances caused by the coincidence of pulsation wavelengths with water passage dimensions inside the machine or external to the machine as well as a large variety of fluid-structure interactions need to be considered.

The time variant and spatial nature of the pressure distributions can be visualized; Franke et al. [4]. Each interaction forcing frequency possesses a global time variant pressure distribution. By inspecting the frequency domain of pressure signals, a number of dominant frequencies appear. By visualizing the pressure variation at the measurement locations at the frequency selected, a pressure characteristic shape (pressure mode shape) appears. Moreover, modal software can correlate geometric transducer locations with their respective data blocks, allowing for animation of the pressure distribution. The largest vibration levels in large pump turbines are, in general, originated in the rotor stator interaction. This vibration has specific

characteristics that can be clearly observed in the frequency domain, namely, harmonics of the moving blade passing frequency and a particular relationship among their amplitudes. The frequencies and their amplitudes depend on the pump design and the operating conditions. The amplitude of harmonics increased when certain conditions are achieved. The rise in the amplitudes is not equal for all harmonics; some are more affected than others.

Rodriguez et al. [5] presented a theoretical analysis to predict and explain, in a qualitative way, such frequencies and amplitudes. The analysis incorporates number of blades, number of guide vanes, the RSI non-uniform fluid forces, and the sequence of interaction. The theoretical analysis is complemented with geometrical and timing considerations that allow going deep in the sequence on interaction rather than assuming excited diameter modes. The distance between the moving and stationary blades helps in determining the origin of the harmonics. Knowing the origin of harmonics guides to effective solutions in order to reduce their amplitudes.

It is known that the performance of a centrifugal pump depends largely upon the flow patterns at the impeller exit to the extent that a small change in the edge form of the impeller blade causes a change in the pump performance. Koji et al. [6] examined the changes in the pump head and the flow pattern experimentally. They used pump impellers whose outlet angles are deformed stepwise by slicing off the blade on the suction or pressure sides. Slicing off the blade edge in the suction or pressure sides was found to increase the pump head due to the increase in the circumferential component in the absolute velocity.

Many cases of impeller failures were caused by unusual radial gap between impeller and diffuser or volute tongue. Srivastav et al. [7] examined the effect of radial gap between impeller and diffuser on vibration and noise in a centrifugal pump under different flow conditions. The original gap was o.6 mm or 0.3% of the impeller outer diameter; which was considered to be very small. Three radial gaps of 0.6, 2.4, and 6 mm were examined. For each radial gap, head, and efficiency were determined at different flow rates. The performance tests of the pump were performed by varying the flow rate in steps by suction and delivery valves. The larger gaps were achieved by trimming the impeller to smaller diameters. Vibration and noise measured in a wide frequency range showed that impeller blade-passing components dominate the frequency spectrum. It was shown that at maximum radial gap between the impeller and diffuser, the overall level of vibration and noise are minimum. Increasing the radial gap reduces vibration and noise levels, however, at the expense of pump performance in terms of head and efficiency. A clear correlation between vibration and noise is observed. If the flow rate is controlled by suction throttling, then the vibration level is higher than that corresponding to delivery throttling for small gaps in general, while this behaviour may be reversed for large radial gaps. Both the impeller blade Passing and diffuser vane Passing components appear in the spectra and depending on the gap values. Vibration at these components is governed by the wake effect at the impeller-diffuser interaction location. This wake causes pressure pulsation which in turn gives rise to vibration and noise. Both impeller blade trailing edge and diffuser vane leading edge control the wake effect. The pressure pulsations and pump performance are strongly affected by the radial gap. Increasing the gap decreases the pump head and efficiency. It was observed that 10 times increase in the radial gap

between impeller and diffuser reduced the vibration level by almost 52% for suction throttling and 32% for delivery throttling; while the efficiency loss was only 4% at best efficiency point. For the noise, 10 times increase in the radial gap between impeller and diffuser; the reduction in the maximum level is more for suction throttling, 8 dB, than the case of delivery throttling, 3dB.

Makay et. al. [8] studied the pressure pulsations arising from the interaction of the impeller and vaned diffuser in a 500 cfs water supply pump, which caused numerous plant problems. Model testing of the pumps was conducted to define and evaluate potential field modifications to the hydraulic components. Two ways to correct the problem were considered:

(1) Increasing the impeller to diffuser clearance.

(2) Changing the number of impeller blades.

When pumps were in operation (a single pump or all six), an objectionable noise and vibration existed. The vibration and noise were measured at 2-times the impeller blade passing frequency. The frequency of this activity corresponded with pressure pulsation amplitudes measured in the discharge pipe. The source had been traced to the interaction between the 7-blade impeller and the 13-vaned diffuser. The pump design was found to accentuate these blade interactions in four possible ways. First, the impeller and diffuser are highly loaded, (high impeller exit angle of 29 degrees plus the low solidity) meaning that even at design flow, it resulted in a large impeller blade-to-blade variation and that the physical size has been kept small in relation to the energy addition. This results in large pressure variations from blade-to-blade and from vane-to-vane. Second, the vane number combination of 7 impeller blades and 13

diffuser vanes cause the 2x blade Passing pulsations. Third, the clearance between impeller and diffuser is small (3% of impeller diameter). Finally, the size, speed and acoustic path length of the impeller and diffuser coincides with criteria known to produce acoustic reinforcement of pressure waves. Two significant changes in measured pump output which indicate the onset of diffuser recirculation are: pressure pulsations and power-flow rate curve. In this study, the changes in impeller to diffuser clearance ranged from the prototypical 3% to the final 12% of the impeller diameter. The change in head characteristic was obvious. A reduction of 10 % in the flow capacity, at the rated head, resulted from this modification. The pulsation amplitude was found to be position sensitive and the 12% clearance reduced the amplitude to less than a third of the prototype configuration. The separation of the sources of the two pressure fields had a positive effect on the magnitude of the resulting pulsation. The efficiency is the same for the 3% and 12% configuration at the rated flow rate and the power input actually decreased in the same proportion as the head decreased. If the rated head is maintained, the pump flow capacity and efficiency should be reduced for larger gaps. It seems that the combination of diameters, rotating speed and speed of sound results in the acoustic reinforcement at the discharge pipe entrance so that the pressure waves (which travel at the speed of sound of the pumped liquid) will arrive simultaneously in the discharge pipe.

Another type of problems where blade passing frequencies dominate is given by Atkins and Tison [9]. A series of six main oil line pumps were experiencing severe vibration problems. The pumps experienced high vibration and noise levels and were generally unreliable with numerous seal failures as well as failures of the attached

small bore piping and gage lines. Two resonant frequencies were excited by blade passing frequency (5x running speed). The noise levels near the pump showed similar spectral content. Initially, it was not known whether these frequencies are mechanical natural frequencies or acoustic natural frequencies. The discharge pulsation data indicated that these were acoustic resonances and identified two response peaks which represented the acoustic natural frequencies of the system. The root cause of failures was identified as an acoustic resonance of the pump internals excited by blade passing frequency. As a means of reducing the pulsation levels generated by the pump, the impeller to cutwater clearance was increased by trimming the cutwater. This was suggested by the pump manufacturer and resulted in a marked reduction in the audible noise. However, the seal and piping failures persisted when the pumps were operated in the upper end of the speed range. In addition to the operating vibration, noise, and pulsation data, impact tests of the bearing housing structure and various piping components were conducted during pumps shut down to identify natural frequencies of mechanical components. In order to solve the acoustic resonance problem, either the acoustic natural frequency or the excitation frequency had to be changed. The most practical solution appeared to be changing the blade passing frequency of the pump by changing the number of impeller vanes. The acoustic natural frequencies would not be excited within the desired operating speed range, if a seven-vane impeller was used.

The application of numerical procedures to pump design and analysis has provided a very valuable tool. Today it is possible to predict the performance curve and static pressure distributions with amazing accuracy, in the very early design stages. Such information accelerates the whole design cycle and achieves enormous time and money saving in the final product.

Many computational fluid dynamics (CFD) studies have been made and applied to pumps. However, experimental data for the internal flow are still needed to verify computational results. Benchmark velocity and pressure data over a wide range of geometries are needed to understand the flow mechanics and to verify CFD predictions. On the other hand, it is difficult to understand the unsteady phenomena only from experimental studies, particularly at off-design conditions, where unsteady phenomena in diffuser pumps become more complicated.

The numerical flow analysis allows the study of different variables which are always difficult to measure experimentally. In particular, the amplitude of the fluctuating pressure field at the blade passing frequency is successfully predicted by numerical models for a wide range of operating flow rates. The main conclusion from many numerical models is the need for a fully unsteady calculation with relative motion of the impeller if the dynamic effects are to be taken into account. The discretization of the geometry should be done keeping the balance between calculation time and the accuracy of the simulation of the flow structure. Special care must be taken in the near cutwaters regions.

Gonzalez and Santolaria [10] implemented the numerical model using a commercial code FLUENT to solve the fully 3D incompressible Navier-Stokes equations, by including the centrifugal force source in the impeller and the unsteady terms. Turbulence is simulated with the standard k-ε model. Initializing the unsteady calculation with the steady solution for few impeller revolutions was necessary to achieve a fully periodic unsteady solution convergence. They reported the effect of flow rate on pressure fluctuations at the blade passing frequency. Also the pressure fluctuations signals at different axial planes were calculated. Pressure fluctuations

were found to be maximum at the central impeller plane. Location of the stagnation point at the tongue region was determined to be variable for variable flow rates.

For the numerical simulation, the viscous Navier-Stokes equations are handled with an unsteady calculation. Sliding mesh technique is applied to take into account the impeller-volute interaction. The unsteady calculation combined with the sliding mesh technique has proven to be a useful tool to investigate the flow field inside a centrifugal pump including the dynamic effects, Gonzalez et al. [11]. The pressure fluctuations at the blade passing frequency reveal the blade-tongue interaction with the flow at the impeller outlet plane. Such interaction clearly increases the fluctuation levels for off-design conditions, which limits operation range, increases losses, etc.

Zhang and Tsukamoto [12] developed an experimental and computational study for unsteady hydrodynamic forces on a diffuser pump impeller excited by the interaction between the impeller and the vaned diffuser. The impeller has a number of blades equal to the number of diffuser vanes. Unsteady flow calculations are made using commercially available CFD software, CFX-TASCflow, as well as the two dimensional vortex method. It was demonstrated that the fluid forces on the impeller with the same number of vanes as the vaned diffuser are smaller compared with other combinations of vane numbers. However, the pressure fluctuations are found to be greater than other cases.

Wang and Tsukamoto [13] developed an experimental and numerical study for the unsteady phenomena at off-design conditions of a diffuser pump. The pressure fluctuations due to the rotor-stator interaction and the rotating stall in a diffuser pump were calculated using the vortex method, and the calculated pressures were compared with the experimental data. They found that the impeller blade passing frequency and

its higher harmonics are always dominant in the pressures downstream of the impeller for the whole flow range because of the rotor-stator interaction.

There exist some lower dominant frequencies in the pressure filed downstream of the impeller for unstable range because of the effects of the complicated flows; such as separating flow, rotating stall and reverse flow in pumps. These lower dominant frequencies are dependent on the flow rate, the unsteady pressures, and are chaotic in such unstable ranges.

The blade outlet angle is one of the most important design parameters which can affect centrifugal pump performance. It controls the strength of the wake at the impeller exit. Shojaee and Boyaghchi [14] studied the performances of a centrifugal pump with different blade outlet angles both experimentally and numerically. The pump was handling water and viscous oils as Newtonian fluids. The 3-D numerical simulation of the flows inside the centrifugal pump with different blade outlet angles was carried for different operating conditions. The k-ε turbulence model is adopted to describe the turbulent flow process. These simulations have been made with a steady calculation using the multiple reference frames (MRF) technique to take into account the impeller-volute interaction. Surface between inlet-impeller and impeller-volute correspond to grid interfaces. The multiple reference frame technique allows the relative motion of the impeller grid with respect to the inlet and the volute during steady simulation. The results show that when the outlet angle increases, the centrifugal pump performance handling viscous fluids improves. This improvement is due to decrease of wake at the exit of impeller. Numerical simulation errors are commonly caused by model and numerical errors which include discretization and calculation errors. The model error,

which describes the difference between the physical model of internal flow and its phenomenon, is mainly caused by the control equations. For a detailed understanding of the internal flow, it is very important to set up and select a good turbulence model for the numerical simulation.

Since the k-ε Turbulence model have been widely used for the numerical simulation of centrifugal pump, LI Xian-hua [15] performed a study of the k-ε turbulence model for numerical simulation of centrifugal pump using FLUENT software. It includes the standard k-ε model, the renormalization group (RNG) k-ε model and the Realizable k-ε model. In order to examine their applicability, a series of steady numerical simulations of centrifugal pump at the design point and at eight off-design points were carried out with these three kinds of turbulence models. During the simulations, the influence of the changes of the relative position between the impeller and volute was considered and the impeller/volute interaction was roundly reflected. The head, shaft power and efficiency were calculated and the simulated performance curves of a centrifugal pump were compared with the experimentally obtained performance curves. It was confirmed that the three models were suitable for the numerical simulation of the internal flow inside a centrifugal pump and especially the result of the numerical simulation from the Realizable k-ε model had a best agreement with the experimental result.

Under ideal conditions, the pressure within the volute is symmetrical around the impeller. When the pump operates away from its design point, however, the pressure within the volute varies, resulting in a net radial load on the impeller and the pump shaft. To limit shaft stresses and subsequent shaft deflections, many pumps are

designed with a double (or split) volute as shown in Fig. 1.1. The pump volute is partitioned into two flow ways. There are actually two cutwaters in the volute, 180° from each other. When the pump is operated away from its best efficiency point (BEP), the radial forces are approximately equalized and the stresses on the pump shaft are almost unchanged [16]. Double volute designs are not available in small pumps and hold the promise of better operation over a wide range of operating heads. On the other hand, large and high pressure pumps are usually available only in the double (split) volute design. The double volute pump demonstrates its value when a pump operates away from the best efficiency point (BEP). The design of the volute results in less radial force on the pump shaft and improve mechanical and hydraulic performance.

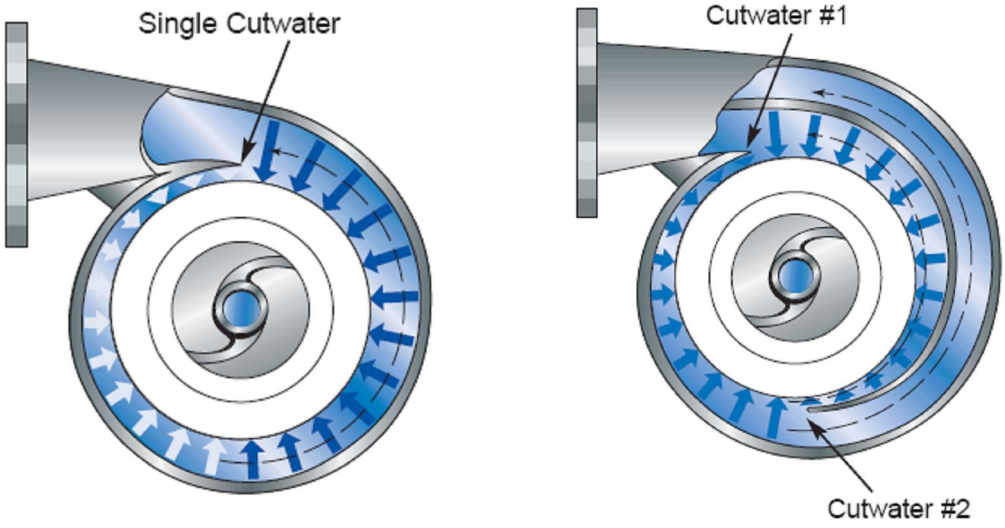

Single volute **Double volute**

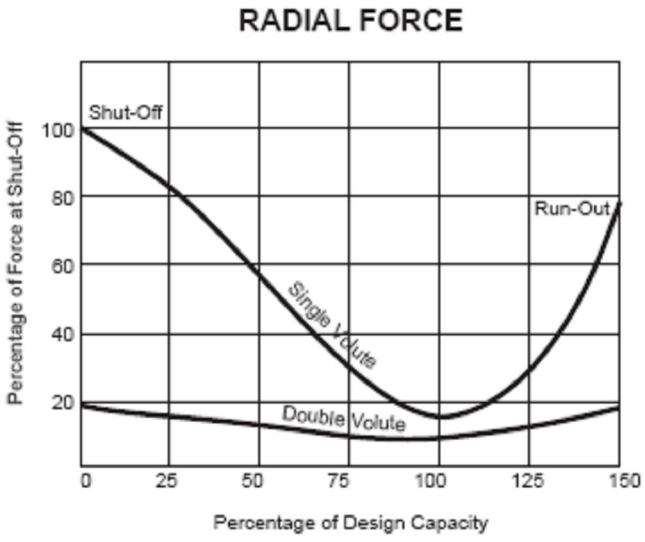

Figure 1.1 Variation of radial unbalance force with pump flow rate for single and double volute pumps [16]

1.2 RESEARCH MOTIVATION

The main boiler feed pumps (BFP), both turbine and motor driven, at one of Saudi Electricity Company (SEC) power plants are experiencing high vibration behavior. The Pumps are MHI- Horizontal-axis, 4-Stage, Double Case Centrifugal Pumps with five blades rotating impellers. Sketch of the boiler feed pump and its components is shown in Fig. 1.2. Figure 1.3 shows the dismantle procedure of the pump. The flow arrangement and a typical double volute pump stage design are shown in Fig. 1.4. The pumps have a special V-shaped cut at the impeller blades exit. Figure 1.5 shows the BFP cartridge (inner casing and impeller) of a retired pump provided by SEC.

The pumps vibration behavior exceeds the adopted standard limits (Seismic 0-peak, 0.25 in/sec, API standard), particularly at high speeds and off-design operating conditions. This vibration problem was transferred to other related/connected components of the equipment, such as instrument gauges and welded pipes, which led to their frequent failures. The pumps are required to operate at variable load (off design conditions) based on electricity consumption. They should maintain a certain water level inside the boiler at a given pressure. Load control is done by changing pump rotational speed. As per the analysis of the seismic vibration data (casing movement) collected on the main BFPs, it was noticed that the vibration spikes are mainly appearing at 5xRPM and 10×RPM frequencies; corresponding to the first and second blade passing frequencies (BPF) as shown in Fig. 1.6. At the same time, the relative vibration (Shaft movement) of the main BFP is smooth. Moreover, other equipment connected to BFP are not experiencing vibration behavior same as the main BFP.

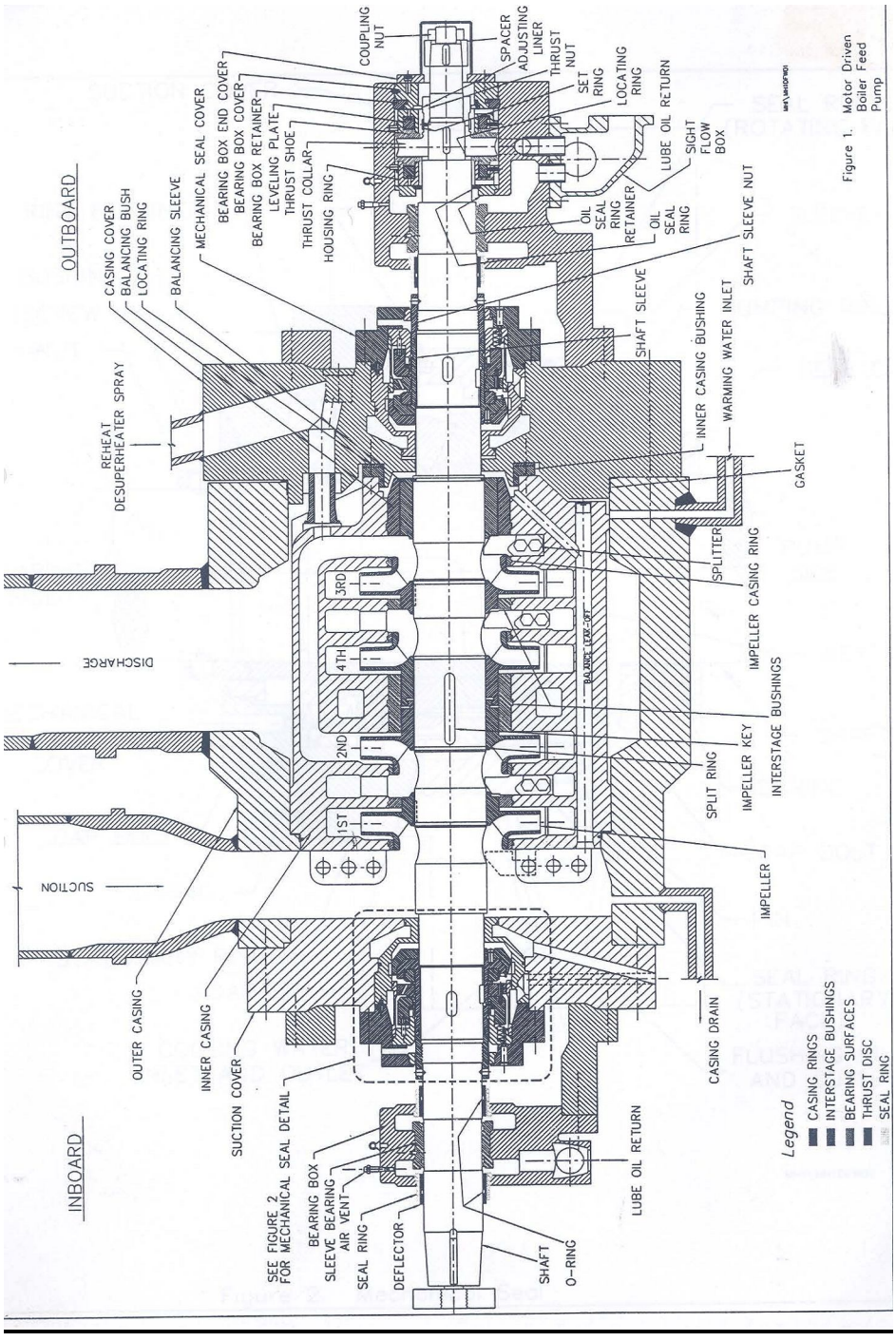

Figure 1.2 Sketch of the boiler feed pump and its components (provided by SEC)

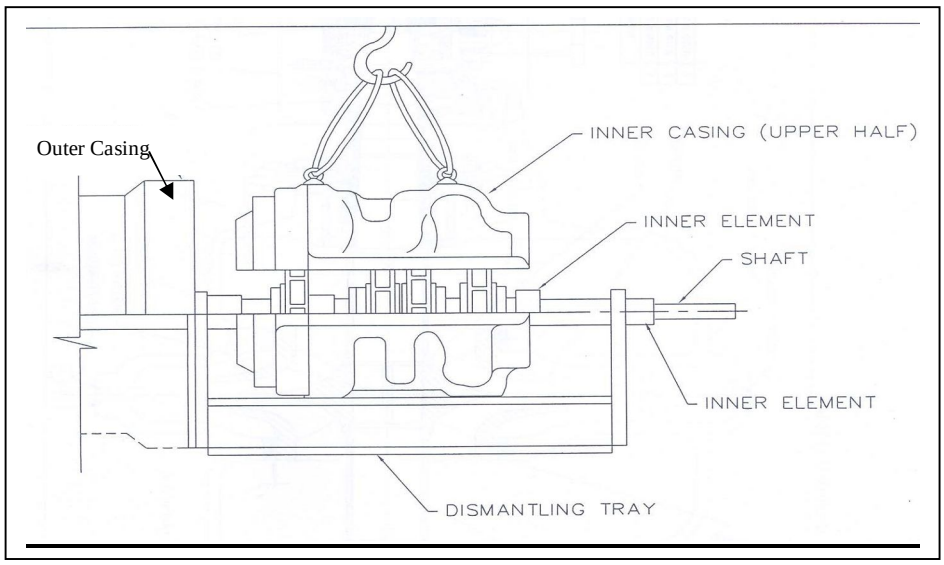

Figure 1.3 Dismantle of pump inner casing: upper half (provided by SEC)

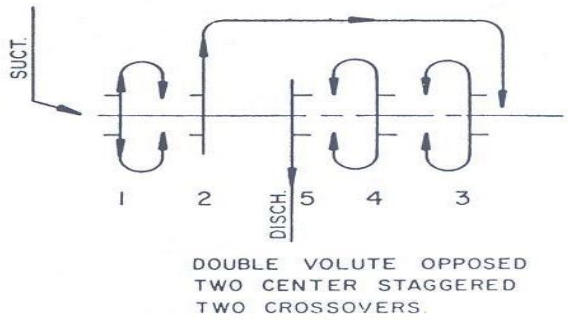

(a)

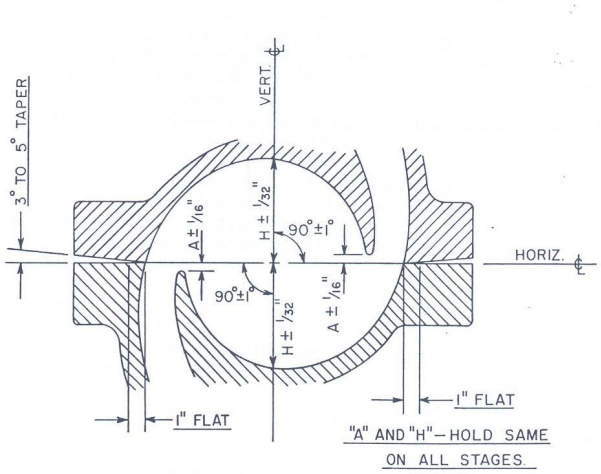

(b)

Figure 1.4 Boiler feed pump flow arrangement and typical double volute pump stage design, with tolerances [17]

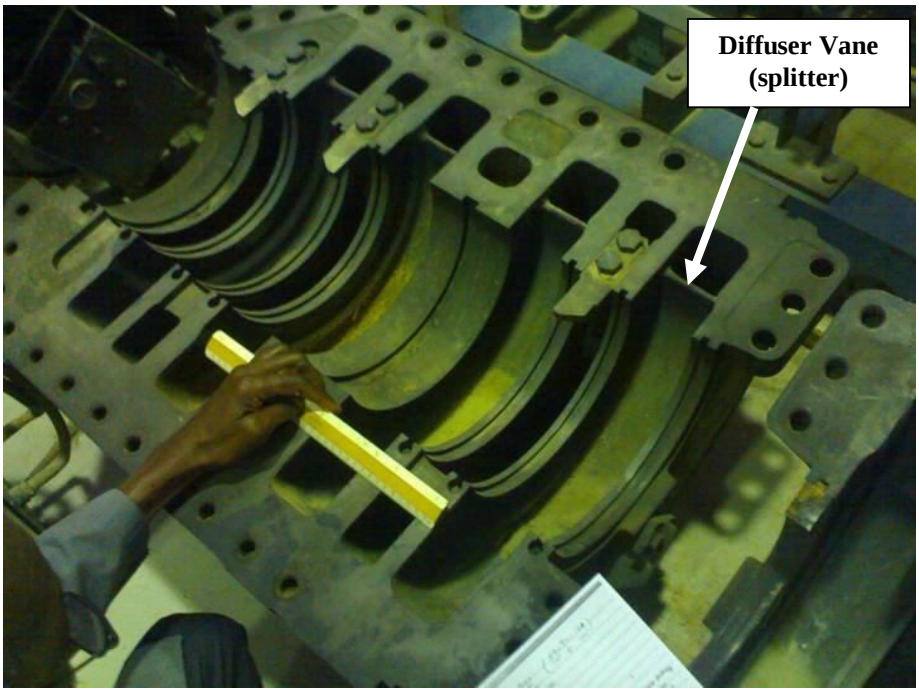

(a) Split Volute

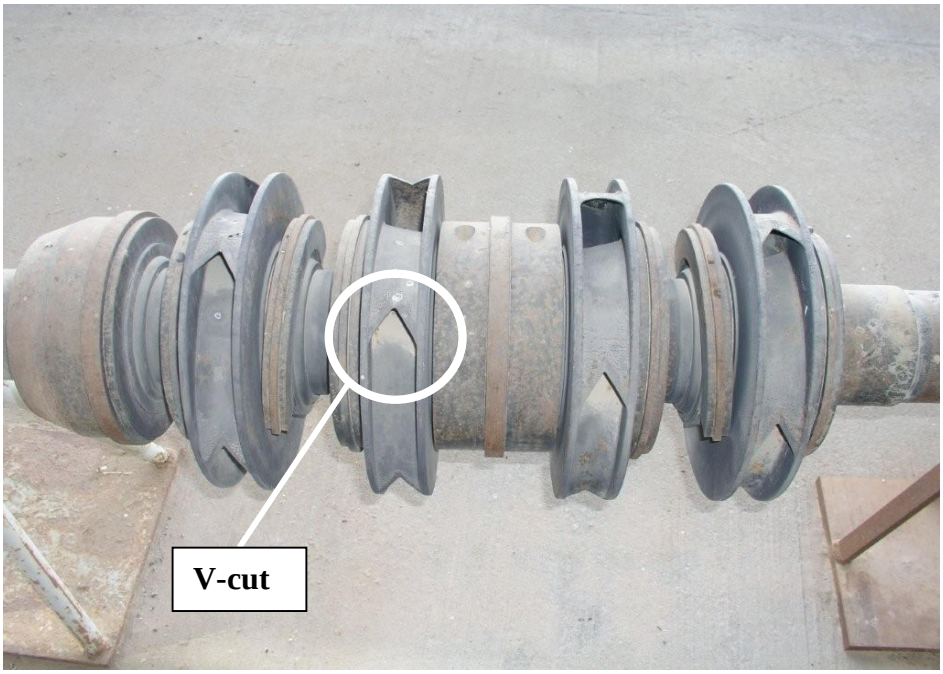

(b) Impellers with V-cut at blade exit

Figure 1.5 Boiler feed pump cartridge provided by SEC

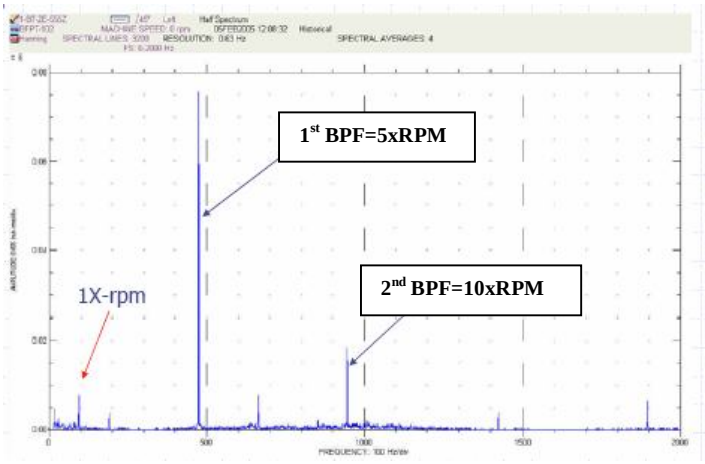

(a) PFB-PIA

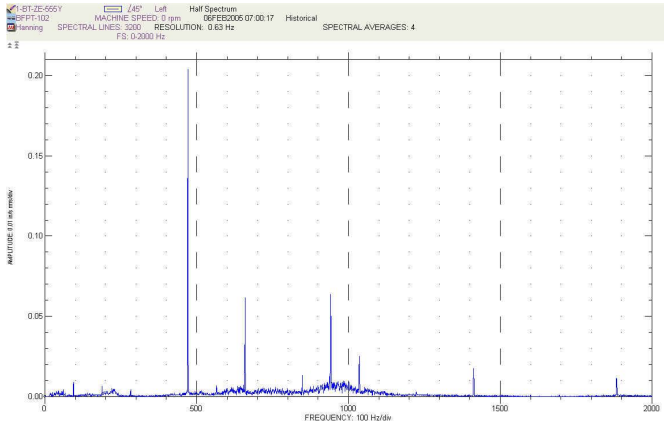

(b) PFB-PIV

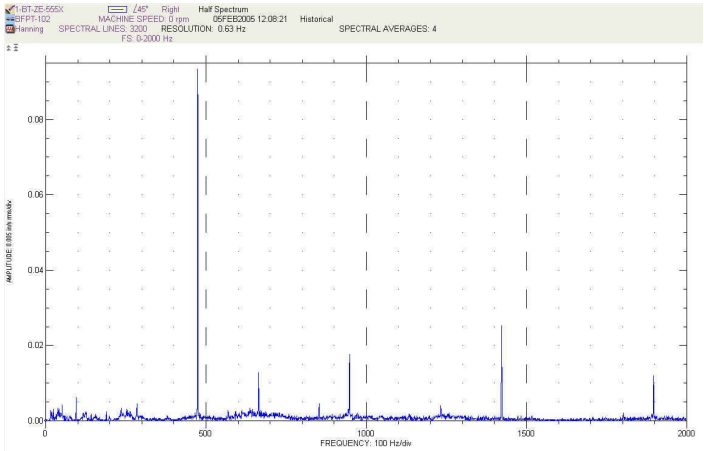

(c) PFB-PIH

Figure 1.6 Sample of field vibration records for BFP at SEC power plant

Different trials were made to reduce the vibration level, such as conducting hot train alignment and replacing one pump cartridge with a new one, but the vibration behavior had not changed much. Also, different vibration engineers from different companies, such as OED/SEC, BW/IP-Holland, and MHI- Japan, were involved to study the problem. All of them came to the same conclusion that the vibration problem is caused by impeller vane passing frequency and are predominant at 5th and 10th harmonics of the rated RPM. To rectify the problem, they suggested to modify the design of the impellers of the main boiler feed pump and to replace the rotor wear rings. Finally, Mechanical engineering department at KFUPM was contracted to find a simple applicable solution for this problem.

Based on collected field data, the vibration amplitude at BPF changed with speed in a pattern that can be attributed to the influence of the flow pattern, and pressure field inside the pump. Also, the vibration amplitude at 1^{st} BPF (5xRPM) changed with misalignment. No dimensional drawings of the boiler feed pump were provided and hence Reverse-Engineering was required. The tools provided by SEC included:

1) Maintenance drawings, no dimensions, and not to scale.
2) An actual impeller (spare part).
3) An inner casing of a retired pump.

1.3 ANALYIS

The problem of high vibration at the blade passing frequency and its harmonics, in high pressure centrifugal pumps, is usually associated with high impeller-volute interaction due to clearance problems (gap between the impeller and the stationary diffusers). It may also appear for improper combination of impeller/volute blades numbers, rotational speed, and working fluid. It is also possible that the 1^{st} BPF (or its higher harmonics) coincides with a system natural frequency causing high vibration. Other minor possible causes include asymmetric gaps between impeller and stationary vanes, early separation due to improper vane angle of attack.

In order to trace the root causes of the vibration, a laboratory setup of a scaled pump is necessary. Model testing is required considering the pump large size and its hydraulic design. Investigation of dynamic operating conditions and pump design features is needed. Through the use of an appropriate model testing, the degree of modification could be identified and the impact on the pump performance is assessed.

Numerical simulation, CFD model, will help to investigate the flow-induced vibration phenomenon and guide qualitatively the experimental work. Both experimental measurements and numerical simulations will be used to investigate the pump design in order to reduce the flow induced vibration to acceptable levels according to the established standard.

1.4 OBJECTIVES

The objective of this work is to perform experimental and numerical studies, on a scaled model pump, to investigate the flow-induced vibration problem of the double volute pump design. The effect of dynamic operating conditions (flow rate and speed) and the pump design (double volute with V-shaped cut at impeller blades exit) are considered. This study leads to the root cause the flow induced vibration problem of the boiler feed pump caused at the blade passing frequency. A simple applicable solution is desired after all. Based on the experimental and numerical results, new modification(s) will be applied and tested. We may divide the research work into four phases as follows:

Phase-I: General experimental investigation on the flow induced vibration for this pump design under different operating conditions (speeds and flow rates) in order to identify the source of vibration, the physical causes, and major controlling factors.

Phase-II: Study the effect of the special V-shaped cut at the impeller blade exit; see Fig (1-5b), on performance, pressure distribution and pressure fluctuations inside the pump, vibration of pump casing; at different operating conditions.

Phase-III: Study the effect of the radial gap between the rotating impeller and the stationary volute vanes on the performance, pressure distribution and fluctuations inside the pump, vibration of pump casing; at different operating conditions.

Phase-IV: Perform a comprehensive unsteady 2D numerical CFD simulation for the model pump under different operating and design conditions similar to experimental conditions. Comparisons with the experimental results will be made to assess the validity of using CFD in such a problem.

1.5 METHODOLOGY

1. Literature review includes the following:
    a. Effect of dynamic and geometrical parameters on the flow induced vibration in pumps.
    b. Experimental field testing, methods of vibration measurements and analysis for identification of blade passing frequencies (BPF).
    c. Existing or proposed remedies for BPF and related vibration problems.
    d. CFD work previously done on modeling flow in pumps, in general, and modeling techniques dealing unsteady phenomena in pumps in particular.
2. Study of the boiler feed pump assembly, geometry, and dimensions.
3. Production of the scaled impeller and volute of model pump.
4. Preliminary uncertainty analysis for experimental planning and designing.
5. Experimental Design (layout, pump selection, model pump specifications, instruments, etc….).
6. Acquiring equipment and instrumentations, (pump, pipes, valves, transducers,….).
7. Setup of the experiment and initial tests.
8. Conducting tests which include the following:

a. Measurements of the performance for the model pump (compare with similarity calculations).
b. Measurements the pressure fluctuation signals around the impeller at different radial and angular locations to identify the critical locations and frequencies.
c. Study the effect of the V-cut at impeller blades exit on the pump performance and pressure fluctuation as well as pressure distribution inside the pump.
d. Study the effect of different radial gaps between the impeller and volute stationary vanes (splitters).
e. Experimental testing of the asymmetry in volute cutwaters locations relative to the horizontal volute centerline.
f. Measurements of vibration on the pump outer casing at different conditions

9- CFD modeling includes:

a. Collection of geometrical data from actual pump with the help of available drawings, information from SEC, actual measurements on the pumps supplied by SEC. The geometric shape of the impeller blades is very complicated. It has a 3D complexity due to its variable thickness, variable twist, and a V-shape cutting at the exit trailing edge. Hence it requires measurements of all the four edges of the blade and the V-cut at trailing edge.
b. Establishing 2-D geometrical models.
c. Design and generate the mesh for optimum solution requirement.
d. Develop the mathematical model (PDE equations, boundary conditions, ….).
e. Testing the 2-D transient simulations for different flow rates/speeds.
f. Analyze the CFD simulation results and extract numerical data such time varying pressure at selected locations, pressure distribution, FFT analysis, etc.

g. Identification of critical frequencies and pressure fluctuations magnitudes.

h. Recommendations and outline of possible design modifications.

i. Testing the model for the new recommended design(s).

10. Analyzing results and comparing the numerical solutions with experimental results.

11. Modify the design and experimentally apply new modification(s) to the pump.

12. Test the new design(s) and recommend a solution to minimize pump vibration.

1.6 DISSERTATION LAYOUT

Chapter 1 is an introduction and literature review about the flow induced vibration problem in centrifugal pumps. It gives the possible causes and ways applied for remedy and the scope of the problem under investigation. Chapter 2 explains the details of the experimental setup, design, instrumentations, and calculations. The experimental results regarding the effect of operating conditions, namely flow rate and speed, the V-cut at impeller blades, radial gap are given in chapter 3. Chapter 4 explains the technique and the model used in the numerical simulation. Simulation results are compared with experimental measurements. Chapter 5 concludes the study with future work recommendations.

CHAPTER 2

EXPERIMENTAL SETUP

2.1 DESCRIPTION OF TEST LOOP

A closed test loop was constructed for testing the model pump at different operating conditions. A photograph of the test loop is shown in Fig. 2.1 and the test loop is shown schematically in Fig. 2.2. A movable steel structure carries the water tank, pipelines, pump, and instrumentation. The dimensions of this structure are 4 meters long, 2 meters wide, and 4 meters height. The pump suction line is 4 inches in diameter, while the delivery line is 3 inches in diameter, all PVC; SCH80. The flow is controlled by a gate valve at delivery line; with a ball valve at suction line for the system drainage. Flexible connection was installed between the pump suction nozzle and pipeline to isolate pump vibration from the pipelines. A special pump base was designed to center the pump weight with rubber isolators carrying the pump to minimize the vibration transmitted to/from the structure.

A water tank of capacity 2.4 m^3 is used as the water reservoir and settling chamber. The tank is provided with two different perforated circular plates of 92 cm diameter each to suppress the tank waves and to smooth the flow into and out of the tank as shown in Fig. 2.3. The first perforated screen is made of PVC and has 143 holes of 10 mm diameter each. It was positioned at one third of the tank length from tank inlet and is made of two half circles to enter inside the tank easily and then assembled and

fixed. The second perforated screen is made of stainless steel circular mesh of 1 mm size. This screen is positioned at one third of the tank length from the exit (suction line). The tank inlet and exit ports had been changed to be at the middle of the tank sides and long bend elbows are used to reduce the turbulence and vortices in the suction and discharge pipes.

The model pump (Goulds pumps Inc. Model 3656) has a speed of 3450 rpm at 60 Hz. However, the measured rotational speed was found to be 3540 rpm at 60 Hz. The motor power factor is 0.92 and the maximum available power is 15 hp. Available pump power supply is a three-phase, 220 Volts. The impeller and volute of this commercial pump are replaced by the scaled model impeller and volute, as shown in Fig. 2.4.

The pump is equipped with a frequency inverter (LG, SV-iP5A) with maximum available frequency of 60 Hz to control pump peed. The inverter was programmed and modified with external knob for manual control. Also, the pump was earth grounded with the steel structure.

A tube bundle flow straightener was installed in the suction line to minimize the flow turbulence and stabilize the meters readings. The tube bundle consists of 19 tubes of 0.5 inch diameter PVC, SCH-40 and has a length of 30 cm; as shown in Fig. 2.5. The flow straightener was placed 12 times the hydraulic diameter upstream of the orifice meter.

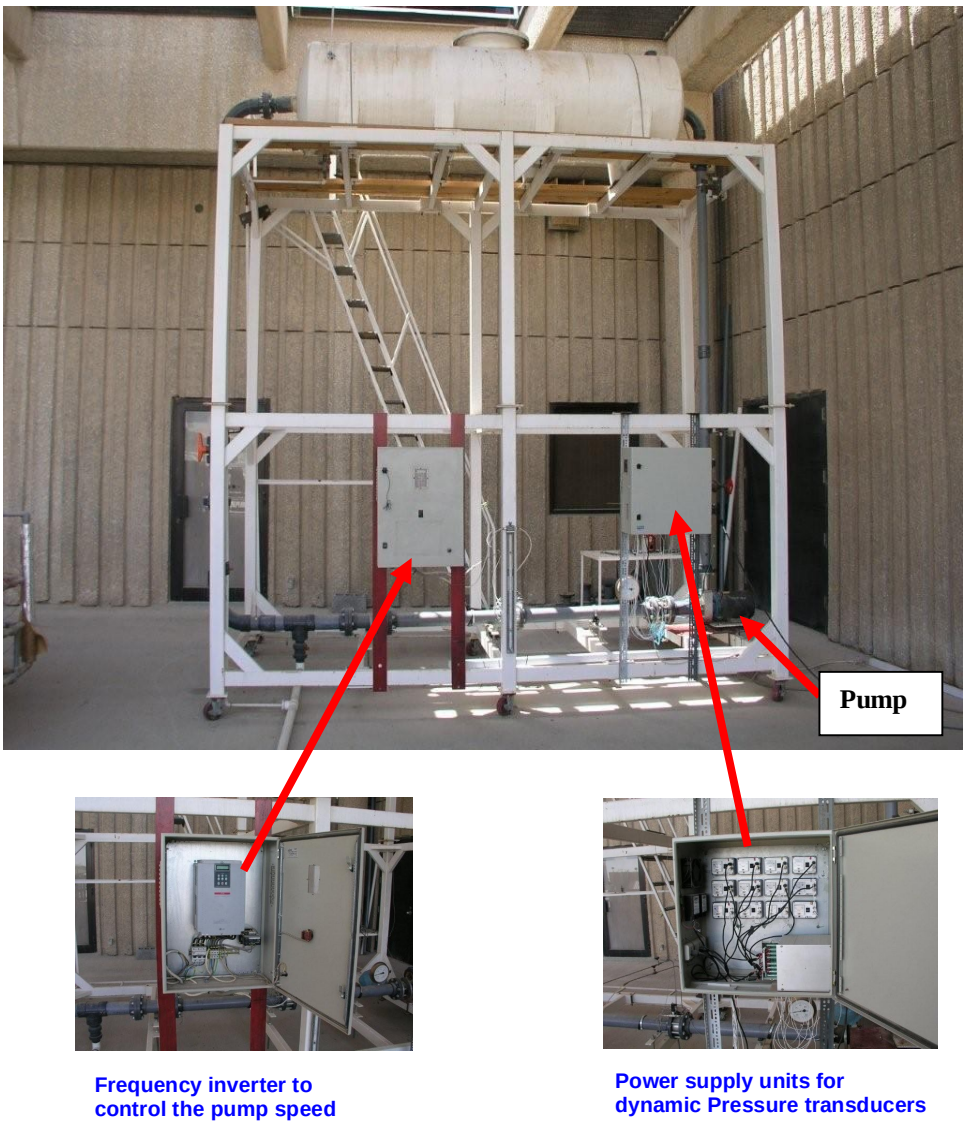

Figure 2.1 Photograph of the test loop

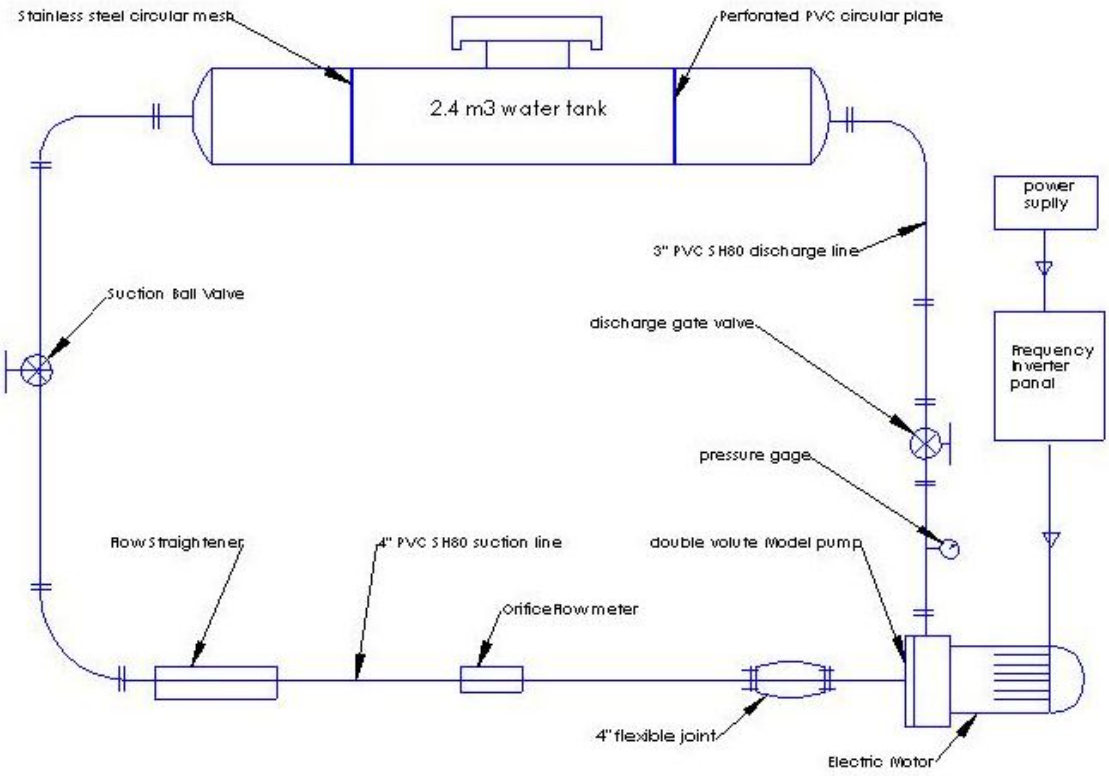

Figure 2.2 Single line diagram for the test loop

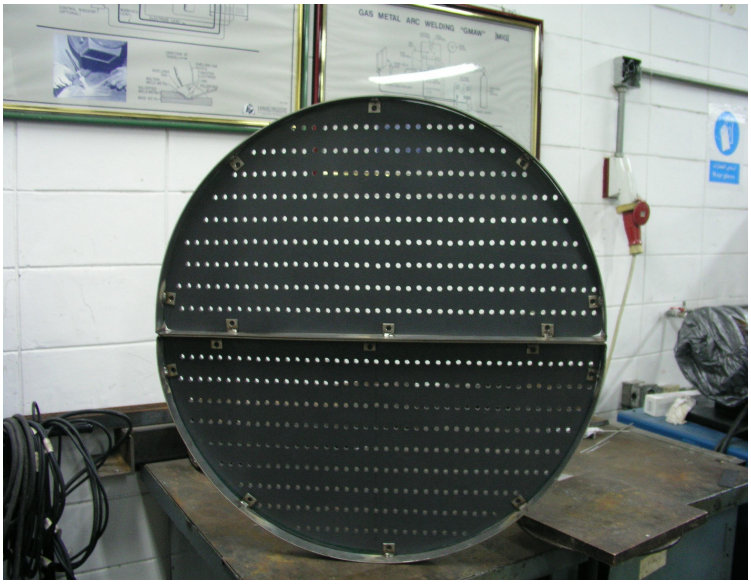

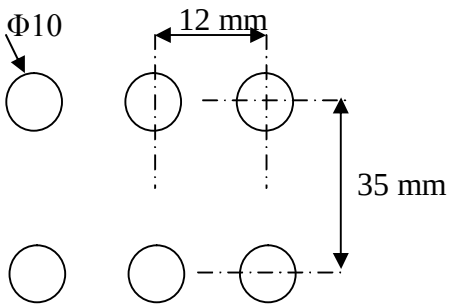

(a) PVC perforated plate

(b) Stainless steel mesh

Figure 2.3 Perforated screens installed inside the tank

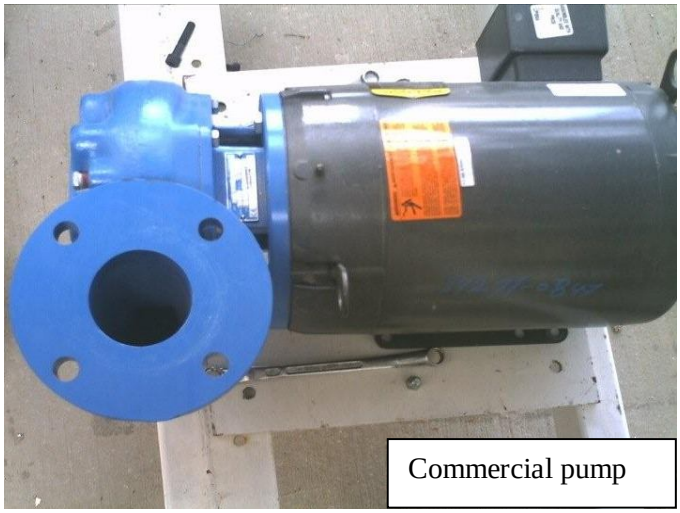

(a)

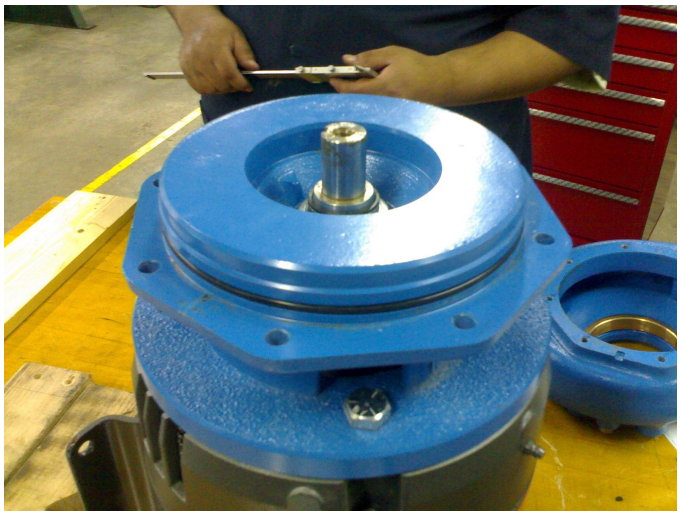

(b)

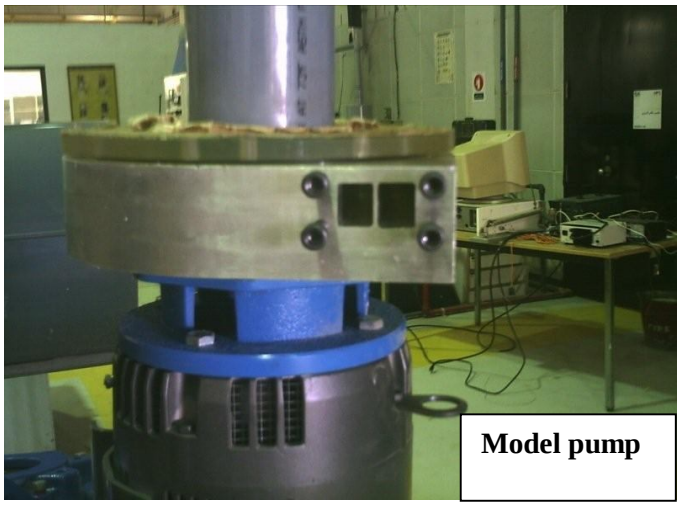

(c)

Figure 2.4 Commercial pump used to test model impeller and volute

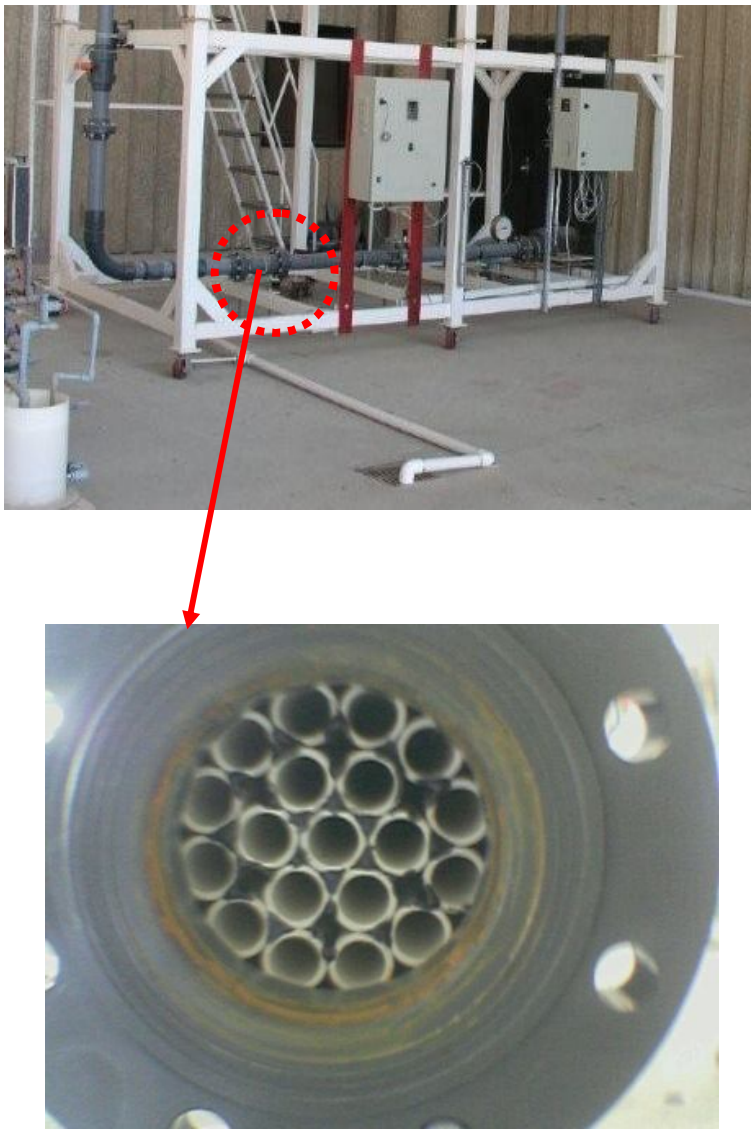

Figure 2.5 Tube bundle flow straightener

2.2 MODELING THE PUMP VOLUTE AND IMPELLER

Reverse engineering was done to produce both volute and impeller for the scaled model pump. Collected geometrical data from the original BFP are used to generate CAD files. These CAD files are then scaled to a ratio of 0.4.

2.2.1 MODELING THE VOLUTE

The geometrical dimensions of the original boiler feed pump split inner case were collected manually as shows in Fig. 2.6. The diffuser vane (splitter) profile and curvature were measured as well as the dimensions of clearances around the leading edge of the vane. The volute 3D geometrical file was designed and scaled using SolidWorks software. 3-axes CNC machine available at ME workshop was used to manufacture the volute of the scaled pump as shown in Fig. 2.7. Dimensions of the pump volute are shown in Fig. 2.8.

2.2.2 MODELING THE IMPELLER

The scaled impeller production process follows the same strategy but it was more tedious and time consuming. This is due to the fact that the blades have high 3-D twisting and curvature. Also, the blade thickness is not constant and there is a special V-shaped cut at the blade exit. A spare impeller was provided by SEC to collect the geometrical dimensions. The original size impeller was fixed on the table of a milling machine which is capable of moving in X, Y and Z directions and has a 3-D coordinate monitor; see Fig. 2.9. The origin was selected to coincide with the impeller center with a reference point on the fixed impeller blade lower leading edge.

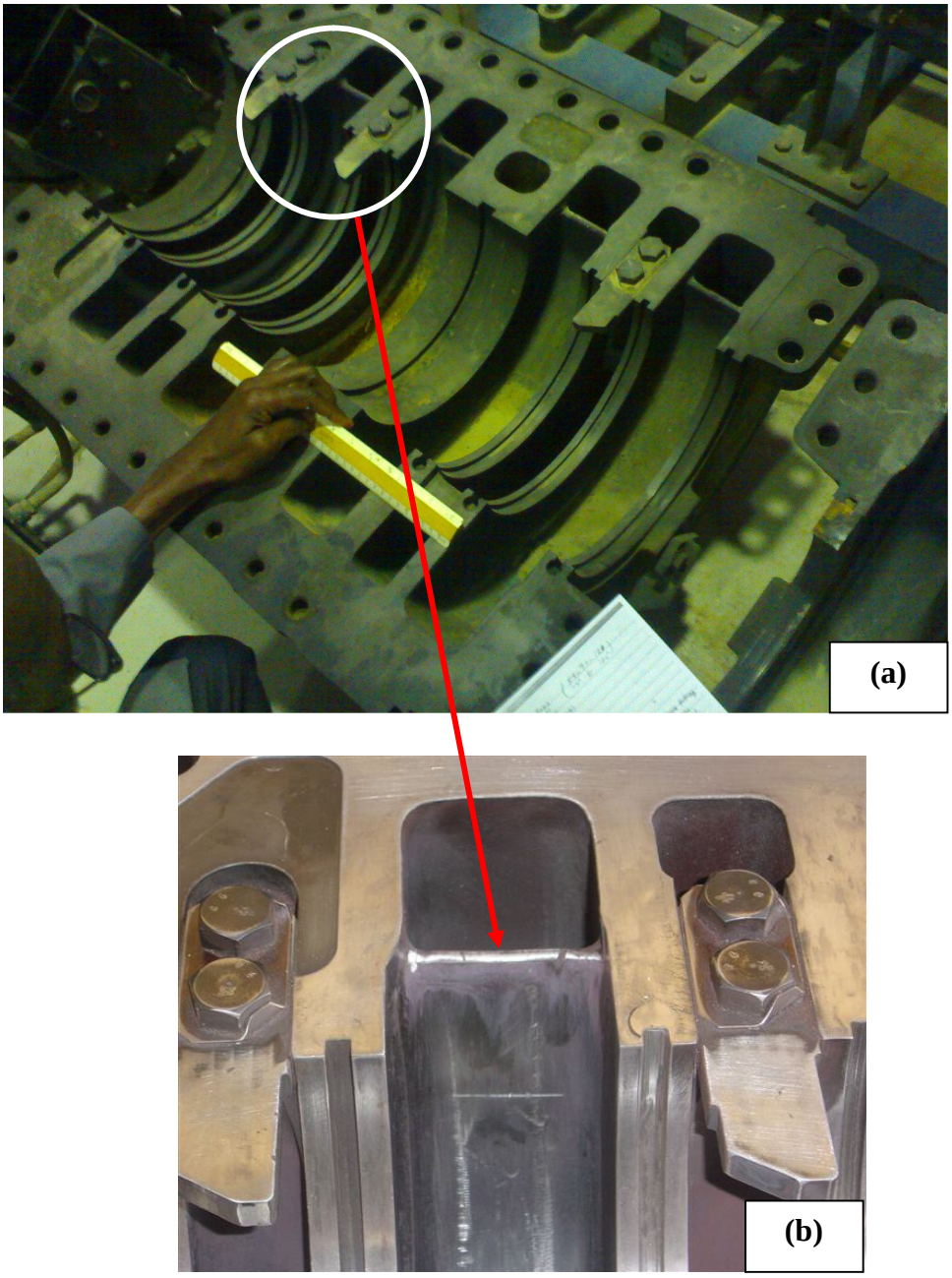

Figure 2.6 Collection of geometrical data for original PFB inner split casing

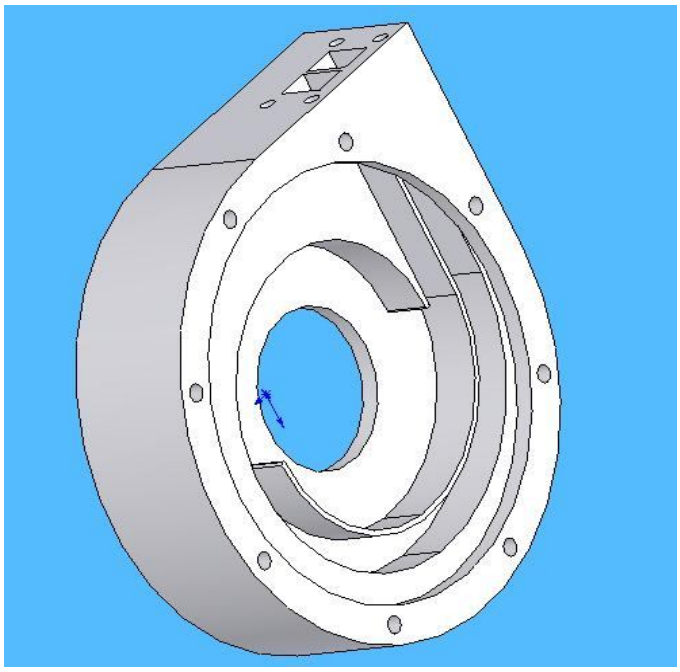

(a) Single stage double volute design for model pump: Solidworks software

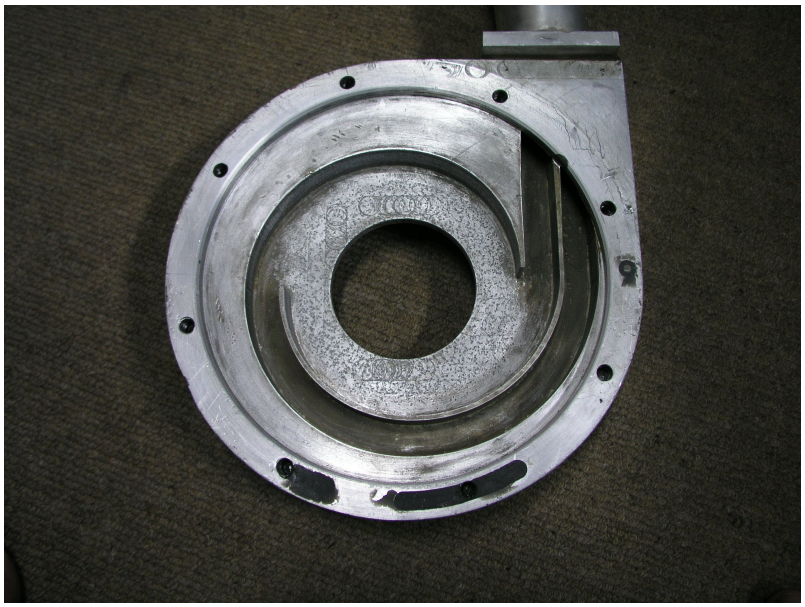

(b) Single stage volute manufactured by CNC machine

Figure 2.7 Modeling pump volute

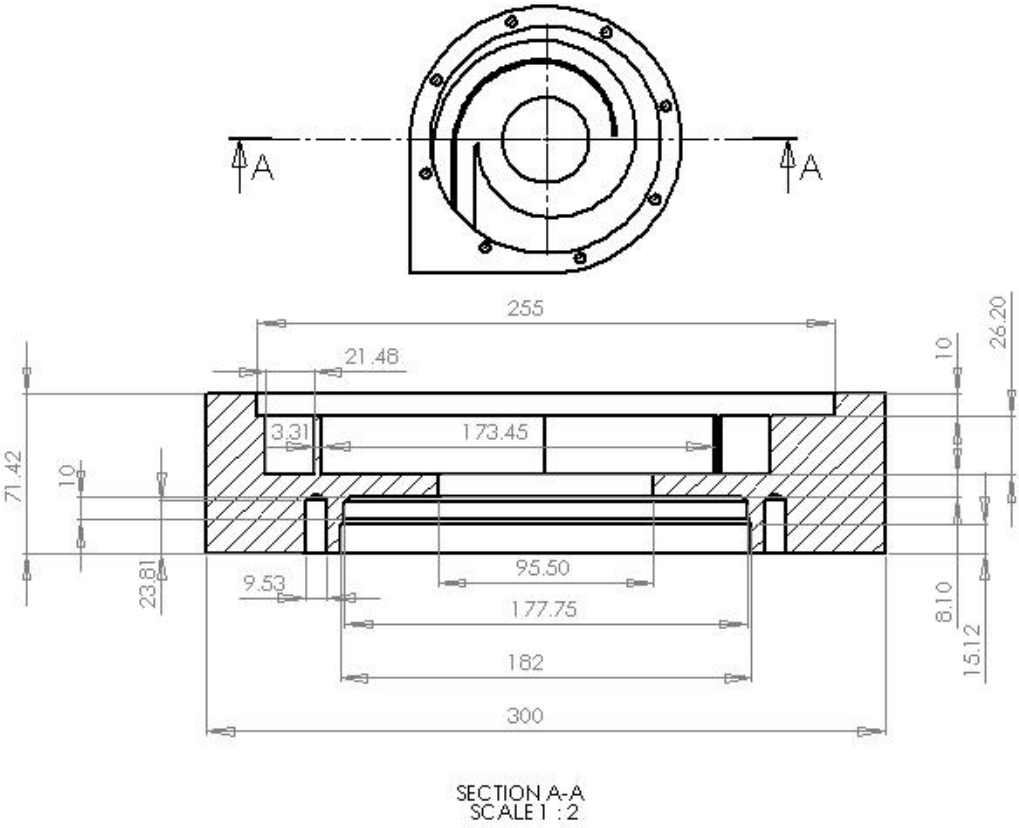

(a) cross sectional view

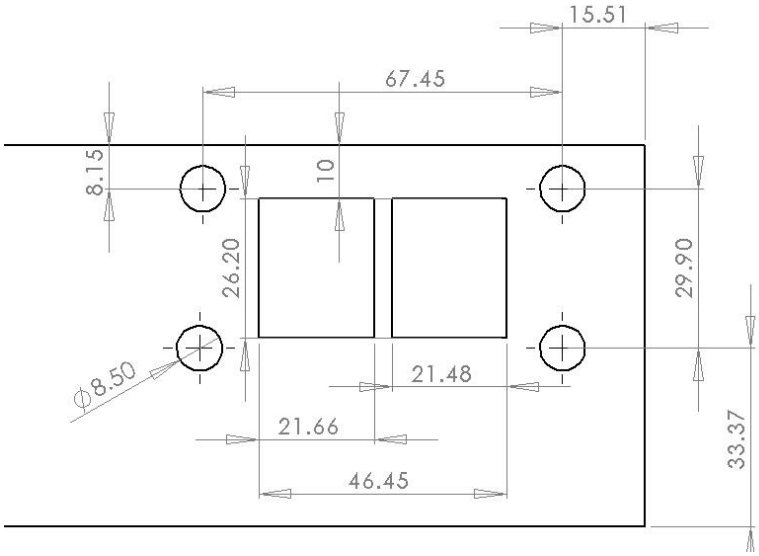

(b) Volute discharge

Figure 2.8 Volute dimensions: Model pump

To reach different parts of the impeller; upper shroud, lower shroud, vane upper front, vane lower front, vane upper back, vane lower back, and V-notch shape, a set of six probes were used for flexible measurements. The procedure of collecting the impeller dimensions is shown in Fig. 2.10. The CAD files for the impeller were generated using Gambit software from the collected data. Figure 2.11 shows the process of developing the impeller geometry files. Using Gambit software at this stage provides also the geometry files needed for numerical simulations by FLUENT.

A 5- axes CNC machine is used to produce the impeller from the CAD files. The impeller was manufactured in two separate parts. The hub with the blades represents the first part while the upper shroud is the second part. They are welded together then cleaned and finally the impeller was dynamically balanced on a two-planes balancing machine. The volute is made of aluminum alloy while the impeller material is brass.

The reverse engineering process included also a shaft like extension attached to impeller to simulate the actual flow characteristics at boiler feed pump suction.

In order to test the effect of the special V-shaped cut at the impeller blade exit, two identical impellers were produced. The first impeller has no V-cuts at blades exit and the second one has the V-cuts. A special V-shaped tool, with the scaled dimensions, was designed to cut the impeller blade trailing edge on the lathe machine. The two model impellers are shown in Fig. 2.12. Dimensions of the impeller and the shaft extension are shown in Fig. 2.13. The assembly of the impeller, the volute, and the driver are shown in Fig. 2.14.

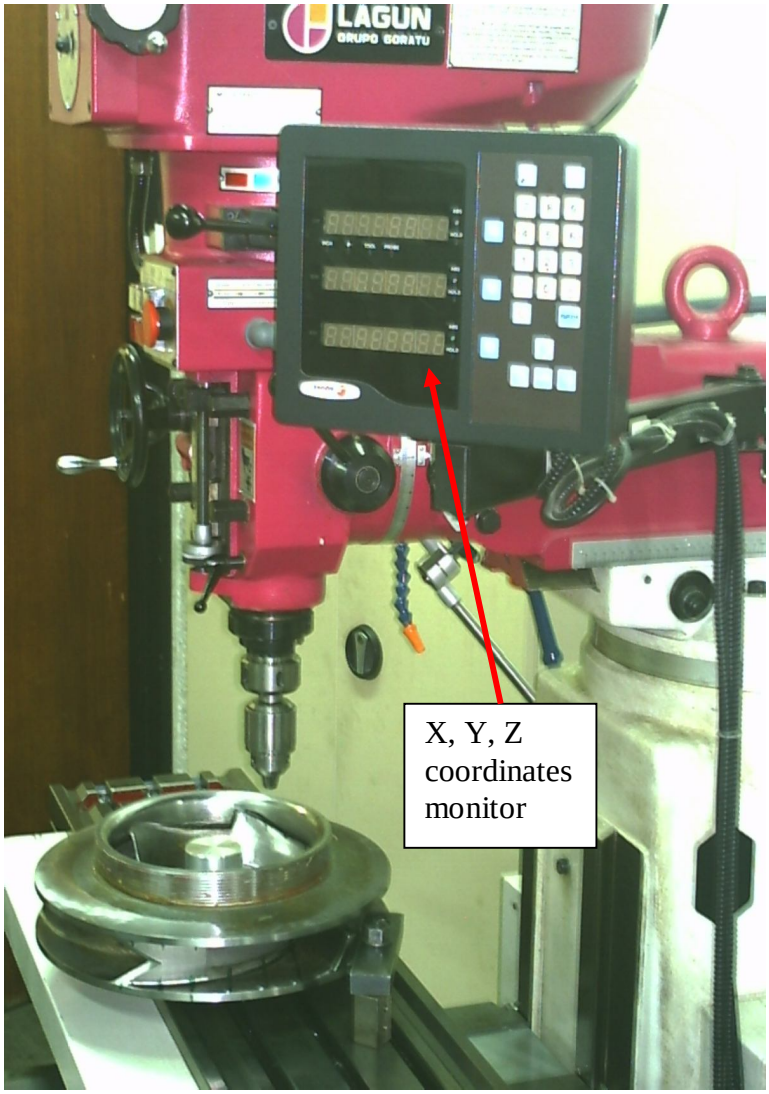

Figure 2.9 Geometrical data collection of BFP impeller using milling machine

(a)

(b)

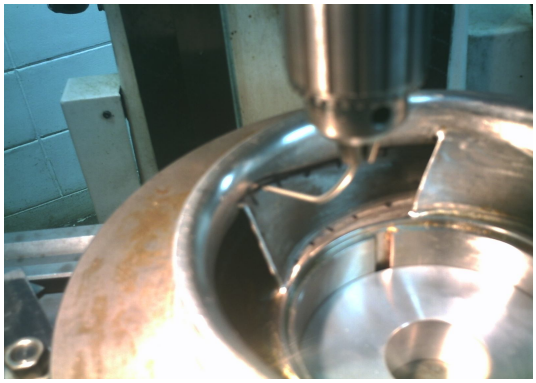

(c)

(d)

Figure 2.10 Procedure of geometrical data collection of BFP impeller

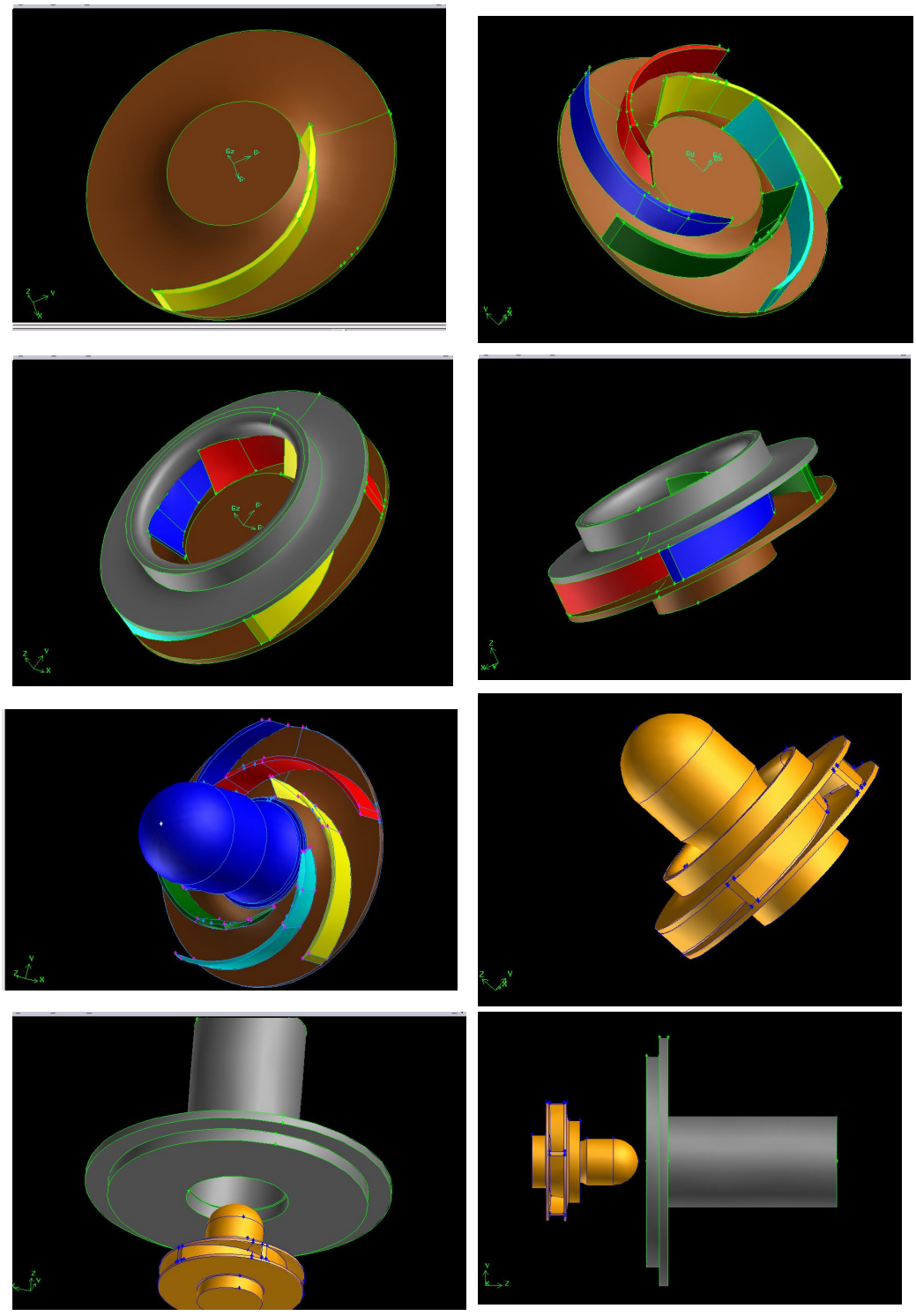

Figure 2.11 Generation of impeller geometry using Gambit/Fluent Software

(a) Without the V-cut at blade exit

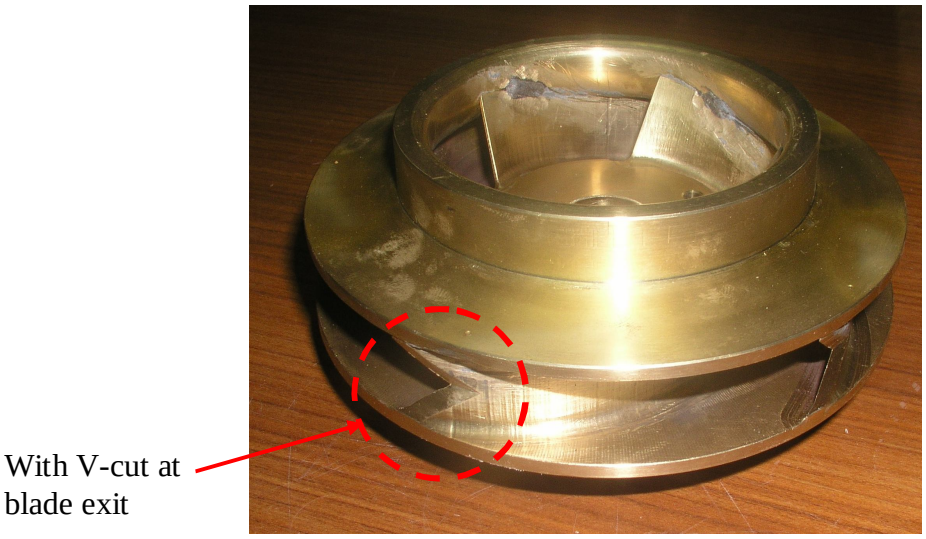

(b) With the V-cut at blade exit

Figure 2.12 Model impellers: without and with the V-cut at blades exit

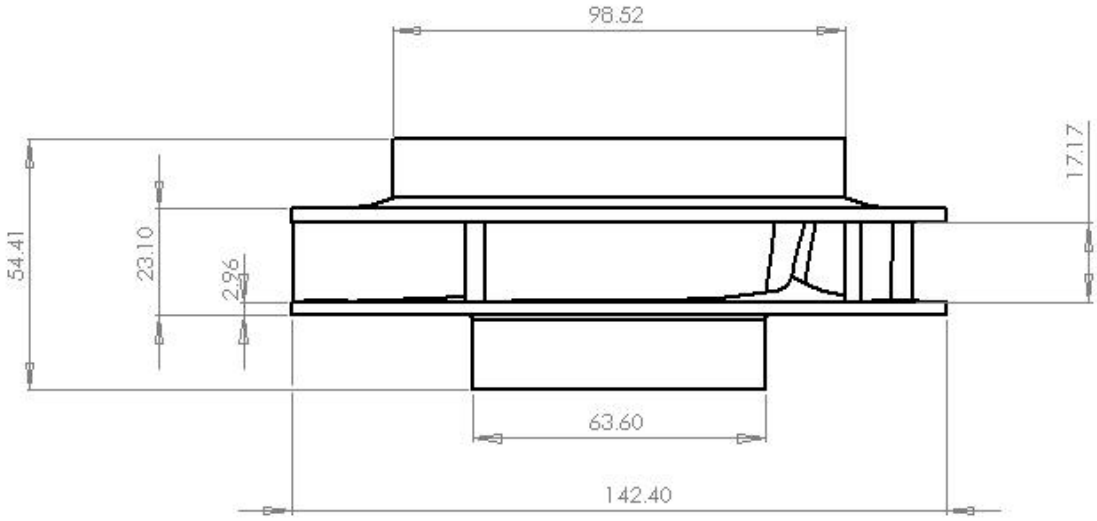

(a)

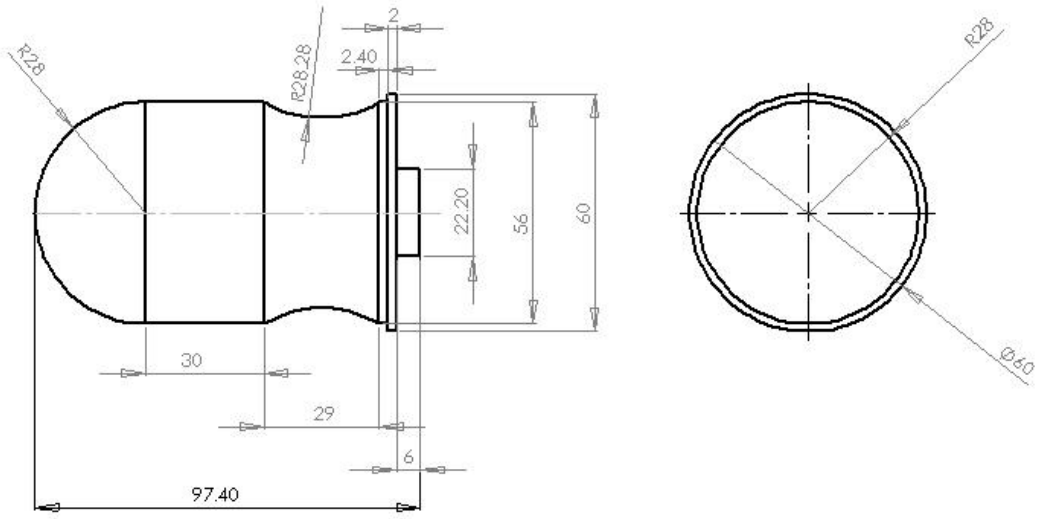

(b)

Figure 2.13 Dimensions of the impeller and the shaft extension

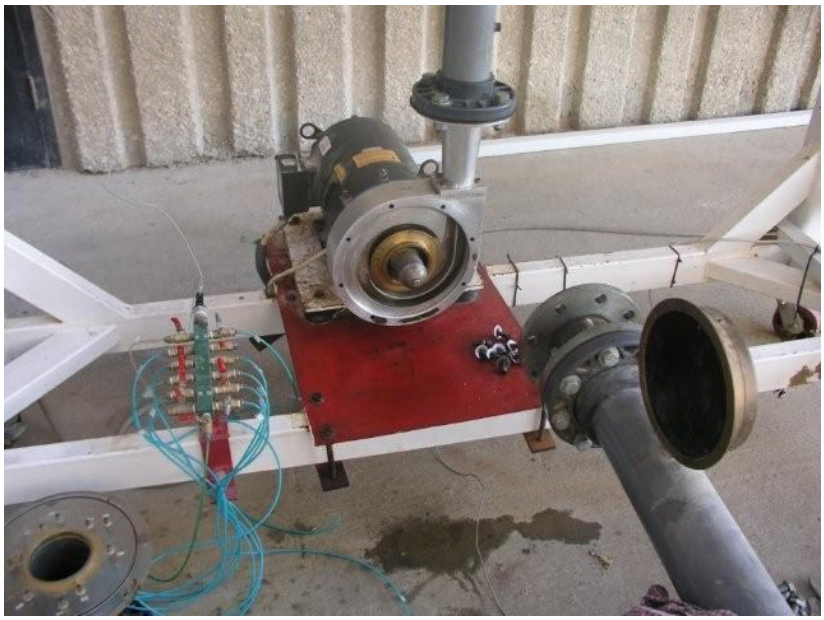

(a)

(b)

Figure 2.14 Impeller and volute assembly

2.3 IMPELLERS BALANCING

A soft-bearing two-plane balancing machine for production and laboratory balancing of rotors up to 10 kg, type 3905 (Bruel & Kjaer); was used to balance the impeller. The balancing speed for the machine was 1800 rpm. The impeller is carried on adjustable vee-bearings and direct-driven via a Cardan shaft from a bidirectional two-speed asynchronous motor. Unbalance vibrations are measured by inertial sensors contained within the bearing supports. An angle reference generator is fitted to the drive shaft to transmit rotor position to the console. The console (2504) accepts two-plane vibration signals and shaft angle data and process them to display digitally the unbalance magnitude and position referred to two user-chosen correction planes. Rotor speed and rotor position are also displayed. The console provides electronic unbalance compensators for calibration using unbalanced rotor.

A 50 cm steel shaft was designed and manufactured at ME-KFUPM workshop to fit both the balancing machine and the impeller dimensions.

The shaft has a middle step diameter of 22.2 mm with a keyway to fix the impeller and another keyway at the shaft end (19 mm dia.) to secure the shaft in its designed position on the machine. Two glands with two small screws are used to prevent the axial impeller movement and secure it in place.

After the final balancing, it was found that there is a balancing tolerance of 0.5 gram which is within the permissible residual unbalance for the rotor using the ISO 1940/1 chart. Figure 2.15 shows the steps for balancing process.

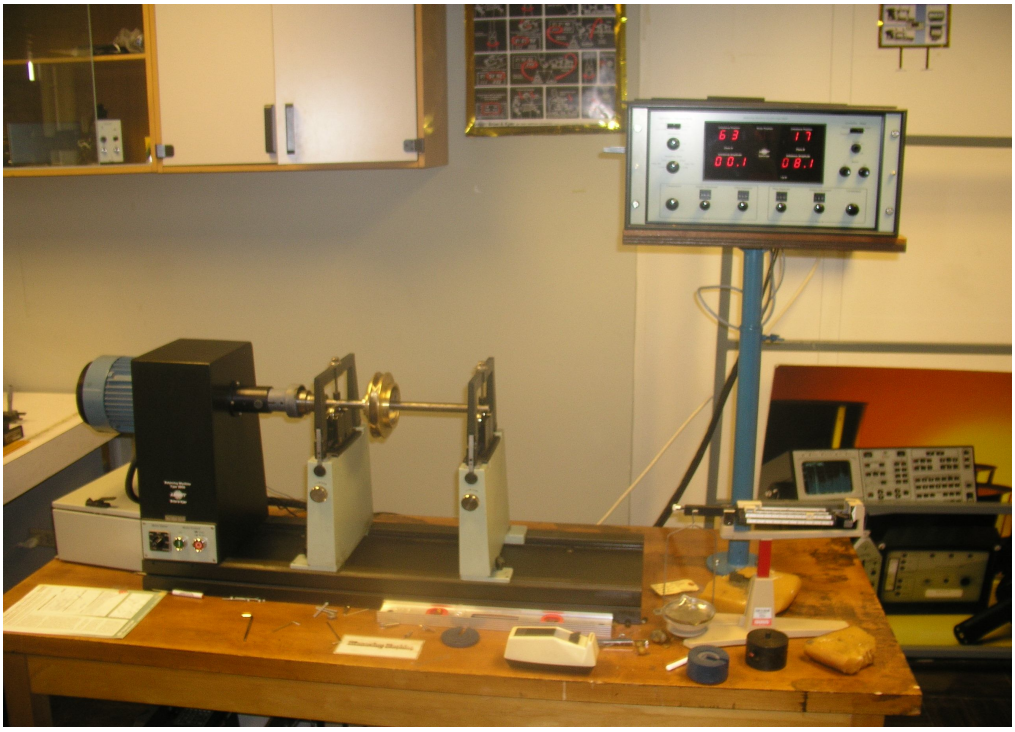

(a) two-planes dynamic balancing machine

(b) removing unbalance mass

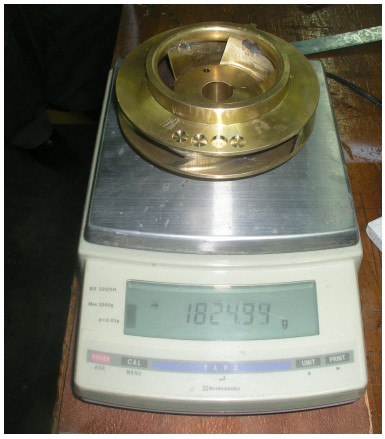

(c) checking the impeller weight

Figure 2.15 Impeller dynamic balancing process

2.4 EXPERIMENTAL MEASUREMENTS

4.2.1 MEASUREMENT OF FLOW RATE

The flow rate is measured using a standard (ASME) stainless steel 4 inches orifice meter (1 inch taps) with a discharge coefficient, C_d, of 0.618. The flow rate is controlled by a gate valve in the discharge pipe. The orifice is designed to match the pipe centerline accurately (± 0.05 mm) by flanges and is sealed using O-rings. Figure 2.16 shows the orifice meter, its dimensions, and the installation in the pipeline.

The orifice is equipped with a DRUCK, PDCR 4170, 700 mbar differential pressure transducer to measure the pressure drop across the orifice directly within ±0.08% FS accuracy with millivolt output ratiometric to supply voltage.

Orifice flow rate, Q, is calculated as

$$Q = C_d \frac{A_2}{\sqrt{1-\left(A_2 / A_1\right)^2}} \sqrt{\frac{2\Delta p}{\rho}} \tag{2.1}$$

where ΔP is the pressure drop across the orifice, ρ is the fluid density, A_1 is the cross sectional area of the pipe, A_2 is the cross sectional area of the orifice plate.

(a)

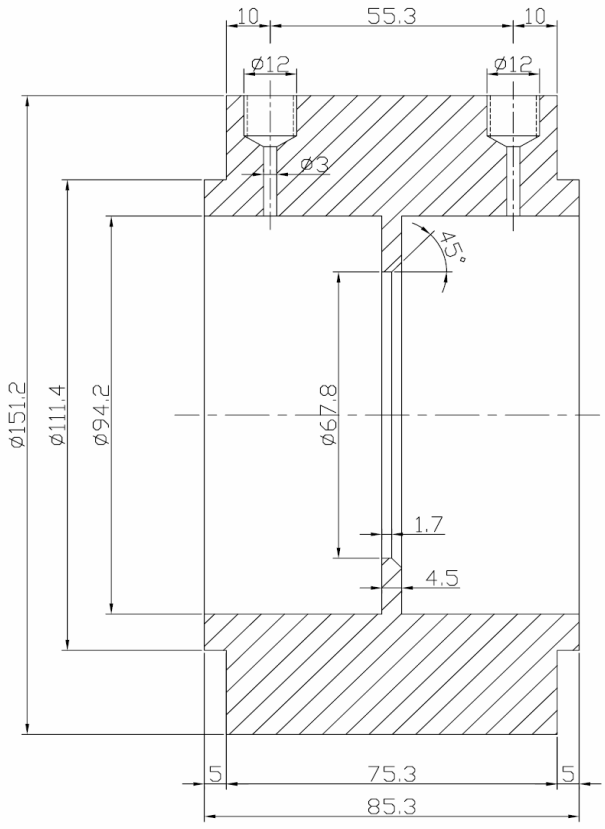

(b)

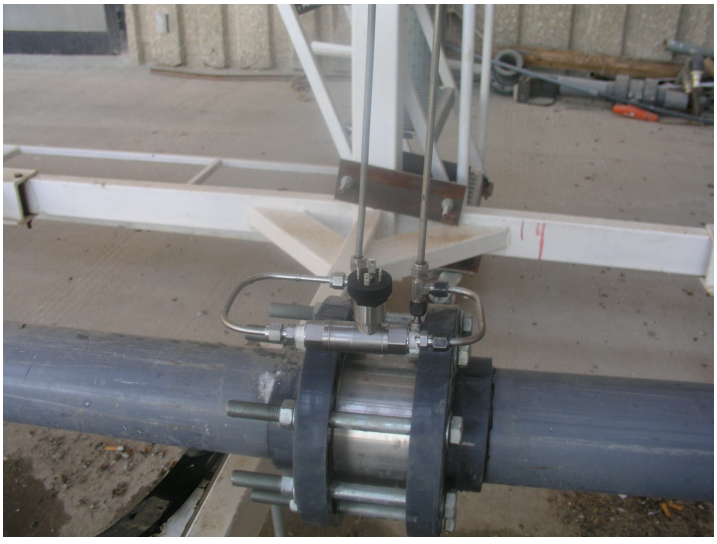

(c)

Figure 2.16 Orifice meter: installation and dimensions

2.4.2 MEASUREMENT OF PUMP TOTAL HEAD

The time-averaged static pressures are measured in the suction and delivery pipes. One pressure transducers is installed at pump discharge pipe at elevation of 50 cm above pump horizontal centerline and another one in suction pipe 4 cm ahead of the impeller eye. The velocities in the suction and delivery pipes are calculated using the measured flow rate. The energy equation is applied to the pump to obtain the pump total head.

Pump Head:

$$H = \frac{p_d - p_s}{\gamma} + \frac{V_d^{\,2} - V_s^{\,2}}{2g} + \Delta z \qquad (2.2)$$

The pressures p_d & p_s represent the delivery and suction pressures respectively; V_d & V_s represent the flow velocities in delivery and suction pipes respectively; Δz is the elevation difference between the two measuring points of p_d & p_s; and γ is the fluid specific gravity.

A balance check was performed for the flow rate measurement. The orifice taps connected to the differential pressure transducer are also connected to a u-tube manometer via three-ways tee-connection. Another balance check for the pump head was made; two pressure gages are installed in the pump suction and discharge lines near the locations of pressure transducer taps.

2.4.3 MEASUREMENT OF PRESSURE FLUCTUATIONS

To measure the effect of operating and design variables on pressure fluctuations inside the pump, sensors locations are selected carefully based on literature of the critical areas inside the pump and around the impeller circumference. Also the sensors are arranged in a geometrical symmetry positions around the impeller as shown in Fig. 2.17. Table (1) gives the coordinates of these locations. Nine pressure transducers are placed flush within the volute plexiglass cover plate at the impeller discharge and near splitters lips, at different angular and radial positions. To measure the pressure fluctuations in the suction and delivery pipes; one dynamic pressure transducers was installed at pump discharge pipe at elevation of 50 cm above pump horizontal centerline. Another one was installed in suction pipe only 4 cm ahead of the impeller eye to be more sensitive to the fluctuation in pressure under different conditions. OMEGA DPX101-250 high-response dynamic pressure transducers were used to measure the dynamic pressure pulsations inside the pump at the mentioned locations. The dynamic pressure sensors have excitation of 2 mA nominal @ 18 to 30 Vdc, constant current, rated Output of 5 V nominal FS, resonant Frequency of 500 kHz, high frequency range of 170 kHz (approx 1 /3 of resonant frequency) with discharge time constant of 2 sec. It can measure dynamic pressure events with rise times as fast as 1 μsec utilizing pure synthetic quartz crystals under high compressive preload. In the present study, the important expected frequencies of pressure fluctuation are in the range of 1000 Hz only. Figures 2.18 and 2.19 show the dynamic pressure transducer dimensions and flush installation in volute plexiglass cover plate. Pressure fluctuations are measured and presented in units of psi throughout the dissertation.

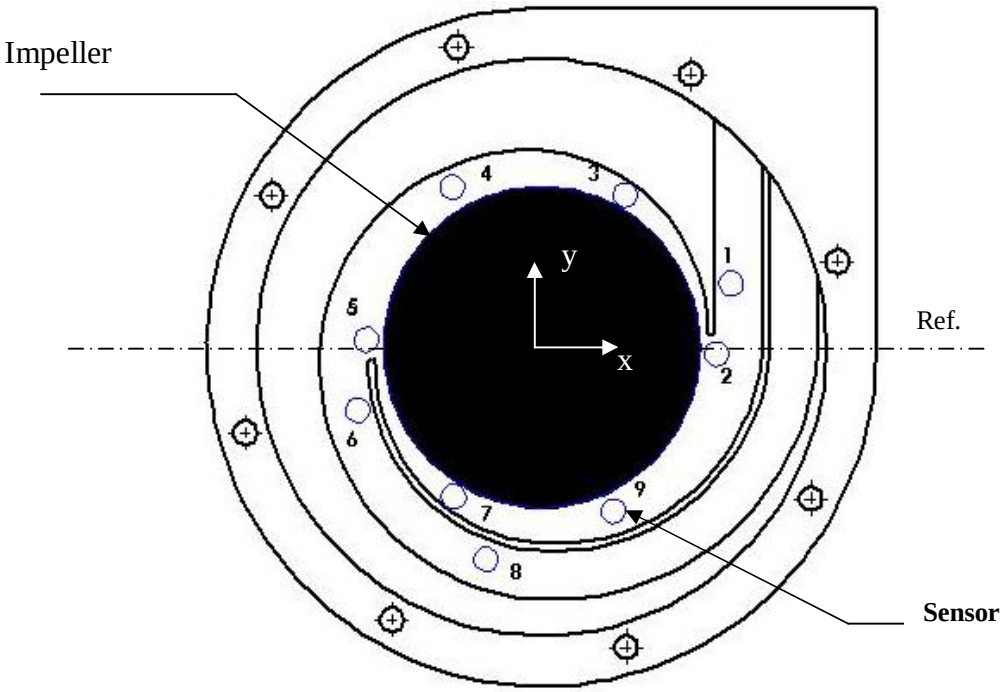

Figure 2.17 Locations of measuring sensors inside the pump

Table 2.1 Coordinates of measuring locations

Location of holes relative to volute horizontal centerline (Ref.)				
sensor #	**radius (mm)**	**angle (deg.)**	**X (mm)**	**Y (mm)**
1	90	19	85.10	29.3
2	78	358	77.95	-2.73
3	77	61	37.33	67.34
4	81	120	-40.49	70.15
5	79	178	-78.95	2.76
6	88	199	-83.20	-28.64
7	77	239	-39.66	-65.99
8	97	255	-25.11	-93.69
9	80	294	32.52	-73.08
10	Suction pipe			
11	discharge pipe			

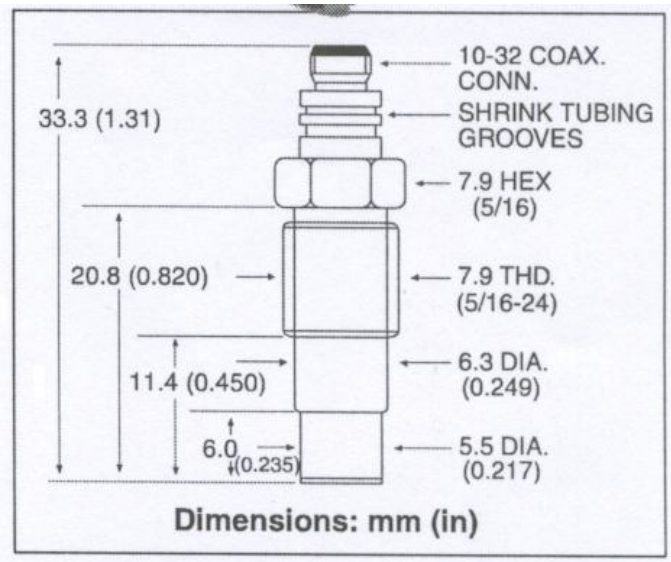

(a) Dimensions of the dynamic pressure transducer

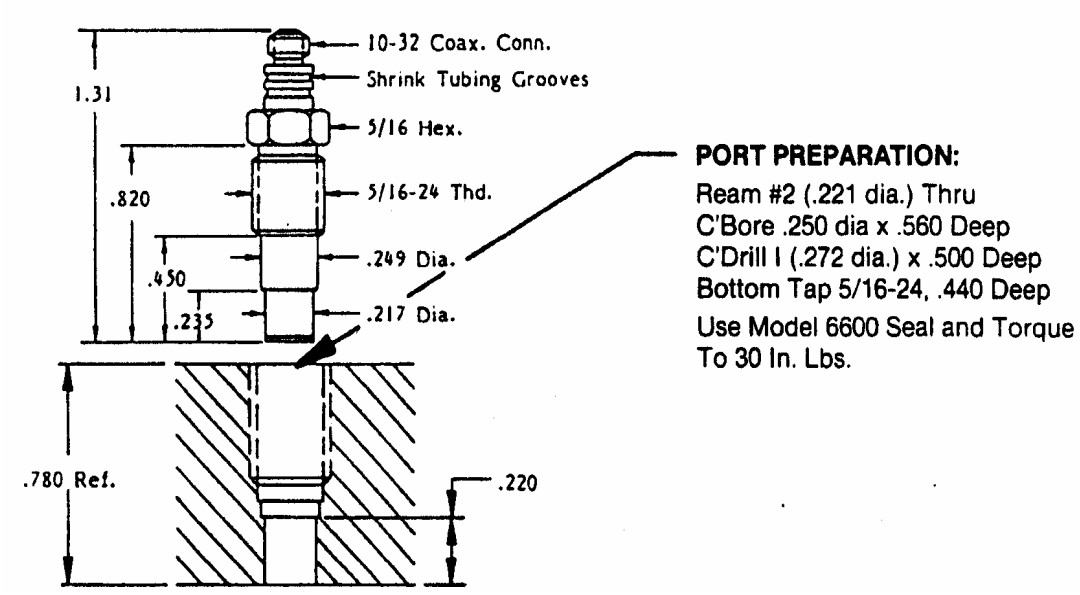

(b) Flush installation of the dynamic pressure transducer

Figure 2.18 Dimensions of the dynamic pressure transducer and flush installation (Omega manual)

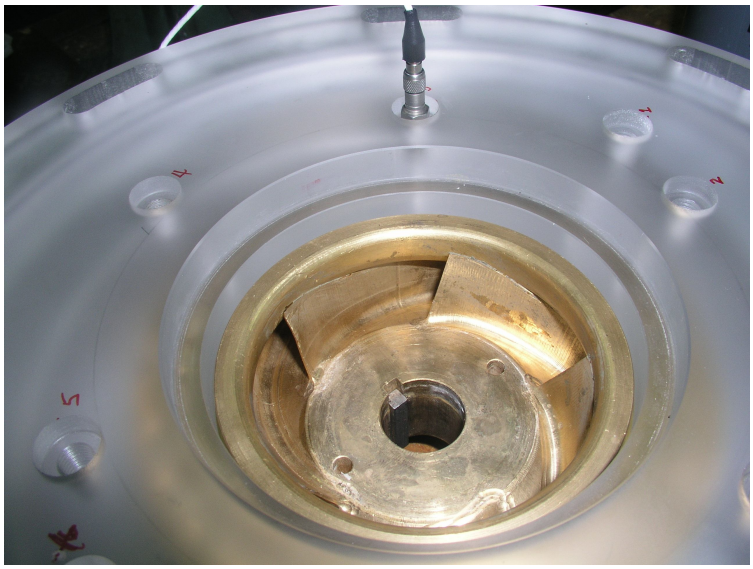

(a) Plexiglass cover with holes for pressure measurements

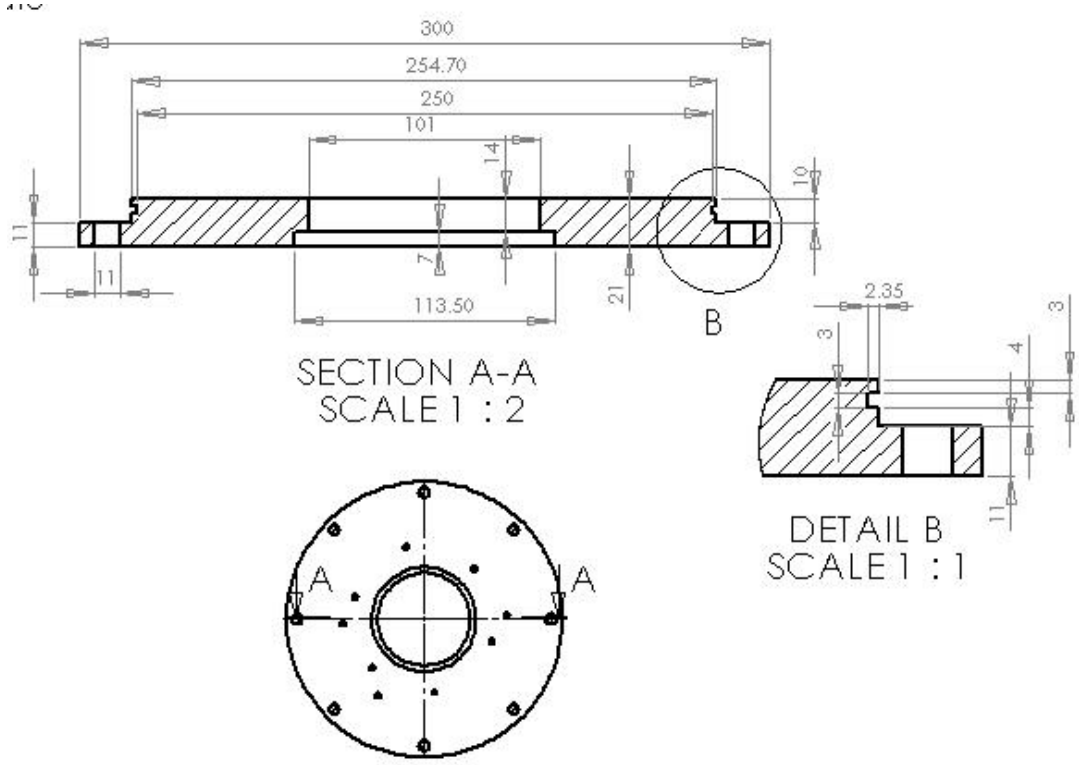

(b) Dimensions of plexiglass cover plate

Figure 2.19 Plexiglass cover plate installation and dimensions

In order to measure the time-average static pressure, at the same locations as dynamic pressure signals, a pressure manifold with 12 outlets was designed with special fittings and connected to a static pressure transducer (RS, 0-6 bar, output 0-100 mV, ± 0.25 mV accuracy). Thus the same plexiglass cover plate is used for dynamic and static pressure measurements inside the pump. The time-average static pressures are measured and presented in Pascals (Pa) throughout the dissertation.

The static pressure transducer and the orifice differential pressure transducer are powered by 10 VDC using a MCH-305A（30V /5A）power supply. With the help FLUKE 189 true RMS multimeter, the accuracy of this power supply can be improved manually to 1 mV as shown in Fig. 2.20. Figure 2.21 shows a sketch for the static pressure manifold and its connection to the test pump and Fig. 2.22 shows the dimensions of the manifold and the pressure fittings.

The dynamic pressure transducers are powered by OMEGA's model ACC-PS1. It is a battery-powered, single-channel, high-performance power supply. It operates from two standard 9 volt batteries and includes a built in battery test meter. ACC-CB2- 10 foot, 10-32/BNCM, coaxial cables are used to connect the sensor and the power supply. Figure 2.23 shows the power supply box for the dynamic sensors.

All sensors output are connected to NI-DAQ drivers, NI PCI-MIO-16E -1 DAQ board 16Ch,1.25MS/s,12-Bit, Multifunction I/O with SCXI-1520/1530 Analog Input Module and SCXI-1314 Terminal Block. The complete instrumentation wiring diagram is shown in Fig. 2.24. Figure 2.25 shows the model pump assembly for the measurements of dynamic pressure fluctuation and measurements of static pressure distribution.

Figure 2.20 Power supply used for static and differential pressure transducers

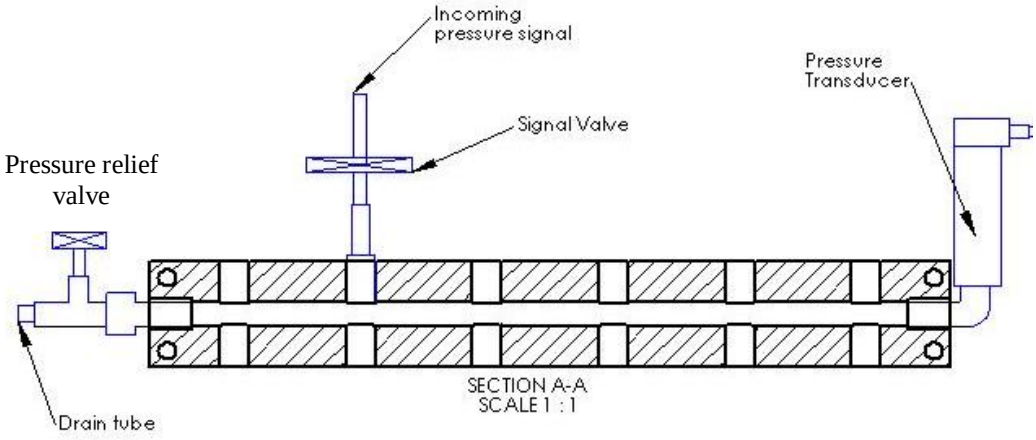

(a)

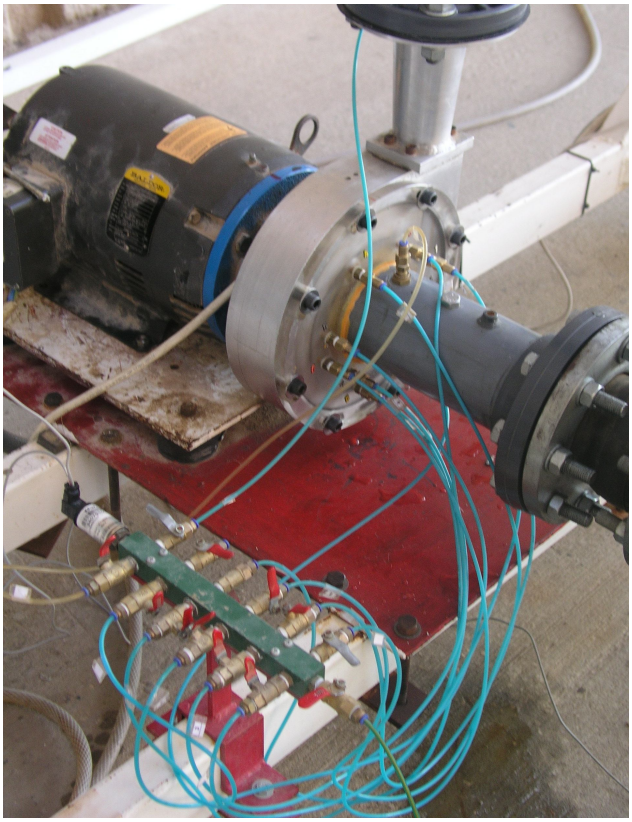

(b)

Figure 2.21 Static pressure manifold

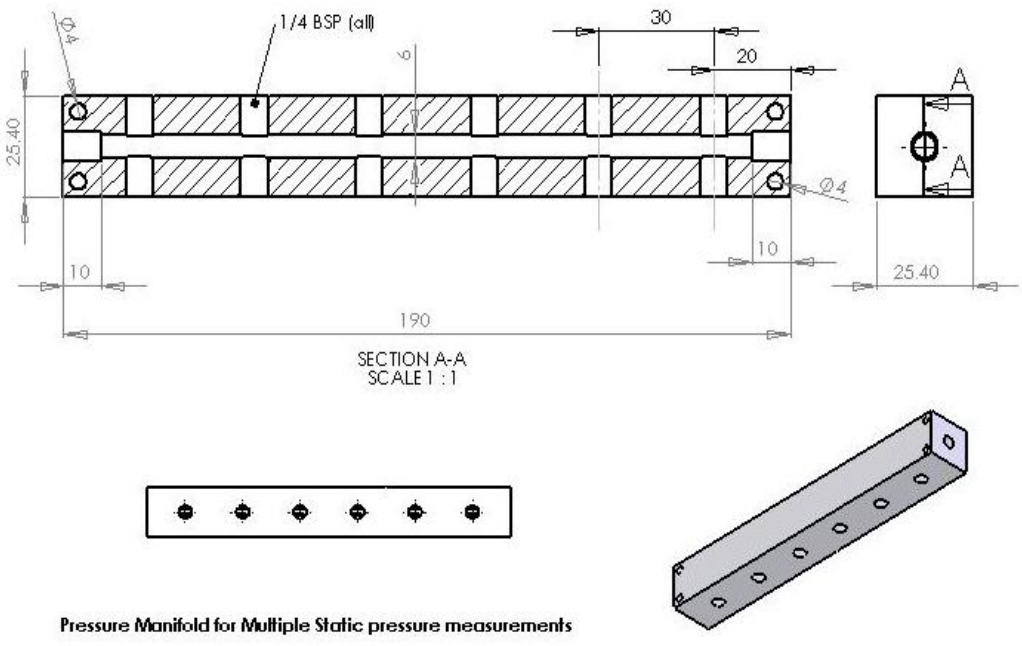

(a) Dimensions of the static pressure manifold

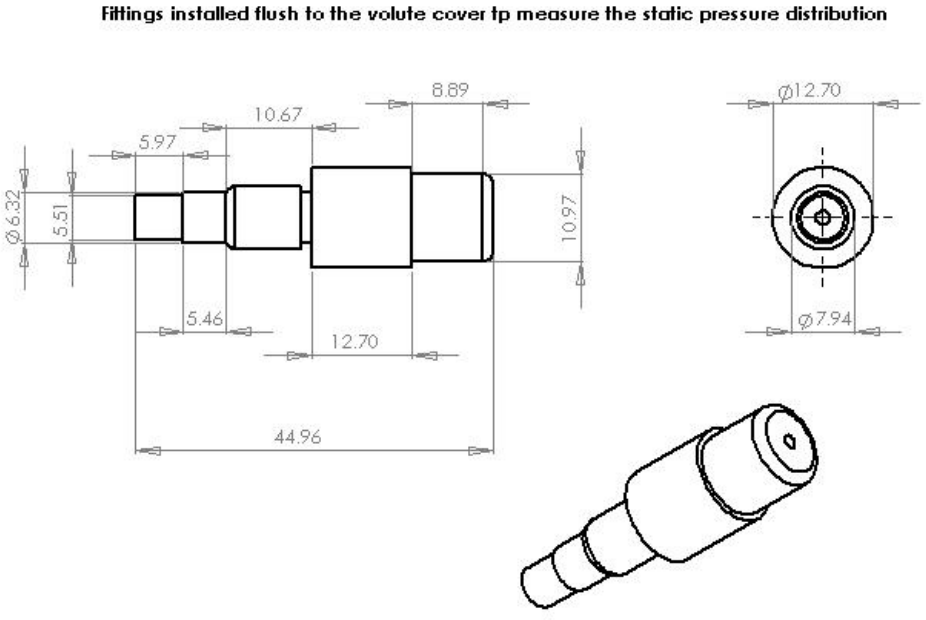

(b) Dimensions of the static pressure fittings

Figure 2.22 Dimensions of the static pressure manifold and its fittings

(a) DAS and power supply box

(b) Power supply connections

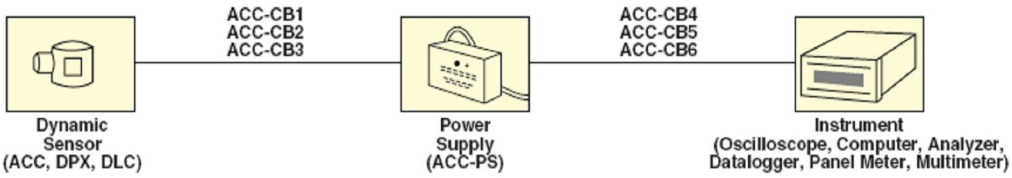

(c) Typical block diagram (Omega manual)

Figure 2.23 Power supply box for dynamic pressure transducers, DAS and a typical block diagram

2.4.4 MEASUREMENT OF BRAKE POWER

The pump brake power is calculated using the power supply Voltage and Ampere. The frequency inverter reads out the current (accuracy of 0.1 Amp) as well as the frequency. The voltage is measured using FLUKE 189 true RMS multimeter with accuracy of 0.0025 V. Knowing the efficiency of the electric motor and its power factor and; the pump shaft power is calculated.

The pump efficiency is calculated as follows

$$\eta = \frac{\gamma QH}{\sqrt{3} * V * I * PF * \eta_{motor}} \tag{2.3}$$

where

V the voltage (volts)

I the pump current (amp)

PF the motor power factor

η_{motor} the motor efficiency

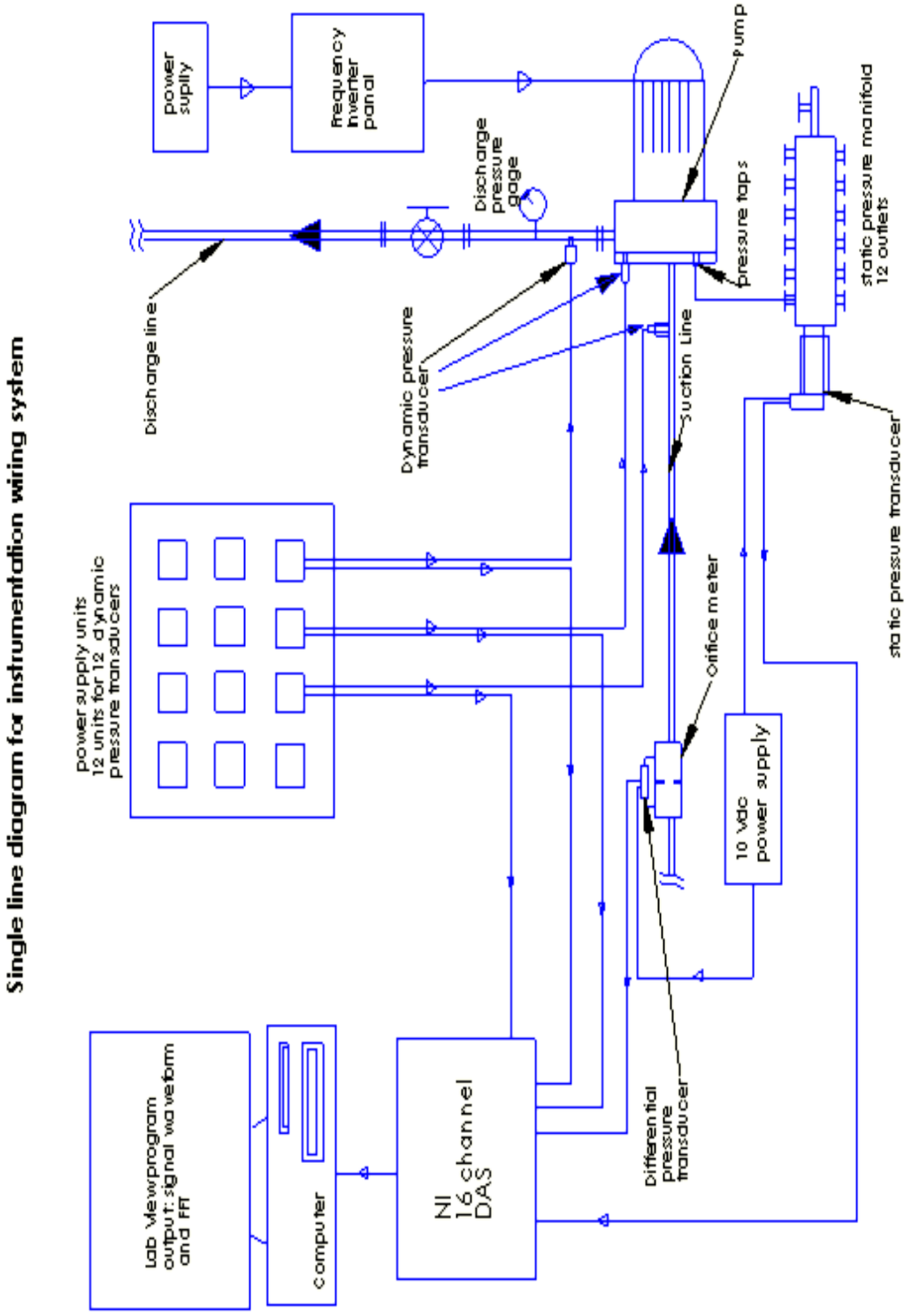

Figure 2.24 Instrumentation wiring diagram

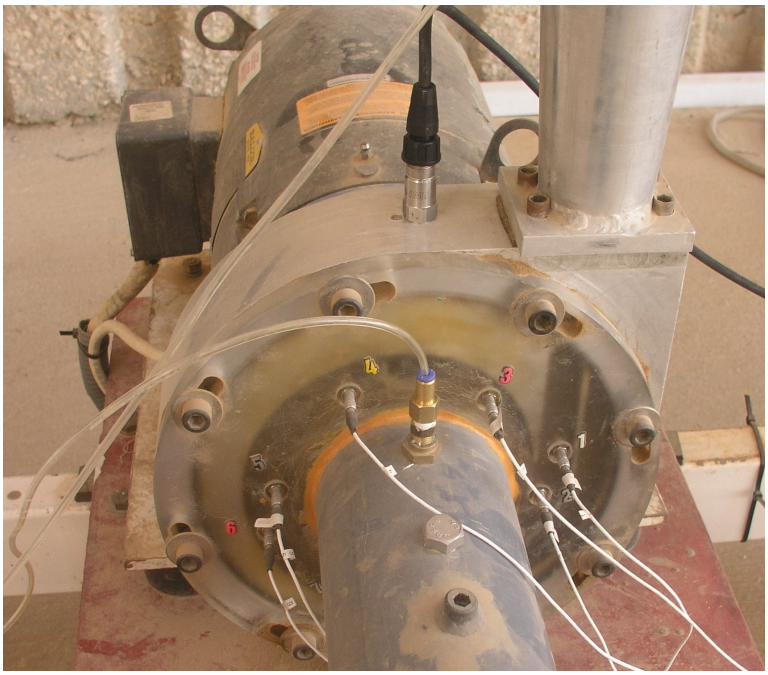

(a) Dynamic pressure transducers connected to measuring locations

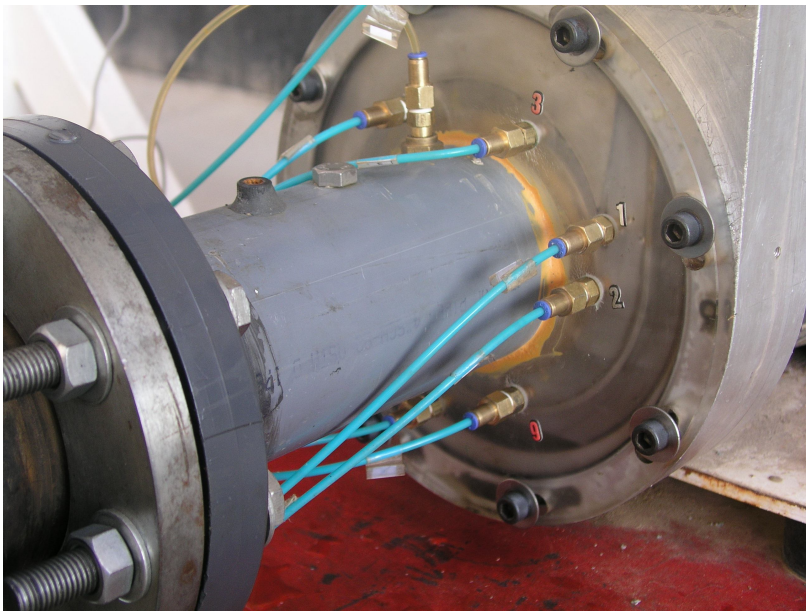

(b) Static pressure fittings connected the plexiglass cover plate of pump volute

Figure 2.25 Model pump assembly: measurements of dynamic pressure fluctuation and static pressure distribution

2.4.5 MEASUREMENT OF CASE VIBRATION

B&K 4507 Delta Tron miniaturized accelerometer, with 100mV/g sensitivity, were used for vertical and horizontal vibration measurements on the model pump case as shown in Fig. 2.26. A combination of high sensitivity, low mass and small physical dimensions make them ideal for modal measurements. Miniature DeltaTron® Accelerometers Type 4507 consists of a ThetaShear® accelerometer and a DeltaTron preamplifier in light weight titanium housing with integrated 10 - 32 UNF connectors. Frequency range is 0.3 Hz to 6 kHz and sensitivity of 100 mV/g.

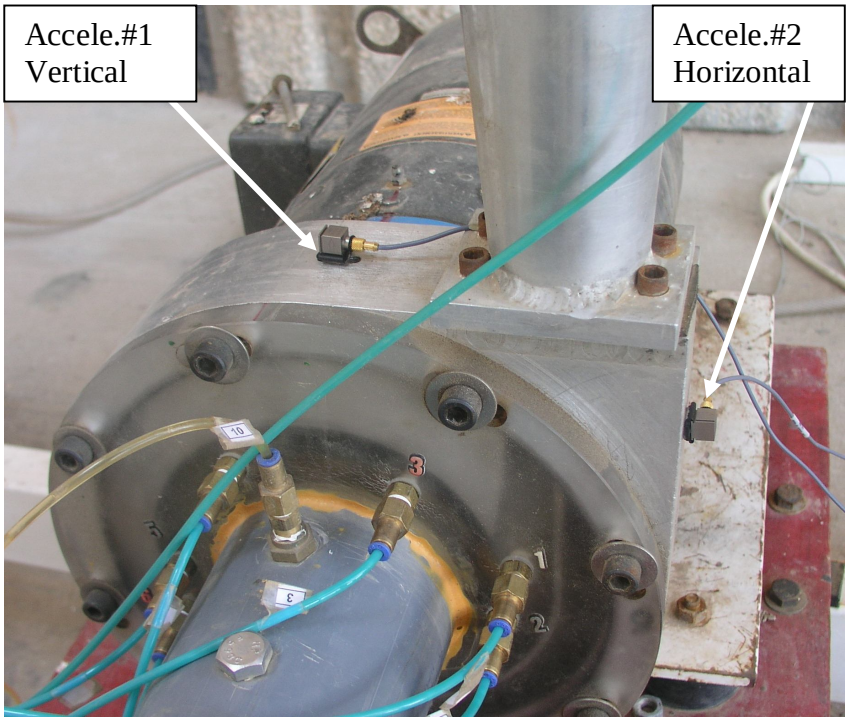

Figure 2.26 Vibration measurements of pump casing

2.5 SIMILITUDE ANALYSIS

A Scale factor of 0.4 (D_m/D_p) between the model and prototype pumps was selected based on market availability and experiment practicality. With the scaling factor of 0.4 and model pump speed of 3540 rpm at 60 Hz; the similarity laws can be applied considering full dynamic similarity between the two pumps to predict the model pump head and capacity at its rated conditions. According to the boiler feed pump manufacturer specifications, the rated conditions for a single stage are: rated flow rate= 0.3056 m^3/s, rated head= 495 m, and rated pump speed= 5950 rpm. The pump specific speed (SI) is n_s = 0.09424 (or N_s=1620 in imperial system). With the scaling factor of 0.4 selected for the model pump, similarity laws can be applied considering the geometrical, kinematical, and dynamic similarities between the model pump and the prototype pump, that is

Head coefficient
$$\psi = \left(\frac{gH}{N^2 D^2} \right)_p = \left(\frac{gH}{N^2 D^2} \right)_m \tag{2.4}$$

Flow coefficient
$$\phi = \left(\frac{Q}{ND^3} \right)_p = \left(\frac{Q}{ND^3} \right)_m \tag{2.5}$$

Power coefficient

$$P = \left(\frac{P}{\rho N^3 D^5} \right)_p = \left(\frac{P}{\rho N^3 D^5} \right)_m \quad (2.6)$$

Specific speed

$$N_s = \frac{N\sqrt{Q}}{(gH)^{3/4}} \quad (2.7)$$

Where N is the pump rotational speed, P is the power consumed by the pump. For a speed of 3540 rpm, the similitude results showed that the expected values for the model pump at rated conditions are:

- Flow rate = 11.64 L/s
- Head = 28 m
- Brake power = 4.8 KW
- Efficiency = 67 %

CHAPTER 3

EXPERIMENTAL RESULTS

3.1 INTRODUCTION

In this chapter, the experimental results are being presented. First, a study on the effect of dynamic operating conditions, flow rate and rotational speed, on the unsteady pressure field inside the pump volute and around the impeller is presented. This detailed study is considered to be the base for later comparisons and includes the effect of flow rate and rotational speed on static pressure distribution, pressure fluctuations, frequency spectrum, and vibration of the pump outer casing. The impeller without V-cut at blade exit was used in this general study and analysis.

The effect of measuring location relative to impeller-volute interaction, fluctuations unevenness, and geometrically similar locations are being highlighted. Also the behavior of the unsteady pressure signals at the pump suction and delivery sides (pips) are shown under variable flow rates and speeds. The relation between pump internal pressure signals and pressure signals collected at suction and discharge pipes are compared.

The second part of experimental work is related to the effect of the geometrical (design) parameters of the impeller and volute. A study of the effect of the special V-shaped cut at the impeller blades exit is presented and compared to the case of impeller with without V-cut at blade exit. In order to reduce the flow induced vibration

problem for this pump, a study of different values of the minimum radial gap between the impeller outer diameter and the volute vanes leading edges is presented. The two impellers (without and with V-cut at blade exit) are used to study the gap effect.

The *experimental matrix* consists of testing the following variables:

- **Flow rate**: Flow ratios Q/Qn = 0, 1, 0.75, 0.5, 0.25, and the max available flow rate for each running speed are examined. The symbol Q represents the flow rate while Qn represents the rated (design) flow rate corresponding to best efficiency point for each speed.
- **Rotational Speed**: speed of 3540, 3000, 2500 rpm are examined.
- **V-cut at the exit of impeller blades**: comparison with impeller without V-cut at blade exit at different flow rates and rotational speeds.
- **Radial gaps**: gaps of 2, 3, 3.6 (original design), 4.85, 6, and 7 mm are tested under different flow rates and rotational speeds, with and without the V-cut.

The performance results for the pump at 3540 rpm are compared to similitude calculations. The uncertainty calculations are given in the appendix and a detailed example at the best efficiency conditions is given also in the appendix.

3.2 EFFECT OF OPERATING VARIABLES ON FLOW INDUCED VIBRATION

Figure 3.1 shows a typical performance curves for the scaled model pump at 3540 rpm with the impeller having no V-cut at blade exit (without the V-cut). The minimum radial gap between the impeller outer diameter and the volute vanes leading edge is 3.6 mm (the original design).

The best efficiency conditions were found to be:

Flow rate, Qn =0.01207 [m3/s] ±0.0001771	(uncertainty = 1.94 %)
Pump Total Head =26.95 [m] ±0.2657	(uncertainty = 1.046%)
Overall Efficiency =0.5514 ±0.01071	(uncertainty = 0.987 %)

Table 3.1 compares between the data of single stage boiler feed pump, similitude calculations, and actual model pump experimental data at best efficiency point. The deviations in pump capacity and head are less than 4% which is lower than the acceptable limits reported in literature (up to 10%). As shown in Fig 3.1, pinpointing the best efficiency conditions is not an easy job. The difference between the highest two efficiencies falls within calculated uncertainty of efficiency which may even decrease this deviation. Power depends on the pumping system and mechanical components and the deviation in efficiency is related to the power deviation.

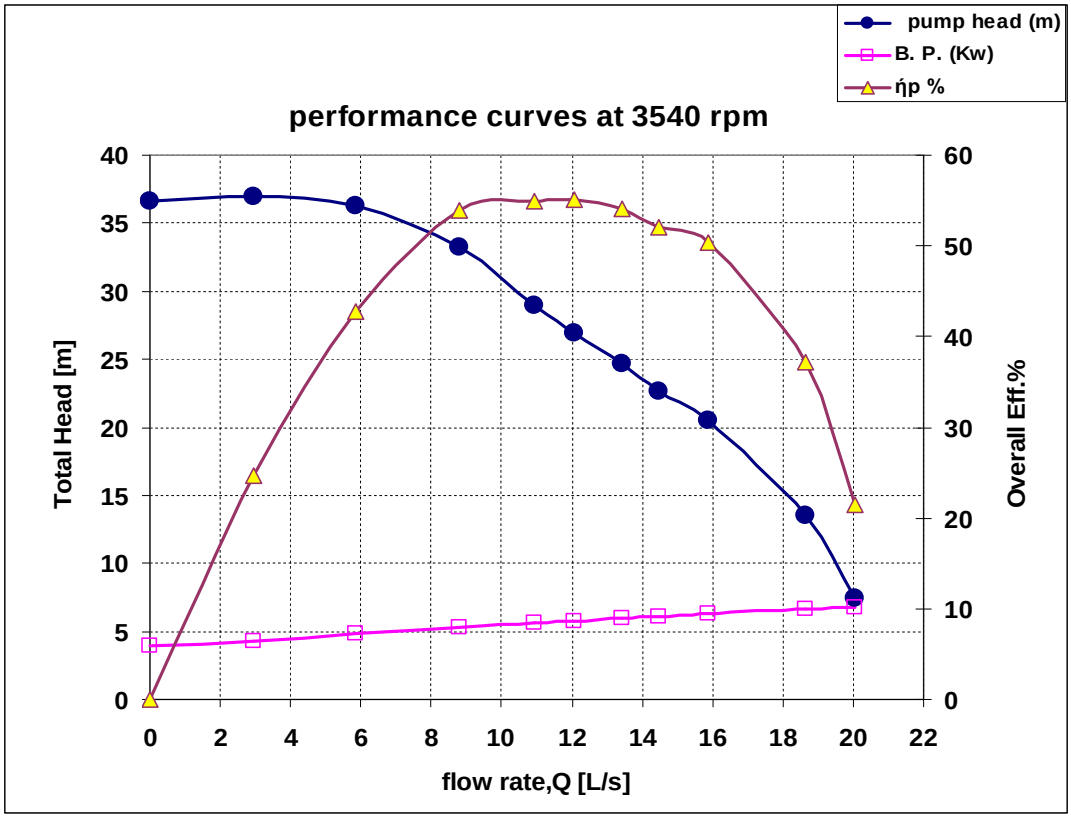

Figure 3.1 Performance characteristics of the model pump at 3540 rpm

Table 3.1 Similitude and experimental results at best efficiency point, 3540 rpm

Variable	Boiler Feed Pump	Similitude calculation	Model pump experimental data	Deviation from similitude %
Flow rate, m3/s	0.3056	0.01164	0.012	+ 3.1
Total head, m	495	28	26.95	- 3.75
Power, KW	2200	4.8	5.75	+ 19.8
Efficiency %	67	67	55.14	- 17

3.2.1 EFFECT OF FLOW RATE

Figure 3.2 shows the effect of the flow rate on the time-averaged static pressures at all measuring locations (Table 2.1) inside the pump volute. The pump rotational speed is constant at 3540 rpm. The pressure is approximately equal for all locations when the pump operates at the nominal capacity (flow ratio Q/Qn =1). At off-design flow rates, the pressure distribution becomes location-dependent with large variations in the local point-to-point pressure values. Measuring locations around the impeller were arranged in symmetrical positions. Figure 3.3a focuses on the geometrically similar pairs around the impeller; namely, locations (2,5), (3,7), (4,9). The double volute design keeps the pressure at the same value at similar locations around the impeller, even at off-design flow rates. This effect of the pump volute design minimizes the net radial forces on the impeller and shaft for all operating flow rates. Figure 3.3b shows the variation of static pressure with the angular position around the impeller. It starts with location 3 (angle=61 deg) followed by locations 4, 5, 7, 9, and 2 respectively. The variation is minimum at design flow rate while operating off-design increases the variation of pressure around the impeller.

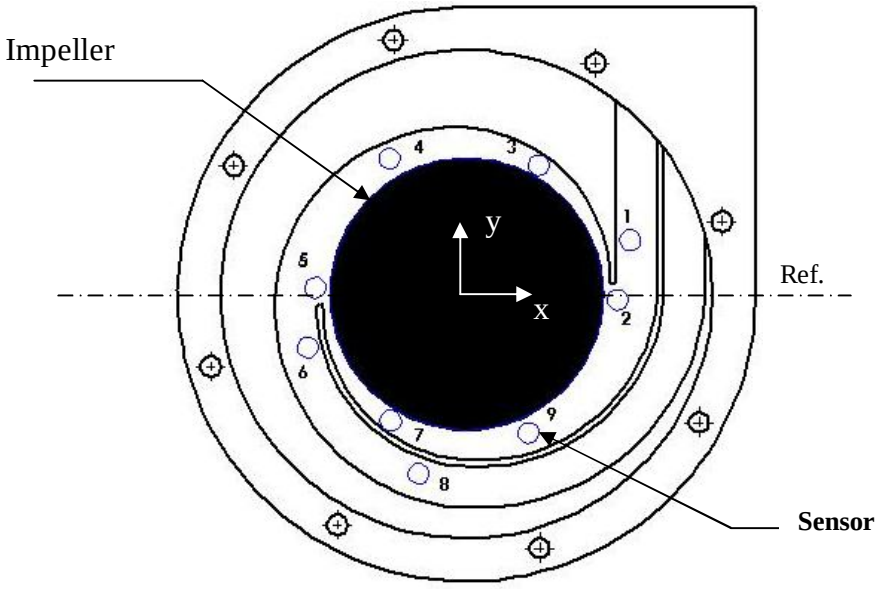

(a) Locations of measuring sensors inside the pump

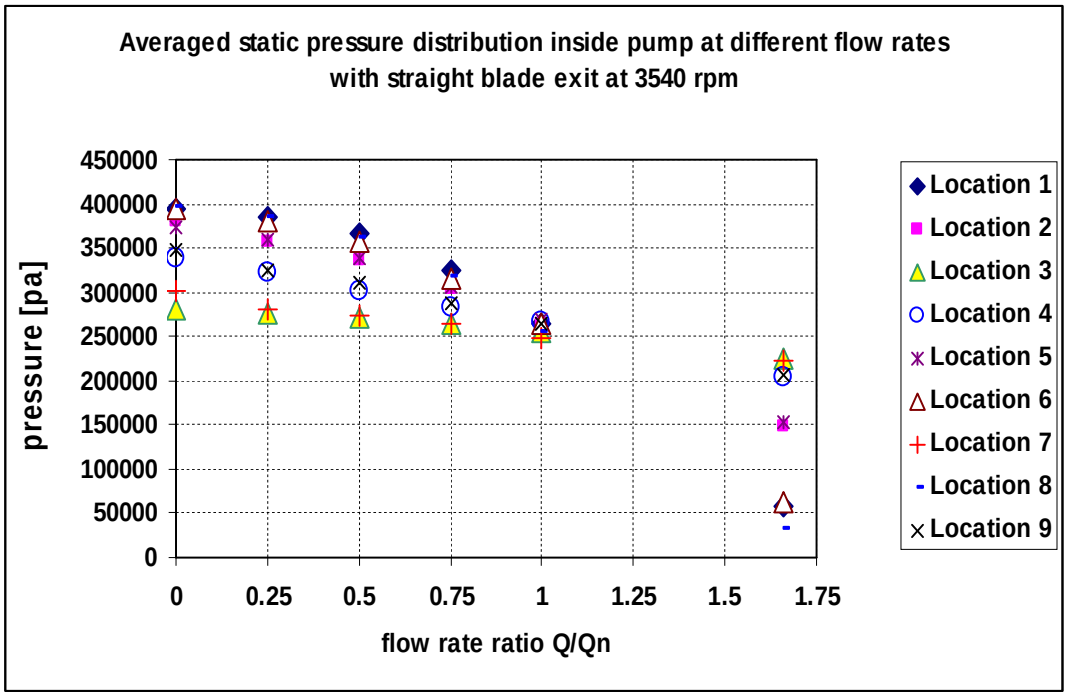

(b) Static pressure variation with flow rate

Figure 3.2 Effect of flow rate on static pressures at measuring locations

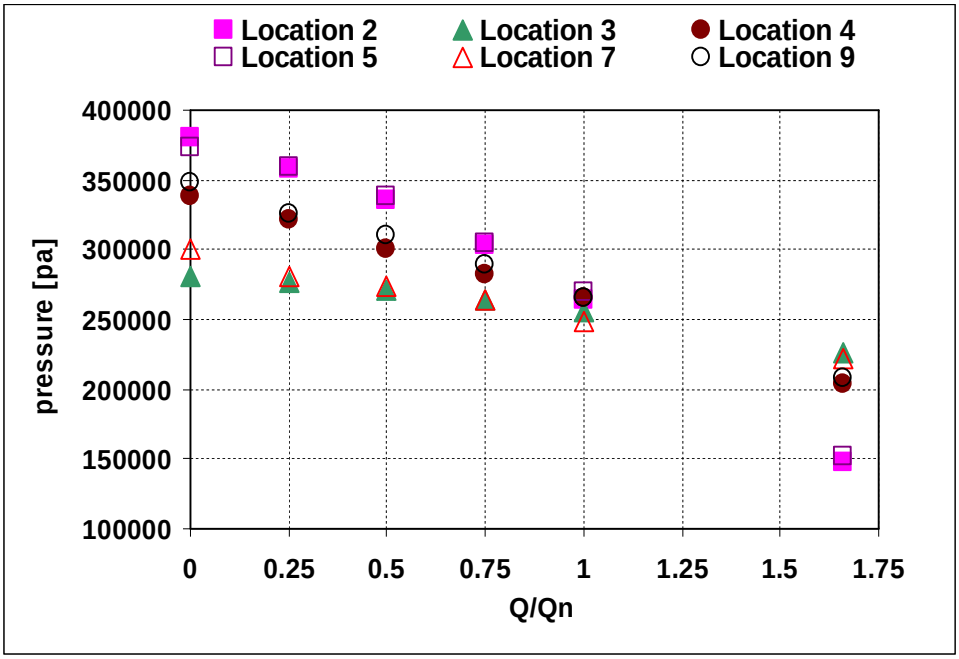

(a)

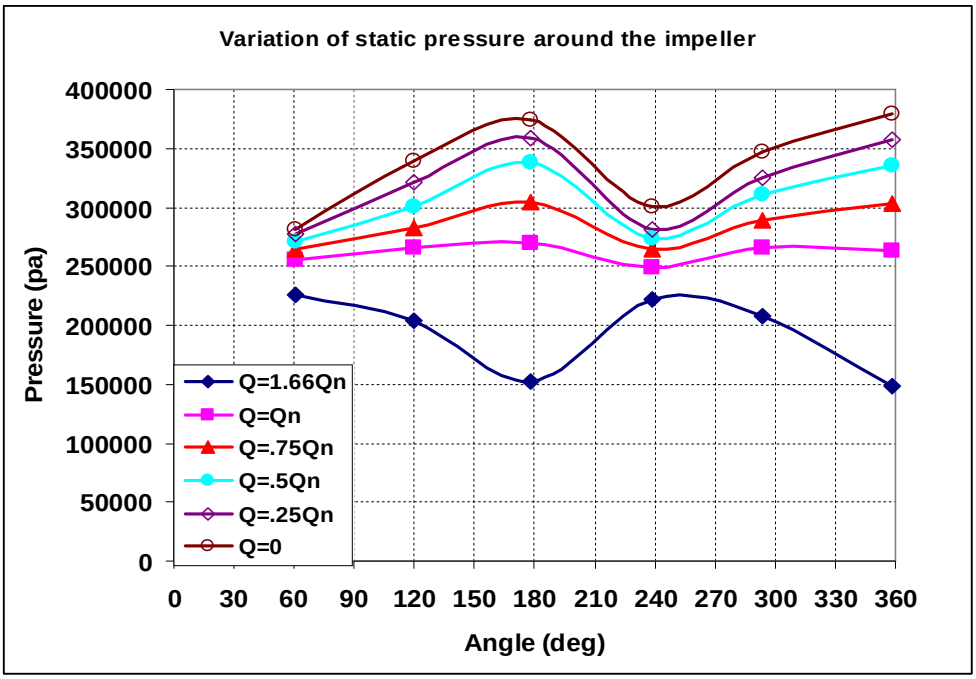

(b)

Figure 3.3 Effect of flow rate on time-averaged static pressure distribution around the impeller at 3540 rpm

The uniformity of the pressure distribution inside the pump and around the impeller has a great impact on the magnitude of pressure fluctuations as mentioned in many references. To clarify the effect of flow rate on the uniformity of the pressure distribution inside the pump, Figure 3.4 shows the same data like Fig 3.2 but with different presentation to identify the locations of maximum variations in pressure under variable flow rate. It is very clear from this Figure that operating at off-design flow rates promotes the pressure variation from location to another inside the pump. Locations 1, 2, 5, 6, and 8 experiencing the largest pressure variations, they are located at the interaction zone. The exception is location 8 in the flow passage after the volute cutwater where the effect of the interaction between the impeller and volute tongue propagates. If the pump runs with closed discharge valve, the pressure inside the pump is maximum with non-uniform distribution, and the pump casing gets hot within a minute. If the pump runs with fully opened discharge valve, the pressure inside the pump drops to minimum with non-uniform distribution and noticeable high noise. Both operating conditions are not recommended.

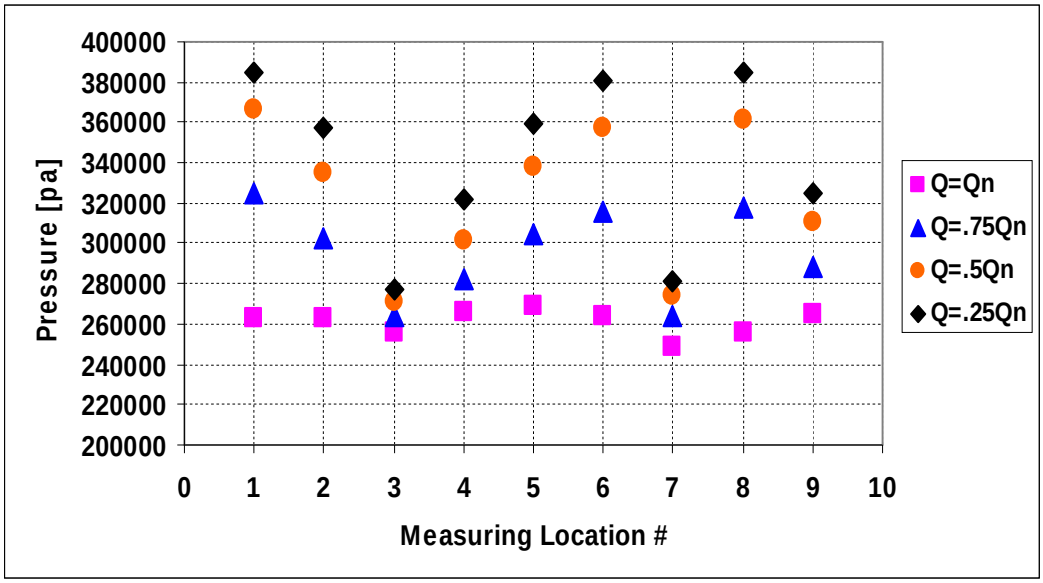

(a) Effect of reduced flow rates

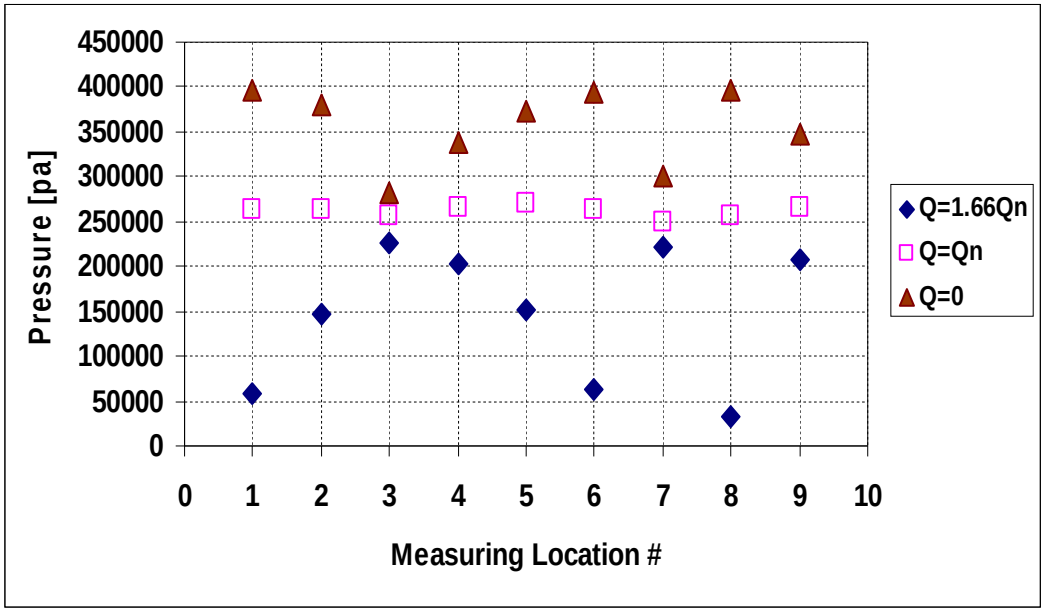

(b) Operating at design conditions against maximum and zero flow rates

Figure 3.4 Effect of flow rate on pressure uniformity inside the pump

Pressure fluctuations at the measuring locations inside the pump, suction side, and delivery side of the pump were measured by dynamic pressure transducers. TL data logger and data viewer software provided by Teclution Company are used for real time monitoring of the waveform and FFT analysis for the pressure fluctuations. As an illustration, Fig. 3-5 displays the waveform (for two shaft revolutions, 0.0324 second) and the spectral analysis (FFT magnitude) for location 3 at three different flow ratios (Q/Qn) of 1, 0.5, and 1.66. Location 3 is the closest measuring point to the impeller-volute interaction zone. The waveform of the pressure fluctuation is displayed in units of psi. The spectrum dominant peak occurs at a frequency of 295 Hz which corresponds to 5xRPM or the first blade passing frequency (1^{st} BPF). Smaller peaks appeared at 10xRPM (2^{nd} BPF) and 15xRPM (3^{rd} BPF). A small peak appeared at the running speed (59 Hz in case of 3540 rpm) due to residual unbalance. Reducing the flow rate to 50% almost doubles the pressure fluctuations range and the same effect for the FFT magnitude measured at the 1^{st} BPF as shown in Fig. 3.5b. Reducing the flow rate has a small effect on higher harmonics (2^{nd} and 3^{rd} BPF). All other locations inside the pump experienced a comparable increase in pressure fluctuations and FFT magnitude with reduced flow rate.

A remarkable effect on the 2^{nd} BPF is noticed when the flow rate is max, Q/Qn=1.66, as shown in Fig. 3.5c. At maximum flow rate, the fluctuations are significant at both the 1^{st} and 2^{nd} BPF. Separation vortices and cavitation bubbles, observed at the volute tongues and extended downstream, excite the 2^{nd} BPF. It is also important here to mention that points 1, 6, and 8 experienced the highest fluctuations amplitudes and energy when the flow ratio is 1.66 due to separation vortices at volute vanes leading edges.

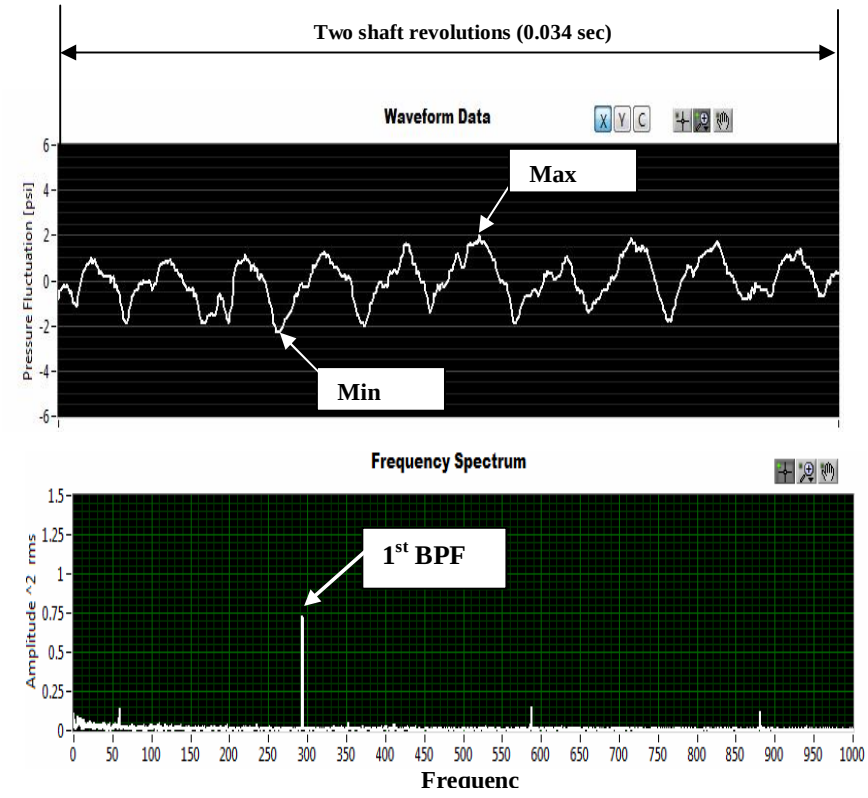
Two shaft revolutions (0.034 sec)
Waveform Data
Max
Min
Pressure Fluctuation [psi]
Frequency Spectrum
1st BPF
Amplitude ^2 rms
Frequenc

(a) Q= Qn

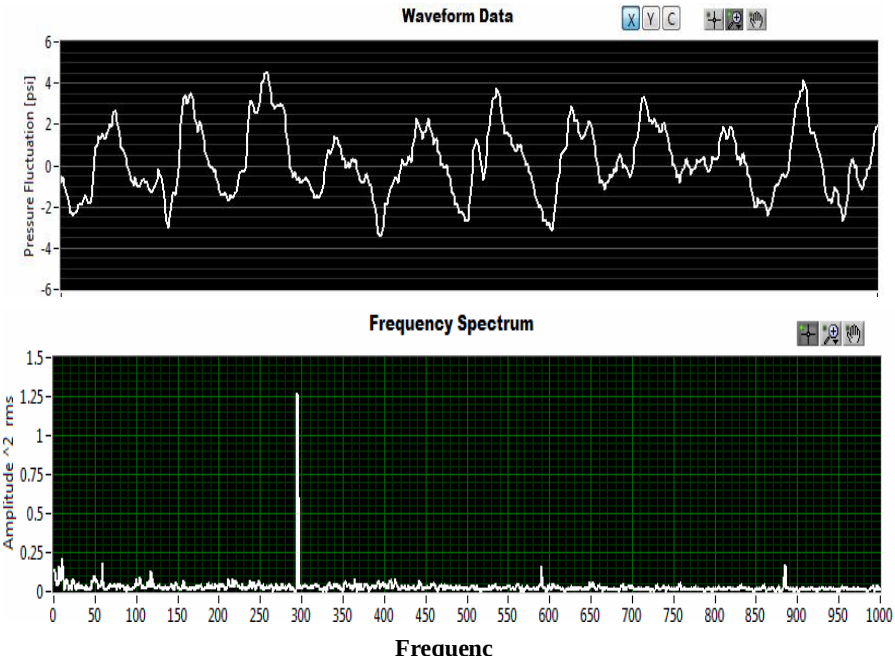
Waveform Data
Pressure Fluctuation [psi]
Frequency Spectrum
Amplitude ^2 rms
Frequenc

(b) Q=0.5 Qn

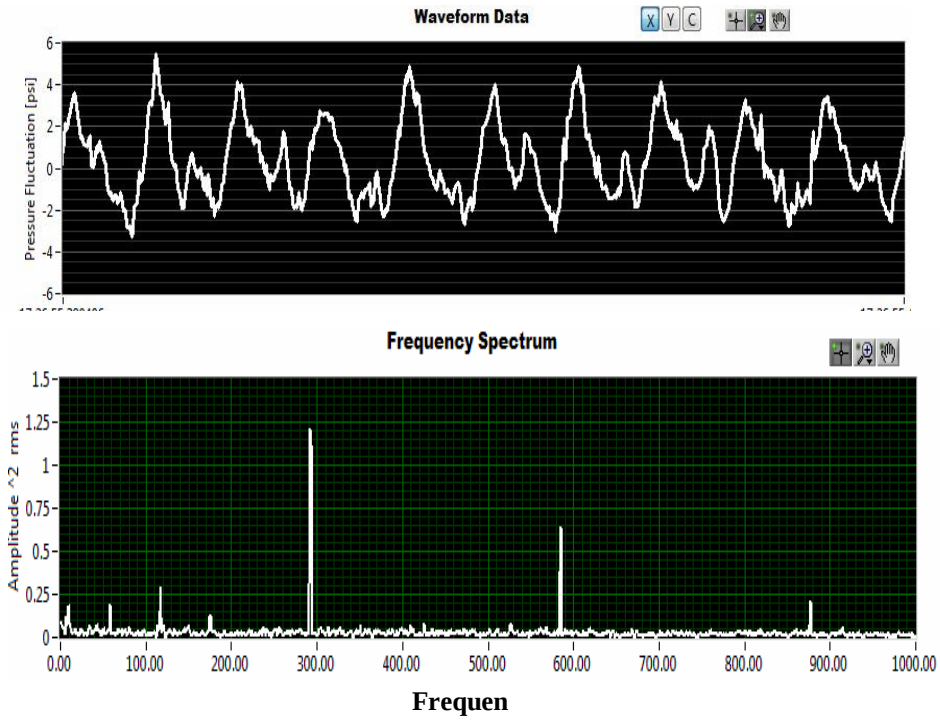

(c) Q =1.66 Qn

Figure 3.5 Effect of flow rate on pressure fluctuation at location 3

Based on the speed of sound in water (about 1500 m/s) and the dimensions of test section, the acoustic resonance was excluded as a source of the pump vibration at a frequency of 295 Hz or its higher harmonics. In order to pinpoint the source of these fluctuations and to study the effect of measuring location on these fluctuations, Fig. 3.6 compares the measured fluctuations amplitudes, measured Peak-to-Peak, at all measuring locations (including pump suction and delivery sides, locations 10 and 11) at reduced flow rates. The peak-to-peak measurement of pressure fluctuation amplitude means the max peak minus the min peak of the signal as shown in Fig. 3.5a. The FFT magnitudes of these signals, measured at the 1^{st} BPF (5xRPM), are also presented. Reducing the flow rate produced higher pressure fluctuations.

For example, fluctuations are doubled when the flow ratio is 0.25 compared to the case when the flow ratio is 1. At off-design flow rates, the flow exiting from the impeller is not tangent to the volute diffuser vanes. This creates circulatory flow inside the pump and impeller resulting in high pressure fluctuation.

Locations 3 and 7 exhibit the largest pressure fluctuation values and the highest FFT magnitudes, especially at low flow rates. They are at the vicinity of the interaction zone located between rotating impeller blades and volute stationary vanes. The fluctuation energy measured in suction and discharge sides are very small compared to inside pump signals since they are away of the fluctuation source. Figure 3.7 compares the measured fluctuations (Peak-to- Peak) at the maximum flow rate (Q/Qn=1.66) to the nominal conditions. The fluctuations and their energies are very high compared to reduced flow rate conditions and Points 1, 2, 6, and 8 show spikes. Again, these points

are close to the vanes lips and are highly affected by the interaction between rotating impeller blades and volute stationary vanes.

Thus the impeller/volute interaction at cutwaters region is the origin of the pressure pulsation inside the pump and this zone is a key factor in the analysis of the flow induced vibration problem of this pump.

The time-averaged static pressure values were equal when measured at similar locations as shown before in Fig. 3.3 but the pressure fluctuations at the same similar locations are not. As an example, Fig. 3.8 compares the pressure fluctuations and their energies at locations 3 and 7, at different flow rate conditions. Although the two locations are geometrically similar with respect to the impeller and cutwaters and have the same averaged static pressure, the dynamic pressure fluctuations (and their energy contents) are not the same due to the impeller/volute interaction. This fact is documented in many literatures (for example, Guo and Maruta [3]) for single volute centrifugal pumps even at Q=Qn and it has been proven here for the double volute pumps.

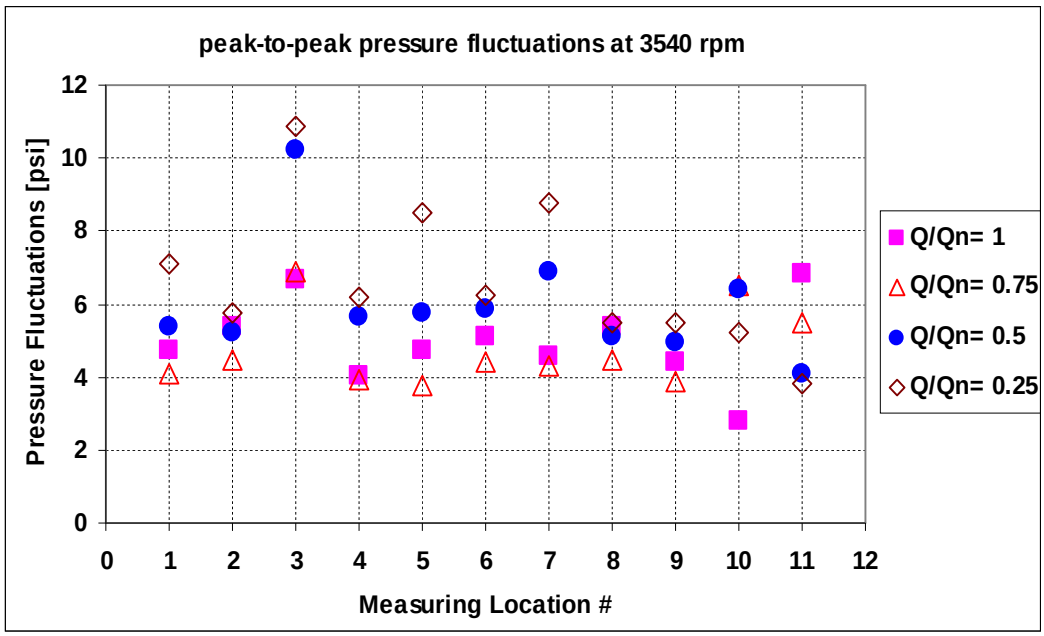

(a)

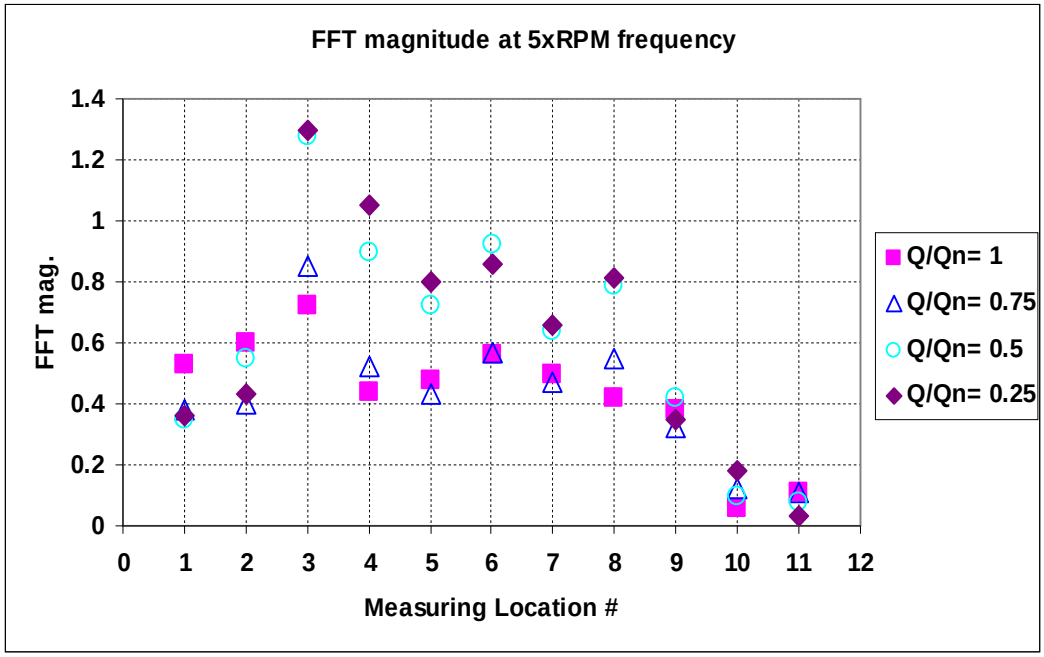

(b)

Figure 3.6 Effect of flow rate on dynamic pressure fluctuation (Peak-to-Peak) and the corresponding FFT at all measuring locations

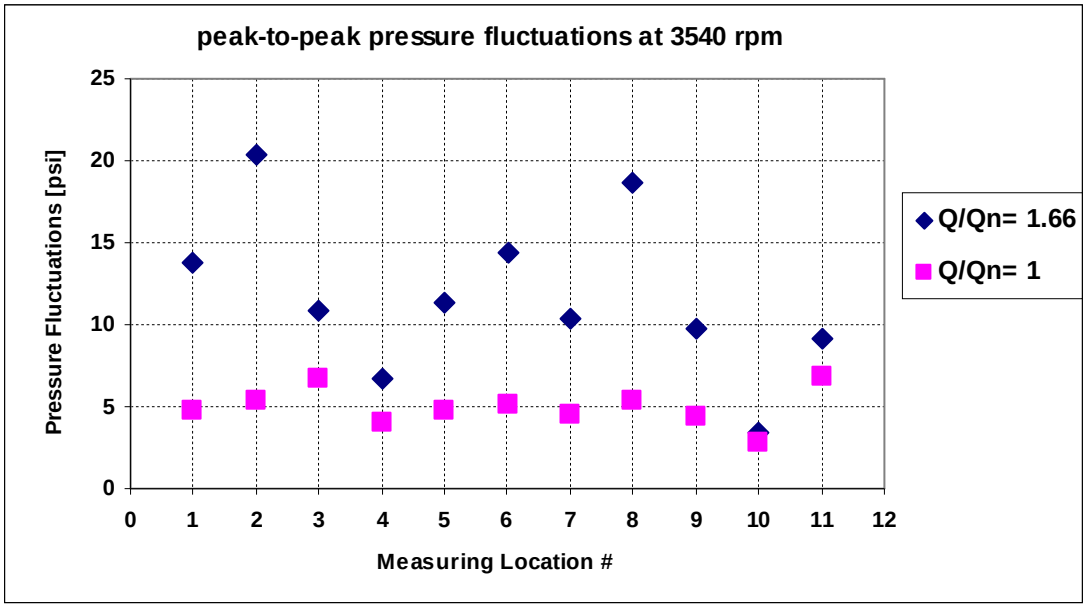

(a)

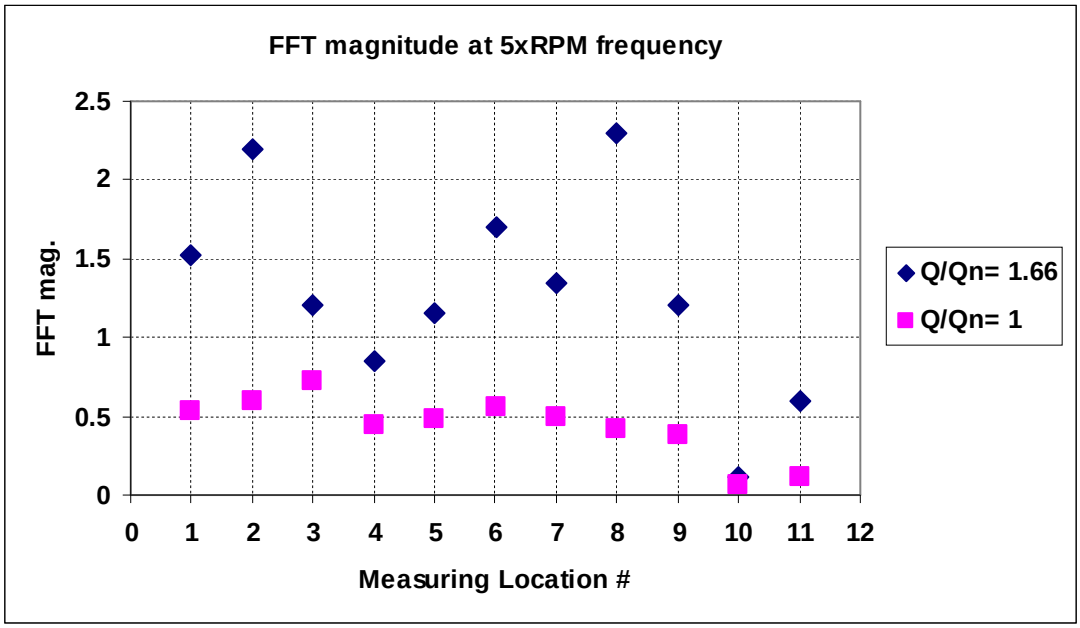

(b)

Figure 3.7 Effect of operating at maximum flow rate on pressure fluctuations compared to operating at design condition

Another feature of the dynamic pressure fluctuations inside the pump volute is the location relative to the interaction zone at volute cutwaters. Figure 3.9 compares the fluctuation amplitudes (peak-to-peak) and FFT magnitudes between the two consecutive locations 3 and 4 where point 3 is closer to the interaction zone. The fluctuation wave is transferred around the impeller and is damped out as it goes away from the cutwater in the angular direction. This also confirms that these fluctuations are originated at the volute tongues due to impeller-volute interaction.

The effect of the flow rate on pressure fluctuation at both discharge and suction sides of the pump is shown in Figs. 3.10 and 3.11 with FFT magnitude measured at the first blade passing frequency (5xRPM), at 3540 rpm. A general behavior of decreasing pressure fluctuations and FFT magnitude was recorded at this speed with decreasing pump flow rate at the discharge pipe, Fig. 3.10. This is an important observation; pressure fluctuation response to change in flow rate at discharge pipe is different from pressure fluctuation behavior inside the pump volute. The opposite behavior (to the discharge side) of the pressure fluctuations was measured in suction pipe. Operating the pump at flow rates less then the nominal value resulted in increasing pressure fluctuations and the corresponding FFT magnitude at 5xRPM frequency.

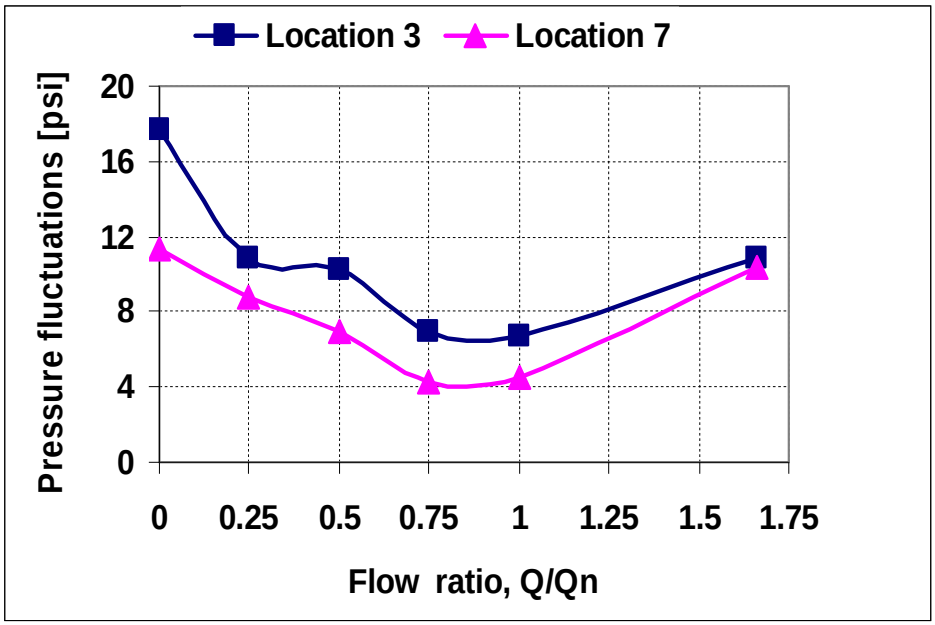

(a)

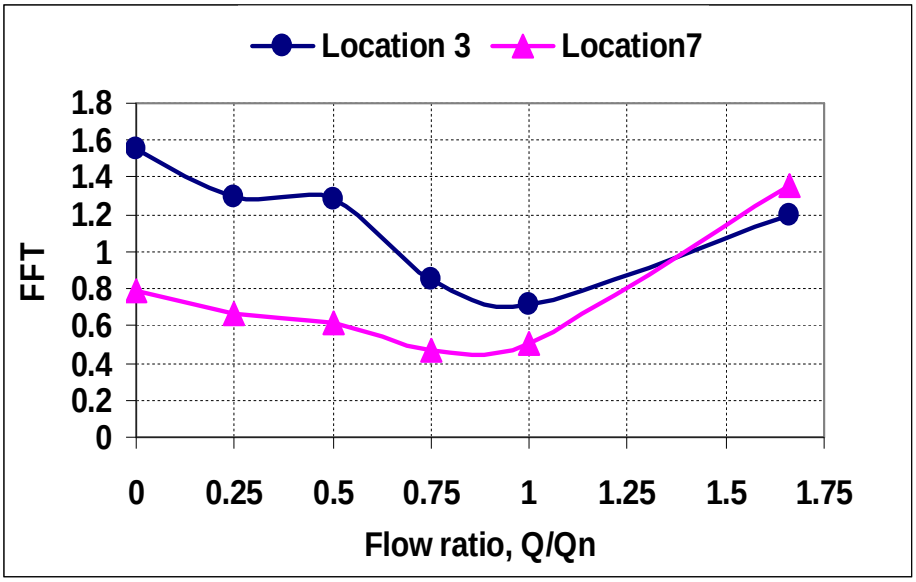

(b)

Figure 3.8 Comparison of pressure fluctuations at geometrically similar locations 3 and 7

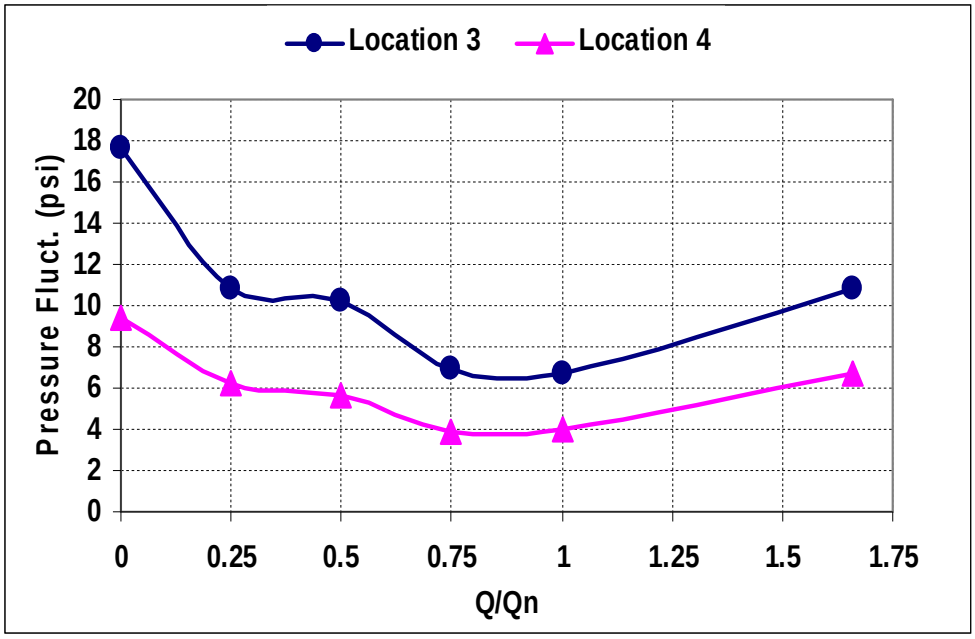

(a)

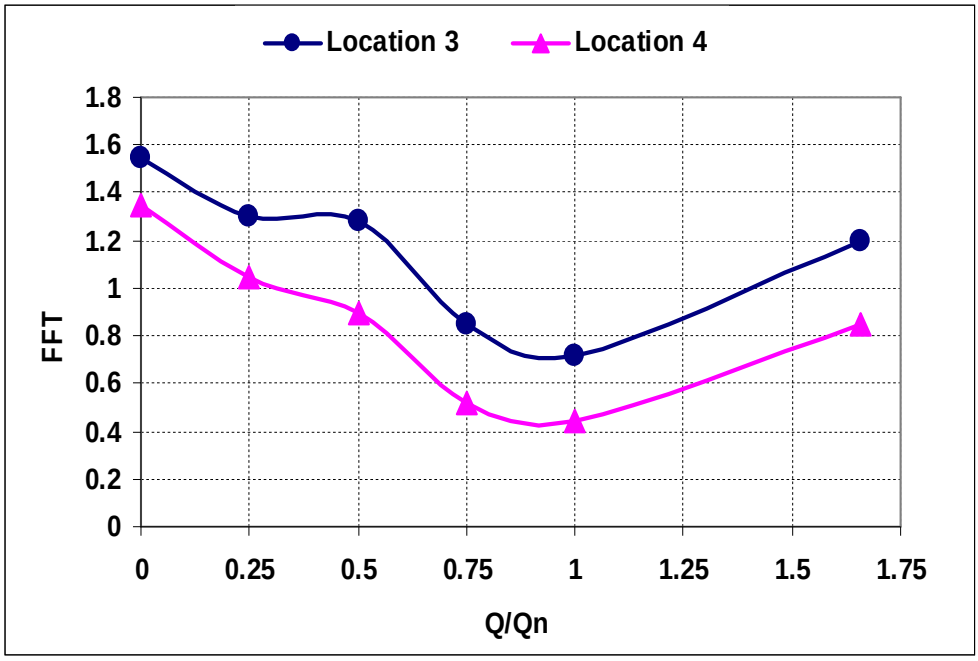

(b)

Figure 3.9 Comparison of pressure fluctuations at consecutive locations 3 and 4

Higher flow rates have small effect on the fluctuations measured at suction pipe, see Fig. 3.11. This is evident since reducing the flow rate increases reverse flow inside the pump and pre-rotation at impeller suction. Based on these results, it is difficult to rely on measurements at discharge and suction pipes for the present pump. For example, at pump speed of 3540 rpm, discharge pipe measurements of pressure fluctuations gave opposite trend compared to measurements inside the pump at various flow rates. The energy content of fluctuation inside the pump is much higher than suction or discharge pipes signals.

The 2^{nd} and 3^{rd} blade passing frequencies also appeared in the spectrum but with smaller peaks compared to the 1^{st} BPF. Figure 3.12 shows that the FFT magnitudes at 1^{st} BPF is much higher than 2^{nd} and 3^{rd} BPFs' when measured at location 7. They become more significant at extreme off-design flow rates. This observation was also noticed in the field seismic vibration test reported for the original boiler feed pump when operating at part loads.

In the suction pipe, FFT magnitude of the second harmonic of the blade passing (10xRPM) was measured to be greater than that for the first harmonic for all tested flow rates as shown in Fig. 3.13.

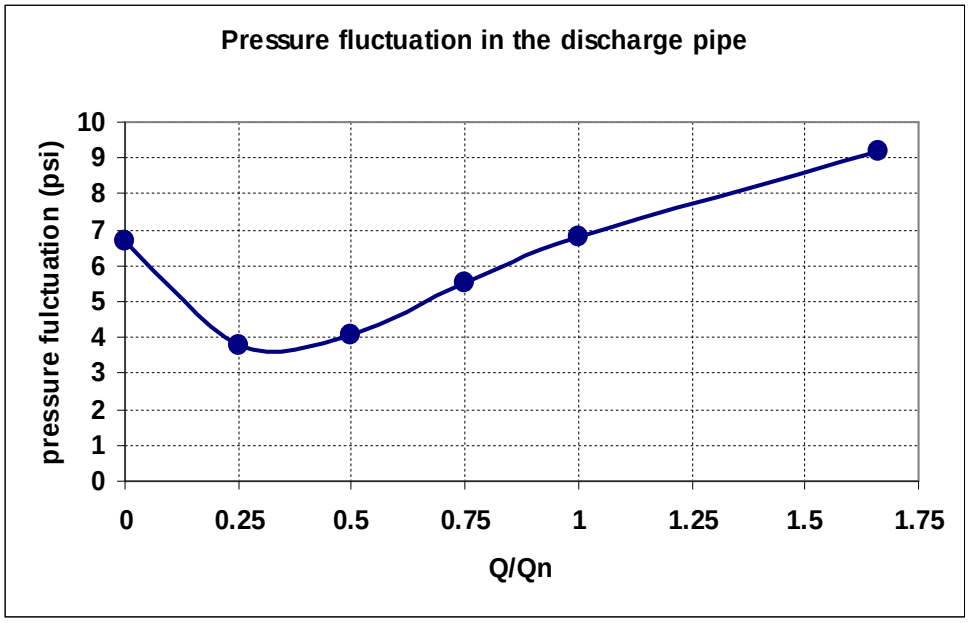

(a)

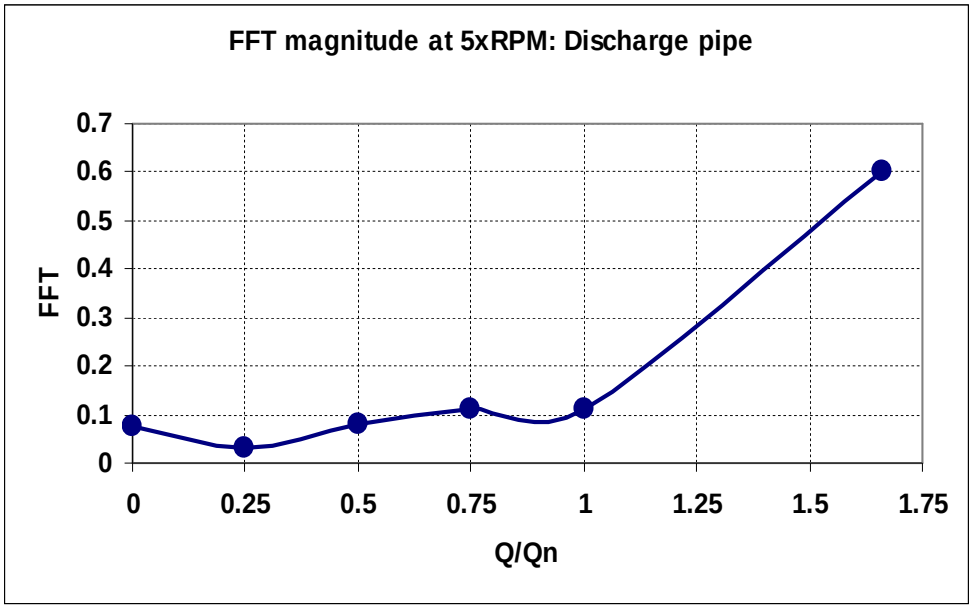

(b)

Figure 3.10 Effect of flow rate on fluctuation and the corresponding FFT Mag. at pump discharge side

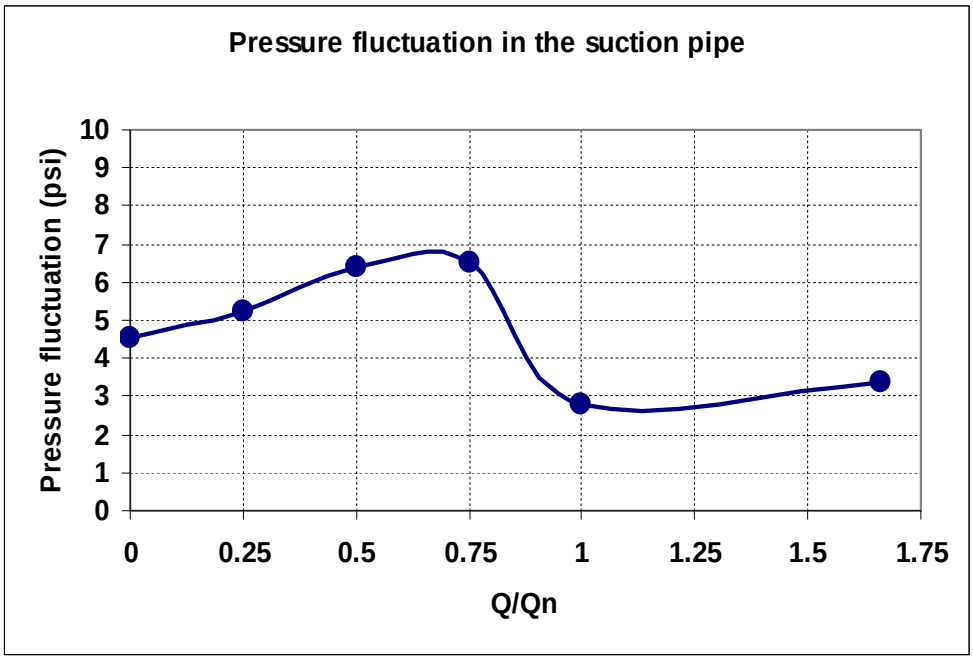

(a)

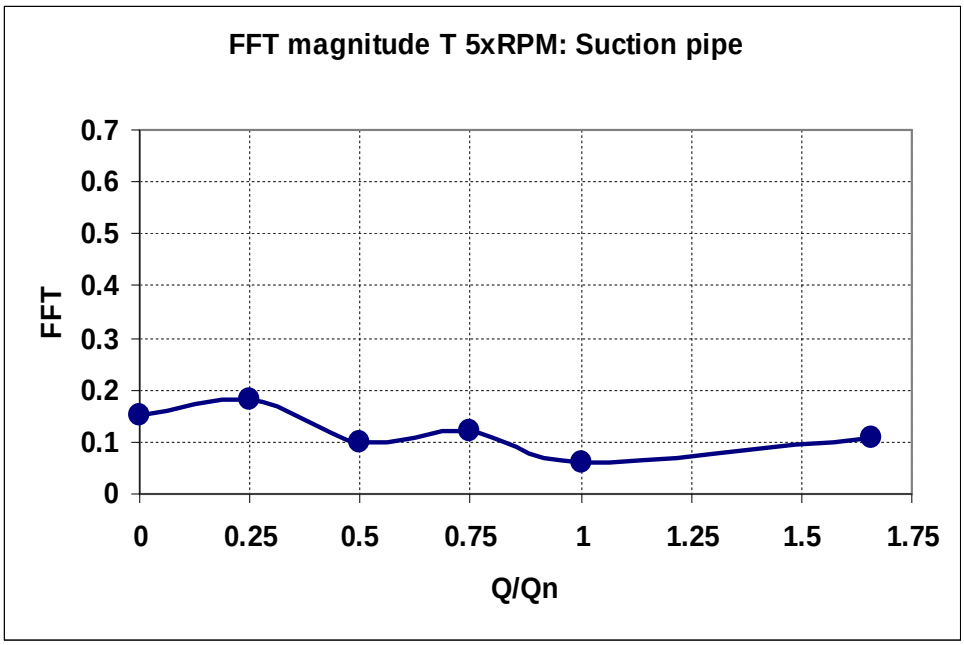

(b)

Figure 3.11 Effect of flow rate on fluctuation and the corresponding FFT magnitude at pump suction side

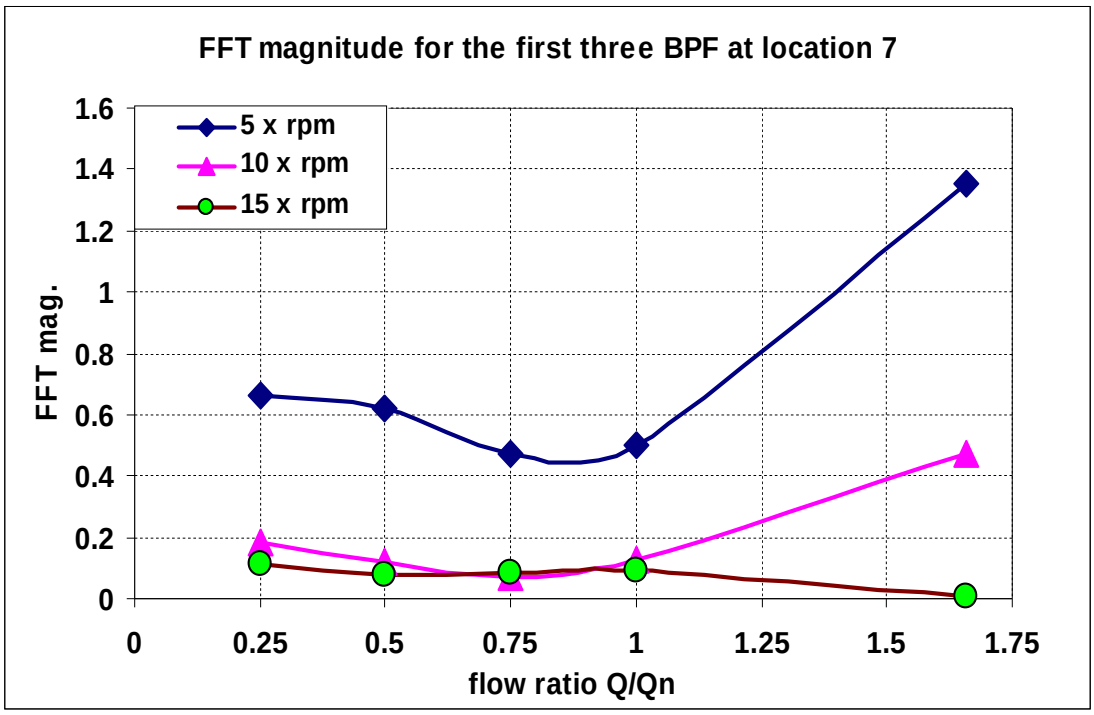

Figure 3.12 FFT magnitudes measured at the first three blade passing frequencies at location 7

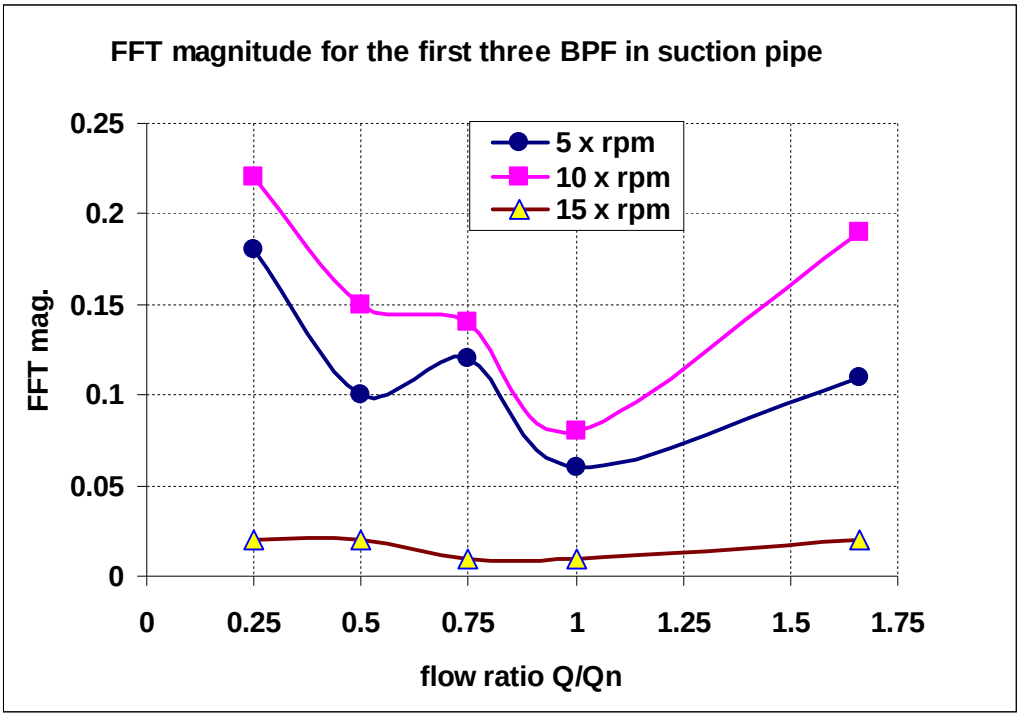

Figure 3.13 FFT magnitudes measured at the first three blade passing frequencies at suction pipe

The measurements of the pump casing vibration were carried out using B&K 4507 Delta Tron accelerometers, with 100mV/g as mentioned in Chapter 2. Figure 3.14 shows a typical spectrum of the vertical vibration of pump casing at 3540 rpm at Q/Qn= 0.5. The vibration occurs mainly at the first blade passing frequency (5xRPM) while smaller peaks appear at the second and third blade passing frequencies. Figure 3.15 shows the behavior of pump vibration in relation to the internal pressure fluctuation and its FFT magnitude (at 5xRPM) measured at location 3, at different flow rates. Location 3 was selected for this comparison since it is the closest location to the impeller-volute interaction zone and it is experiencing the highest fluctuations inside the pump. The minimum pump case vibration and pressure fluctuations were measured at the nominal flow rate; Q/Qn= 1. At off-design flow rates, the pump case vibration and pressure fluctuation increase. The behavior of the pump case vibration is following the behavior of both the pressure fluctuations and the FFT of these fluctuations inside the pump under variable flow rate conditions. This behavior proves that the pump vibration is induced by the flow inside the pump due to the interaction between the impeller rotating blades and volute stationary vanes. It also proves that measurements of the unsteady pressure inside the pump can be used to identify the problem and to seek a solution.

The horizontal case vibration was found to be significant only at low flow rates (less than 50% of the nominal).

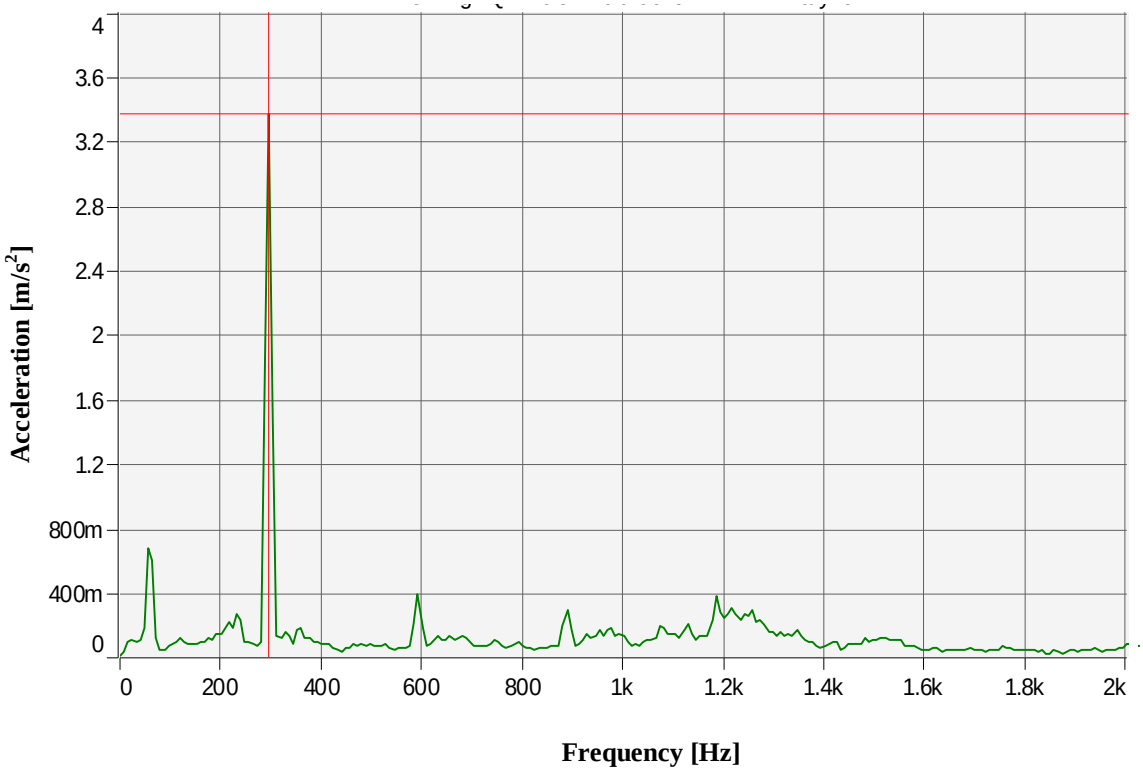

Figure 3.14 Typical Vibration behavior of the pump outer casing: vertical direction (Q/Qn=0.5 at 3540 rpm)

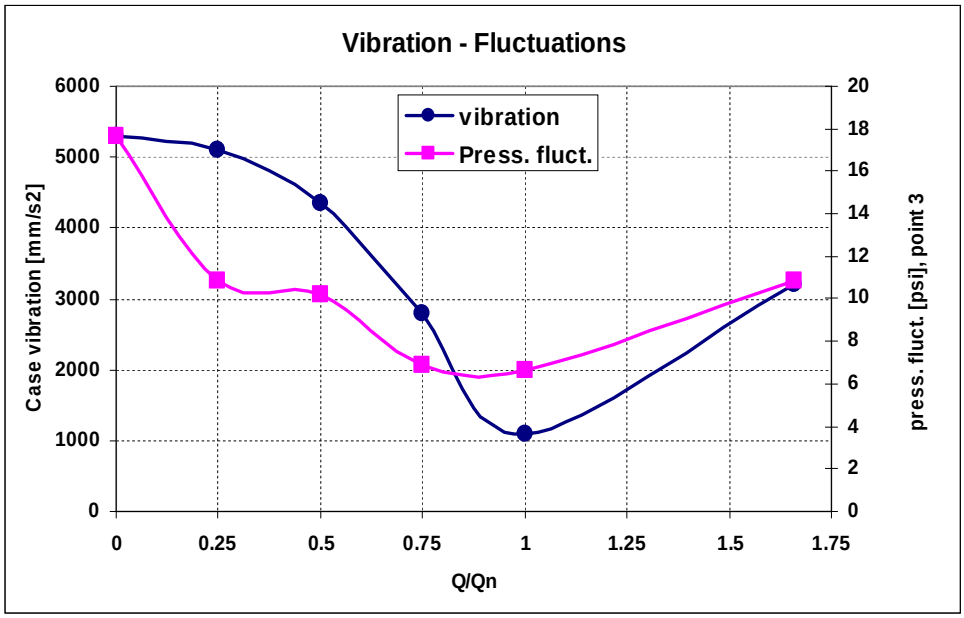

(a)

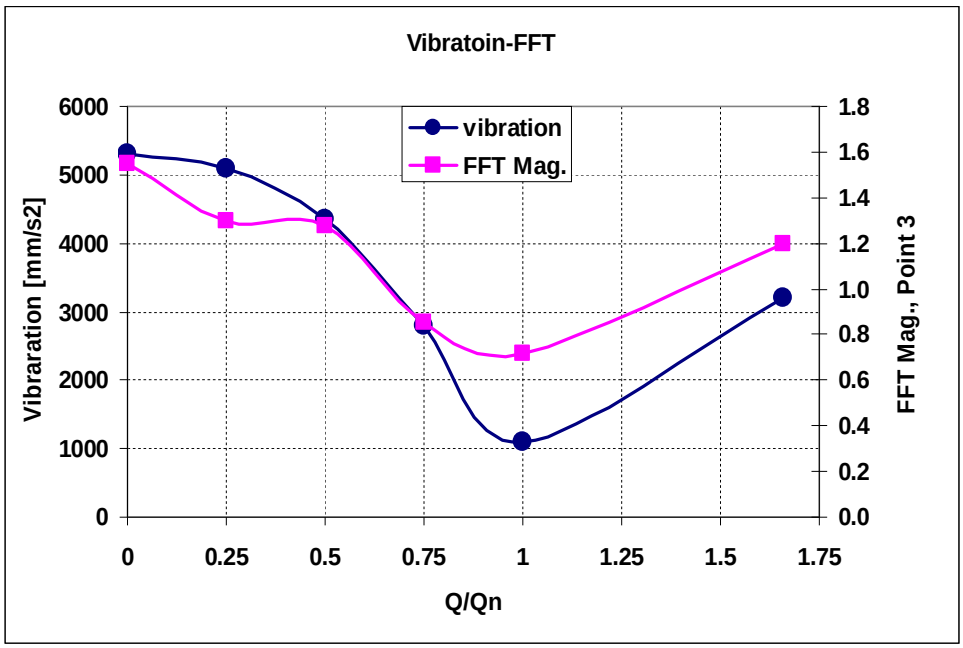

(b)

Figure 3.15 Comparing pump case vibration with the internal pressure fluctuation and FFT measured at 5xRPM at location 3, at different flow rates

3.2.2 EFFECT OF PUMP SPEED

In this section, the effect of pump rotational speed on performance, pressure distribution, pressure fluctuations is presented. The performance characteristics of the model pump are shown in Fig. 3.16 where the H-Q, ή-Q, and B.P-Q curves are plotted for speeds of 3540, 3000, and 2500 rpm. The pump speed is controlled by a frequency inverter which gave maximum speed of 3540 rpm at 60 Hz. No higher speeds can be reached using the current setup. For each speed, there is a corresponding best efficiency conditions. The nominal flow rate, Qn, is based on the related pump speed.

Figure 3.17 shows the effect of the pump rotational speed on the time-averaged static pressure distribution inside the pump at measuring locations. The pressure is almost constant inside the pump for each speed when the flow rate equals to that corresponding best efficiency capacity. Reducing the pump flow rate resulted in unequal pressure values locally inside the pump.

Large variation of pressure from point to point inside the pump gives rise to higher local pressure fluctuations as demonstrated in Fig. 3.18. Figure 3.19 gives the FFT magnitude for the fluctuations presented in Fig. 3.18 under the same conditions.

Increasing the speed increases the pulsation originated at the impeller-volute interaction region. When high speeds are combined with off-design flow rates, pressure fluctuations and pump vibration are expected to be very high and to exceed the standard limits.

The amplitude and strength of pressure fluctuations depend on the pump speed, the flow rate, and the location of each point relative to the interaction zone. A typical behavior is shown in Fig. 3.20 for location 3 under variable speed and a wide range of

flow rates. Minimum fluctuation amplitude and energy were measured at the best efficiency flow rates.

The behavior of pressure fluctuation and its FFT analysis at discharge and suction sides of the pump under variable speeds and flow rates is shown in Figs. 3.21 and 3.22. The discharge pipe feels higher pressure fluctuation energy than the suction pipe due to the movement of fluctuation waves downstream the pump. Higher speeds when combined with maximum flow rate resulted in higher fluctuation at the pump discharge side, which is comparable in amplitude and FFT magnitude to the values measured inside the pump, and lower fluctuation in the suction side. The fluctuation energies measured at suction and discharge side of the pump are small compared to inside pump values in general.

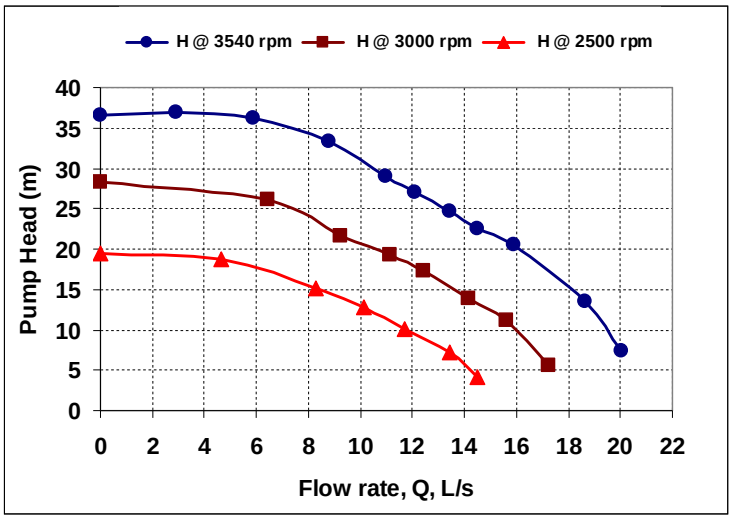

(a)

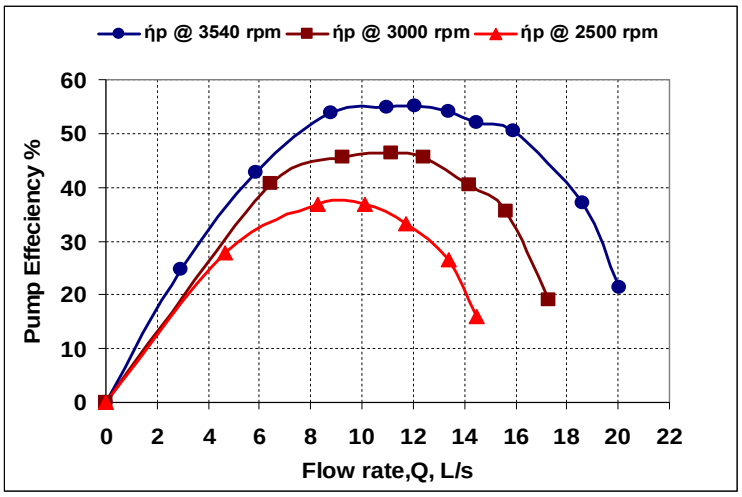

(b)

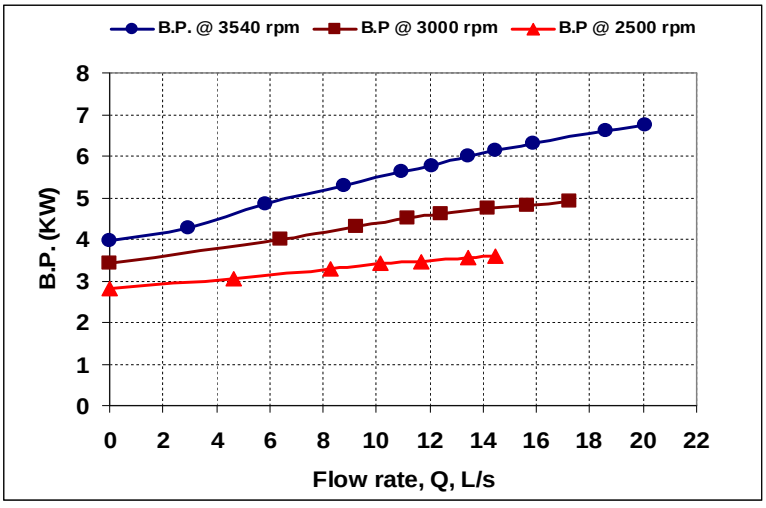

(c)

Figure 3.16 Effect of pump speed on performance curves

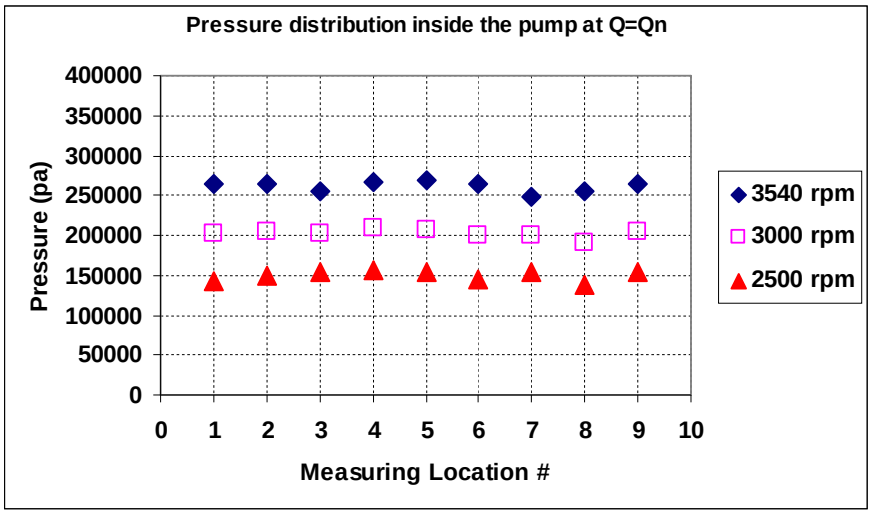

(a)

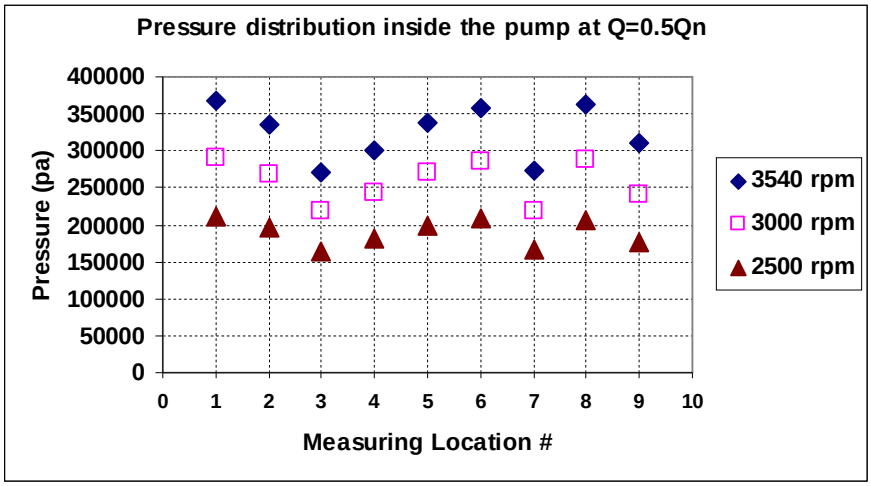

(b)

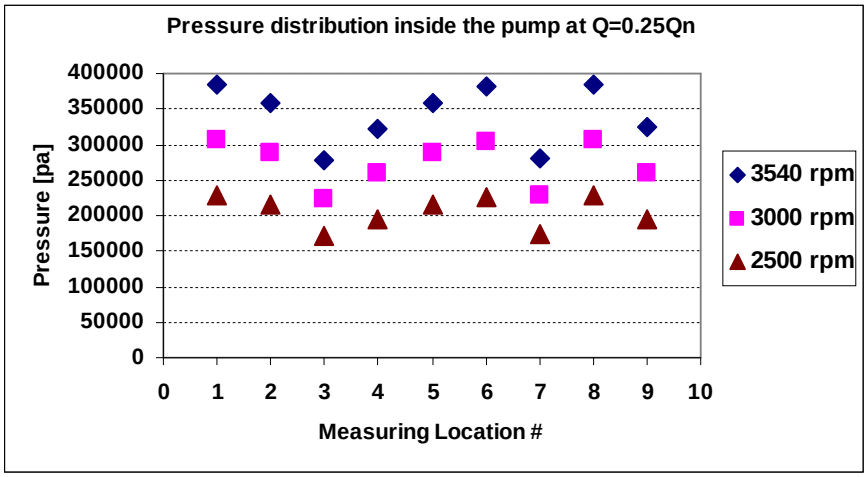

(c)

Figure 3.17 Effect of speed on pressure distribution at different flow rates

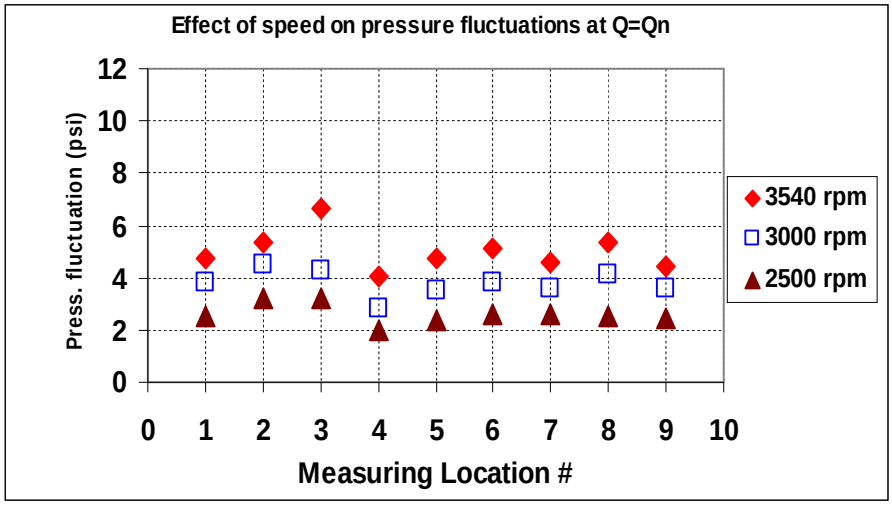

(a)

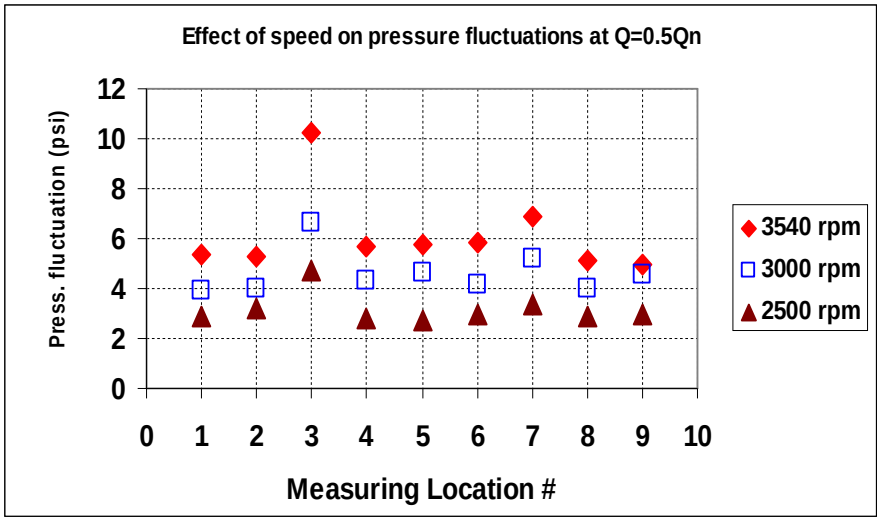

(b)

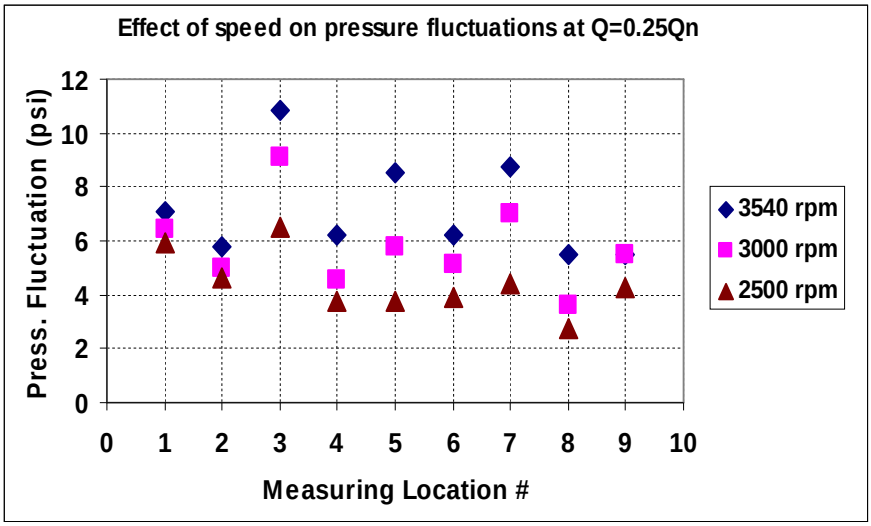

(c)

Figure 3.18 Effect of speed on pressure fluctuations at different flow rates

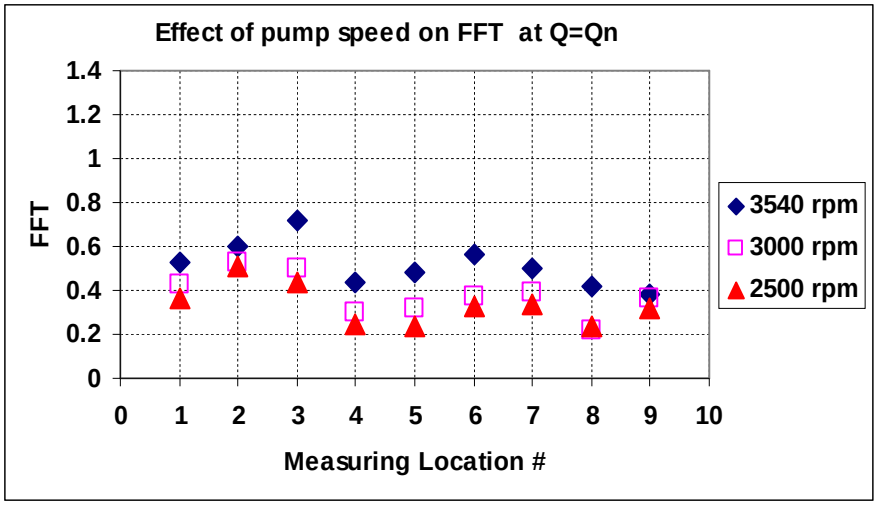

(a)

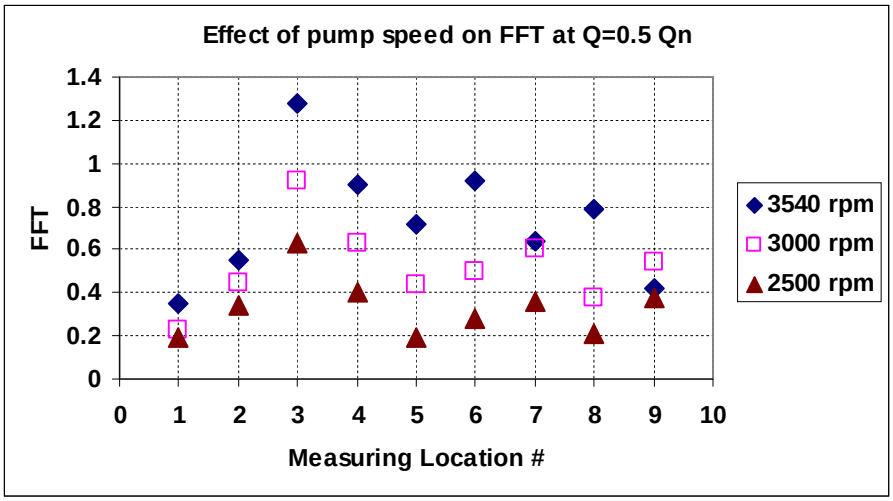

(b)

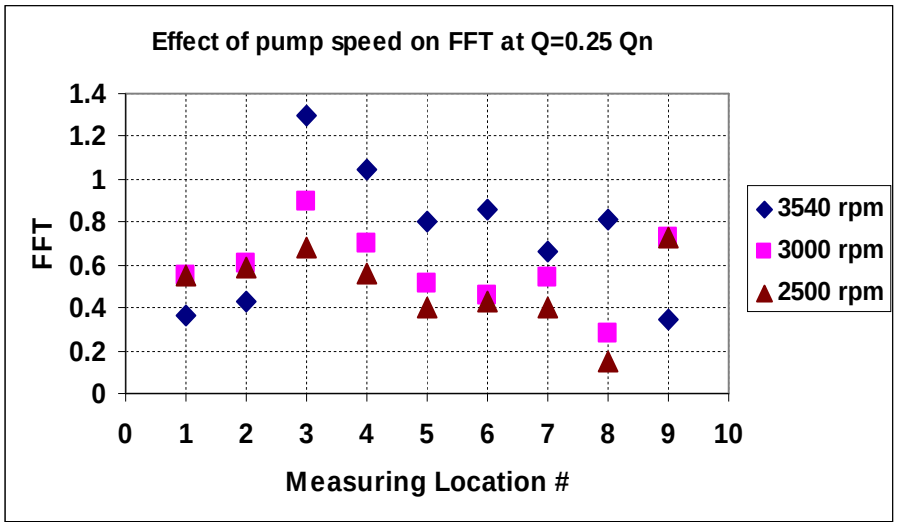

(c)

Figure 3.19 Effect of speed/flow rate on FFT magnitude of pressure fluctuations

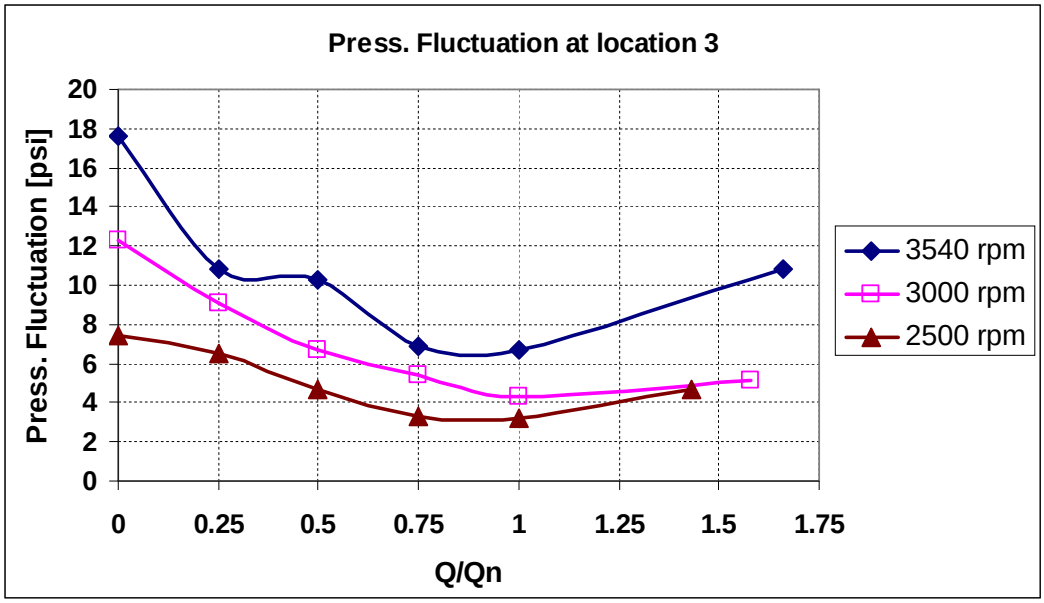

(a)

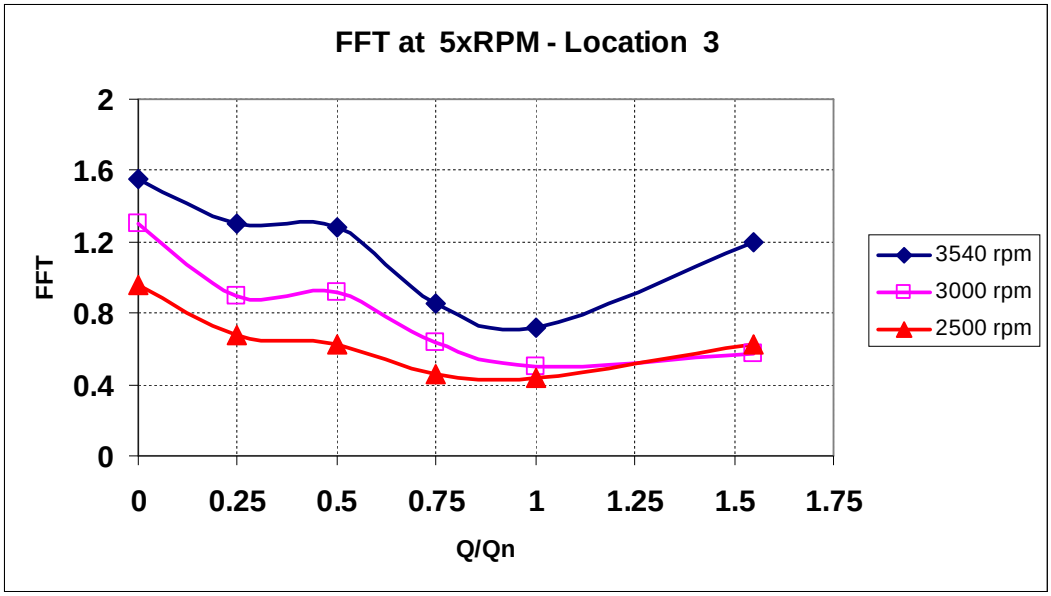

(b)

Figure 3.20 Effect of speed/flow rate on pressure fluctuation and FFT magnitude at measuring location 3

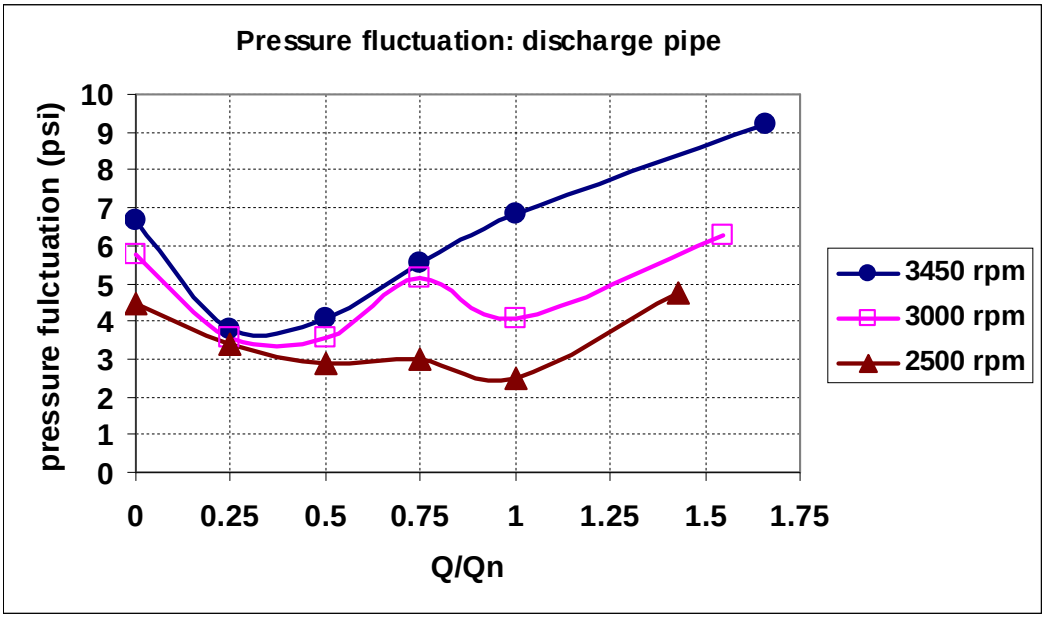

(a)

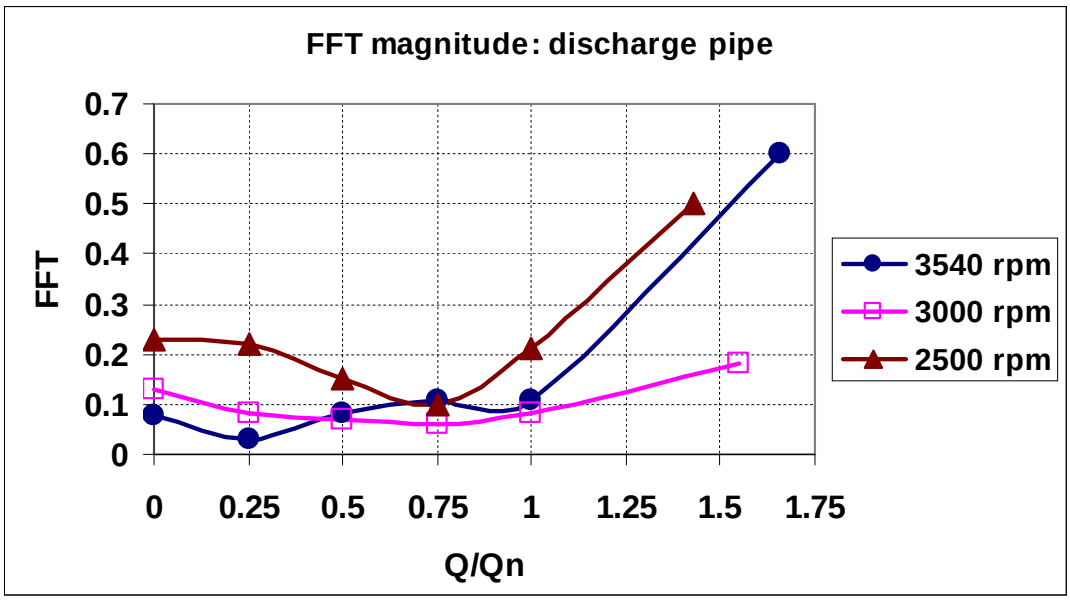

(b)

Figure 3.21 Effect of speed/flow rate on pressure fluctuation and FFT magnitude at pump discharge side

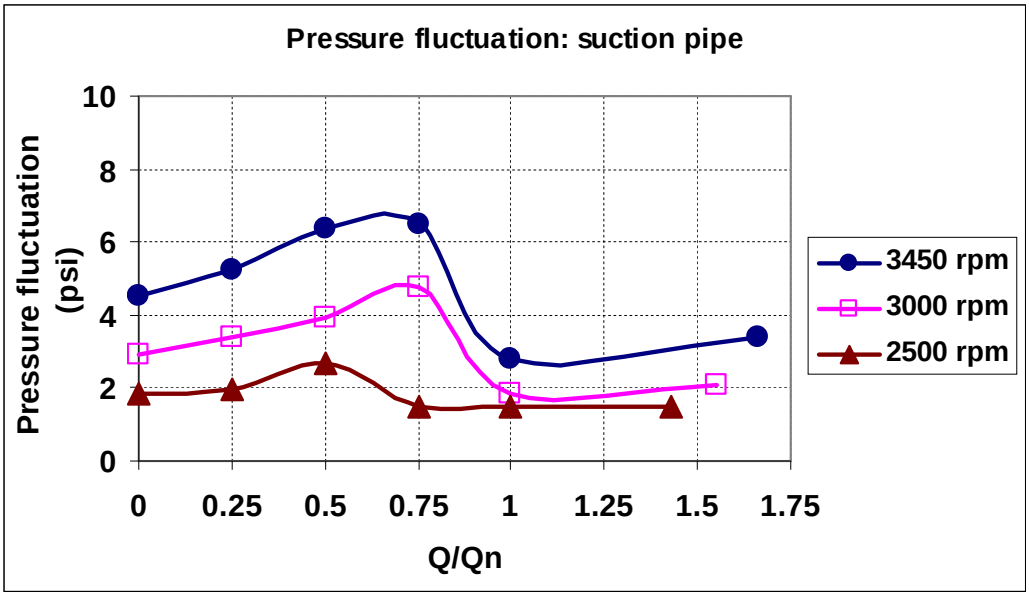

(a)

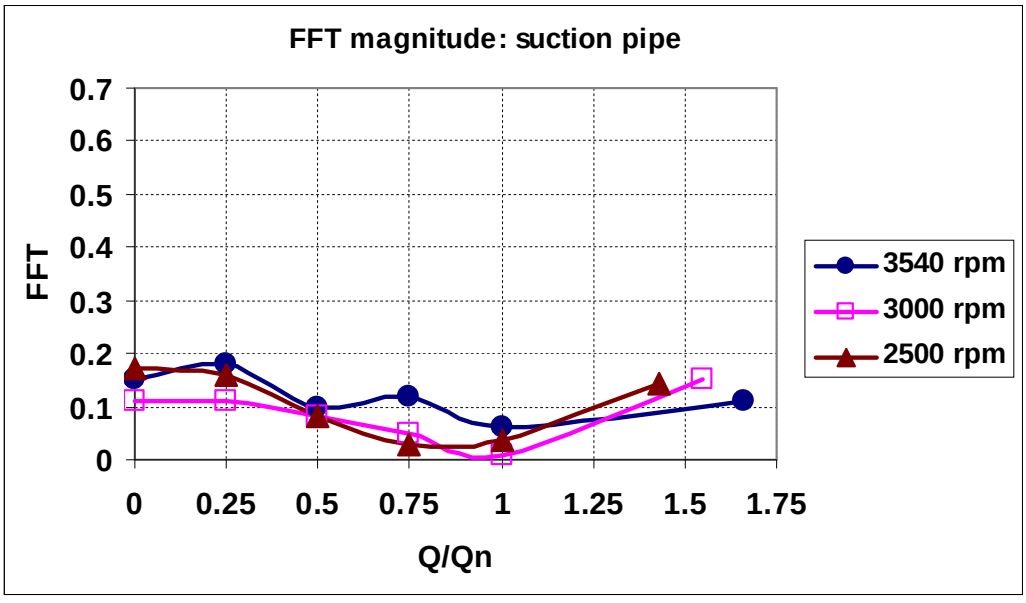

(b)

Figure 3.22 Effect of speed/flow rate on pressure fluctuation and FFT magnitude at pump suction side

3.3 EFFECT OF THE V-SHAPED CUT AT IMPELLER BLADES EXIT

Based on the previous comprehensive analysis for the impeller without V-cut at blade exit, a comparative study was done on the effect of the V-cut at blade exit which exist in the original boiler feed pump impeller. A second (but identical) impeller was manufactured and a V-cut was made according to the selected scale (scale=0.4) as shown in Fig. 3.23. The cut was done by a specially designed cutting tool at KFUPM/ME workshop. The effect of this V-cut on performance, pressure distribution, pressure fluctuation and FFT magnitude, and the vibration of pump casing are presented and discussed in this section.

3.3.1 EFFECT OF THE V-CUT ON PERFORMANCE CURVES

The best efficiency conditions (with calculated uncertainty) for the pump with V-cut at impeller blade exit at a rotational speed of 3540 rpm were measured to be:

- Pump total head = 25.13 m ±0.2511 (or 25.13 m ± 1%)
- Nominal flow rate, Qn = 0.01242 m^3/s ±0.0001769 (or 12.4 L/s ± 1.42%)
- Overall Efficiency = 0.5546 ±0.01102 (or 0.55 ± 2%)

Figure 3.23 Scaled impeller with V-cut at blades exit

Figure 3.24 shows a comparison on the pump performance curves between the impeller with V-cut at blade exit and the impeller without V-cut at blade exit, at three different speeds of 3540, 3000, and 2500 rpm. Based on the best efficiency nominal conditions of the impeller without V-cut at blade exit (Qn=12 l/s, efficiency=55.14 %, and head=26.95 m), the V-cut reduces the head developed by the pump by 5% at the 12 l/s for a speed of 3540 rpm. Equivalent reduction in head was found for a speed of 3000 rpm. At 2500 rpm, the reduction in head due to the existence of the V-cut was around 2% at the corresponding best efficiency flow rate. When the pump operates at off-design flow rates, the head reduction due to the V-cut was slightly increased above the previously mentioned values. The efficiency is reduced by small amount measured to be less than 2% at the best efficiency point for a speed of 3540 rpm and about 1 % for speeds of 3000 rpm and 2500 rpm. The efficiency is more affected by the V-cut if the pump operates at flow rates higher than the nominal ones (corresponding to each speed). The existence of the V-cut reduces the power consumption by the pump by a small amount at the higher speed of 3540 rpm. This may be the reason behind the small loss in efficiency (< 2%) compared to the reduction of 5% in the head. The efficiency loss falls within the calculated uncertainty limit.

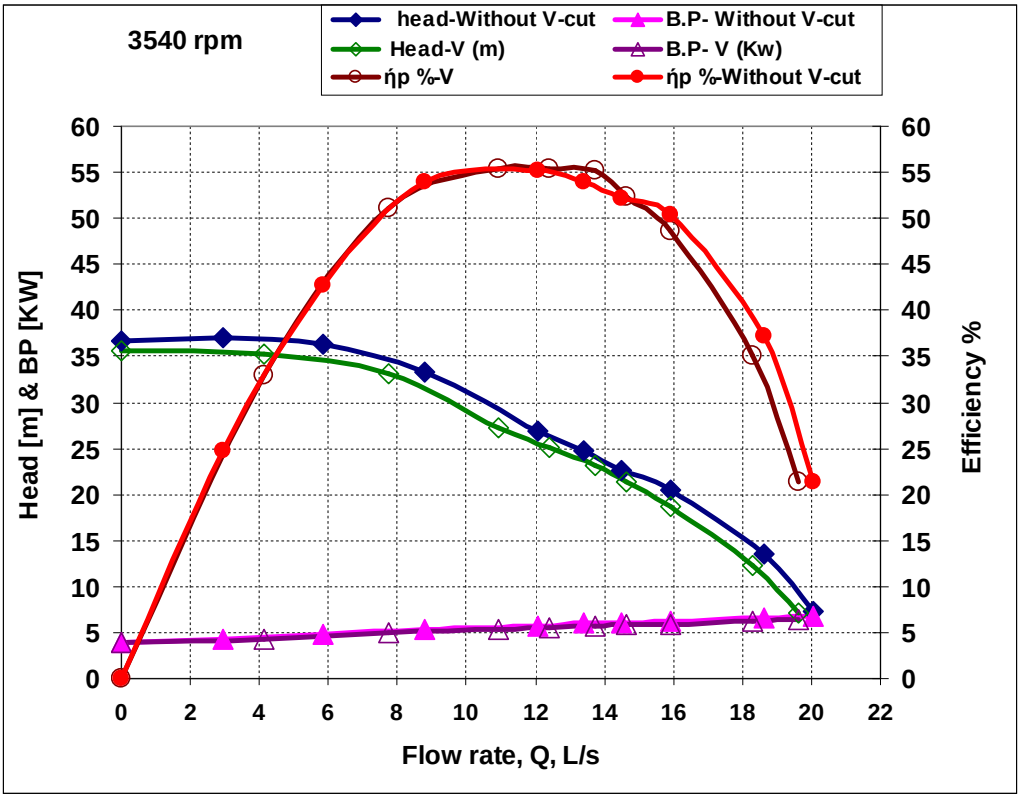
3540 rpm
head-Without V-cut
B.P- Without V-cut
Head-V (m)
B.P- V (Kw)
ήp %-V
ήp %-Without V-cut
Head [m] & BP [KW]
Efficiency %
Flow rate, Q, L/s

(a)

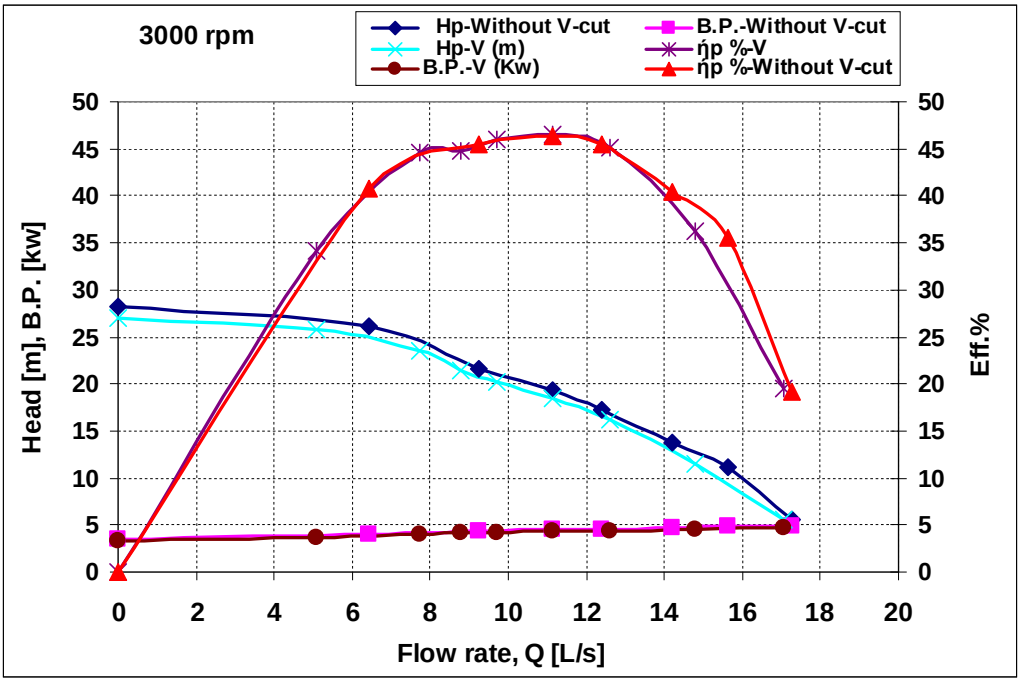
3000 rpm
Hp-Without V-cut
B.P.-Without V-cut
Hp-V (m)
ήp %-V
B.P.-V (Kw)
ήp %-Without V-cut
Head [m], B.P. [kw]
Eff.%
Flow rate, Q [L/s]

(b)

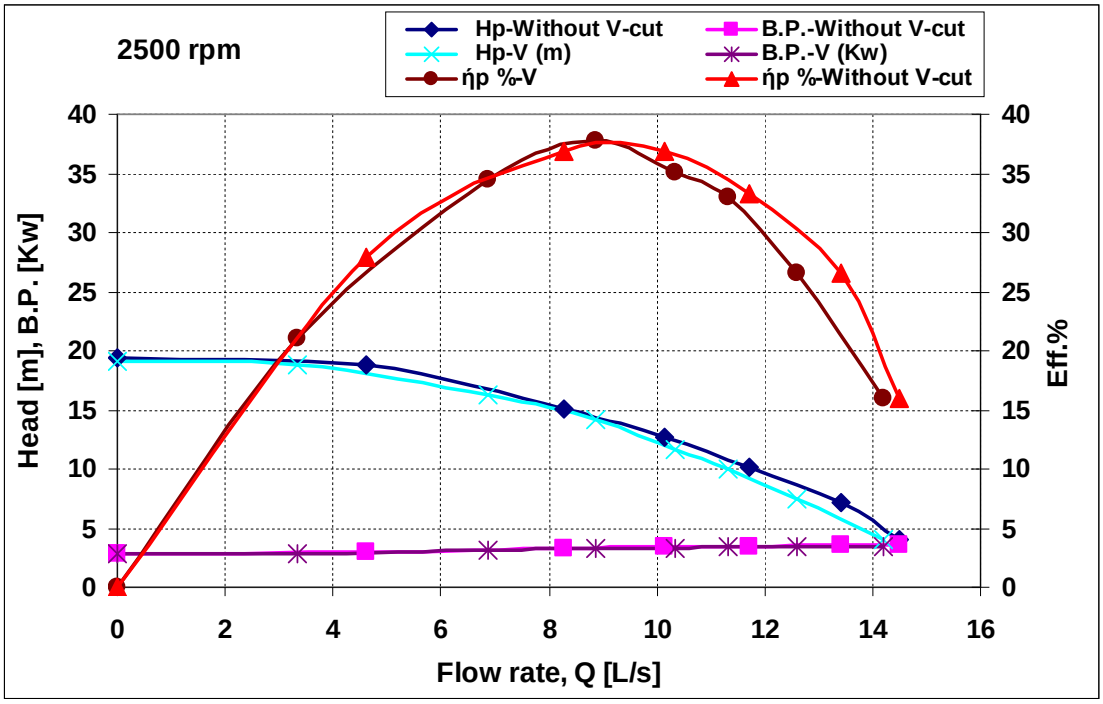

(c)

Figure 3.24 Effect of the V-cut at impeller blades exit on the pump performance at different speeds compared to the case of impeller without V-cut at blade exit

3.3.2 EFFECT OF THE V-CUT ON THE PRESSURE DISTRIBUTION

The V-cut at impeller blade exit was proven to reduce the head developed by 5% as mentioned above. More details about the pressure distributions inside the pump are given in Fig. 3.25 where the static pressures measured at different flow rates, including the max and zero flow rates, at 3540 rpm. When the pump operates at the nominal flow rate, Q=Qn, the pressure inside the pump is the same for the two impellers and the V-cut has no effect on the pressure distribution. This is the reason of getting the minimum loss in head due to the V-cut at the design flow rate. As the flow is reduced, the impeller with V-cut gives lower pressure inside the pump compared to the impeller without the V-cut. Again, the reduction of pressure inside the pump due to the existence of the V-cut is estimated between 5 to 8% when the flow ratio is less than 0.75. At maximum flow rate conditions, the two impellers gave the same pressure distribution but the impeller without the V-cut produced higher flow rate which turns to higher total pump head developed. Figure 3.26 displays the effect of the V-cut on the time averaged pressure value measured at location 3. It is a typical behavior for all locations of measurements inside the pump. Minimum difference in measured pressure for the two impellers was recorded at the best efficiency flow rate. Operating at off-design increases this difference in general and lower flow rates provide the maximum differences.

The effect of the V-cut on static pressure at the discharge side of the pump has been investigated. Figure 3.27 shows that the behavior for the discharge pipe is similar to the pump inside measurements and the V-cut reduced the pressure especially at off-design flow rates.

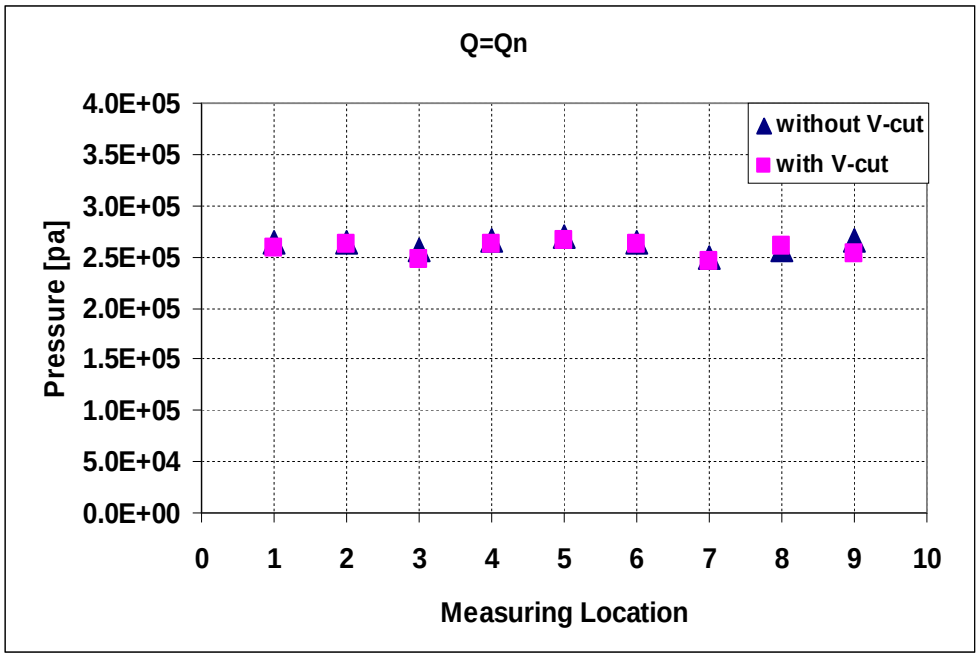
Q=Qn
4.0E+05
3.5E+05
3.0E+05
2.5E+05
2.0E+05
1.5E+05
1.0E+05
5.0E+04
0.0E+00
Pressure [pa]
0 1 2 3 4 5 6 7 8 9 10
Measuring Location
without V-cut
with V-cut

(a)

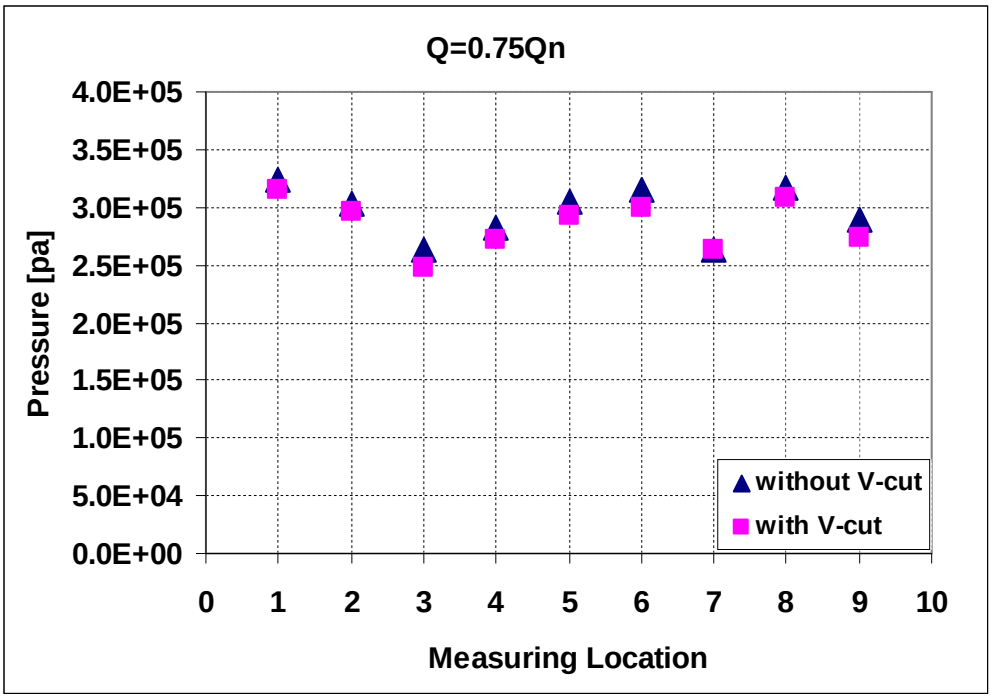
Q=0.75Qn
4.0E+05
3.5E+05
3.0E+05
2.5E+05
2.0E+05
1.5E+05
1.0E+05
5.0E+04
0.0E+00
Pressure [pa]
0 1 2 3 4 5 6 7 8 9 10
Measuring Location
without V-cut
with V-cut

(b)

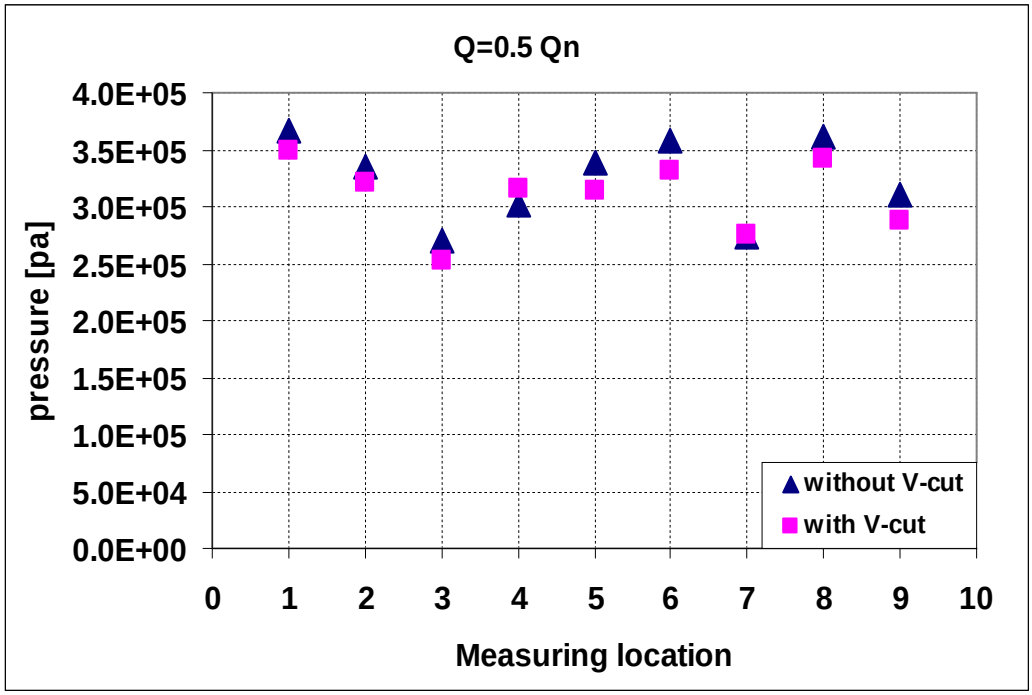
Q=0.5 Qn
4.0E+05
3.5E+05
3.0E+05
2.5E+05
2.0E+05
1.5E+05
1.0E+05
5.0E+04
0.0E+00
pressure [pa]
0
1
2
3
4
5
6
7
8
9
10
Measuring location
without V-cut
with V-cut

(c)

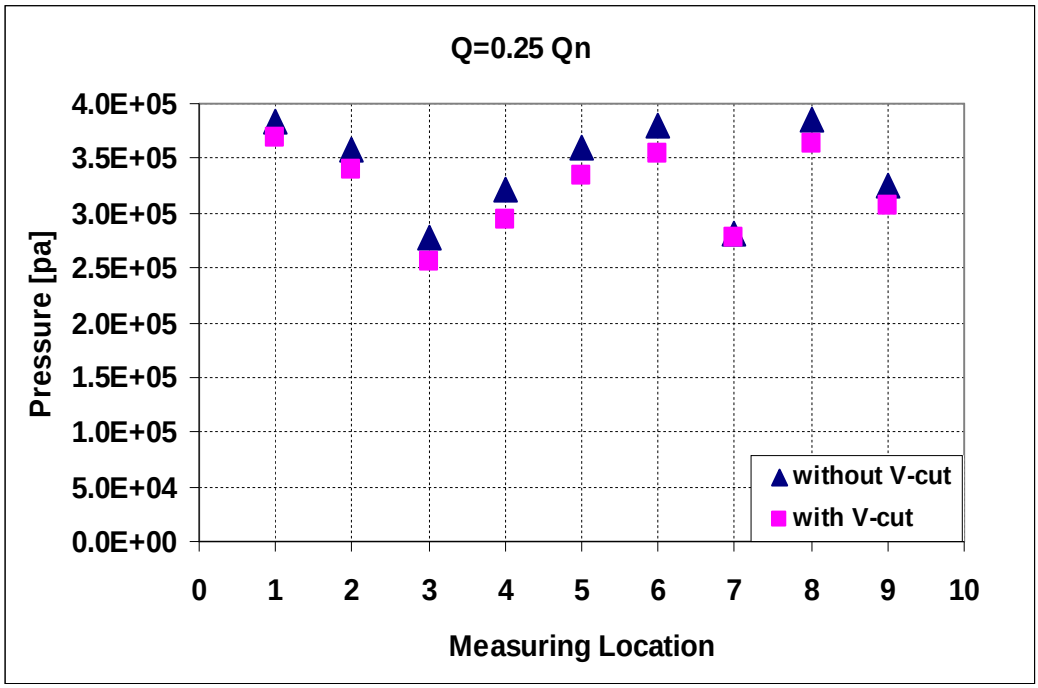
Q=0.25 Qn
4.0E+05
3.5E+05
3.0E+05
2.5E+05
2.0E+05
1.5E+05
1.0E+05
5.0E+04
0.0E+00
Pressure [pa]
0
1
2
3
4
5
6
7
8
9
10
Measuring Location
without V-cut
with V-cut

(d)

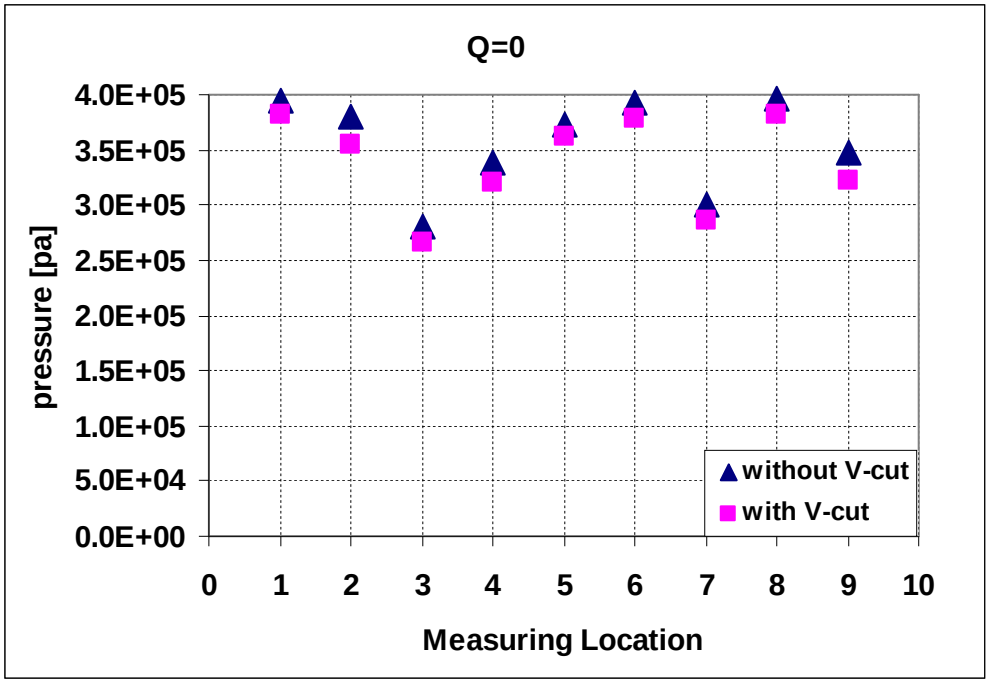

(e)

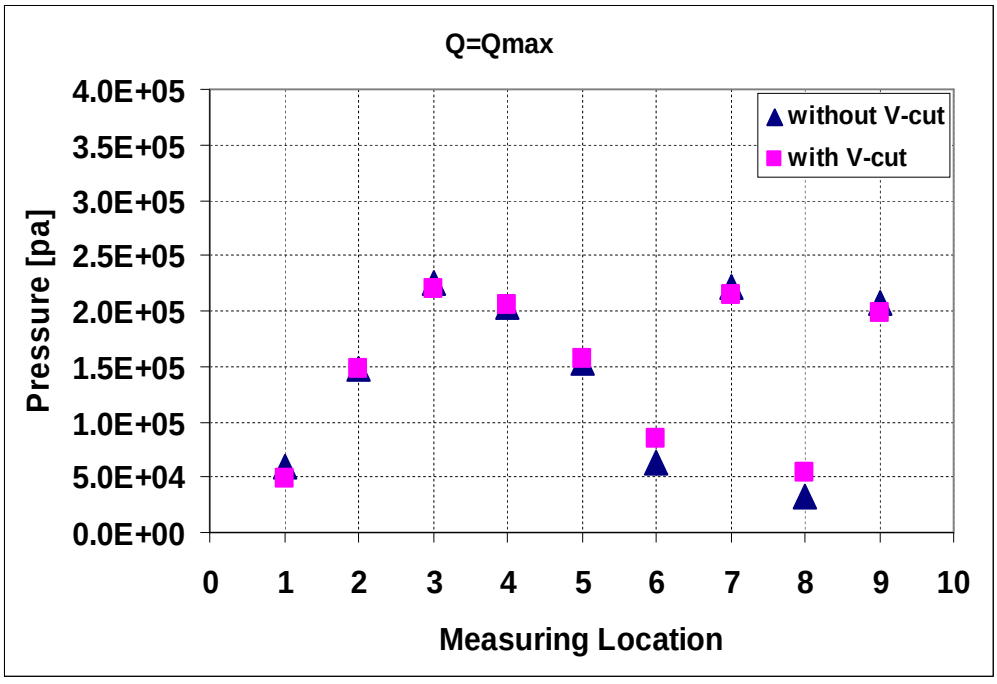

(f)

Figure 3.25 Effect of the V-cut on static pressure distribution inside the pump at different flow rates, 3540 rpm

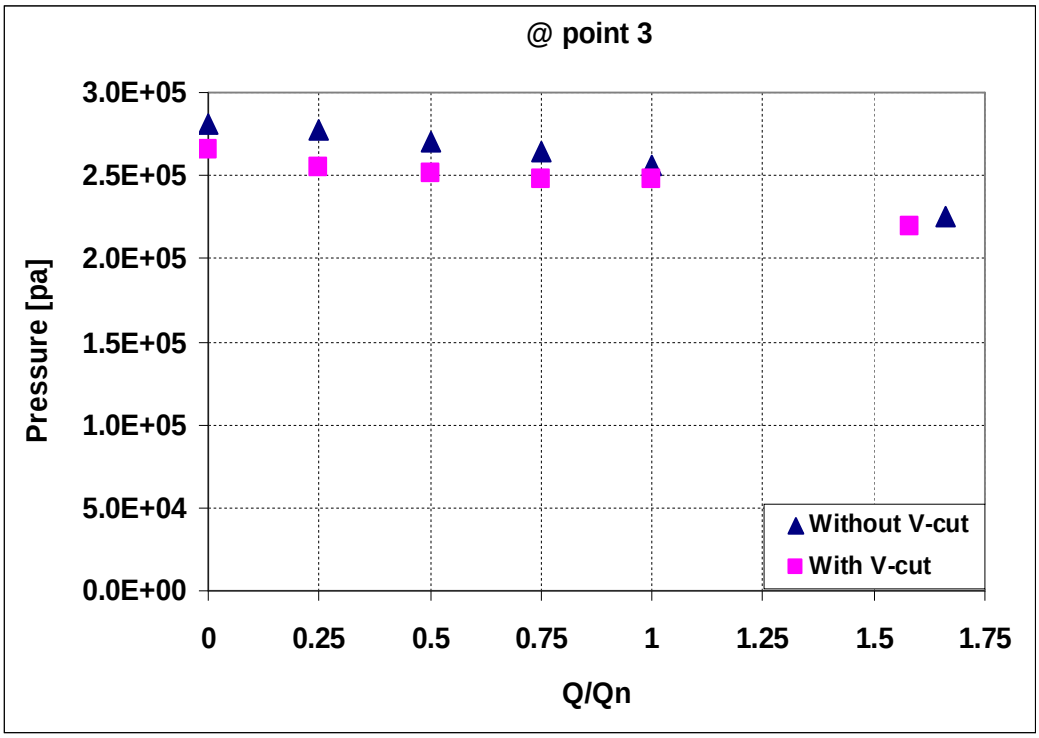

Figure 3.26 Effect of the V-cut on static pressure at location 3 at different flow rates, 3540 rpm

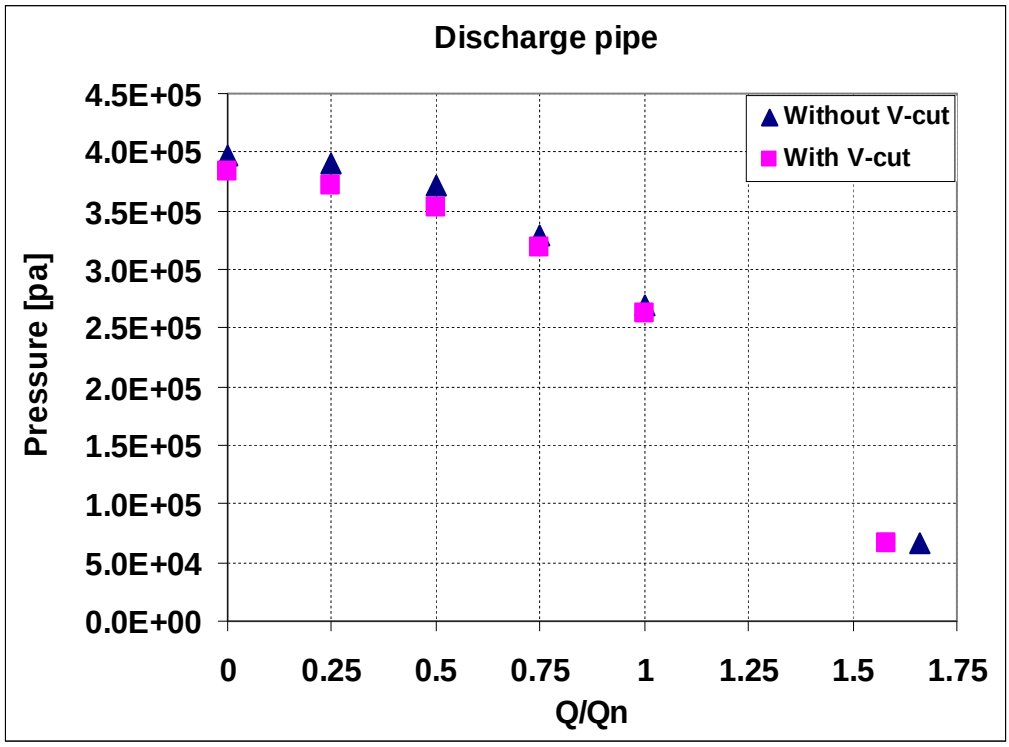

Figure 3.27 Effect of the V-cut on static pressure in discharge pipe, under different flow rates, 3540 rpm

3.3.3 EFFECT OF THE V-CUT ON THE PRESSURE FLUCTUATIONS

The two impellers, without and with V-cut blade exits, were tested for the pressure fluctuations inside the pump. Figure 3.28 shows the amplitude (peak-to-peak) of the unsteady pressure fluctuations at all measuring locations inside the pump at different flow rates. The V-cut is effective in reducing the fluctuations at all measurement locations. A special case was found at Q/Qn=0.75 where the effect of V-cut on fluctuations is minimum. At flow rates less than 75%, a reduction of 30 to 45% in fluctuations was measured (depending on the location and flow rate) due to the existence of the V-cut. The impeller with the V-cut gave lower fluctuations at the limits of zero and maximum flow rates. To complete the analysis of pressure fluctuations, the effect of the V-cut on the FFT magnitude, at 1st blade passing frequency, is shown in Fig. 3.29. The energy contents of the fluctuations are dependent on flow rate and measuring location. At the nominal flow rate, the FFT magnitude is equivalent for both impellers (without and V-cut). At off-design flow rates, the existence of the V-cut reduces the FFT magnitudes and it was found to be very effective at flow rates lower than 75%. It is also effective at maximum and zero flow rates, but the magnitudes at these limiting conditions are very high. Again, it is not recommended to operate the pump under these limiting conditions.

The V-cut design was able to reduce the FFT magnitude at the suction and discharge pipes as shown in Fig. 3.30. The reduction in the FFT magnitude was clearer in the suction pipe than the discharge pipe at reduced flow rates.

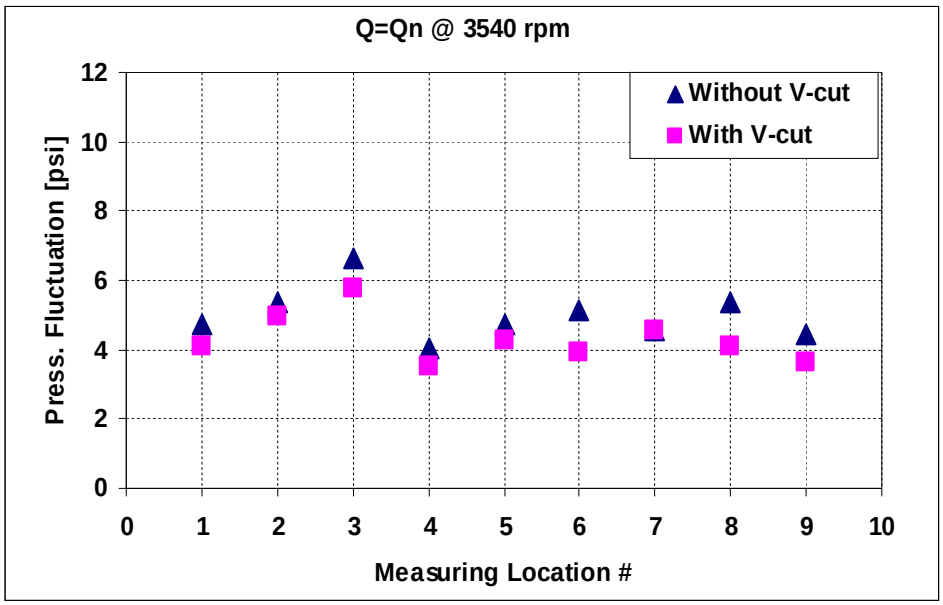
Q=Qn @ 3540 rpm
Without V-cut
With V-cut
Press. Fluctuation [psi]
Measuring Location #
0
2
4
6
8
10
12
0
1
2
3
4
5
6
7
8
9
10

(a)

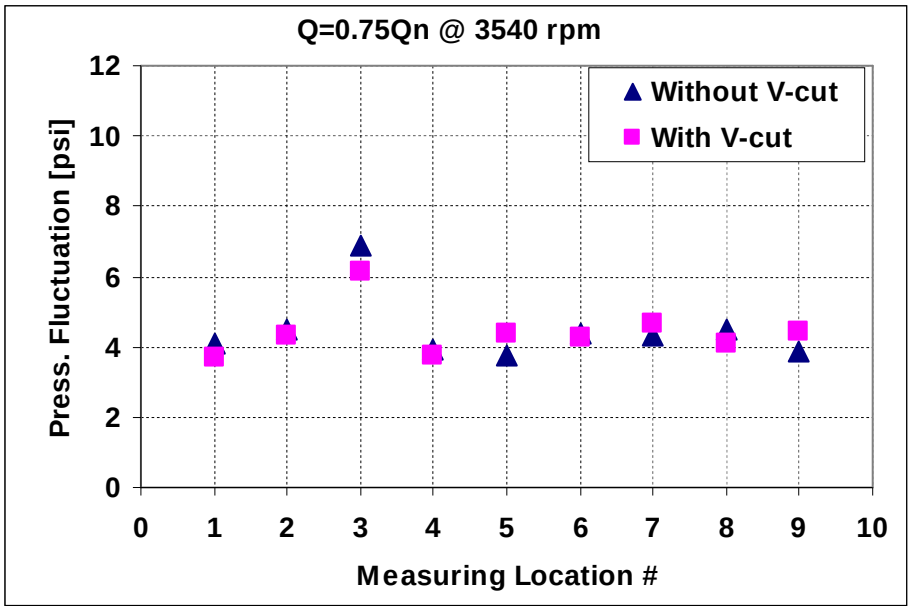
Q=0.75Qn @ 3540 rpm
Without V-cut
With V-cut
Press. Fluctuation [psi]
Measuring Location #
0
2
4
6
8
10
12
0
1
2
3
4
5
6
7
8
9
10

(b)

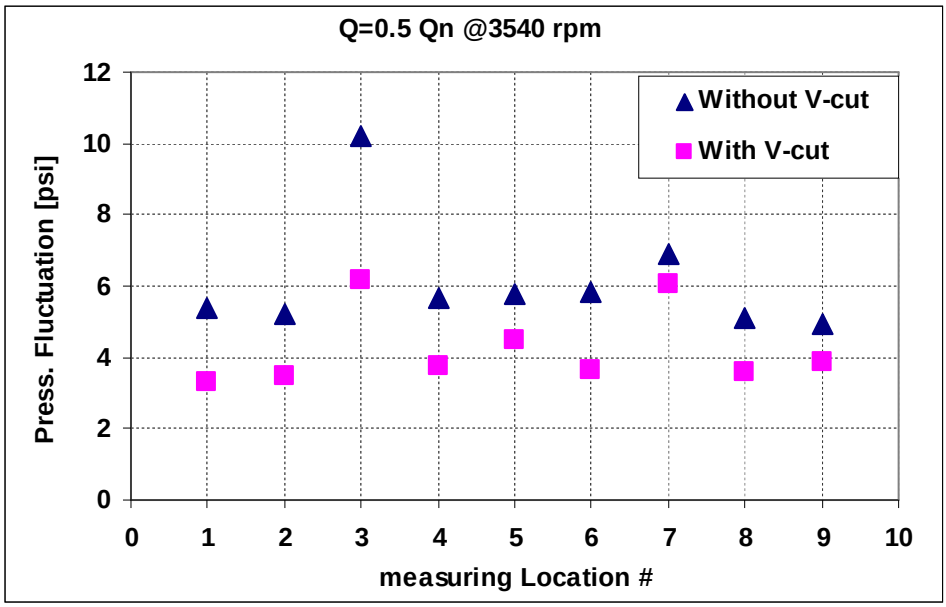
Q=0.5 Qn @3540 rpm
Without V-cut
With V-cut
Press. Fluctuation [psi]
measuring Location #
0
2
4
6
8
10
12
0
1
2
3
4
5
6
7
8
9
10

(c)

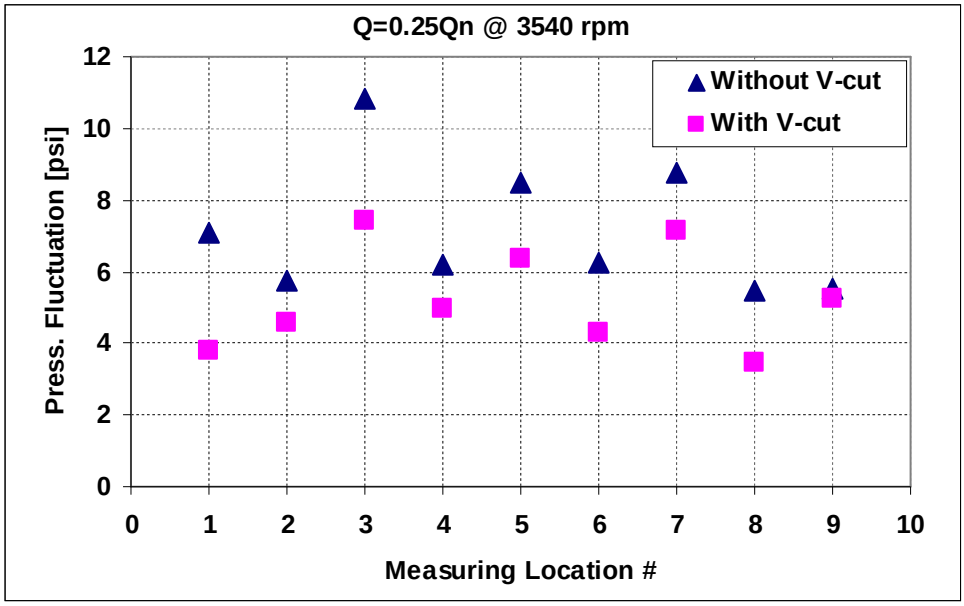
Q=0.25Qn @ 3540 rpm
Without V-cut
With V-cut
Press. Fluctuation [psi]
Measuring Location #
0
2
4
6
8
10
12
0
1
2
3
4
5
6
7
8
9
10

(d)

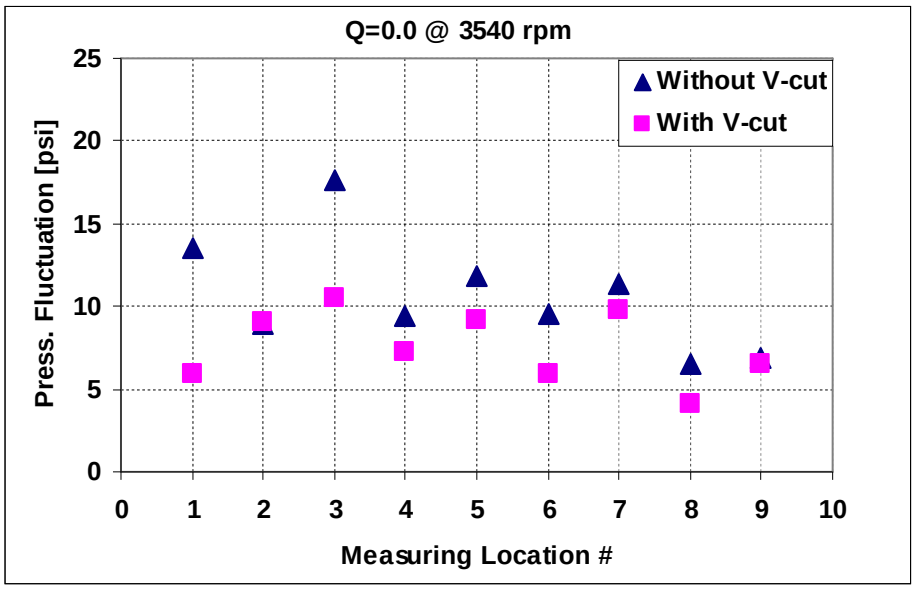

(e)

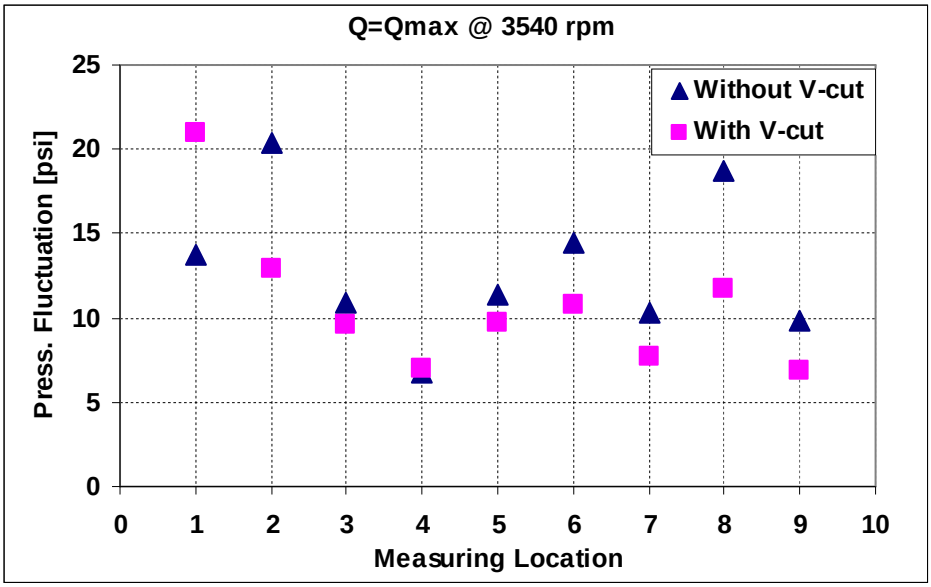

(f)

Figure 3.28 Effect of the V-cut on static pressure distribution inside the pump at different flow rates, 3540 rpm

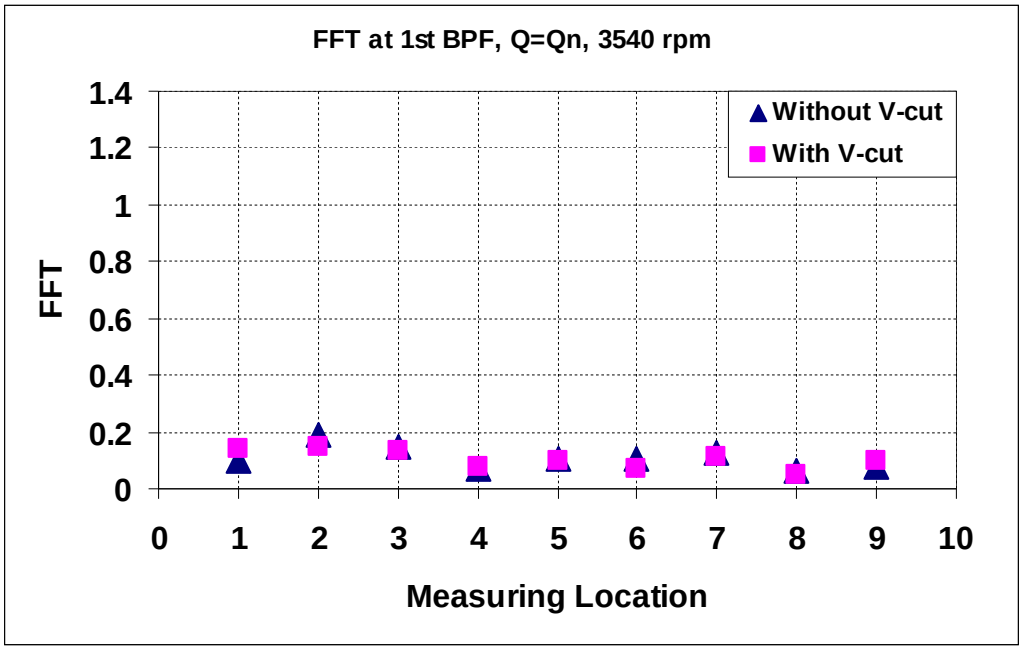
FFT at 1st BPF, Q=Qn, 3540 rpm
FFT
Measuring Location
Without V-cut
With V-cut
1.4
1.2
1
0.8
0.6
0.4
0.2
0
0 1 2 3 4 5 6 7 8 9 10

(a)

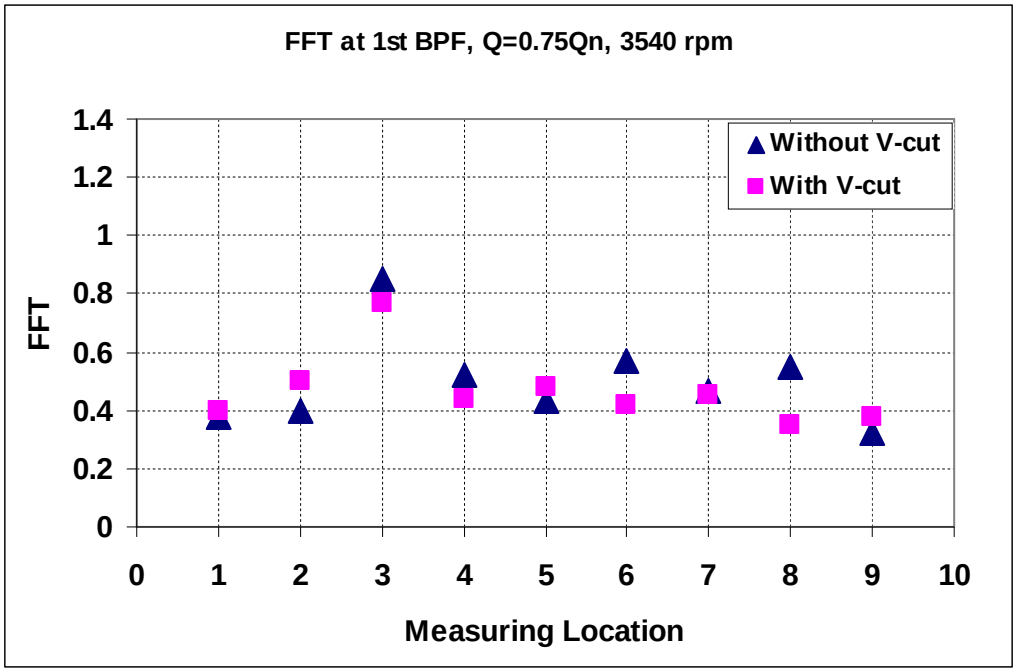
FFT at 1st BPF, Q=0.75Qn, 3540 rpm
FFT
Measuring Location
Without V-cut
With V-cut
1.4
1.2
1
0.8
0.6
0.4
0.2
0
0 1 2 3 4 5 6 7 8 9 10

(b)

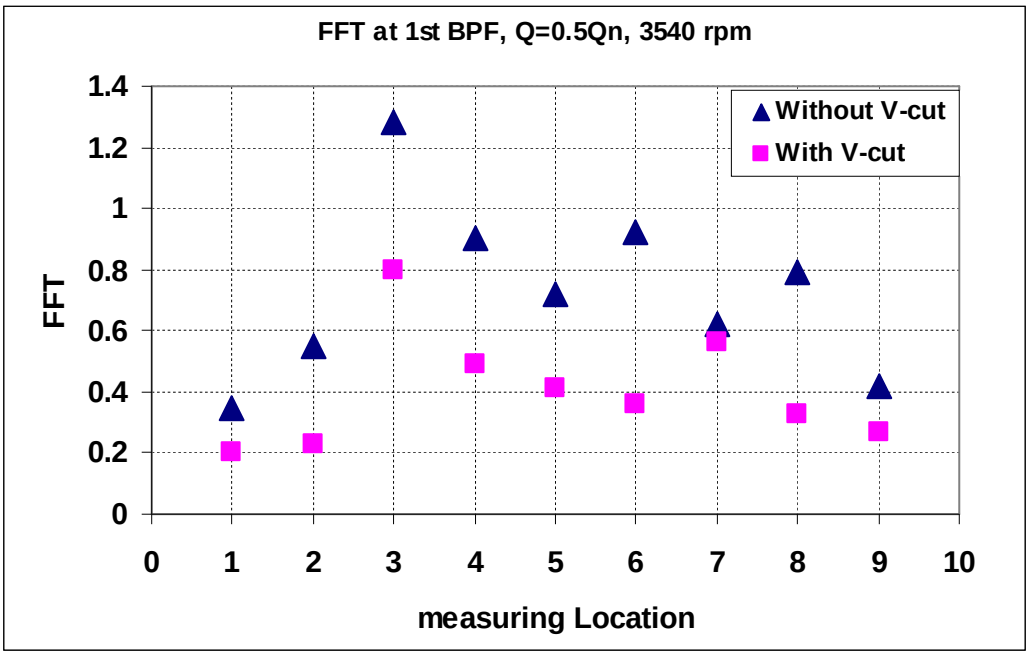
FFT at 1st BPF, Q=0.5Qn, 3540 rpm
Without V-cut
With V-cut
FFT
1.4
1.2
1
0.8
0.6
0.4
0.2
0
0 1 2 3 4 5 6 7 8 9 10
measuring Location

(c)

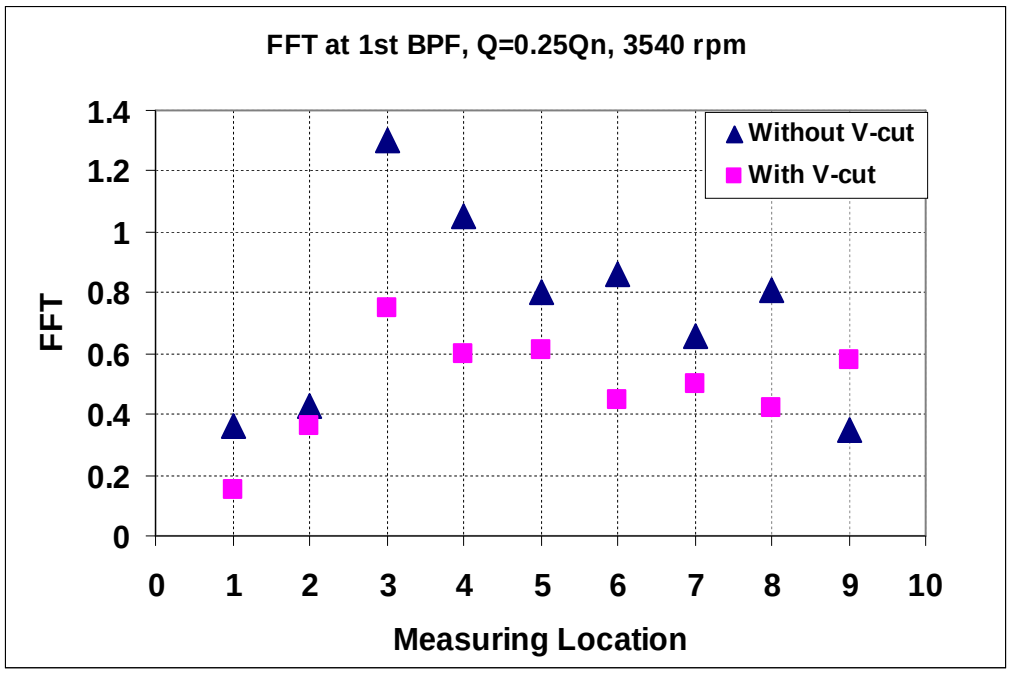
FFT at 1st BPF, Q=0.25Qn, 3540 rpm
Without V-cut
With V-cut
FFT
1.4
1.2
1
0.8
0.6
0.4
0.2
0
0 1 2 3 4 5 6 7 8 9 10
Measuring Location

(d)

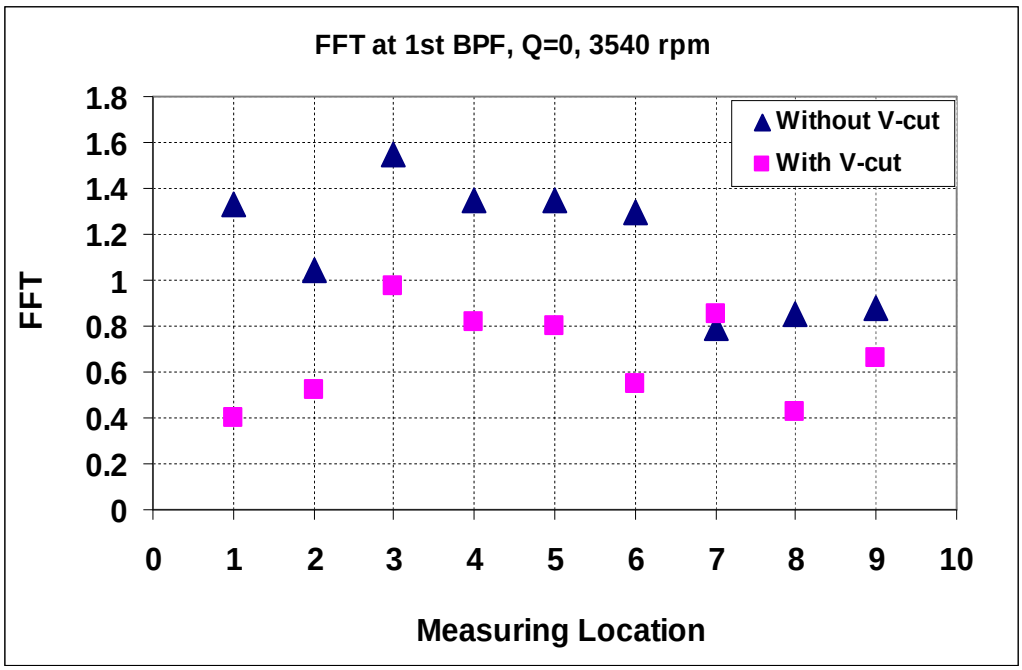

(e)

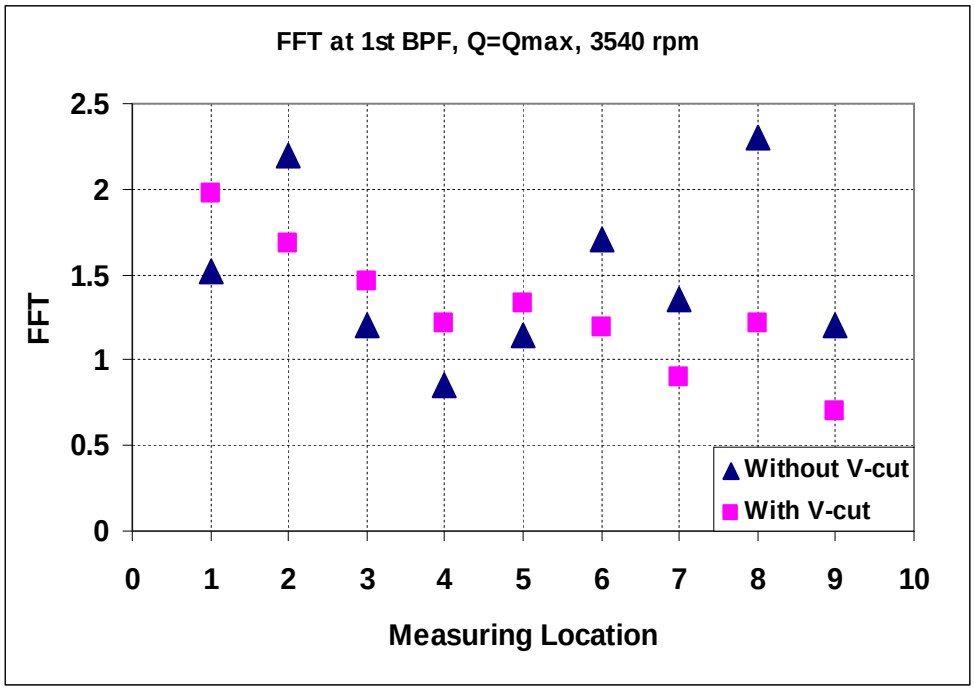

(f)

Figure 3.29 Effect of the V-cut on the FFT magnitude inside the pump, measured at the 1st BPF (5xRPM) at different flow rates, 3540 rpm

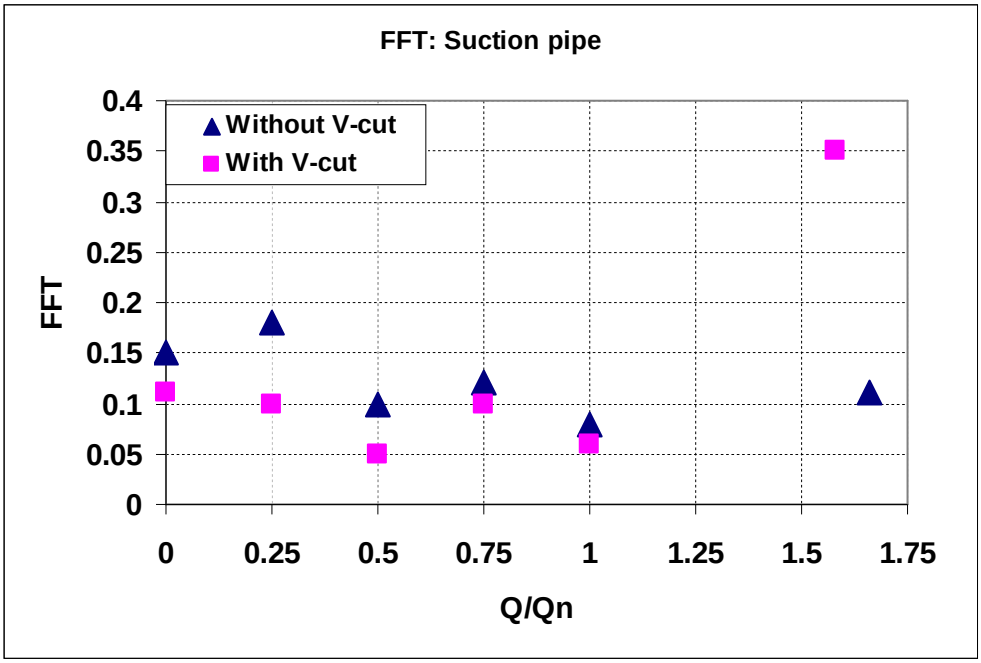

(a)

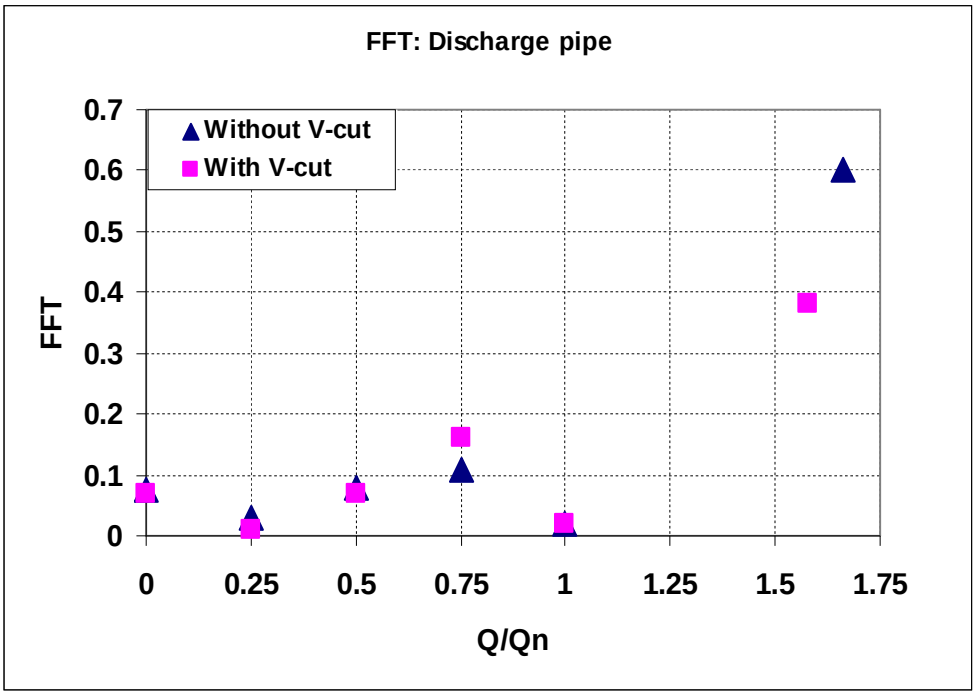

(b)

Figure 3.30 Effect of the V-cut on the FFT Magnitude (measured at 1st BPF) in suction and discharge pipes, under different flow rates, 3540 rpm

3.3.4 EFFECT OF THE V-CUT ON THE PUMP VIBRATION

The vibration of the pump casing (0 ~ peak) was recorded after installing the impeller with the V-cut at its blade exit as shown in Fig. 3.31, at different flow rates. As the flow rate is shifted from the best efficiency conditions, the vibrations increase. Similar behavior to what was found for the impeller without the V-cut at variable flow rates but with smaller vibration magnitudes. The vibration of the pump casing was reduced by 20 to 50 % (depending on the flow rate) when the V-cut was implemented as shown in Fig. 3.32. The V-cut is effective in reducing the pressure fluctuations inside the pump volute and the vibration of the pump casing, particularly at off-design flow rates.

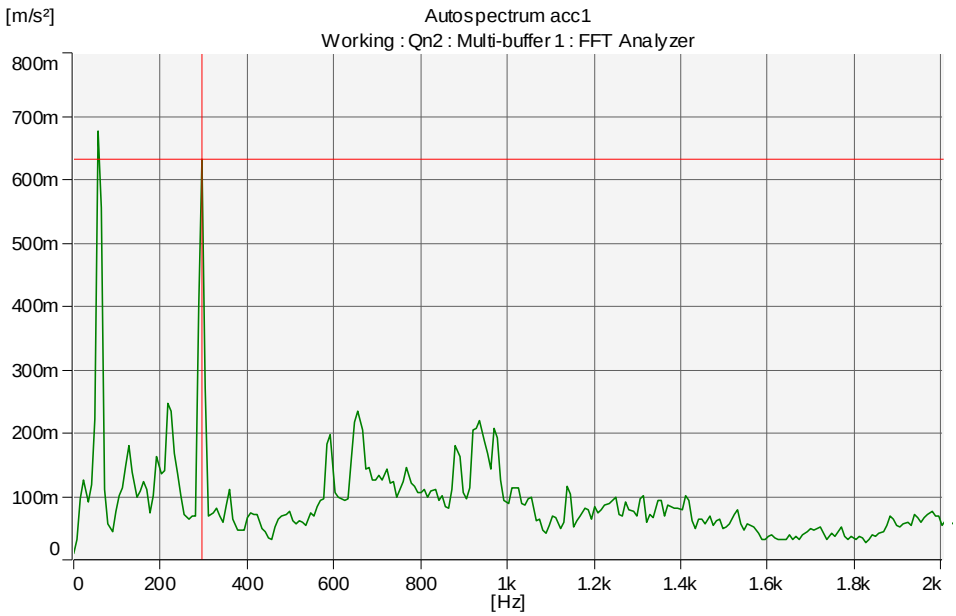

(a) Q=Qn

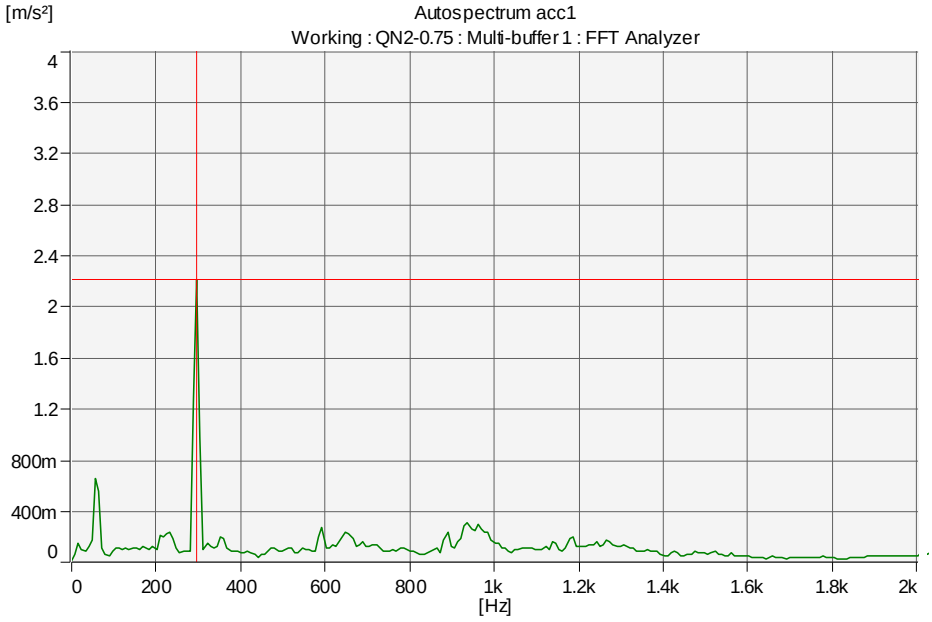

(b) Q=0.75Qn

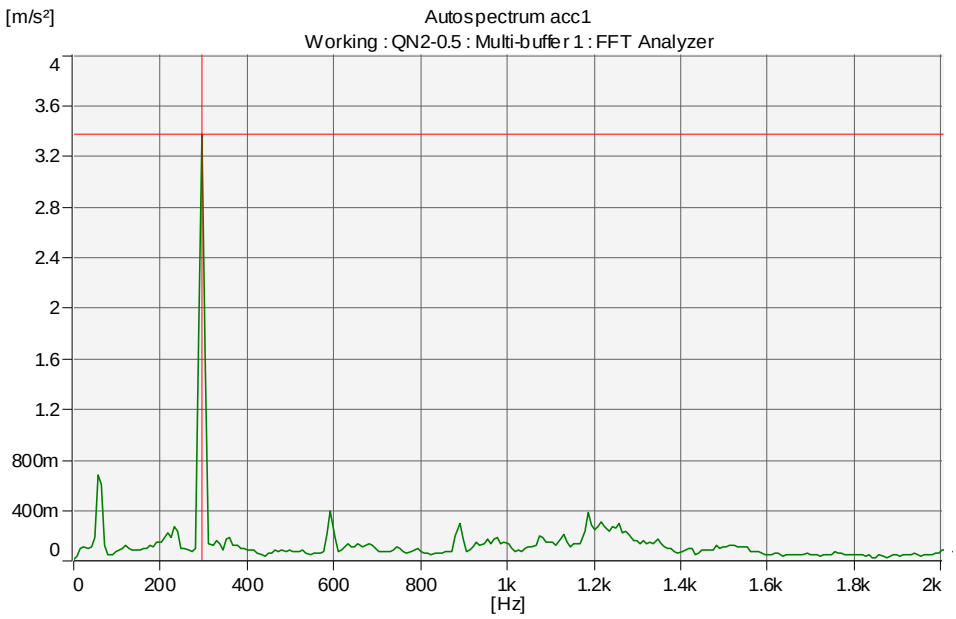

(c) Q=0.5Qn

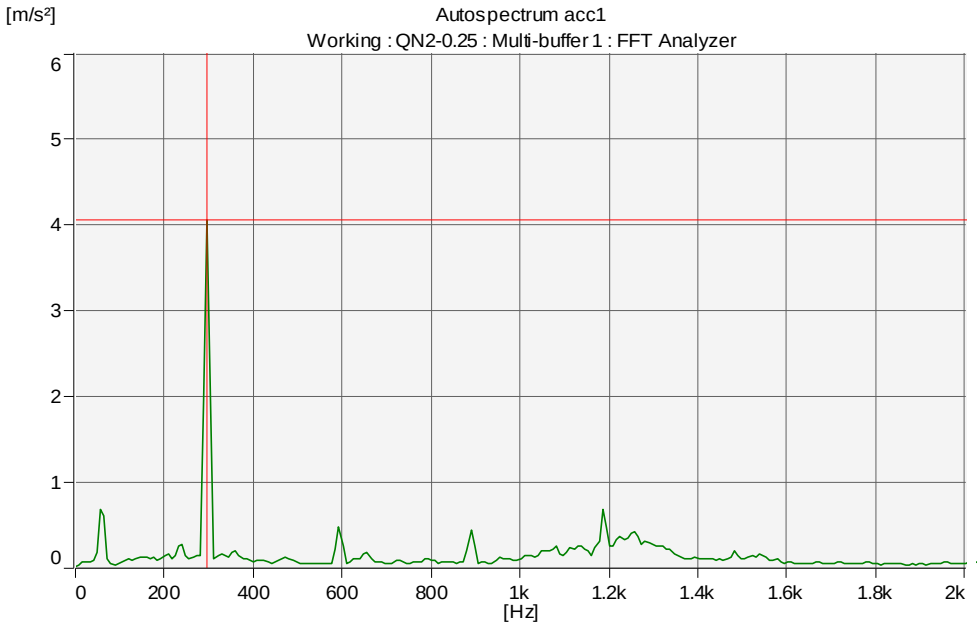

(d) Q=0.25Qn

Figure 3.31 Vertical vibrations of the pump casing with the V-cut at 3540 rpm

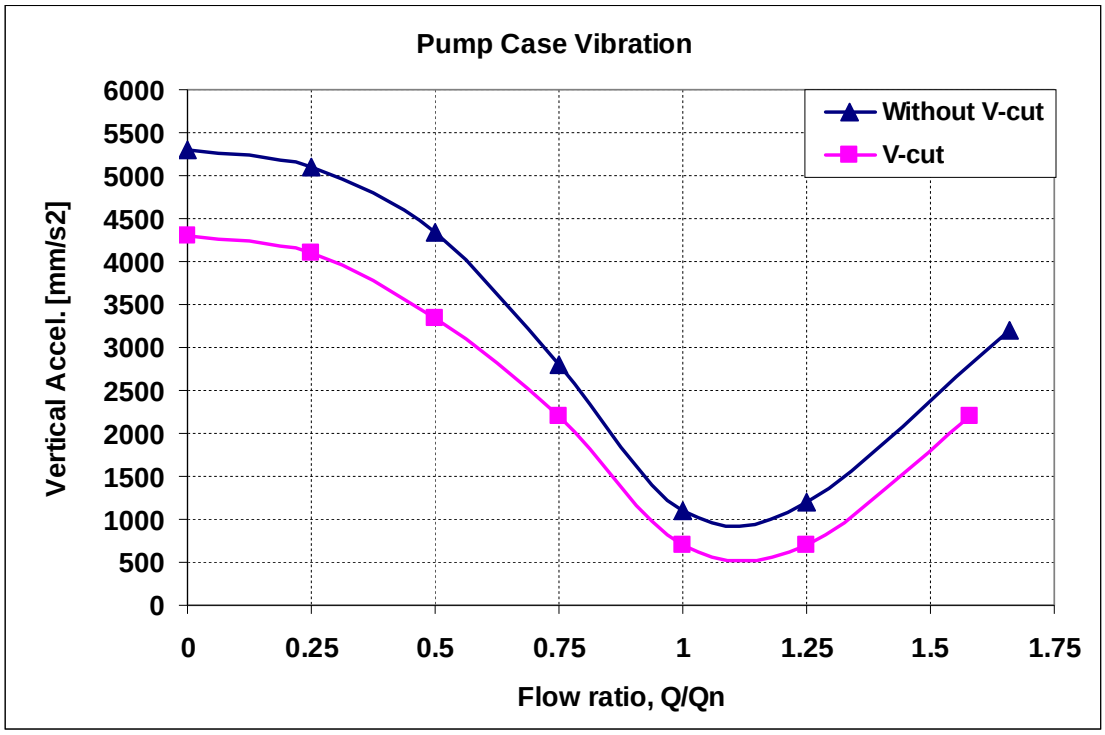

Figure 3.32 Effect of the V-cut on pump vertical vibration at 3540 rpm

3.4 EFFECT OF THE RADIAL GAP ON THE FLOW INDUCED VIBRATION

One of the main sources of flow-induced vibration problems in high-pressure pumps is the inconvenient minimum radial gap between impeller blades and volute vanes leading edges. Very small gap may initiate strong impeller/volute interaction resulting in high pressure pulsation inside the pump and high vibrations appear on the pump case. The special V-cut at impeller blade exit has been proved to be effective in reducing the pressure pulsation inside the pump and consequently the vibration of the pump casing with small effect on the pump performance. However, the prototype boiler feed pump still suffering high vibration levels even with the existence of the V-cut design. Another design modification, with the V-cut, is needed to reduce the vibration levels to the acceptable limits. Different radial gaps between impeller outer diameter and volute vanes were tested experimentally to study the effect of the gap on pressure, fluctuations, case vibration, and performance. Ultimately, a simple applicable solution is desired to minimize the problem of the high flow-induced vibration problem at blade the first passing frequency. The impeller diameter for the model pump is 142.1 mm and the original gap design is 3.6 mm which means that the ratio of this gap to the impeller diameter is 2.5 %. This gap value (3.6 mm) was changed by extending the volute splitters to achieve smaller gaps and cutting the splitters back for larger gaps. This process is accompanied by changing the location/angle of the volute cutwaters.

Gaps of 2, 3, 4.85, 6, and 7 mm were examined and compared with the original gap design (3.6 mm) for the pressure pulsation inside the pump at different flow rates and

to assess their effect on pump performance. This is equivalent to changing the gap from 1.4% (2 mm) to 5% (7 mm) of the impeller diameter. Experiments were carried for both impellers, without and with V-cut at blade exit.

Figure 3.33 shows the process of decreasing the original gap design by extending the volute vanes. A simple mold was produced by wormed candle wax around the vane to keep the same vane curvature for the extension. After drying, the mold was then filled with epoxy and the resulted extension was cleaned after being solid. Extension of 10 mm length decreased the gap from 3.6 mm to 3 mm. Another extension of 10 mm length was required to decrease the gap to 2 mm. Increasing the gap was carried out by cutting back the volute vanes using a milling machine. Consecutive gaps of 4.85, 6, and 7 mm were achieved by cutting back the original volute vanes of the model pump in steps. Each step represents the cutting of 10 mm from the vane leading edge. For example, the maximum gap of 7 mm was achieved by cutting back 30 mm in the vertical direction as shown in Fig. 3.34. The measuring locations are fixed for all tested gaps. Results regarding the effect of changing the radial gap between the impeller outer diameter and volute vanes leading edges are presented in this section. First we will consider the impeller without V-cut at blade exit. The effect of changing the gap on performance, static pressure distribution, pressure fluctuations and their FFT magnitudes, and the vibration of the pump casing at limiting gap design are presented. Later, similar results related to the impeller having the V-cut at blade exit are considered. When the analysis for the performance is combined with the analysis of pressure fluctuations and case vibration, selection of the most effective gap design (optimum gap) will be available.

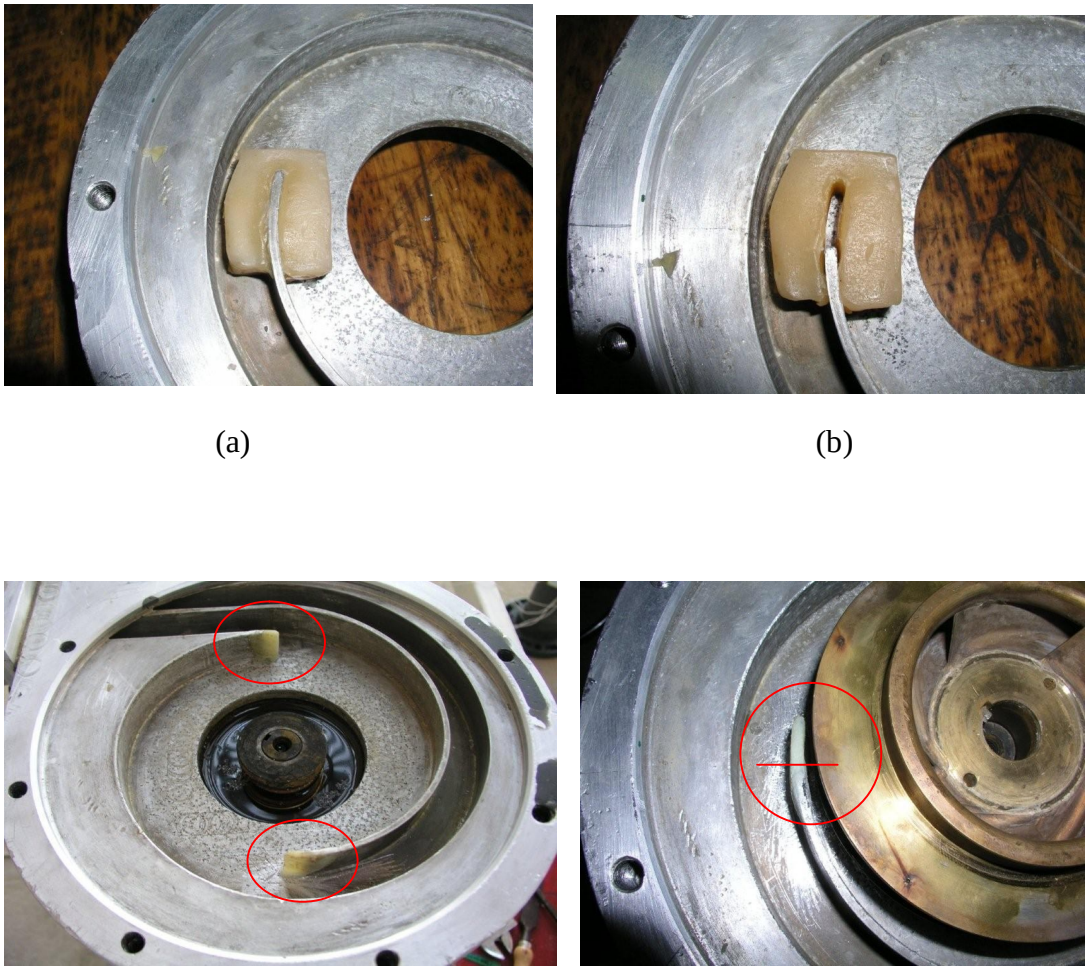

(a) (b)

(c) (d)

Figure 3.33 Extending the volute vanes to decrease the radial gap

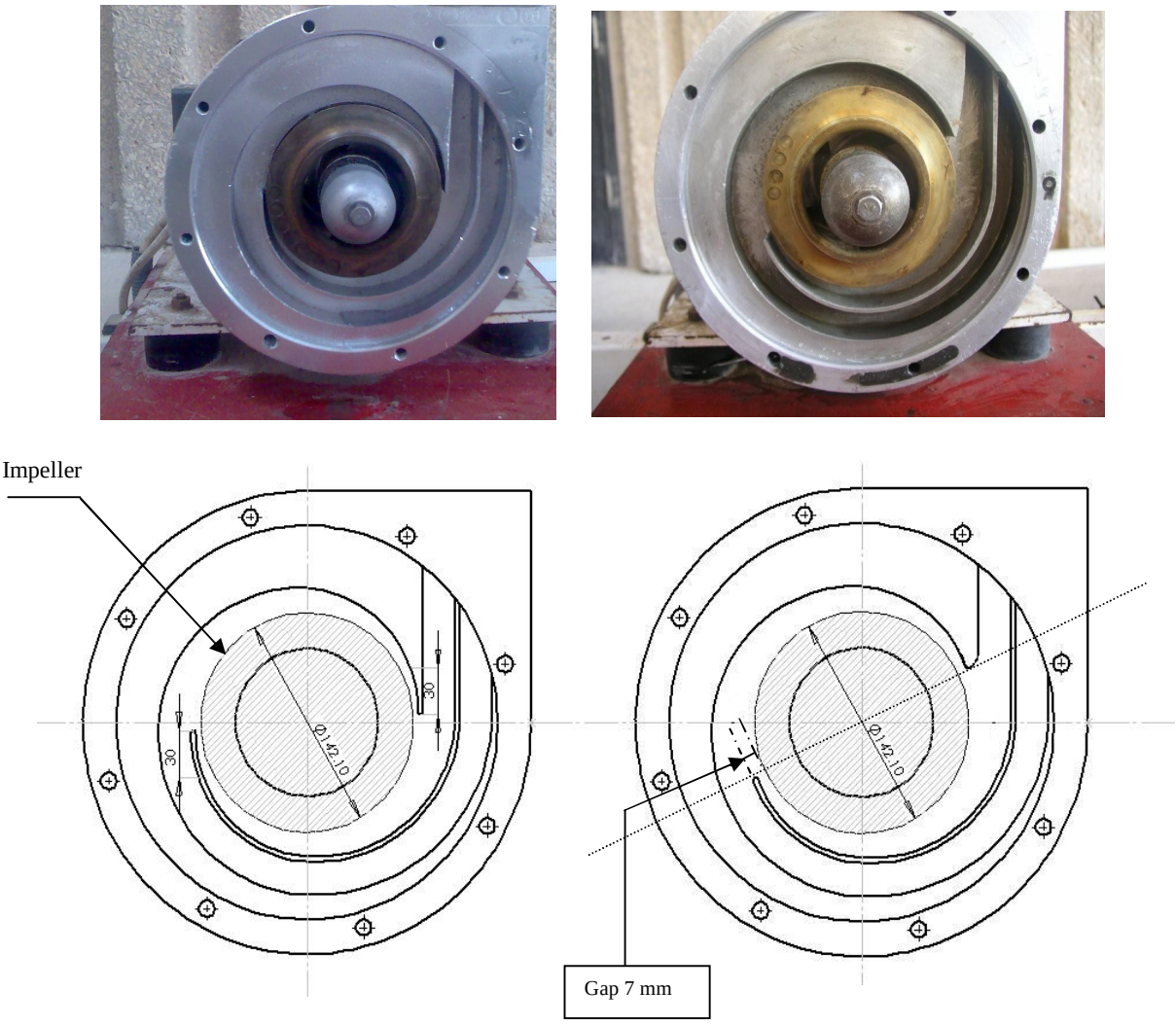

Figure 3.34 Cutting back the volute vanes to increase the gap
(a) Original gap of 3.6 mm (2.5%); and (b) the max gap of 7 mm (5%)

3.4.1 IMPELLER WITHOUT V-CUT AT BLADE EXIT

Figure 3.35 shows the effect of gap design on the pump performance; head and efficiency for the impeller without V-cut at blade exit. The Figure was split into two parts for simplification. At the best efficiency conditions, all gap designs are relatively comparable in performance. Decreasing the gap from 3.6 mm (original design) to 2 mm did not improve the head or the efficiency. Smaller gaps are not recommended for performance at lower flow rates while larger gaps are not recommended at higher flow rates. The original gap design of 3.6 mm (2.5% of the impeller diameter) is considered to be satisfactory for performance over a wide range of flow rates. It should be mentioned here that the comprehensive analysis for uncertainty calculations is based mainly on zero order replication. However, it is actually a first order replication type. For example, the rotational pump speed at 60 Hz was measured to be variable within 10 rpm (about 0.3 % of pump speed) at different times of the day and from gap to gap testing due to re-installation. This variation in the pump speed provides higher uncertainty limits for the head and efficiency. Figure 3.36 gives the variation of pump head and efficiency for different gaps at constant flow rate of 12 L/s (Qn for impeller without V-cut at blade exit). The figure also contains a numeral table for pump performance at different gaps. The error bars (uncertainty limits) are indicated on the figure for the original gap (3.6 mm) as calculated in the detailed uncertainty analysis. Based on uncertainty limits and measured performance, we may conclude that the change in pump performance with different gaps under consideration is negligible, except for pump head at large gap of 7 mm.

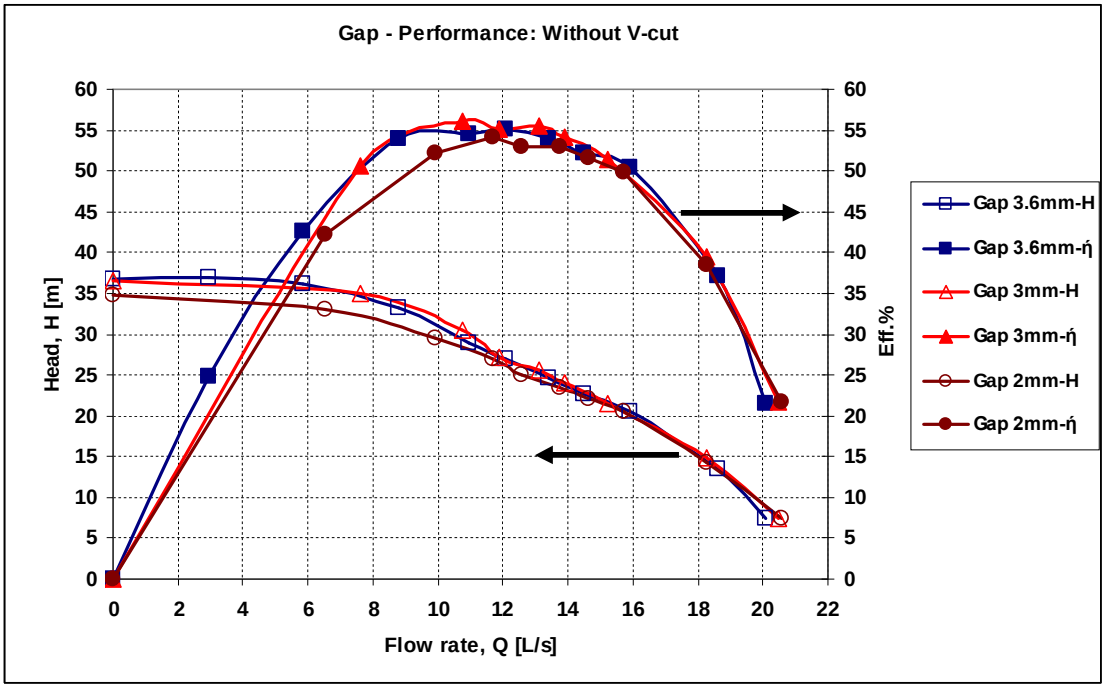

(a)

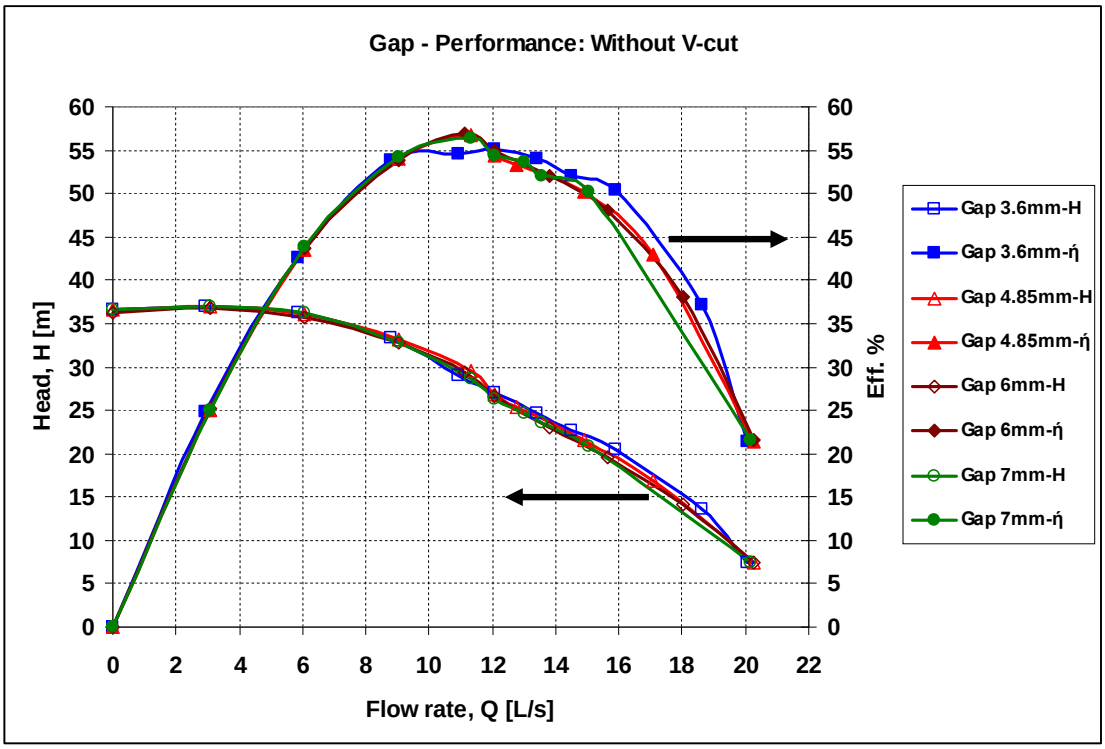

(b)

Figure 3.35 Pump performance at 3540 rpm under different gaps: impeller without V-cut at blade exit

Flow rate = 12 Lit/sec				
Gap (mm)	Head (m)	Efficiency	% change in head	% change in efficiency
2	26.6	54.1	-1.298	-1.88
3	27.1	55.2	0.556	0.108
3.6	26.95 ± 1%	55.14 ± 2%	---	----
4.85	26.91	54.39	-0.148	-1.360
6	26.7	54.86	-0.927	-0.507
7	26.3	54.35	-2.411	-1.432

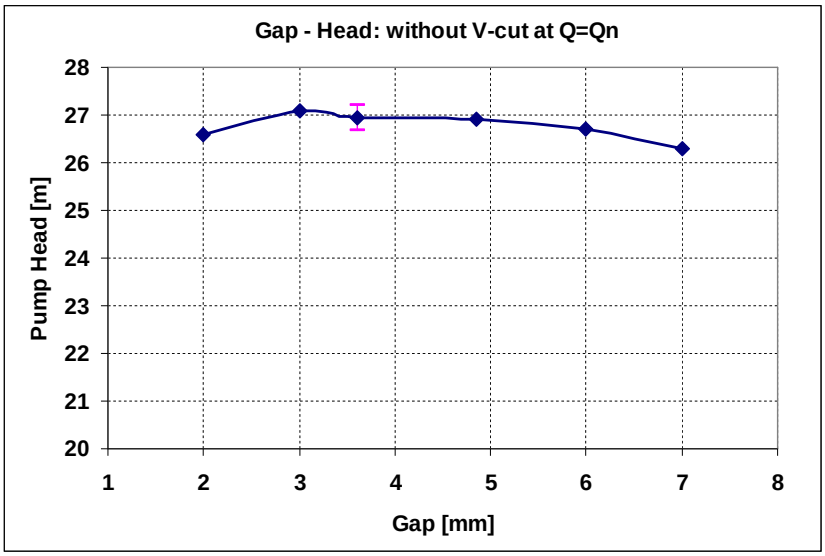

(a)

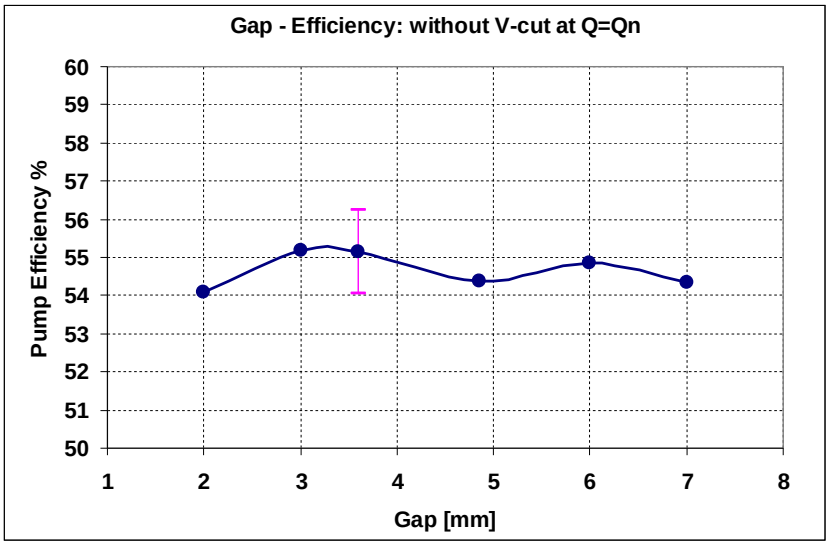

(b)

Figure 3.36 Effect of gap design on head and efficiency at Q=Qn: Without V-cut

The pump head may be investigated more deeply by looking to the pressure distribution. The distribution of the static pressure inside the pump volute is presented in Fig. 3.37. The maximum gap of 7 mm and minimum gap of 2 mm are compared with the original gap of 3.6 mm at two different representative flow rates. Gaps in between are falling within the limits.

At the design flow rate, the pressure is almost uniform with comparable averaged values for all gaps. At 50% of the nominal flow rate, the original gap of 3.6 mm gave the most uniform distribution and the highest average pressure inside the pump. Gaps of 2 mm and 7 mm reduced the average pressure and the smaller gap of 2 mm gave the lowest pressure inside the pump. The effect of decreasing the gap on the pressure fluctuations inside the pump volute is shown in Fig. 3.38, at different flow rates. Similarly, the effect of increasing the gap on the pressure fluctuations inside the pump volute is shown in Fig. 3.39, at different flow rates. Smaller gaps produced higher fluctuations when the flow rate is higher than or equal to 50% of the nominal value. At flow rates lower than 50%, smaller gaps reduced the fluctuations. In general, decreasing the gap is not the choice to reduce the pump vibration. Increasing the gap has a positive effect on reducing the pressure fluctuations inside the pump at all flow rates. Gap of 6 mm gave the lowest fluctuation amplitudes (measured peak-to-peak) inside the pump and particularly at reduced flow rates.

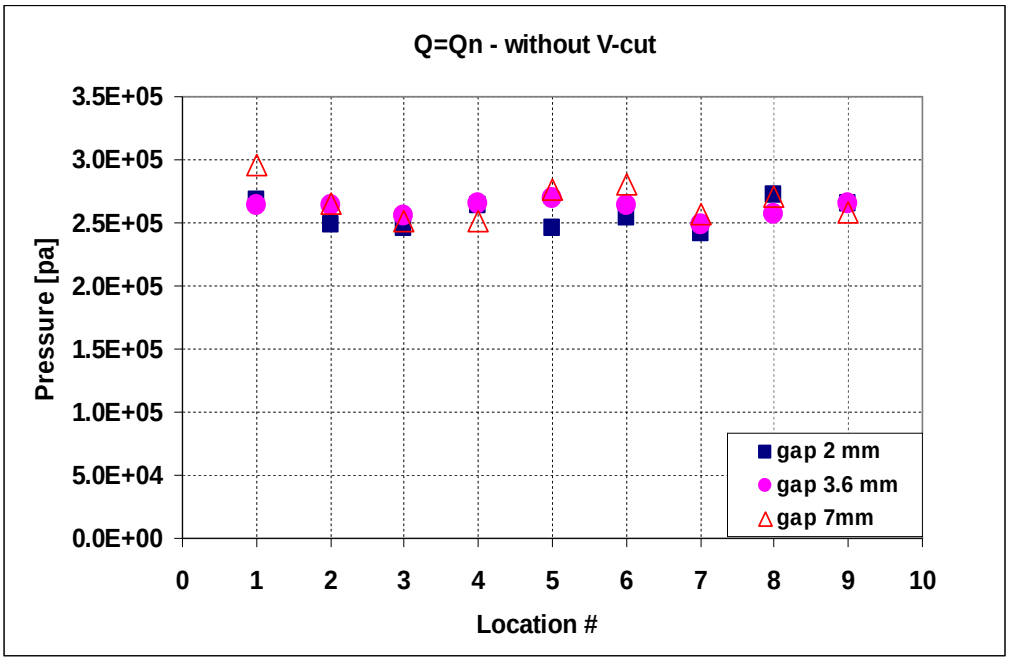

(a)

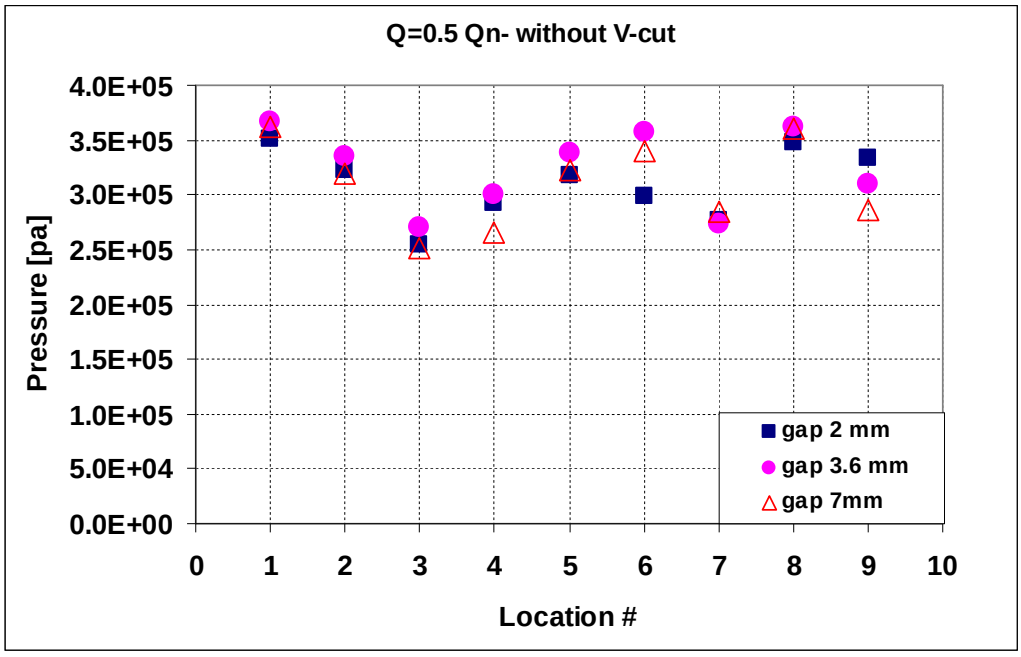

(b)

Figure 3.37 Static pressure distribution: max and min gaps compared with the original design at two different flow rates: Without V-cut

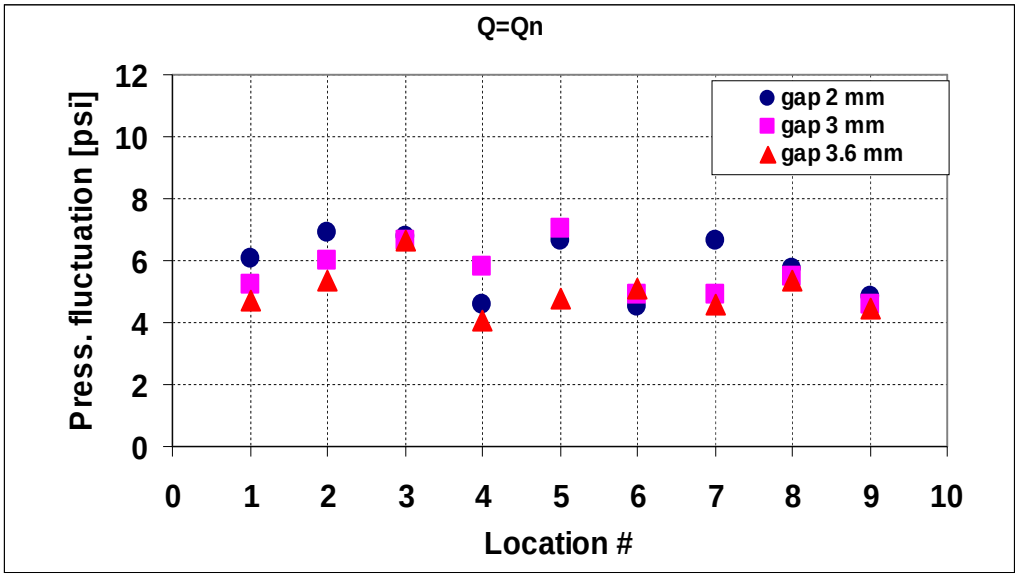
Q=Qn
Press. fluctuation [psi]
Location #
gap 2 mm
gap 3 mm
gap 3.6 mm
0
2
4
6
8
10
12
0
1
2
3
4
5
6
7
8
9
10

(a)

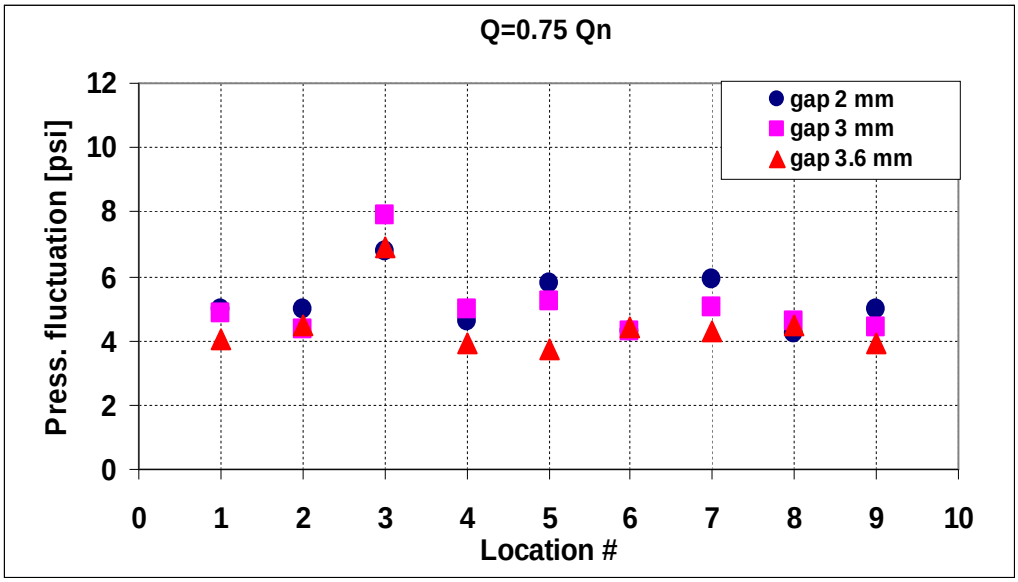
Q=0.75 Qn
Press. fluctuation [psi]
Location #
gap 2 mm
gap 3 mm
gap 3.6 mm
0
2
4
6
8
10
12
0
1
2
3
4
5
6
7
8
9
10

(b)

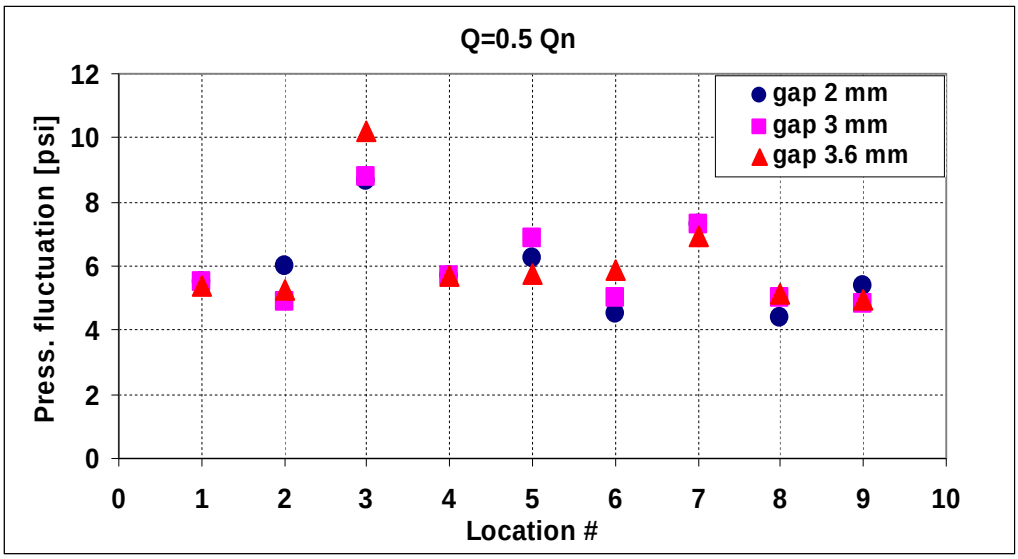

(c)

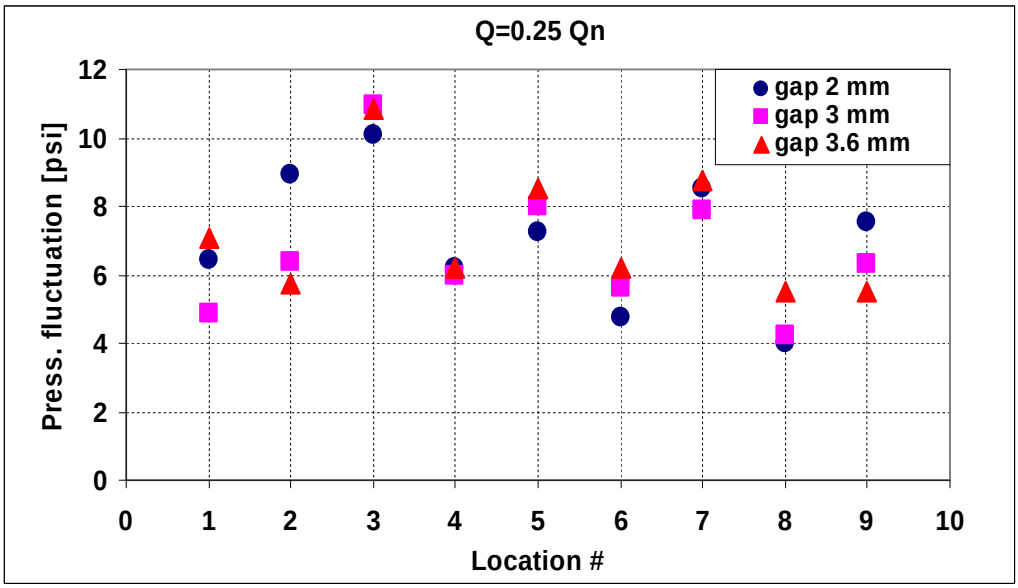

(d)

Figure 3.38 Effect of decreasing the gap on pressure fluctuation at different flow rates: Without V-cut

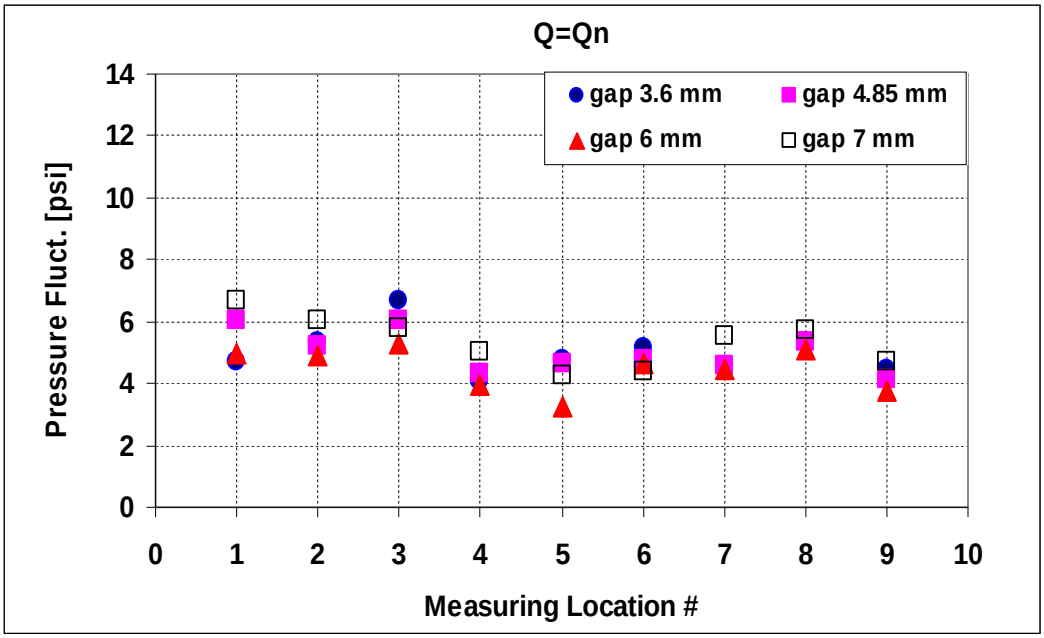
Q=Qn
gap 3.6 mm
gap 4.85 mm
gap 6 mm
gap 7 mm
Pressure Fluct. [psi]
Measuring Location #
0
2
4
6
8
10
12
14
0
1
2
3
4
5
6
7
8
9
10

(a)

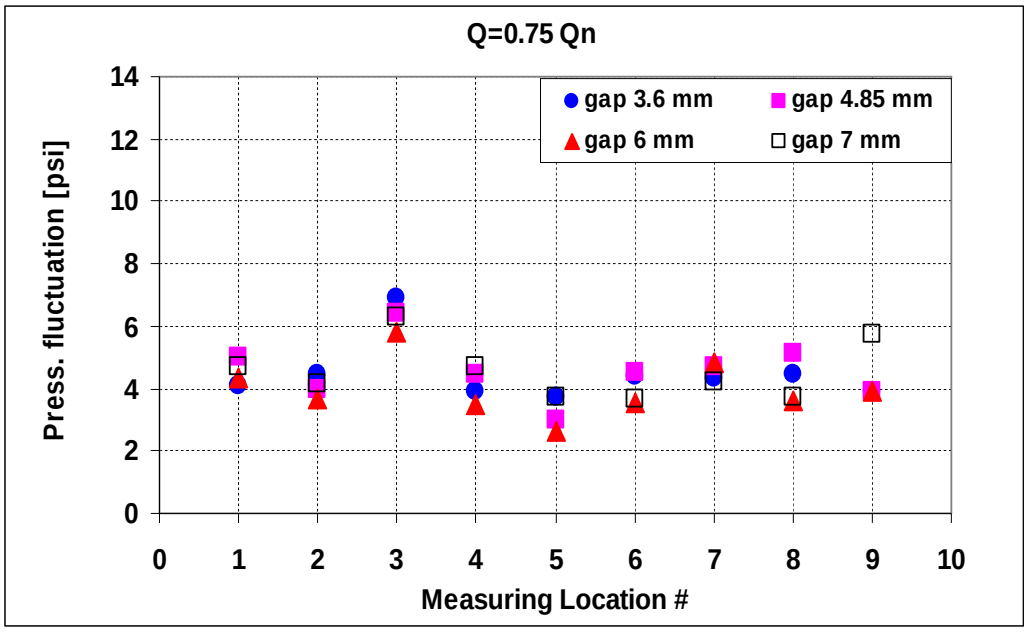
Q=0.75 Qn
gap 3.6 mm
gap 4.85 mm
gap 6 mm
gap 7 mm
Press. fluctuation [psi]
Measuring Location #
0
2
4
6
8
10
12
14
0
1
2
3
4
5
6
7
8
9
10

(b)

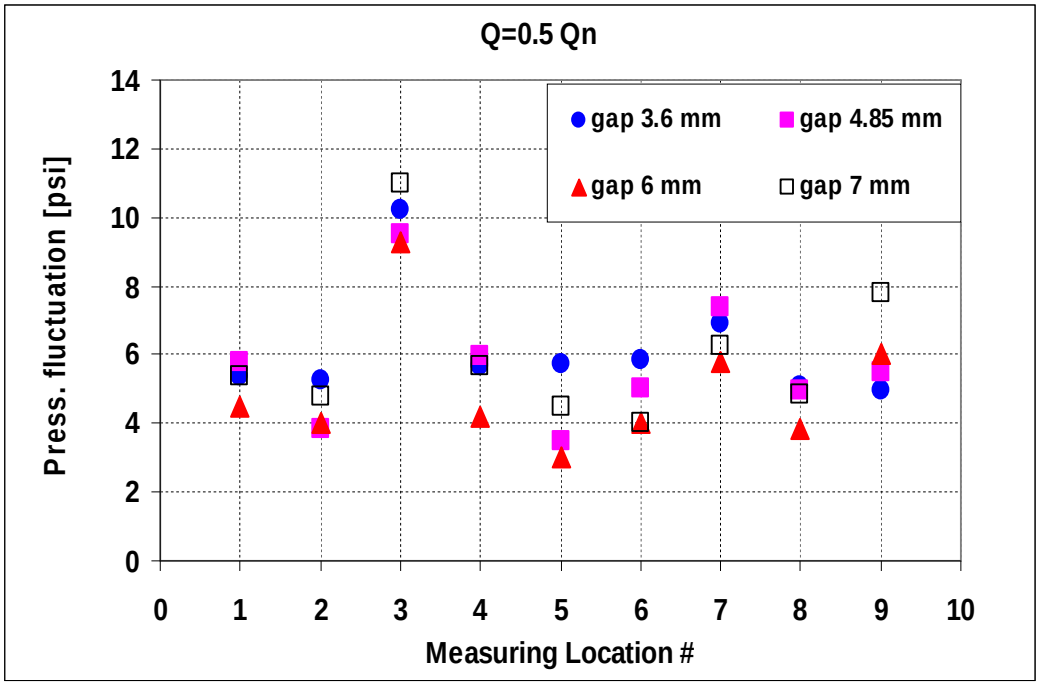

(c)

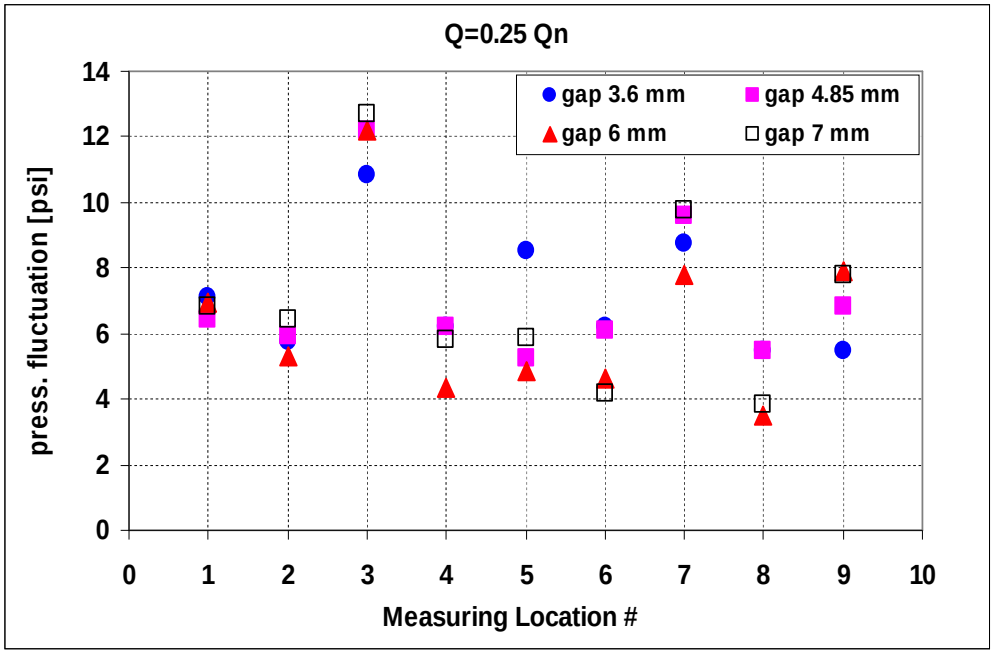

(d)

Figure 3.39 Effect of increasing the gap on pressure fluctuation at different flow rates: Without V-cut

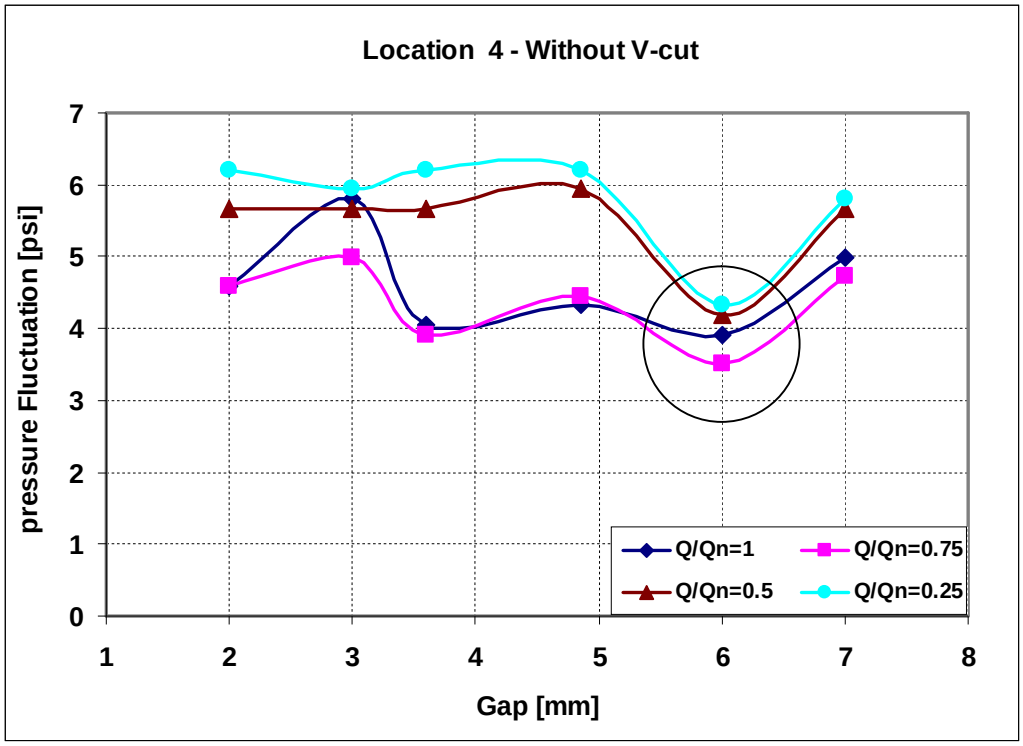

(a)

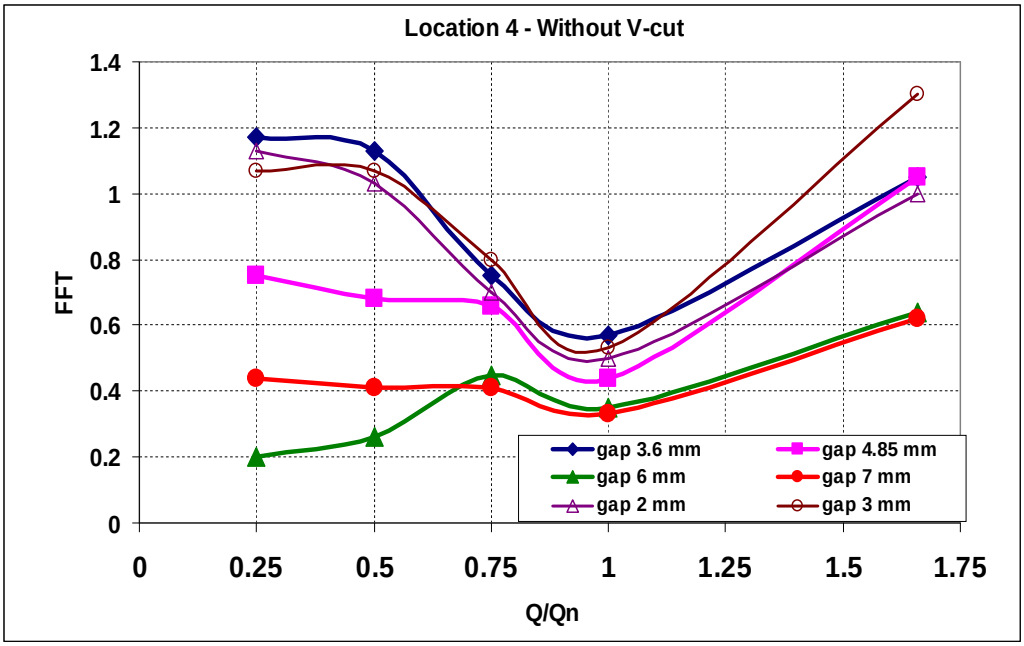

(b)

Figure 3.40 Effect of gap and flow rate at location 4: Without V-cut

Note that increasing the gap by cutting back the volute vanes while keeping the measuring locations fixed means that point like 3, 4, 7, and 9 became closer to the pulsation source due to the interaction between the impeller and volute vanes. For illustration, Fig. 3.40 shows effect of all tested gaps on fluctuations and their FFT magnitudes, for different flow rates, measured at location 4. Gap of 6 mm seems to be the optimum gap for the case of impeller without the V-cut at blade exit. It gives the minimum pressure fluctuations for all flow rates with the lowest FFT magnitude while maintaining acceptable performance. The behavior shown in Fig. 3.40 is dominating inside the pump.

Since increasing the gap has a positive effect on the pressure fluctuations, the gap of 7 mm was expected to perform better than the gap of 6 mm. However, cutting back the volute vanes more than a certain limit produces unsuitable flow angle at the leading edges of volute tongues, and it has a negative effect on the symmetry of the pressure distribution around the impeller. Figure 3.41 is a comparison between pressure distributions at geometrically similar pairs of measuring locations around the impeller for the gaps of 3.6 mm and 7 mm. At the rated capacity, pressure values are equivalent for all measuring locations inside the pump. For the original 3.6 mm gap, the pressure distribution is symmetrical around the impeller, at all flow rates. When the larger gap of 7 mm is implemented, the pressure around the impeller becomes asymmetric, particularly at reduced flow rates. This gives rise to higher amplitudes of local fluctuations, and it produces a net radial force on the impeller.

Although the gap of 7 mm did not give the minimum fluctuations of pressure inside the pump, it does reduce the vibration measured on the pump casing. Figure 3.42

shows the effect of increasing the gap from 3.6 mm to 7 mm on the pump case for the impeller without the V-cut. Average reduction of about 55 to 70% in pump case vibration was obtained when the gap of 7 mm is used instead of the gap of 3.6 mm, depending on the flow rate. In case of using the impeller without V-cut at blade exit, it is desirable to increase the radial gap from 3.6 mm to 6 mm (from 2.5% to 4.25% of the impeller diameter).

Increasing the radial gap between impeller and volute to this '*optimum*' value was found to be effective in reducing the pressure fluctuations at design conditions and at reduced capacities.

Gaps larger than this optimum value may result in higher pressure fluctuations due to asymmetric pressure distribution around the impeller. The reduction in pressure fluctuation amplitudes and vibration level at 6 mm gap was achieved at the expense of 0.92% loss in pump head and 0.5% in efficiency for the rated capacity of 12 L/s. These values of loss in head and efficiency fall within the calculated uncertainty limits of the experiment.

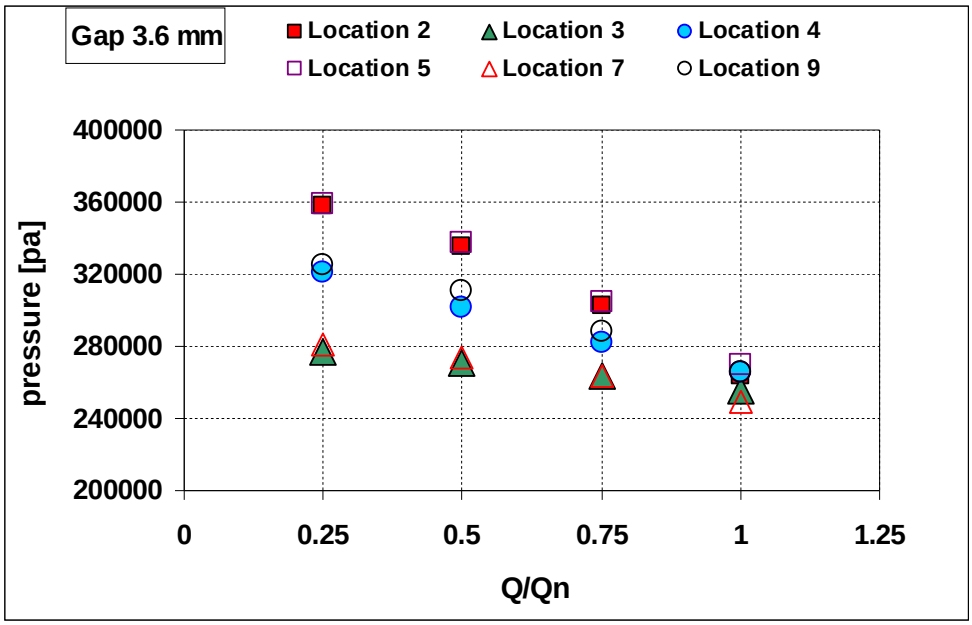

(a)

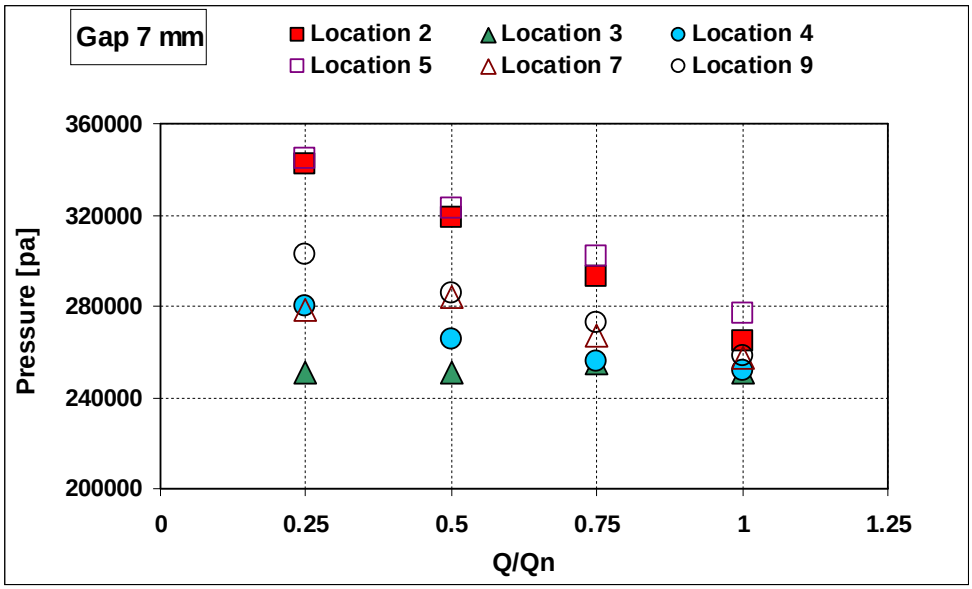

(b)

Figure 3.41 Comparison between pressure distributions at geometrically similar pairs of locations around the impeller for the gaps of 3.6 and 7 mm

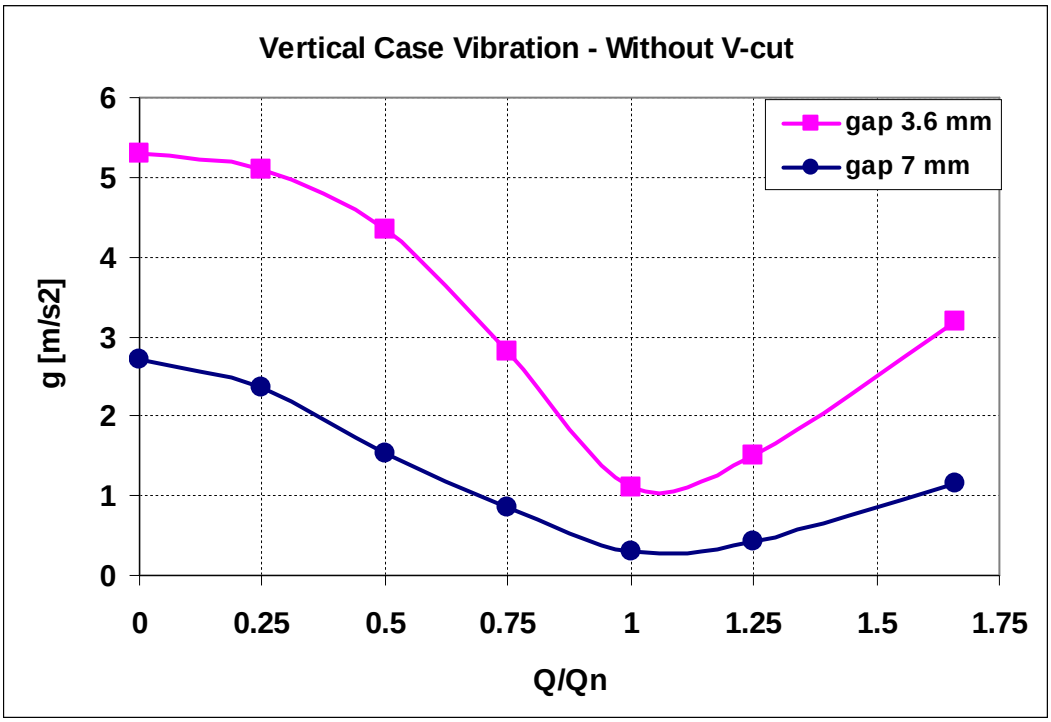

Figure 3.42 Comparison the original gap design and max gap of 7 mm for the case vibration at different flow rates: Without V-cut

3.4.2 IMPELLER WITH V-CUT AT BLADE EXIT

The effects of changing the gap on performance, pressure fluctuation and FFT magnitude, and case vibration are present in this section for the impeller with V-cut at blade exit. Figure 3.43 shows the effect of both decreasing and increasing the gap on the pump performance. Smaller gaps give better performance, in terms of head and efficiency, at flow rates higher than about 130% of best efficiency flow rate. Again, the original gap design of 3.6 mm (2.5% of the impeller diameter) is a good choice for performance at design flow rate and below. Figure 3.44 gives the variation of pump head and efficiency for different gaps at constant flow rate of 12.4 L/s (Qn for impeller with V-cut at blade exit at 3540 rpm). The pump head decrease as the gap increases. When comparing Fig. 3.44 with Fig. 3.36, increasing the gap has more negative effect on pump head in case of impeller with V-cut at blade exit rather than the impeller without V-cut at blade exit. The head drops faster with increasing the gap due to the existence of the V-cut which actually increases the effective gap between the impeller and the volute vanes. The change in pump efficiency due to different gaps falls within the uncertainty limits. Thus, the considered gap values had negligible effect on pump efficiency.

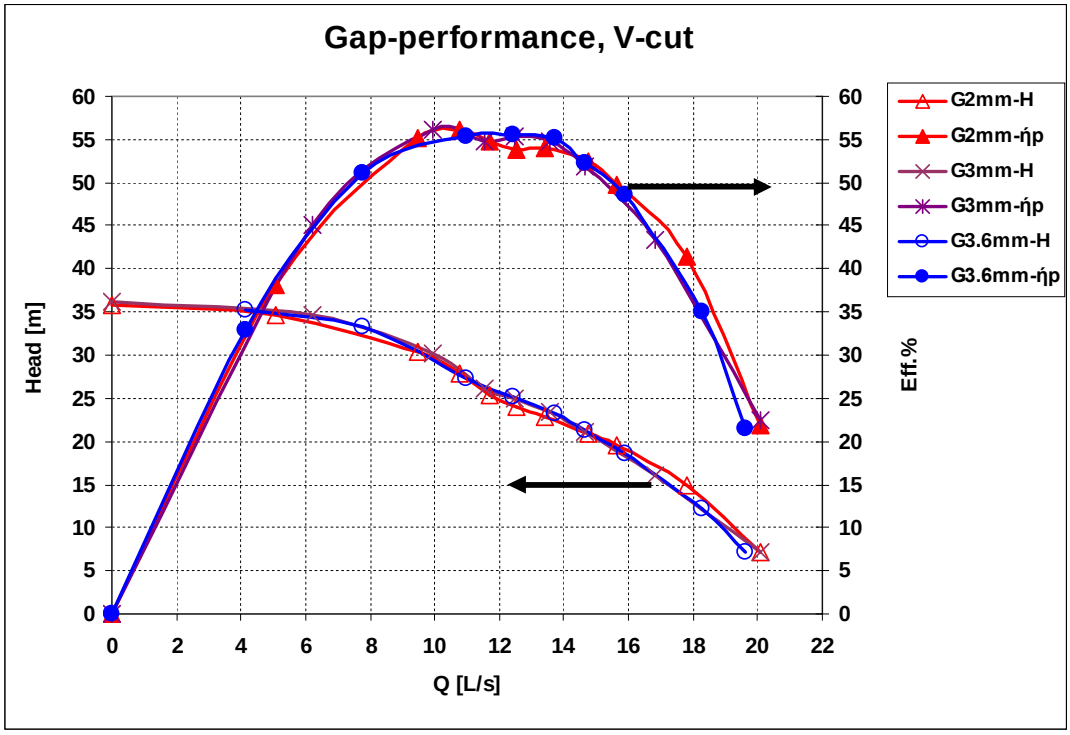

(a)

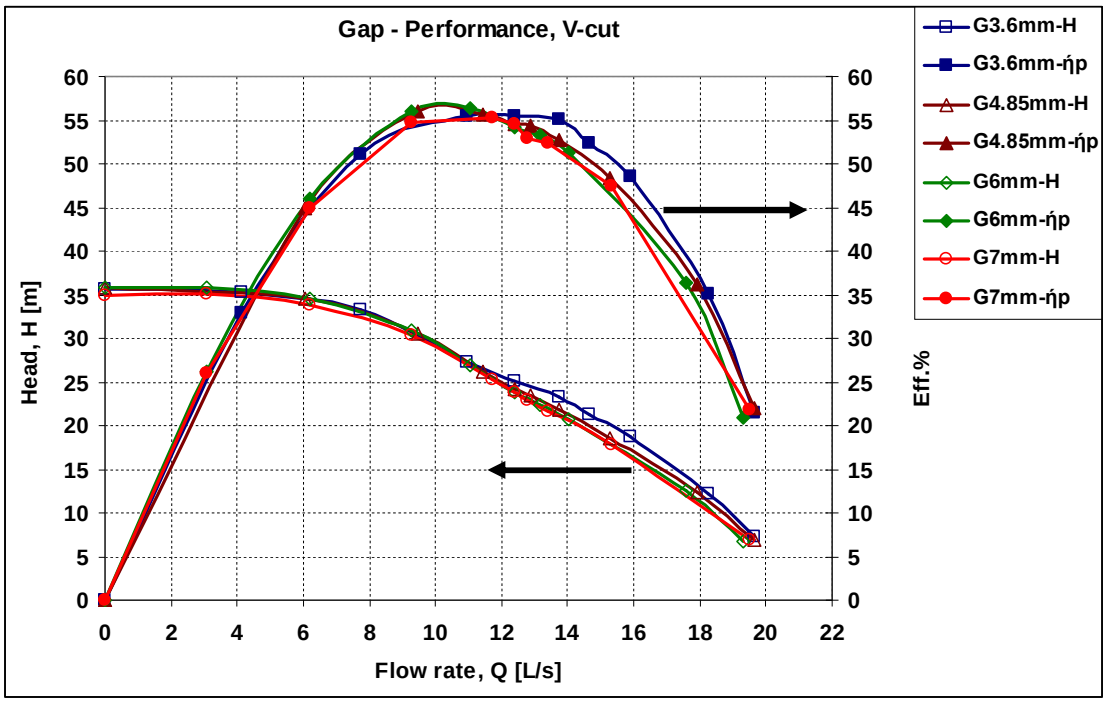

(b)

Figure 3.43 Pump performance at 3540 rpm under different gaps: impeller with V-cut at blades exit

flow rate= 12.4 Lit/sec				
Gap (mm)	Head (m)	Efficiency	% change in head	% change in efficiency
2	25.32	55.86	0.74	0.74
3	25.03	55.6	-0.42	0.27
3.6 (Ref.)	25.13 ± 1%	55.45 ± 2%	----	----
4.85	24.4	54.96	-2.92	-0.88
6	23.88	54.12	-4.99	-2.40
7	23.75	54.6	-5.51	-1.53

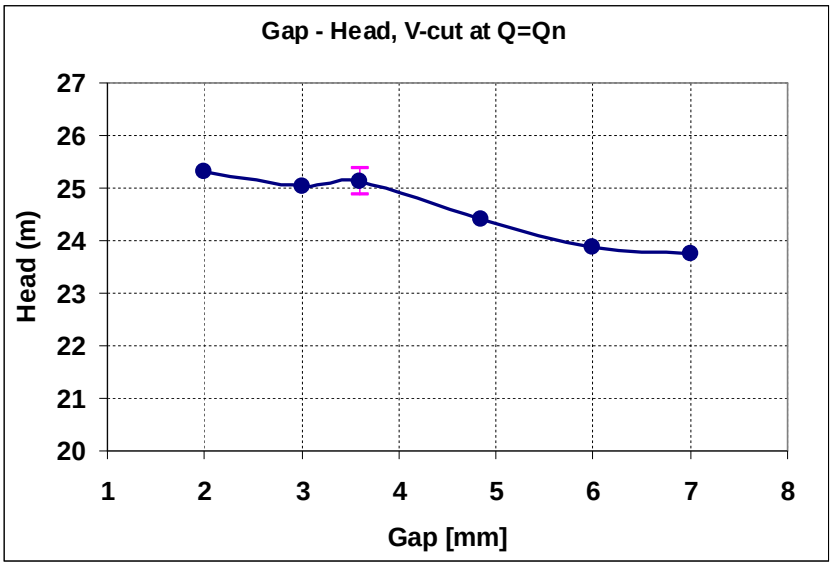

(a)

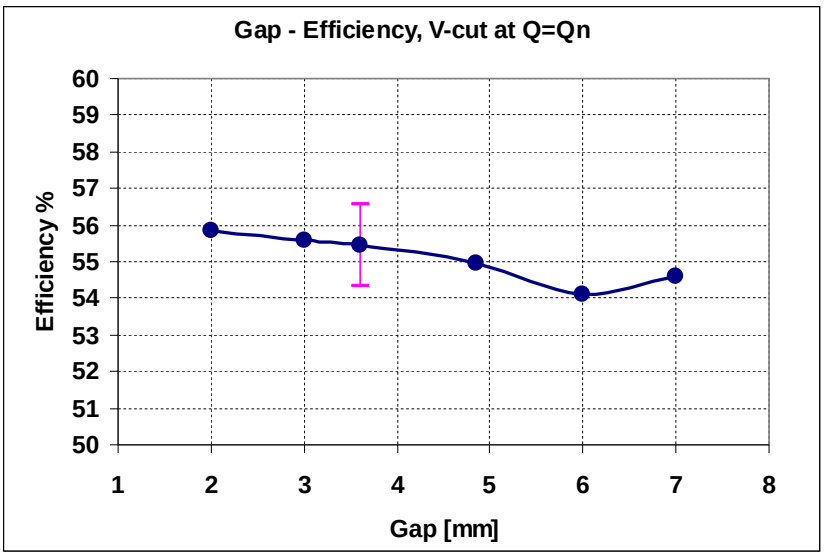

(b)

Figure 3.44 Effect of gap design on head and efficiency: With V-cut at blade exit

The distribution of the static pressure inside the pump volute at different gaps is shown in Fig. 3.45 for different flow rates. The original gap of 3.6 mm is compared with the maximum gap of 7 mm and the minimum gap of 2 mm. At reduced flow rates, the pressure distributions with different gaps are more compatible than at nominal conditions except for location 4 which shows maximum variation due to changing the gap. Locations like 3 and 7 were expected to show higher variations with different gaps due to their closeness to the volute vanes leading edges. This gives indication that the pump head is less sensitive to the gap at reduced flow rates when the V-cut exists. The effect of decreasing the gap on the pressure fluctuations inside the pump volute is shown in Fig. 3.46, at different flow rates. Similarly, the effect of increasing the gap on the pressure fluctuations inside the pump volute is shown in Fig. 3.47, at different flow rates.

Smaller gaps produced higher fluctuations in general, for all flow rates. Fluctuation peaks at Locations 3 and 7 when the pump operates at off-design flow rate. Increasing the gap reduces the pressure fluctuations inside the pump at all flow rates. Gap of 7 mm gave the lowest fluctuation amplitudes (measured peak-to-peak) inside the pump and particularly at reduced flow rates. Figure 3.48 shows the effect of different gaps, at different flow rates, on the FFT magnitude measured at 5xRPM (1^{st} BPF) at different locations around the impeller. Gap of 7 mm is considered to be the optimum design for the case of impeller with V-cut at blade exit. It gives the minimum fluctuations and FFT magnitude for reduced flow rates as well as higher flow rates up to 125% of nominal capacity; approximately.

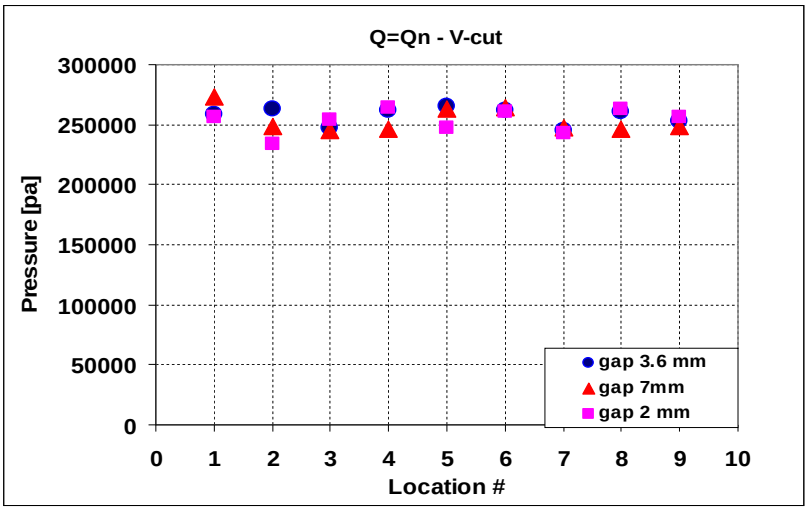

(a)

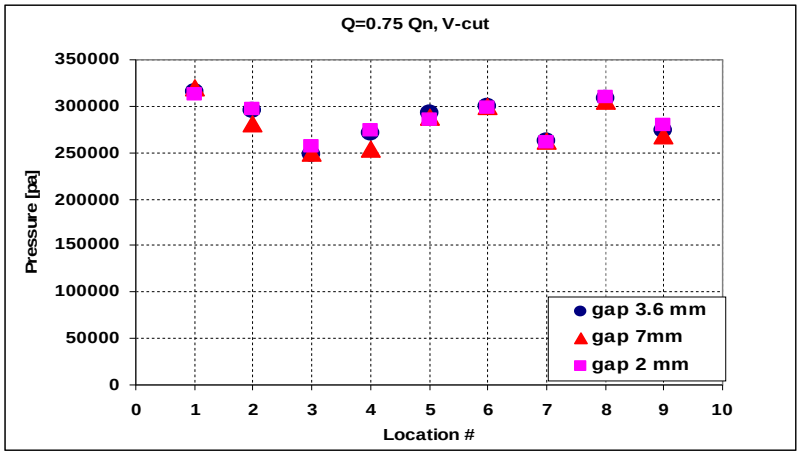

(b)

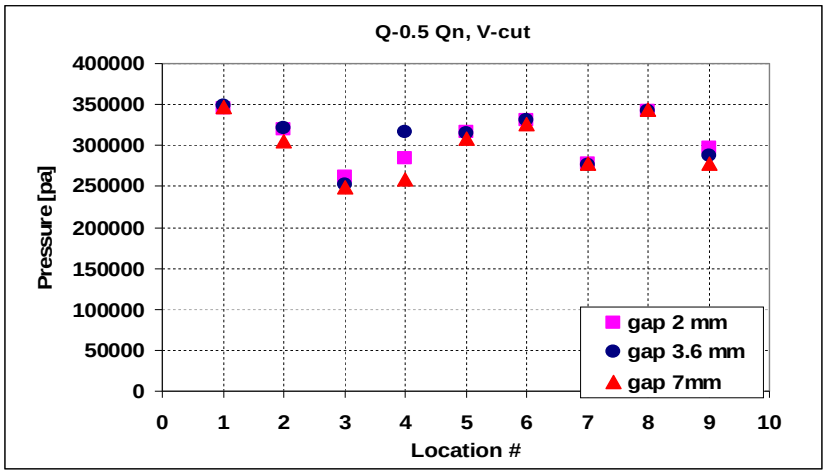

(c)

Figure 3.45 Static pressure distribution: max and min gaps compared with the original design at three different flow rates: With V-cut

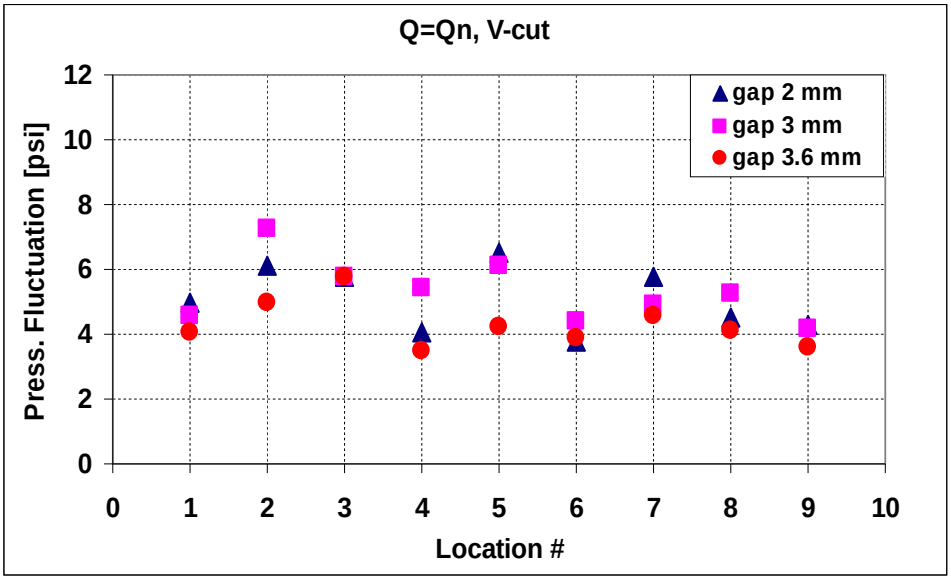
Q=Qn, V-cut
Press. Fluctuation [psi]
Location #
gap 2 mm
gap 3 mm
gap 3.6 mm
0
2
4
6
8
10
12
0
1
2
3
4
5
6
7
8
9
10

(a)

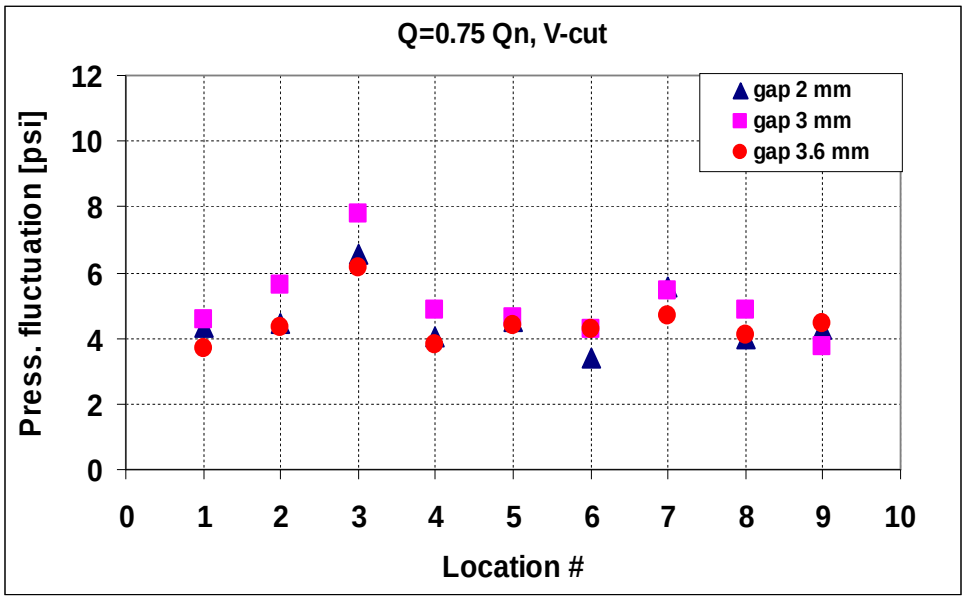
Q=0.75 Qn, V-cut
Press. fluctuation [psi]
Location #
gap 2 mm
gap 3 mm
gap 3.6 mm
0
2
4
6
8
10
12
0
1
2
3
4
5
6
7
8
9
10

(b)

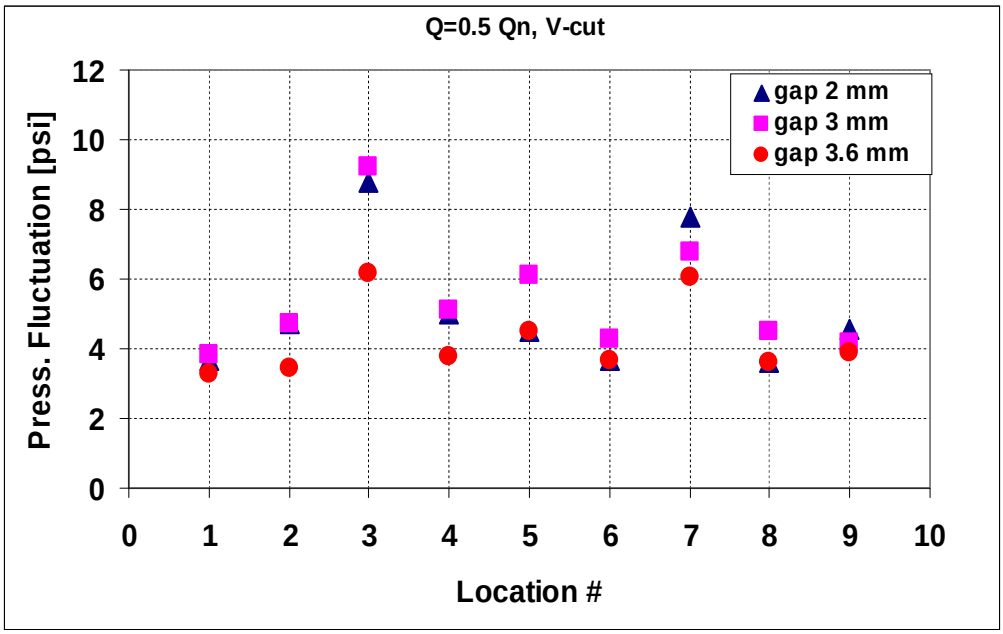

(c)

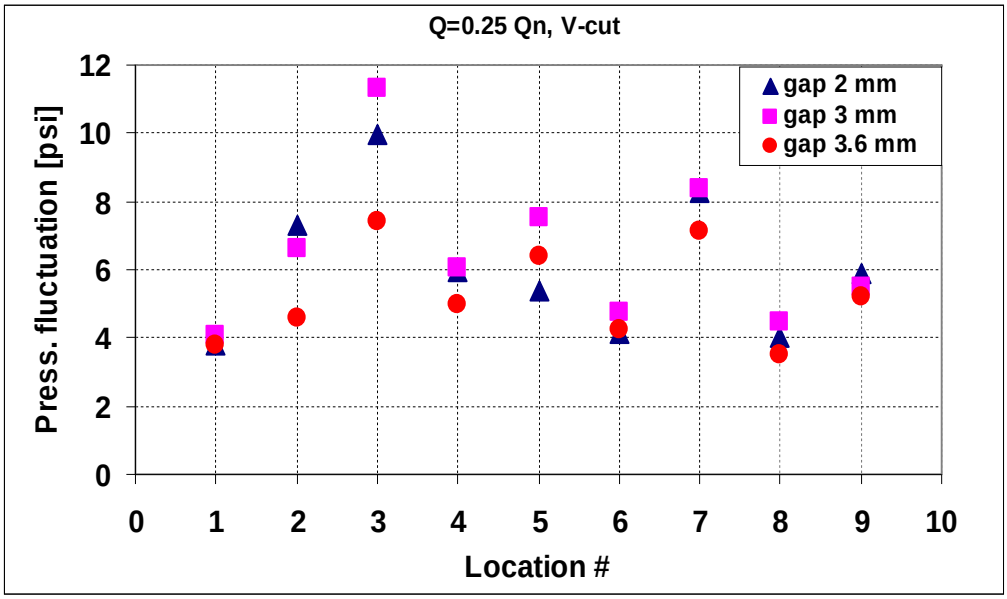

(d)

Figure 3.46 Effect of decreasing the gap on pressure fluctuation at different flow rates: With V-cut at blade exit

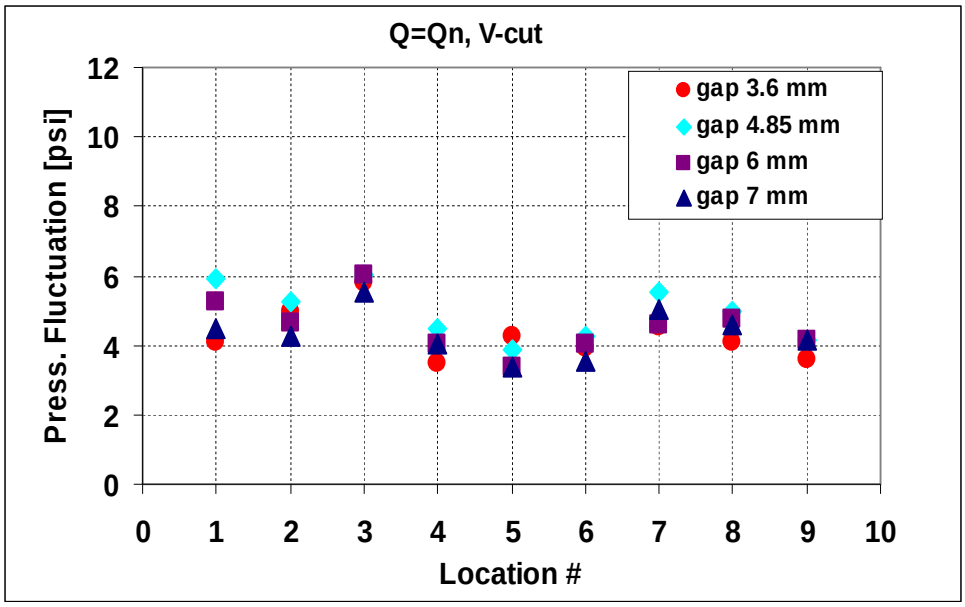
Q=Qn, V-cut
Press. Fluctuation [psi]
Location #
gap 3.6 mm
gap 4.85 mm
gap 6 mm
gap 7 mm
0
2
4
6
8
10
12
0
1
2
3
4
5
6
7
8
9
10

(a)

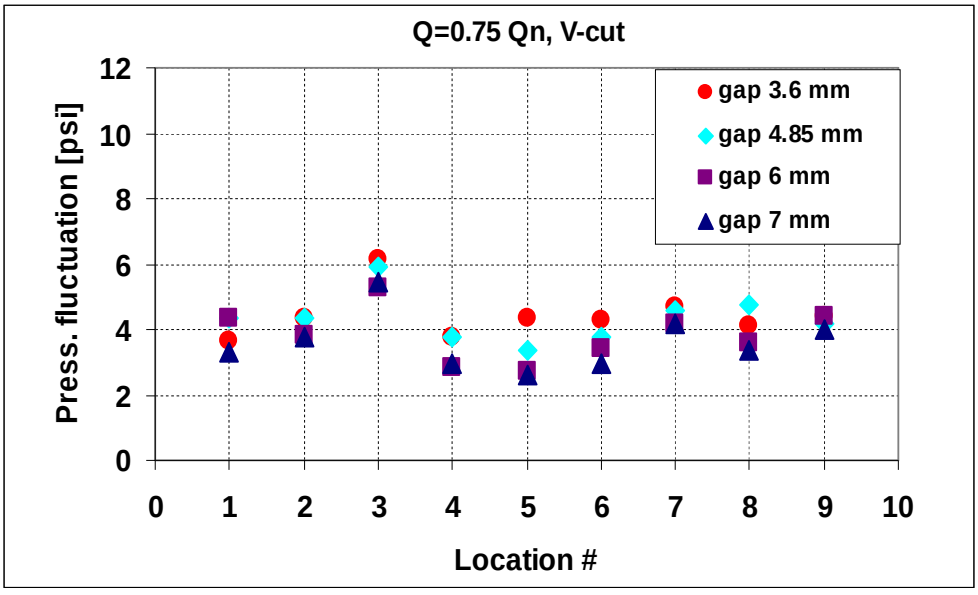
Q=0.75 Qn, V-cut
Press. fluctuation [psi]
Location #
gap 3.6 mm
gap 4.85 mm
gap 6 mm
gap 7 mm
0
2
4
6
8
10
12
0
1
2
3
4
5
6
7
8
9
10

(b)

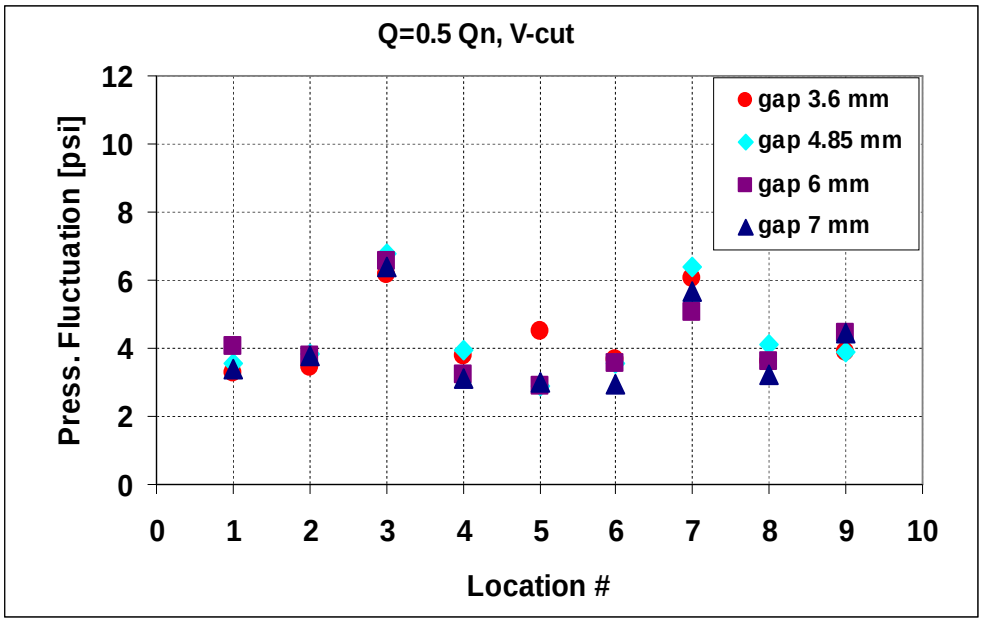

(c)

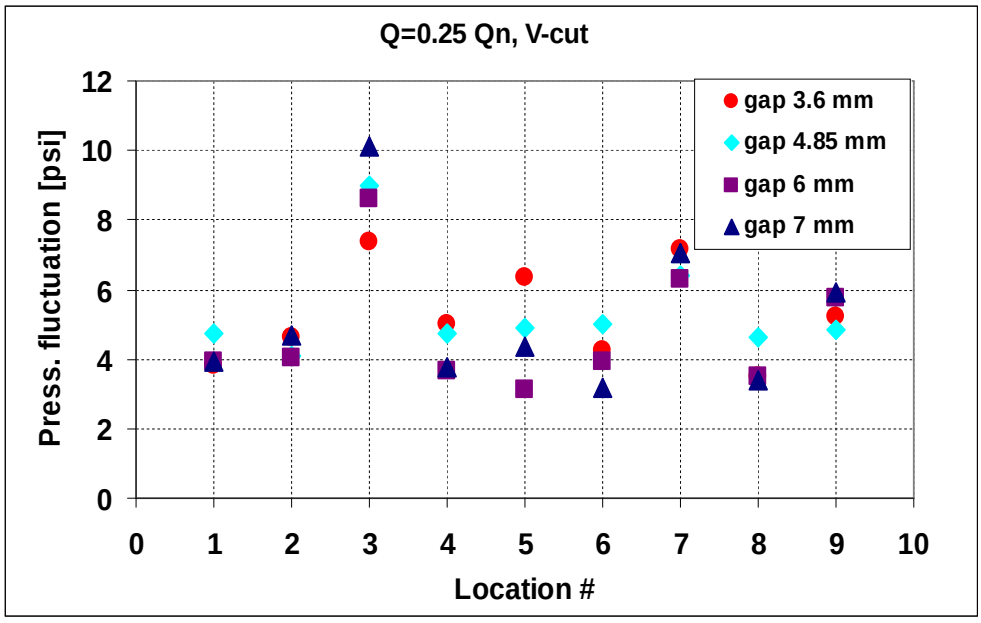

(d)

Figure 3.47 Effect of increasing the gap on pressure fluctuation at different flow rates: With V-cut at blade exit

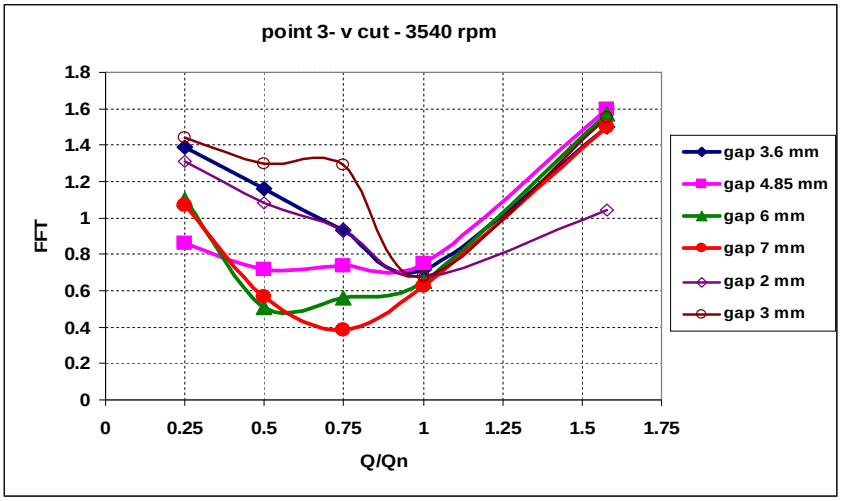

(a)

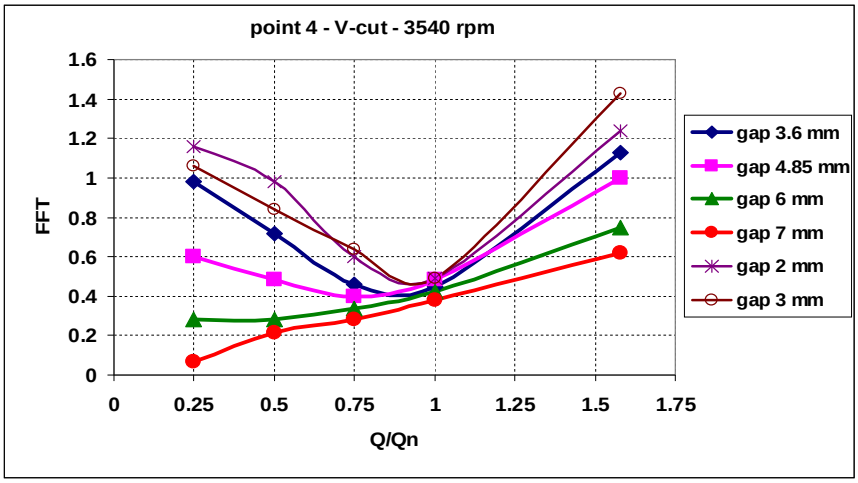

(b)

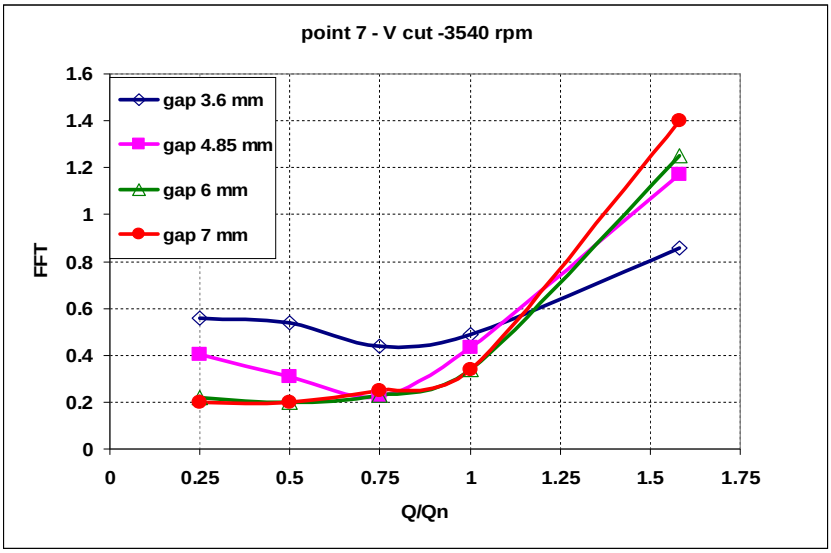

(c)

Figure 3.48 Effect of different gaps and flow rates at different locations with V-cut at blade exit

Figure 3.49 shows the effect of increasing the gap from 3.6 mm to 7 mm on the pump casing for the impeller with V-cut at blade exit. Average reduction of about 50% in pump casing vibration was obtained when the gap of 7 mm is used instead of the gap of 3.6 mm, at all flow rate conditions.

The improvement in reducing the amplitudes of pressure fluctuations and outer casing vibration was achieved at the expense of 5% loss in pump head and 1.6% in efficiency for the rated capacity of 12.4 L/s. Combining the V-cut design with the gap of 7 mm (5% of the impeller diameter) is considered to be a suitable solution to reduce the flow induced vibration problem for the present pump. For the original boiler feed pump, equivalent gap of 5% of impeller diameter would be achieved by cutting back about 75 mm from the splitters leading edges (in the vertical direction while the pump is horizontally positioned). The original pump geometry and dimensions should be studied accurately if gap modification is to be applied to pinpoint the cutting limit for 5% gap, as per the study recommendation, to avoid any discrepancies in scaling between original and model pumps.

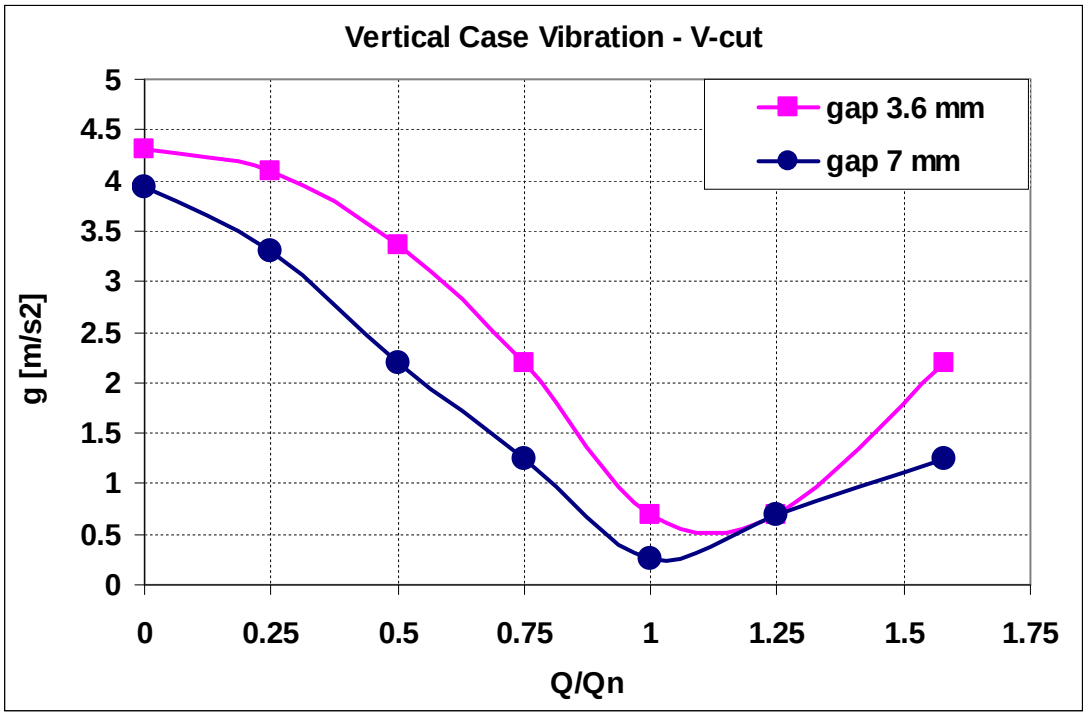

Figure 3.49 Comparison between the original gap design and max gap of 7 mm for the case vibration at different flow rates: With V-cut at blade exit

Finally, the asymmetry measured between the diffuser vanes leading edges for the SEC pump was about 1.5 mm. One vane leading edge was shorted by 1.5 mm and in order to test the effect of this tolerance, one volute vane in the model pump was extended by 5 mm while the other one was kept as designed. Extension of 5 mm is equivalent to 12.5 mm extension for the original boiler feed pump which is very large compared to what measured actually. Experiments on the model pump showed that this asymmetry (5 mm) has negligible effect on pressure fluctuations inside the pump as shown in Fig. 3.50. The slight asymmetry of 1.5 mm observed between the diffuser vanes of SEC prototype pump has negligible effect on pressure pulsation inside the pump.

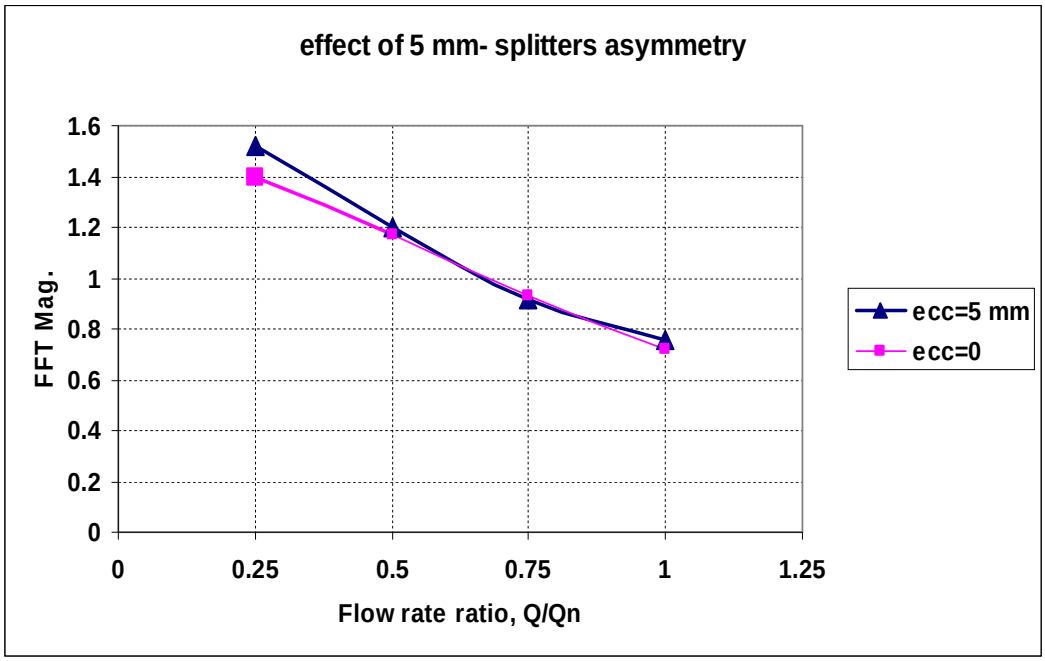

Figure 3.50 Effect of the asymmetry of splitters lips (locations of volute tongues)

CHAPTER 4

NUMERICAL SIMULATIONS

4.1 INTRODUCTION

The application of Computational Fluid Dynamics (CFD) to pump industry has provided a very valuable tool to predict the pump performance and pressure distributions with high accuracy. Numerical simulations make it easy to understand the unsteady phenomena which are difficult to analyze (or measure) from experimental studies alone. This is because of the complicated flow patterns in pumps, especially at off-design conditions. Unsteady phenomena in diffuser pumps become more complicated at off-design operating conditions where the flow and pressure of a pump become increasingly unsteady. The frequencies of the fluctuating pressure field in pumps can be successfully captured by 2D and 3D CFD models for a wide range of operating flow rates. However, 3D CFD models are required to capture the accurate value of the amplitudes of pressure fluctuations at the blade passing frequencies. If the dynamic effects are to be taken into account, there is a need for fully unsteady calculations with an accurate technique to model the relative motion of the impeller. The discretization of the model geometry should be done while keeping the balance between calculation time and the accuracy of the simulation of the flow structure. Special care must be taken at the interaction zones between the rotating impeller and stationary volute.

4.2 GENERATION OF PUMP GEOMETRY

Two dimensional numerical simulations for the model pump geometry were carried out using the FLUENT software. The 3D geometry file for the impeller was generated using the preprocessor software; GAMBIT, to produce the scaled impeller. A planar cross section at the blades mid-height produced the 2D geometry of the blades. Figure 4.1 shows this process. Similarly, the 2D geometry of the volute, Fig. 4.2, is obtained from a 2D cross section of the 3D volute geometry generated by Solidworks for the scaled volute. The discharge nozzle added for more accurate simulation. The geometry and mesh files for the volute and the impeller were built separately. The two geometry files were merged for the use of the sliding mesh technique as shown in Fig. 4.3. Sliding mesh technique is suitable for accurate unsteady flow simulations. Figure 4.4 shows the different components of a sliding mesh for the impeller and volute of the model boiler feed pump stage.

The interface between the mesh of the volute and that of the impeller is circular in shape for this 2D model as shown in Fig. 4.4 The mesh of volute is fixed and does not move as time progresses. On the other hand, the mesh of the impeller moves (slides) with respect to the volute mesh as the transient simulation evolves with the actual flow time.

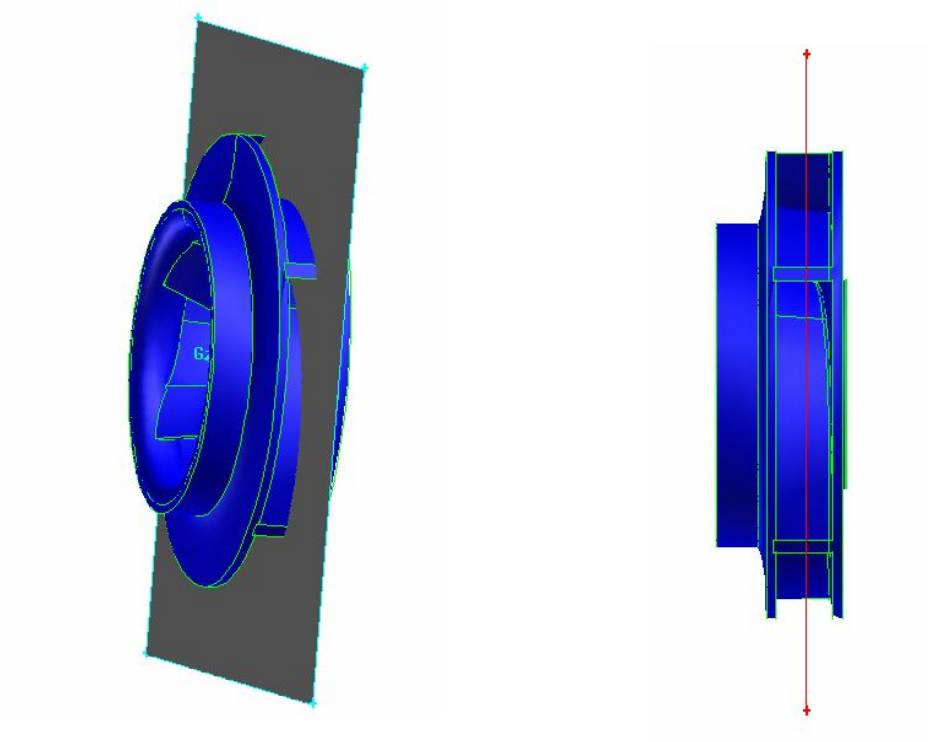

(a) Cutting the 3D impeller at blades mid-height

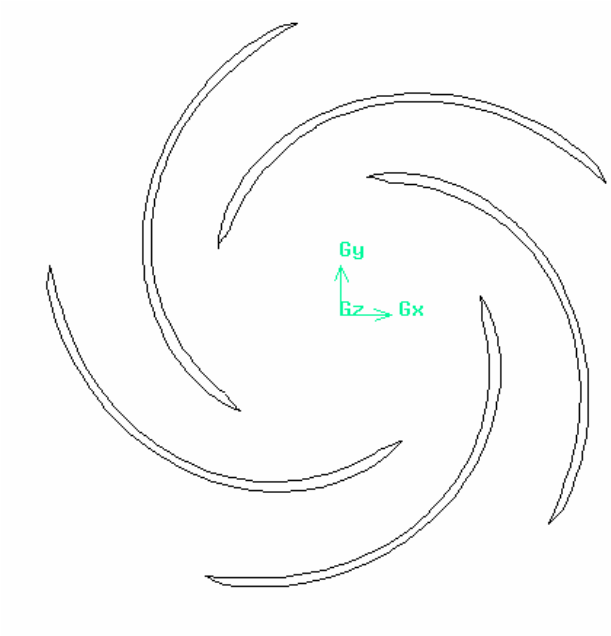

(b) 2D geometry of impeller blades at mid-height

Figure 4.1 Generation of 2D impeller blades geometry

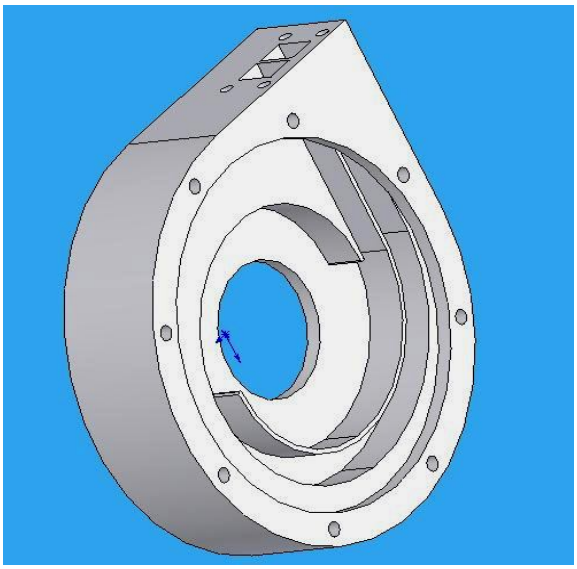

(a) 3D scaled volute for the model pump

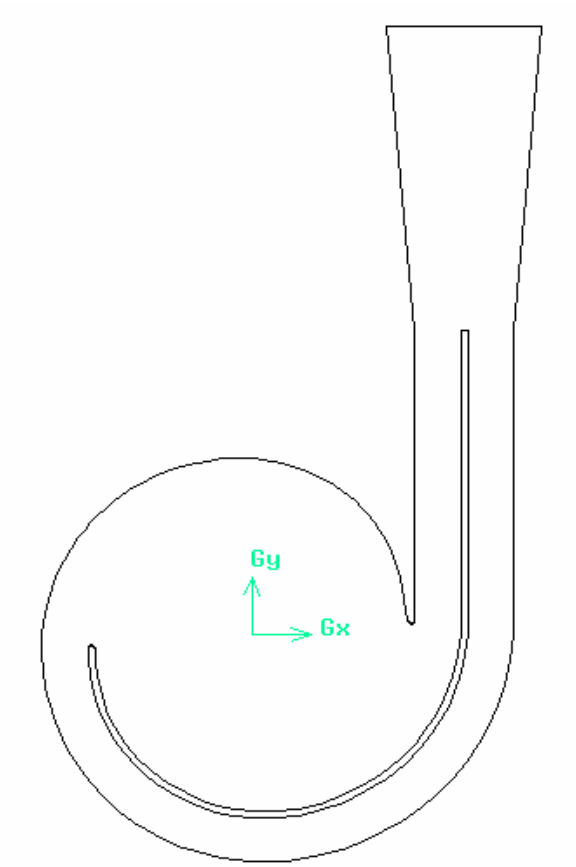

(b) 2D geometry of model pump volute

Figure 4.2 Generation of the 2D geometry of volute

(a) Impeller (b) Volute

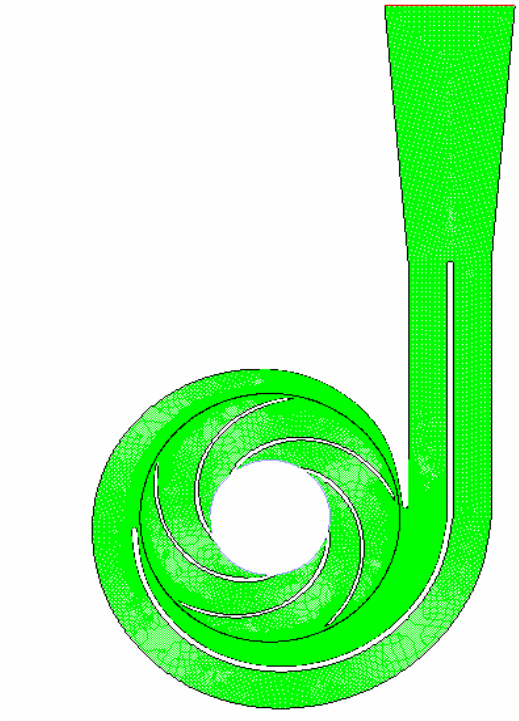

(c) Model pump

Figure 4.3 Merging the impeller and volute mesh files

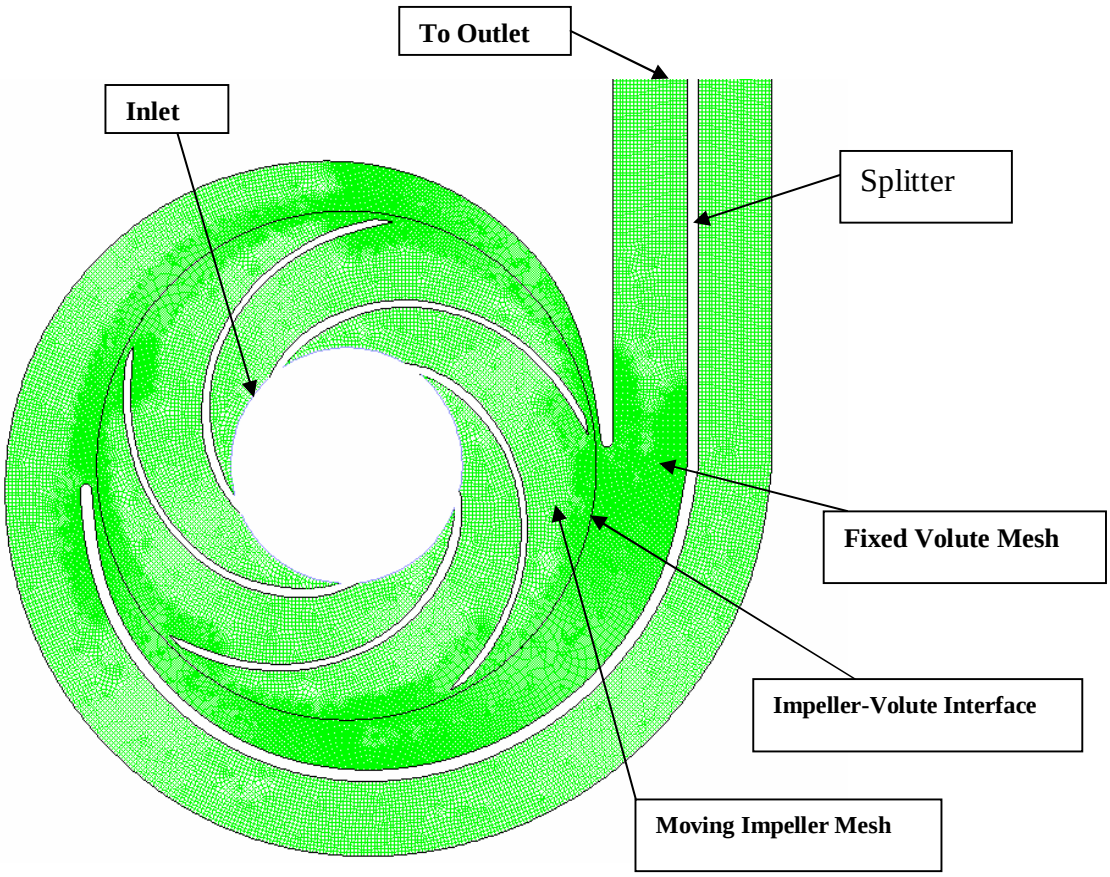

Figure 4.4 Components of a sliding mesh

4.3 NUMERICAL PROCEDURE

4.3.1 GOVERNING EQUATIONS

The model solves the fully 2D incompressible Navier-Stokes equations with an unsteady calculation. The sliding mesh technique is applied to take into account the impeller-volute interaction. Turbulence is simulated with the standard k-ε model. The model solves the unsteady continuity equation (mass conservation), the momentum equations for incompressible flow in both coordinate directions x and y and the turbulence model equations. These equations are integrated in time using a finite volume method .

Mass conservation equation is given by

$$\nabla \cdot \vec{v} = 0 \tag{4.1}$$

Equation (4-1) is the general form of the mass conservation equation and is valid for incompressible as well as compressible flows.

Conservation of momentum in an inertial (non-accelerating) reference frame is described by

$$\frac{\partial}{\partial t}\left(\rho \vec{v}\right) + \nabla \cdot \left(\rho \vec{v}\vec{v}\right) = -\nabla p + \nabla \cdot \left(\bar{\bar{\tau}}\right) + \rho \vec{g} \tag{4.2}$$

where p is the static pressure, $\overline{\overline{\tau}}$ is the stress tensor (described below), and $\rho\vec{g}$ is the gravitational body force . The stress tensor $\overline{\overline{\tau}}$ is given by

$$\overline{\overline{\tau}} = \mu\left[(\nabla\vec{v} + \nabla\vec{v}^{T}) - \frac{2}{3}\nabla\cdot\vec{v}I\right] \tag{4.3}$$

where μ is the molecular viscosity, I is the unit tensor, and the second term on the right hand side is the effect of volume dilation.

4.3.2 TURBULENCE MODEL

The simplest “complete models" of turbulence are two-equation models in which the solution of two separate transport equations allows the turbulent velocity and length scales to be independently determined. The standard k-ε falls within this class of turbulence models and has become the workhorse of practical engineering flow calculations. Robustness, economy, and reasonable accuracy for a wide range of turbulent flows explain its popularity in industrial flow and heat transfer simulations. It is a semi-empirical model, and the derivation of the model equations relies on phenomenological considerations and empiricism.

The standard k-ε model is a semi-empirical model based on model transport equations for the turbulence kinetic energy (k) and its dissipation rate (ε). The model transport equation for k is derived from the exact equation, while the model transport equation

for ε was obtained using physical reasoning and bears little resemblance to its mathematically exact counterpart.

In the derivation of the k-ε model, it was assumed that the flow is fully turbulent, and the effects of molecular viscosity are negligible. The standard k-ε model is therefore valid only for fully turbulent flows. The turbulence kinetic energy, k, and its rate of dissipation, ε, are obtained from the following transport equations:

$$\frac{\partial}{\partial t}(\rho k)+\frac{\partial}{\partial x_i}(\rho k u_i)=\frac{\partial}{\partial x_j}\left[\left(\mu+\frac{\mu_t}{\sigma_k}\right)\frac{\partial k}{\partial x_j}\right]+G_k+G_b+\rho\varepsilon \tag{4.4}$$

and

$$\frac{\partial}{\partial t}(\rho\varepsilon)+\frac{\partial}{\partial x_i}(\rho\varepsilon u_i)=\frac{\partial}{\partial x_j}\left[\left(\mu+\frac{\mu_t}{\sigma\varepsilon}\right)\frac{\partial\varepsilon}{\partial x_j}\right]+C_{1\varepsilon}\frac{\varepsilon}{k}(G_k+C_{3\varepsilon}G_b)-C_{2\varepsilon}\rho\frac{\varepsilon^2}{k} \tag{4.5}$$

In these equations, G_k represents the generation of turbulence kinetic energy due to the mean velocity gradients G_b is the generation of turbulence kinetic energy due to buoyancy. $C_{1\varepsilon}$, $C_{2\varepsilon}$, and $C_{3\varepsilon}$ are constants. σ_k and σ_ε are the turbulent Prandtl numbers for k and ε, respectively. The turbulent (or eddy) viscosity, μ_t, is computed by combining k and ε as follows:

$$\mu_t = \rho C_\mu \frac{k^2}{\varepsilon} \tag{4-6}$$

where C_μ is a constant.

The model constants have the following default values:

$C_{1\varepsilon} = 1.44$;

$C_{2\varepsilon} = 1.92$;

$C_\mu = 0.09$;

$\sigma_k = 1.0$; and

$\sigma_\varepsilon = 1.3$

These default values have been determined from experiments with air and water for fundamental turbulent shear flows including homogeneous shear flows and decaying isotropic grid turbulence. They have been found to work fairly well for a wide range of wall bounded and free shear flows.

Although the default values of the model constants are the standard most widely accepted ones, we can change them (if needed) in the Viscous Model panel. As the strengths and weaknesses of the standard k-ε model have become known, improvements have been made to the model to improve its performance. Two of these variants are available in FLUENT: the RNG k- ε model and the realizable k- ε model.

4.3.4 SLIDING MESH TECHNIQUE

When simulating the pump numerically, the moving cell zone capability provides a powerful set of features for solving problems in which the domain or parts of the domain are in motion. When transient rotor-stator interaction is desired, sliding meshes model is to be used. This situation occurs in turbomachinery applications where rotor and stator blades are in close proximity and hence rotor-stator interaction is important. The sliding mesh model assumes that the flow field is unsteady. Thus, it

models the interaction with complete fidelity. This is the model of choice if rotor-stator interaction is strong and a more accurate simulation of the system is desired. Note that because the sliding mesh model requires an unsteady numerical solution, it is computationally more demanding.

In the sliding mesh technique, two or more cell zones are used. When the mesh is generated in each zone independently, they have to be merged prior to starting the calculation. Each cell zone is bounded by at least one "interface zone" where it meets the opposing cell zone. The interface zones of adjacent cell zones are associated with one another to form a "grid interface". The two cell zones will move relative to each other along the grid interface. The grid interface must be positioned so that it has fluid cells on both sides. During the calculation, the cell zones slide (rotate) relative to one another along the grid interface in discrete steps.

As the rotation or translation takes place, node alignment along the grid interface is not required. Since the flow is inherently unsteady, a time-dependent solution procedure is required. The grid interface and the associated interface zones can be of any shape, provided that the two interface boundaries are based on the same geometry. This situation requires means of computing the flux across the two non-conformal interface zones of each grid interface. Figure 4.5 shows a depiction of sliding mesh configurations at 6 positions during impeller rotation of 0.0025 second in steps of 0.0005 sec, rotational speed is 3540 rpm.

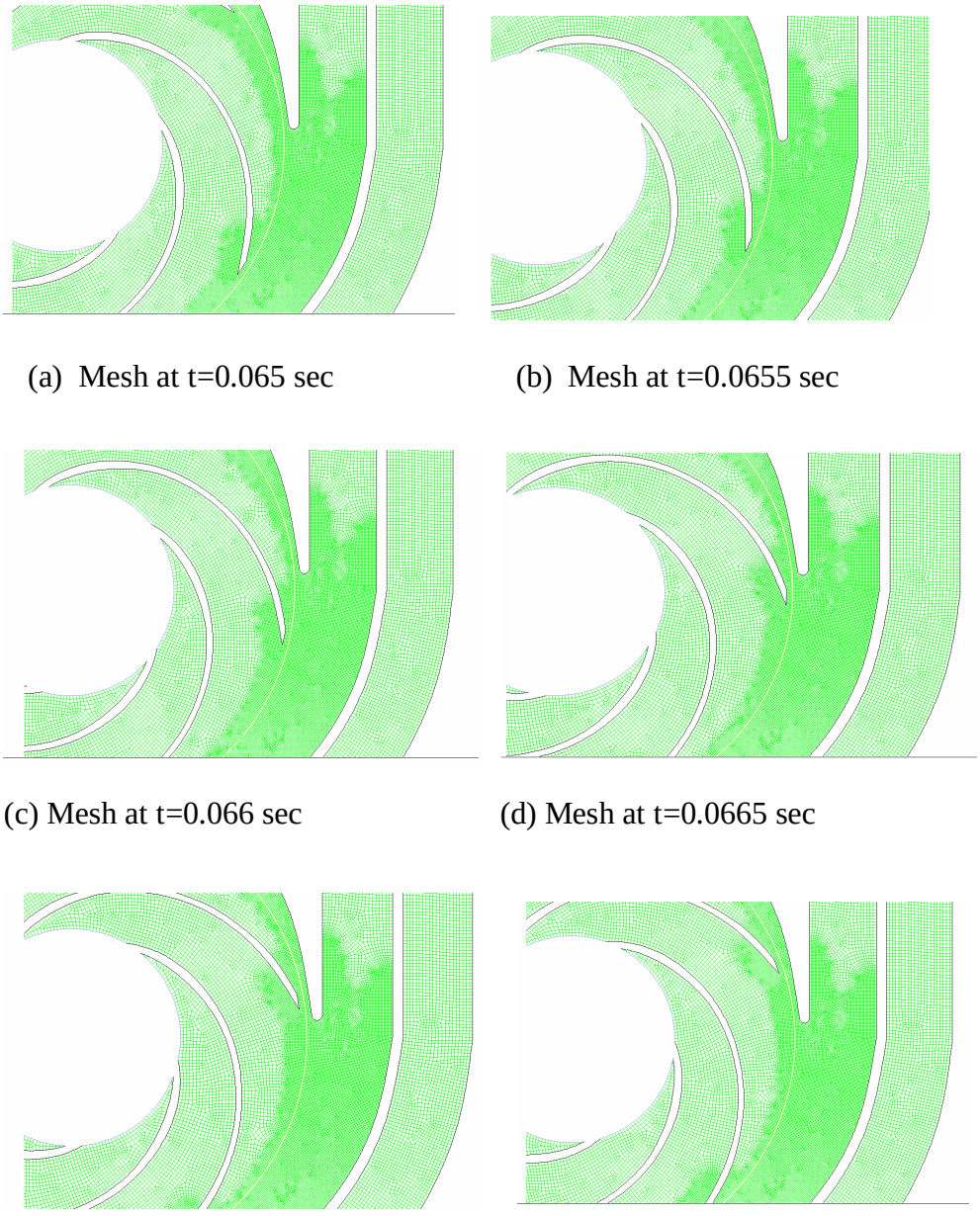

(a) Mesh at t=0.065 sec

(b) Mesh at t=0.0655 sec

(c) Mesh at t=0.066 sec

(d) Mesh at t=0.0665 sec

(e) Mesh at t=0.067sec

(f) Mesh at t=0.0675 sec

Figure 4.5 Depiction of sliding mesh configurations at 6 positions during impeller rotation of 0.0025 second, rotational speed is 3540 rpm

4.3.5 GRID INDEPENDENCE STUDY

4.3.5.1 MESH SIZE

Three different mesh sizes were examined for the unsteady pressure field inside the pump as shown in Fig. 4.6, with time step of 0.0001 sec, as follows:

- M1: Coarse mesh (2955 cells for the impeller and 7415 cells for the volute)
- M2: Fine mesh (11746 cells for the impeller and 29650 cells for the volute)
- M3: Very fine mesh (47785 cells for the impeller and 119630 cells for the volute)
- M4: The mesh has been refined in high gradient areas; close to the interface zone, blades trailing edges, and volute vanes leading edges.

Results showed that the differences in the pressure distributions and pump head between the fine and very fine meshes are small while the coarse mesh over-estimates the pressure values. Refining the mesh in the interaction and high gradient zones was proven to give almost the same results as in the fine mesh case.

The location of the interface between impeller and volute was also examined as shown in Fig. 4.7. To obtain skew-free cells at the interface, about 4 cells are required between the impeller blades and the interface. The same number of cells between the volute vanes leading edge and the interface are needed. This requirement restricts the size of mesh in these narrow gaps.

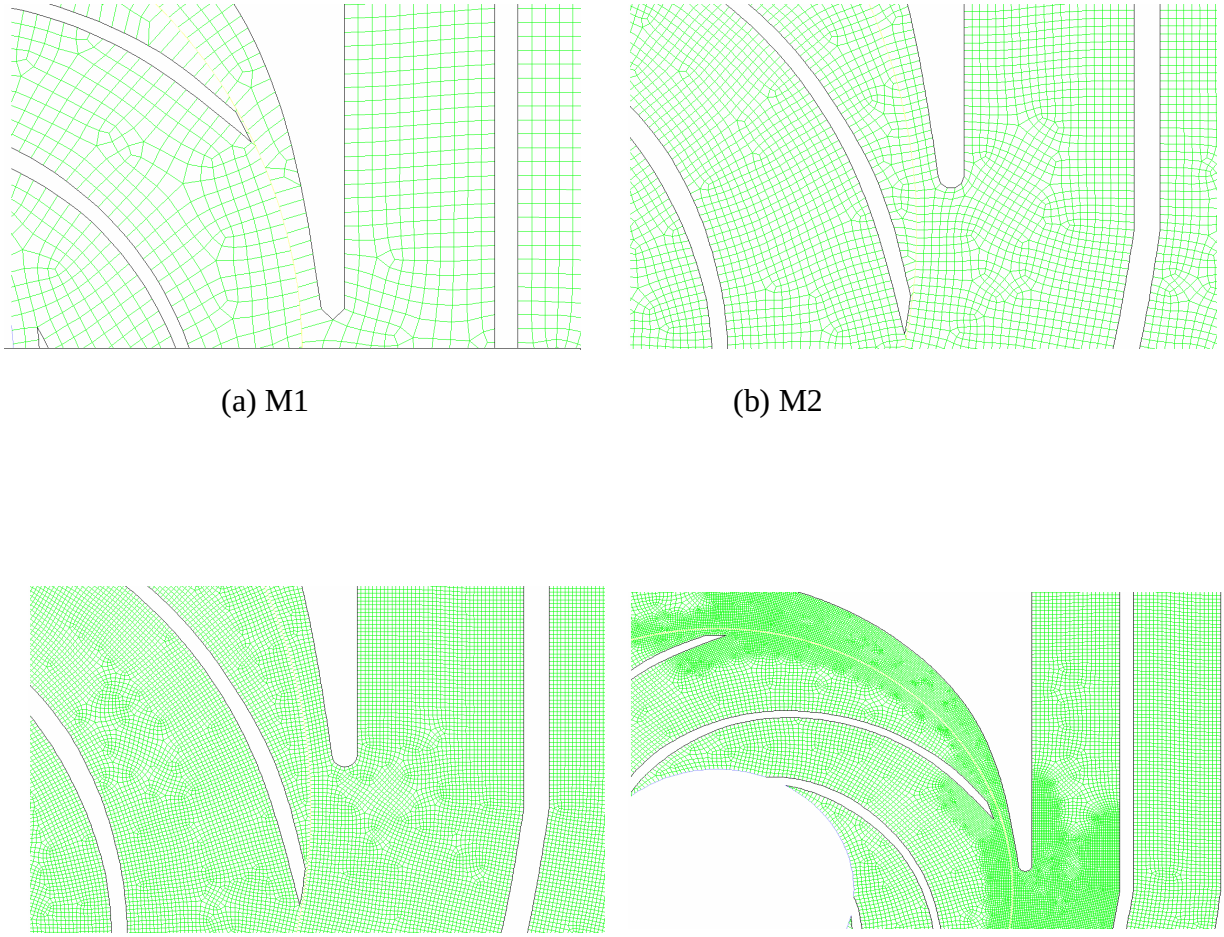

(a) M1 (b) M2

(c) M3 (d) M4

Figure 4.6 Sections of the four meshes used for the grid-independence study

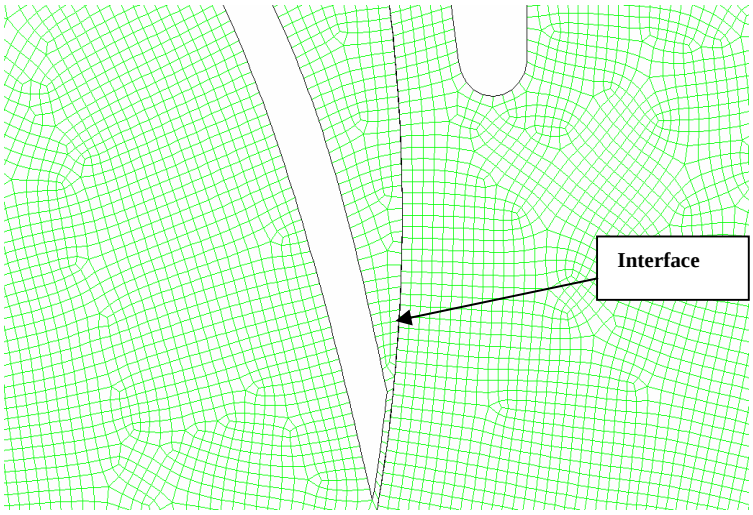

(a)

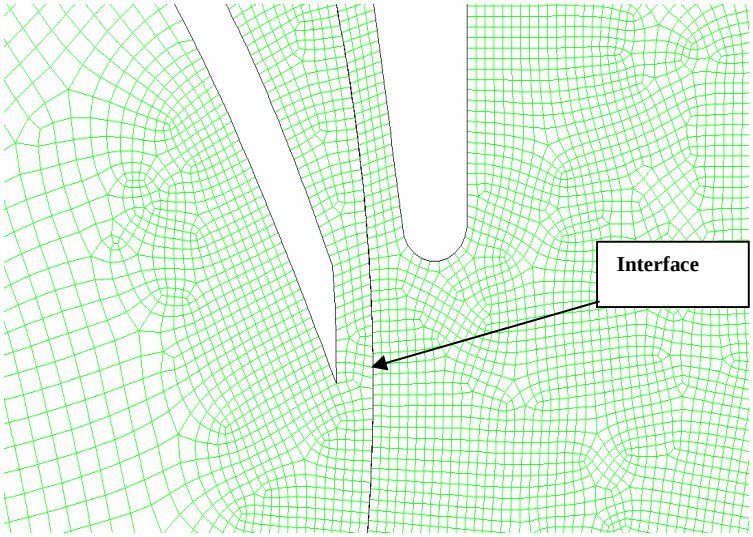

(b)

Figure 4.7 Location of the interface between impeller blades and volute vanes

4.3.5.2 TIME STEP

Experiments on the model pump and filed measurements on the boiler feed pump showed that the first blade passing frequency (BPF) is the dominant frequency in the spectral analysis of pressure fluctuations. The second and the third harmonics of the BPF appeared as small sidebands. Since the model pump has a rotational speed of 3540 rpm, the 1^{st} BPF is 295 Hz (=5xRPM). One cycle of pressure fluctuation inside the pump is expected to take about 0.0034 sec at this speed. In order to capture the correct transient behavior of the flow inside the pump, two time steps are examined. Time increments of Δt=1E-4 sec and Δt=1E-5 sec are tested. Results of the numerical solutions showed that both the time steps give the same results. Therefore, a time step of 0.0001 sec has been chosen for the numerical simulations.

4.3.6 GENERAL PARAMETERS OF SIMULATION MODELS

The following parameters are used for all simulation models of different designs and flow rates at pump rotational speed of 3540 rpm.

- Average number of Cells

Volute: 53600 quadrilateral cells

Impeller: 22000 quadrilateral cells

- Models

Space	2D
Time	Unsteady, 2^{nd} -Order Implicit
Viscous	Standard k-epsilon turbulence model
Wall Treatment	Standard Wall Functions

- Boundary Conditions

Volute flow:

Water-liquid (Density= 998 kg/m^3)

Stationary

Impeller flow:

Water-liquid

Motion Type: rotational

Rotation speed: 370.7 rad/sec (3540 rpm)

Inlet: Velocity, normal to the boundary, Absolute Velocity Formulation

Outlet: pressure outlet

- Unsteady Calculation Parameters

Time Step (s)	1E-4
Max. Iterations per Time Step	50
Convergence tolerance	1E-6

- Discretization Scheme

Pressure	Standard
Momentum	Second Order Upwind
Turbulence Kinetic Energy	Second Order Upwind
Turbulence Dissipation Rate	First Order Upwind

4.3.7 BOUNDARY CONDITIONS

The boundary conditions for the modeled cases were taken to be the same as the experimental conditions of the model pump testing for the sake of later comparison between numerical and experimental results. The velocity inlet boundary condition at the impeller eye represents the flow rate while the pressure outlet was selected for the discharge side at pump exit. Other boundary conditions like velocity inlet-velocity outlet and pressure inlet-pressure outlet were also examined. However, the conditions of velocity inlet and pressure outlet gave the closest pressure distribution to the experimental results and hence they were adopted.

4.3.8 MONITORING LOCATIONS

Figure 4.8 shows the locations at which the unsteady pressure signals are monitored throughout the transient simulations. Table 4.1 gives the coordinates of these monitoring locations inside the pump.

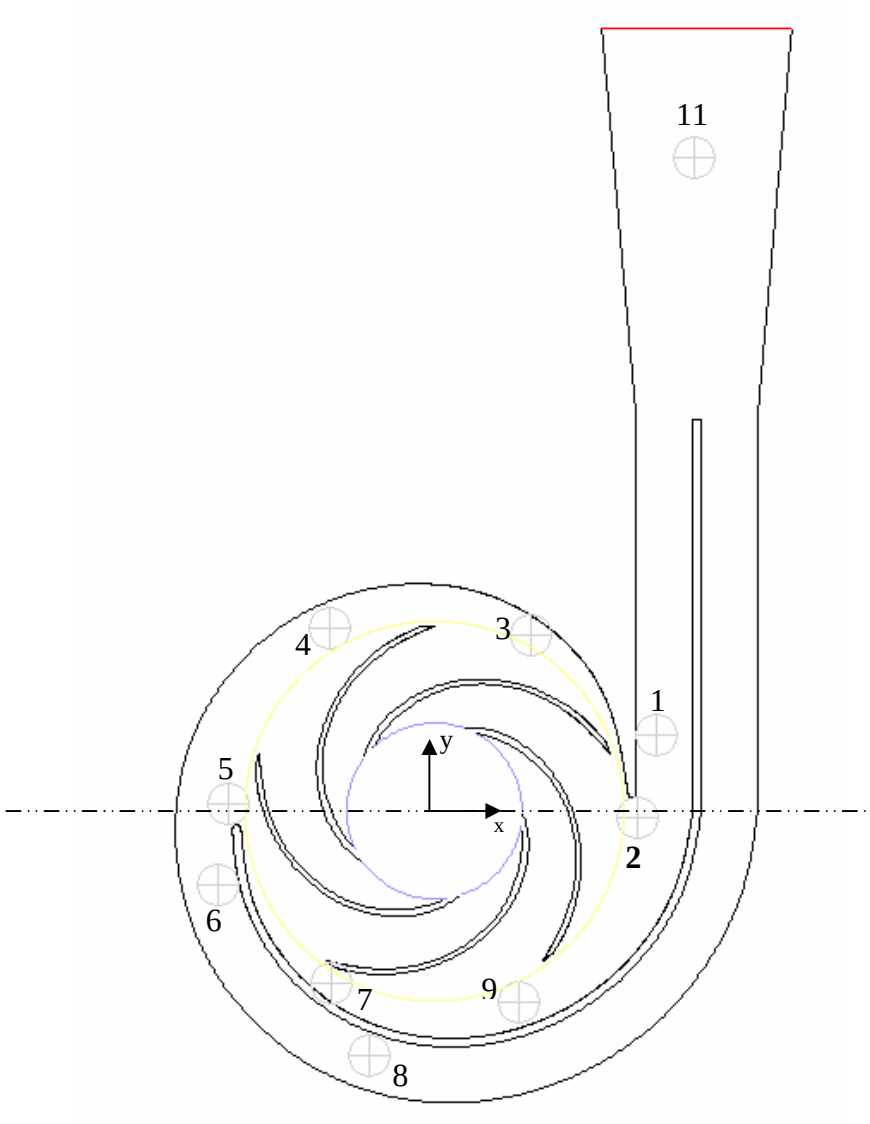

Figure 4.8 Locations of pressure monitoring inside the pump, similar to experimental setup

Table 4.1 Coordinates of monitoring locations

Location of holes relative to volute horizontal centerline

Sensor #	X (mm)	Y (mm)
1	85.10	29.30
2	77.95	-2.73
3	37.33	67.34
4	-40.50	70.15
5	-78.95	2.76
6	-83.20	-28.64
7	-39.66	-66.00
8	-25.11	-93.70
9	32.52	-73.08
11	100	250

4.4 RESULTS OF 2D SIMULATIONS

In this section, the results of the 2D numerical simulations for different pump geometries (impeller and volute) are presented at different flow rates. The simulations follow the experimentally tested geometries and flow rates. The pump rotational speed is fixed at 3540 rpm (370.7 rad/sec). The first geometry to be presented is the impeller without V-cut at blade exit combined with the original volute geometry. A comprehensive analysis is presented for this case as a basic simulation to assess results obtained from other geometry modifications.

4.4.1 SIMULATION RESULTS FOR IMPELLER WITHOUT V-CUT AT BLADE EXIT

Results obtained from the CFD model are presented in this section for the case of 3.6 mm gap and impeller without V-cut at blade exit. It contains five simulations corresponding to five different flow rates for this geometry. Table 4.2 lists the numerical values of the boundary conditions used for the simulations. Q is the flow rate while Qn represents the nominal flow rate corresponding to the best efficiency point, as measured experimentally at 3540 rpm.

Table 4.2 Boundary Conditions for Numerical Simulation: speed 3540 rpm, Without V-cut at blades exit: gap 3.6 mm

Q/Qn	Velocity inlet [m/s]	Pressure outlet [pa]
1.66	5.3	68,000
1	3.2	290,000
0.75	2.4	345,000
0.5	1.6	375,000
0.25	0.8	395,000

A= flow area at impeller inlet= πD*width

Width= 15 mm between the hub and shroud

D= 80 mm = average eye diameter

Inlet velocity = Q/A, Q is measured experimentally.

Figures 4.9 and 4.10 show the contours of static pressure and velocity vectors for the pump at the nominal flow rate (Q=Qn), respectively. These Figures are presented to distinguish the areas with high and low pressures and velocities inside the pump. The lower pressure was found at impeller inlet (suction) while the highest velocity was located at impeller blade exit as expected. Figure 4.11 compares the static pressure contours inside the pump for different flow rates, namely; Q/Qn = 1, 1.66, 0.25. When the pump operates at maximum flow ratio of 1.66, the leading edges of volute diffuser vanes are exposed to very low pressure. If the pressure drops below the vapor pressure at these locations, cavitation is expected. This expectation is supported by the observation of local separation at the leading edges of the volute vanes during the experiments on the scaled pump at this flow rate.

The predicted values for the static pressure at impeller inlet are very low, even below the vapor pressure (cavitation onset). The results of the 2D simulations for the pressure close to the impeller inlet are not realistic and can not be compared with actual values. This is because the flow field in this area is highly 3D with complicated inlet geometry. The pressure field starts to have a 2D behavior close to the exit of the impeller.

Another comparison is shown in Fig. 4.12 for the velocity vectors at different flow ratios of Q/Qn= 1, 1.66, 0.25. At the design flow rate, the flow coming out of the impeller is tangential to the volute vanes. At maximum flow rate, the flow exiting the impeller is not tangential to the vanes and the velocity vectors are directed out of the impeller to the pump exit near the volute cutwaters with high speeds. A reverse flow with small vortices trying to escape from the gap between the impeller and the volute vanes to the exit was also noticed. When the flow ratio is reduced to lower value of

Q/Qn = 0.25, the flow at the interaction zone at the volute cutwaters tends to be reversed inside the impeller. Operating at part loads increases the circulatory flow and causes the pre-rotation at the suction eye/pipe and excites the pressure fluctuations inside the pump. The CFD prediction for the H-Q curve is shown in Fig. 4.13. The pressure at exit is a given boundary condition while the pressure at impeller inlet is the area-weighted averaged pressure at inlet boundary. The velocities used to calculate the head are the delivery and suction pipes velocities based on the flow rate.

A typical waveform and FFT analysis of the unsteady pressure signal at point 3 is shown in Fig. 4.14. The 2D numerical simulation is capturing the fluctuation frequencies very well as found by experimentation. The first blade passing frequency is the dominant and its higher harmonics appear with smaller magnitudes. The pressure signal in the discharge nozzle (point 11) is shown in Fig. 4.15. It shows that the energy content of fluctuations in the discharge nozzle/pipe are very small (check the scales of y-axes) and not comparable to fluctuations inside the pump (e.g. point 3). This result for the discharge pipe is found to be in a good agreement with experimental measurements.

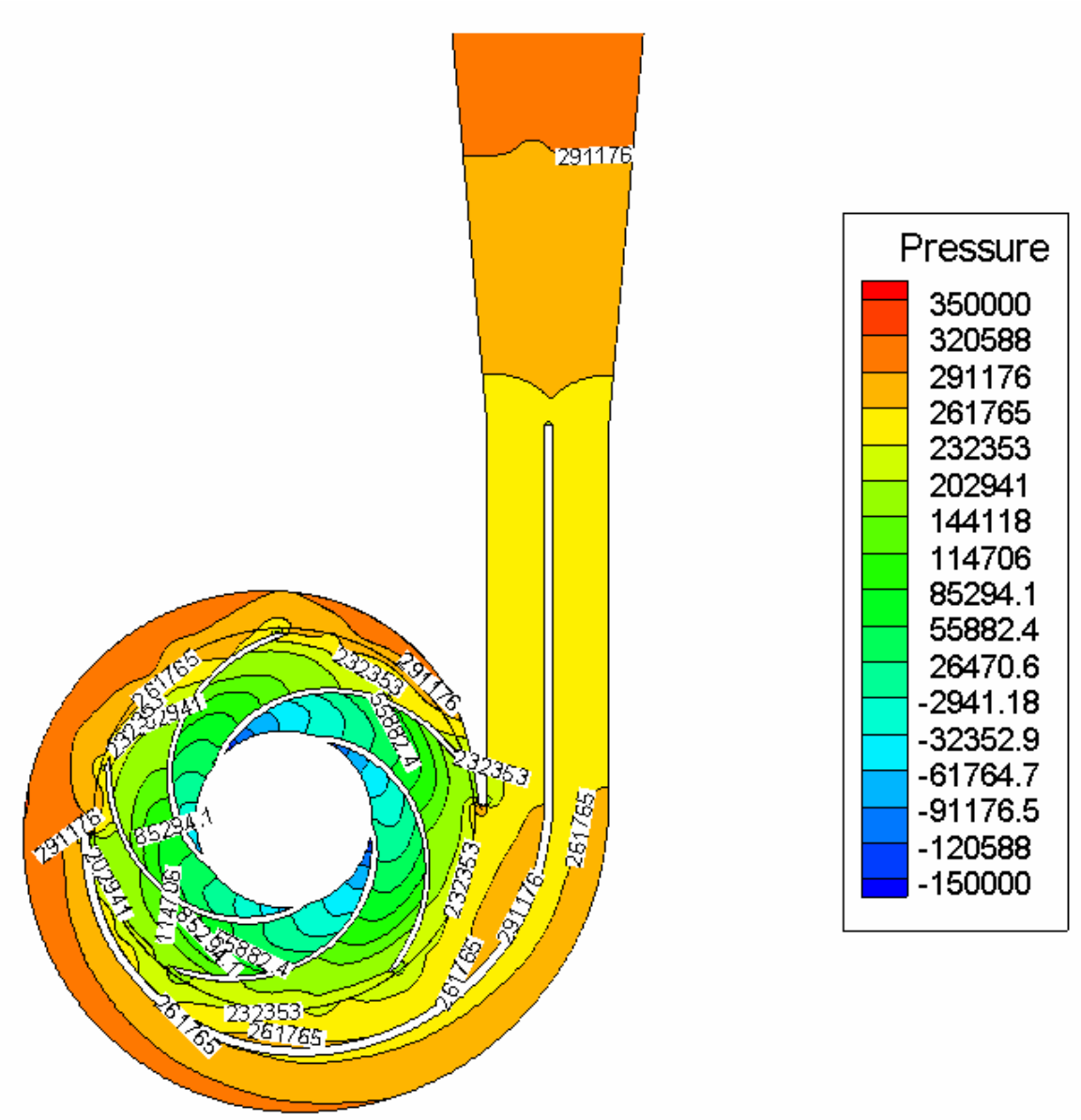

Figure 4.9 Contours of static pressure (pa), Q=Qn, without V-cut at exit, gap 3.6 mm

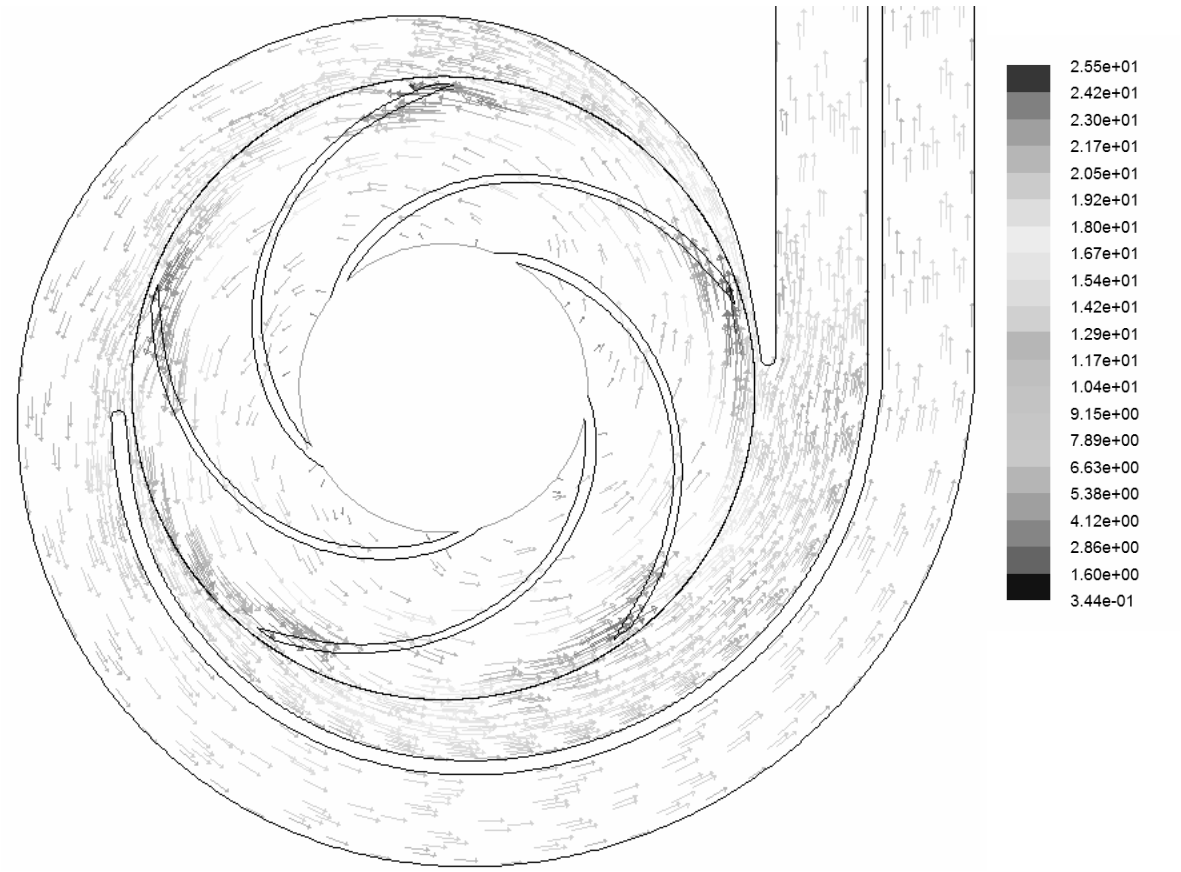

Figure 4.10 Velocity vectors (m/s), Q=Qn, without V-cut at exit, gap 3.6 mm

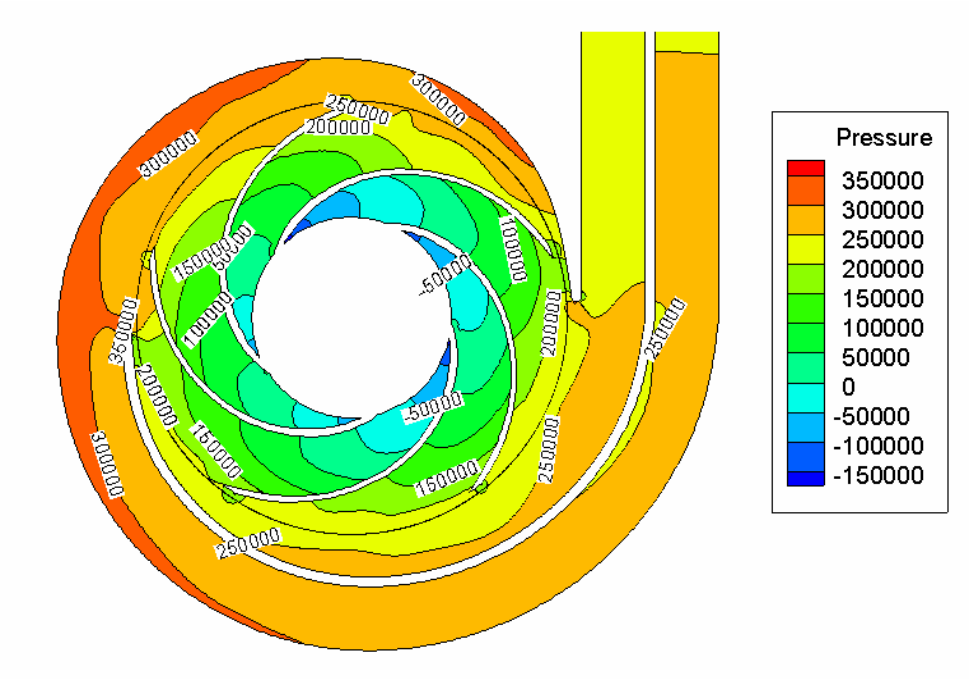

(a) Q=Qn

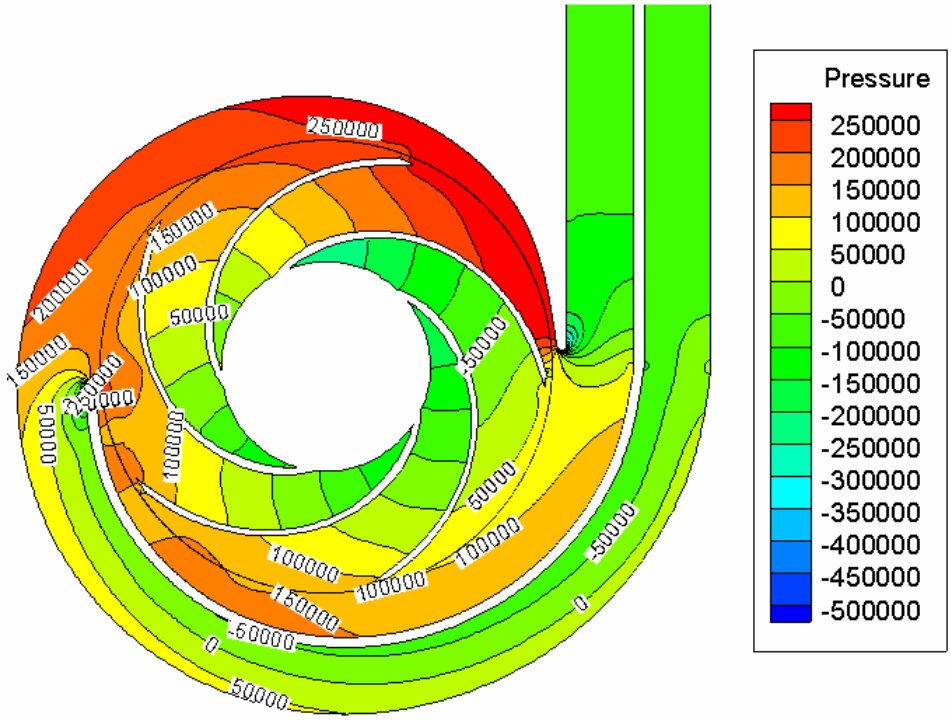

(b) Q=1.66 Qn

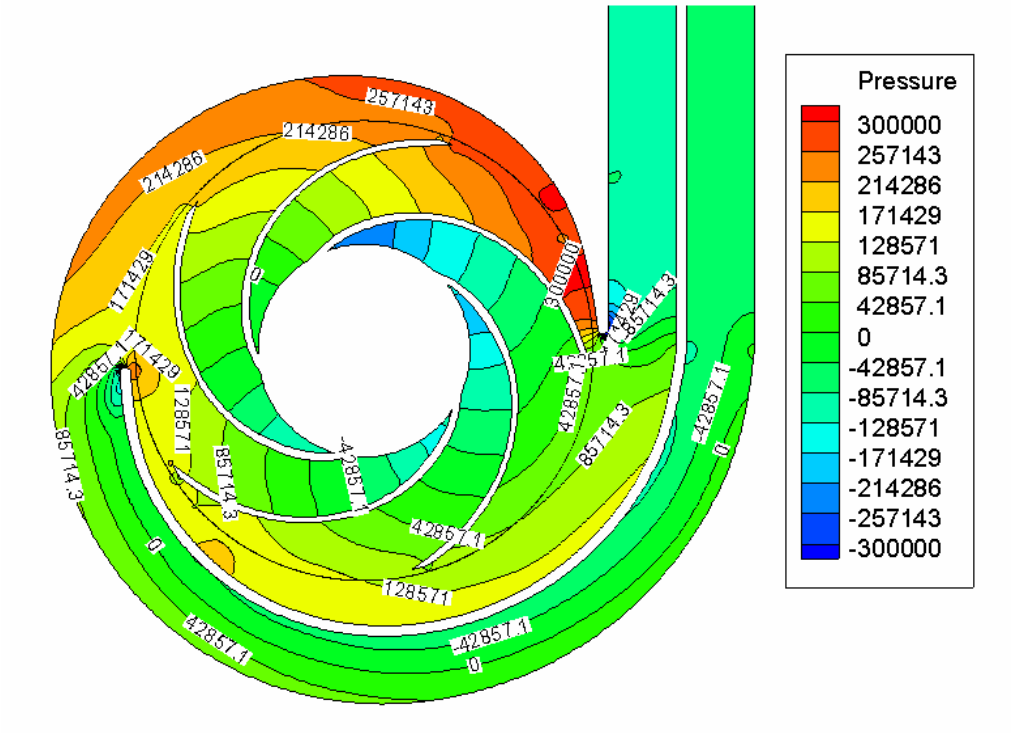

(c) Q=0.5 Qn

Figure 4.11 Contours of static pressures at different flow rates

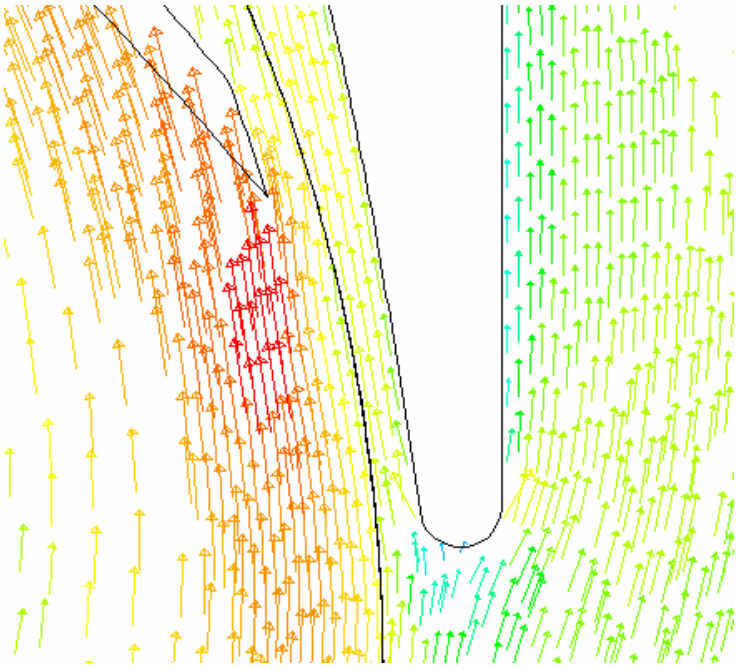

(a) Q=Qn

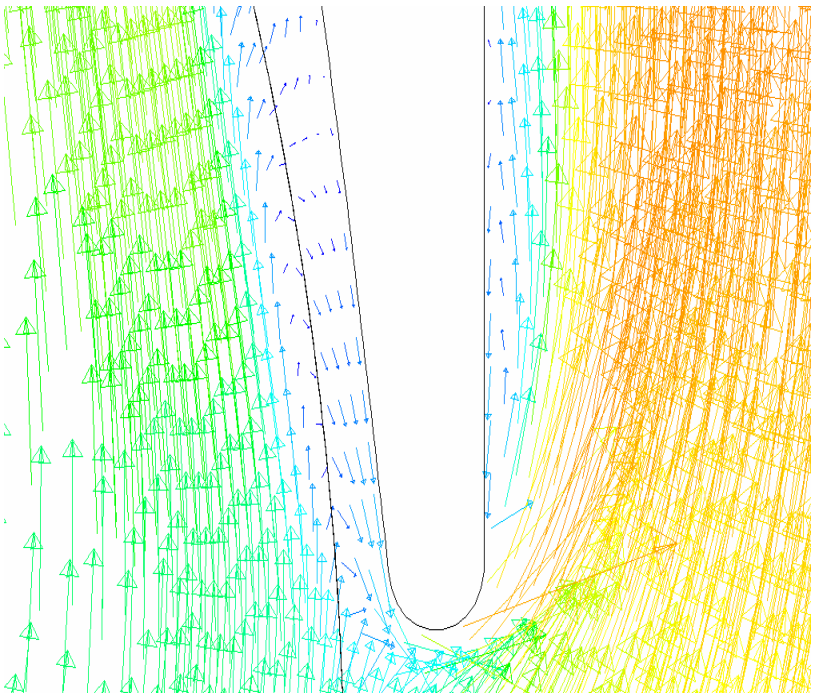

(b) Q=1.66Qn

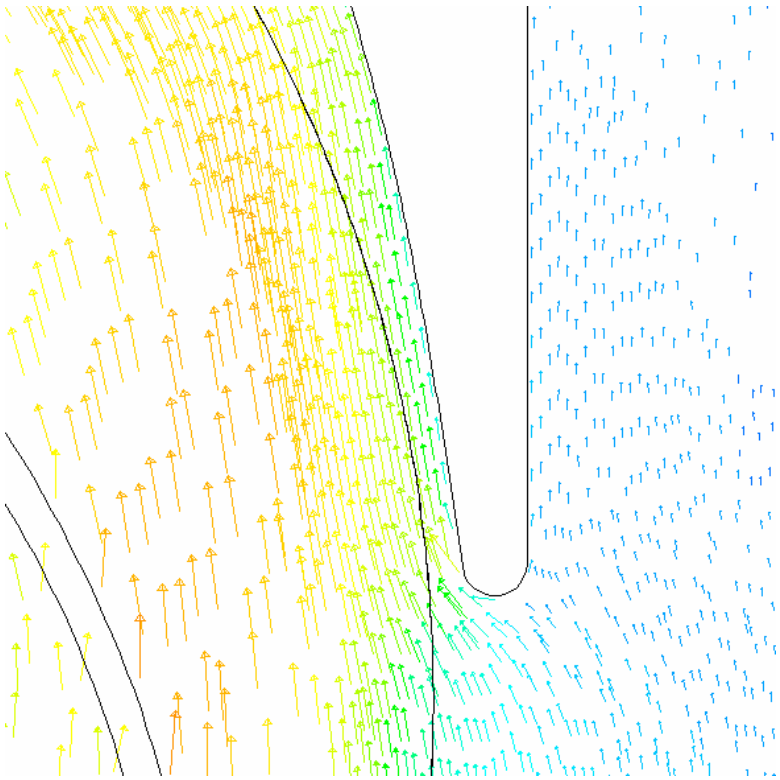

(c) Q=0.25Qn

Figure 4.12 Velocity vectors close to interaction zone; at different flow rates

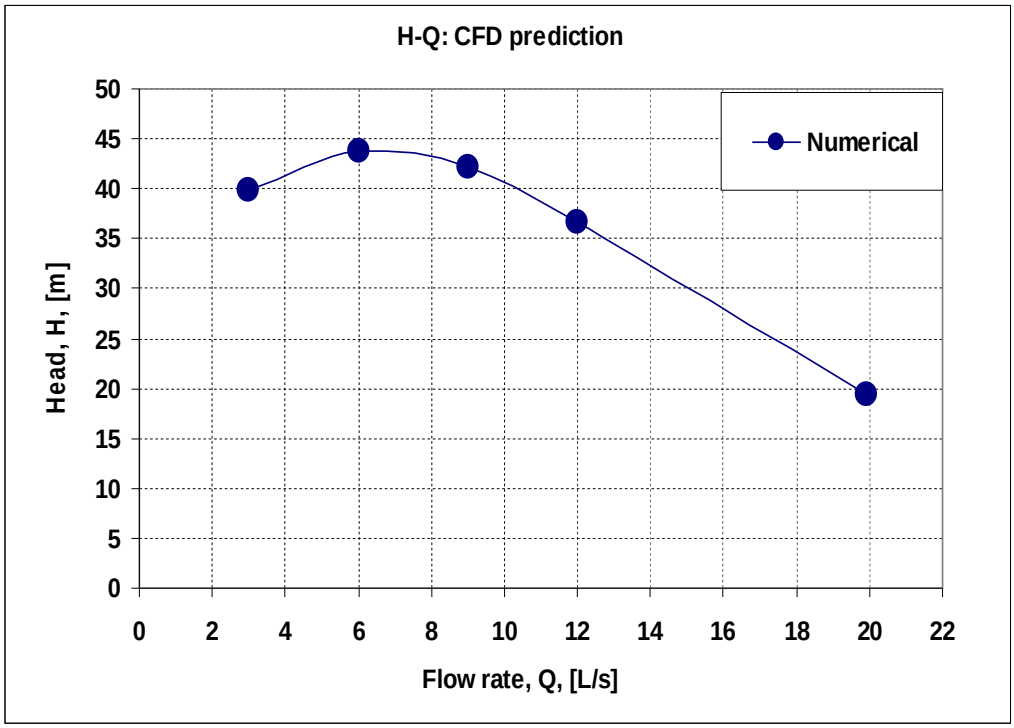

Figure 4.13 CFD prediction for H-Q curve

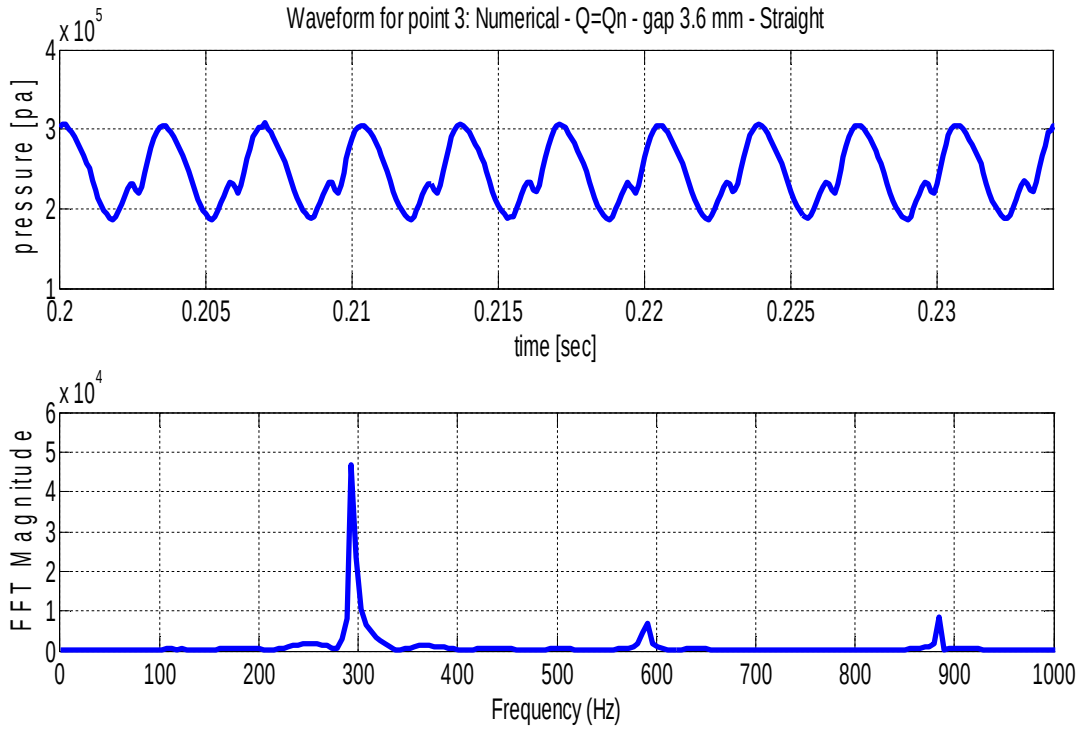

Figure 4.14 Typical waveform and spectral analysis of the unsteady pressure history at point 3

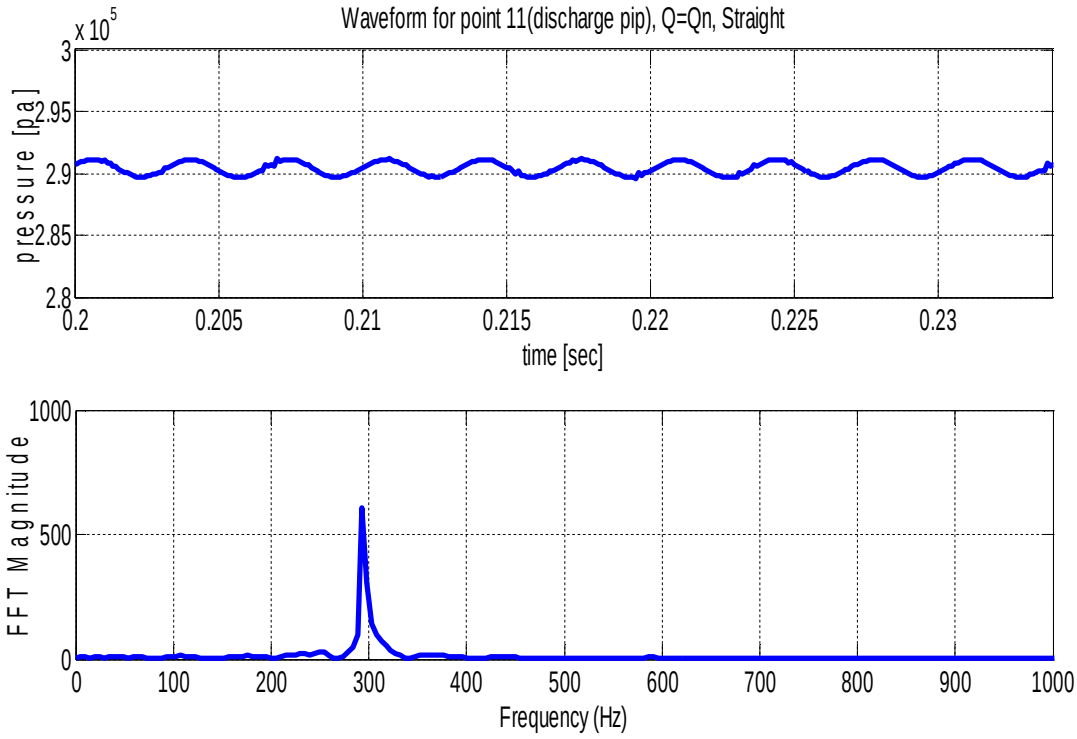

Figure 4.15 Waveform and spectral analysis of the pressure signal at the discharge nozzle

The simulation results for the time-averaged static pressure distribution inside the pump under different flow rates are given in Fig. 4.16. At the nominal flow rate, the pressure is considered to be constant around the impeller while at off-design flow rates, there is a large variation in the pressure values from point to point, i.e. the pressure is not uniform. As done in the experimental testing, the locations of monitoring points around the impeller were selected such that they are geometrically symmetrical pairs of locations with respect to the volute cutwaters (vanes leading edges). They are in similar locations and expected to have similar flow conditions. These pair of locations around the impeller are (2,5), (3,7), (4,9).

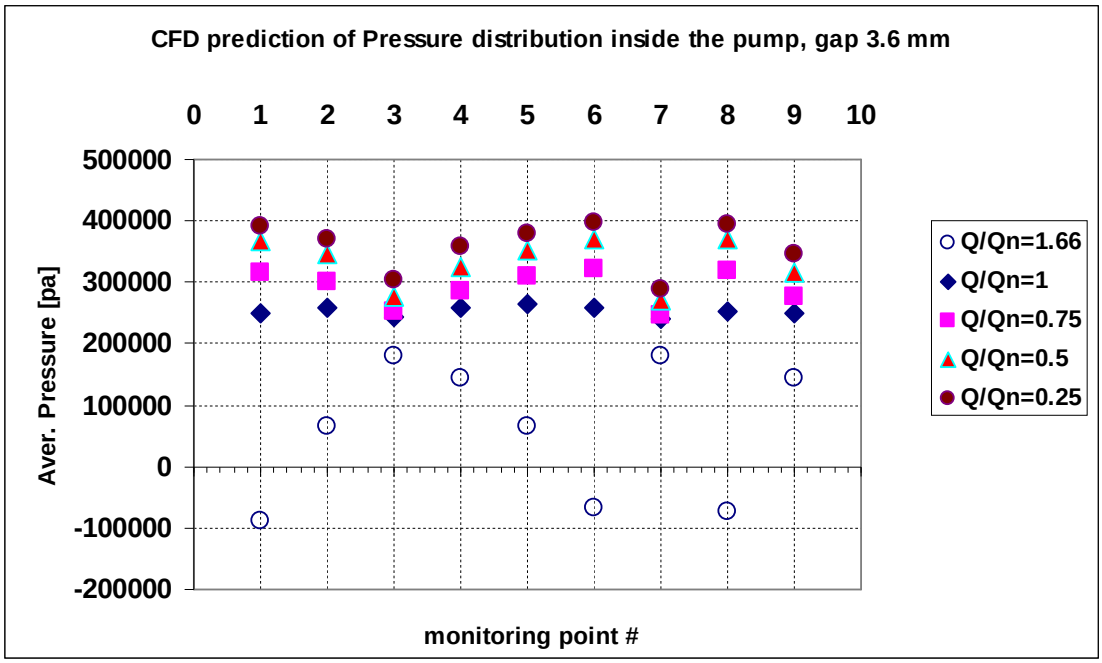

Figure 4.16 Time-averaged pressure distribution inside the pump at different flow rates

Figure 4.17 proves that geometrically similar pairs of locations around the impeller have the same pressure values at all flow rates. These results of pressure are similar to the experimental ones.

Pressure fluctuations for all selected points inside the pump are shown in Fig. 4.18a for reduced flow rate conditions and in Fig. 4.18b for flow rate of 166% of the nominal. Operating at off-design flow rates increases the pressure fluctuations around the impeller. Point 3 showed the maximum amplitude of fluctuation (measured peak-to-peak) due to its closeness to the interaction zone between the impeller and volute vanes. Flow rates much higher than the design capacity produce high pressure fluctuations which are comparable to those at flow rates much lower than design value.

The effect of flow rate on the unsteady pressure signal at location 3 is given in Fig. 4.19. Location 3 is selected since it is experiencing the highest pressure fluctuation inside the pump. Operating at off-design conditions increases the pressure fluctuation and its energy content. Figure 4.19 was produced using Matlab software. Figure 4.20 shows the effect of flow rate on the FFT spike magnitude, measured at 1^{st} BPF, at point 3. The minimum fluctuations energy is recorded at the design flow rate.

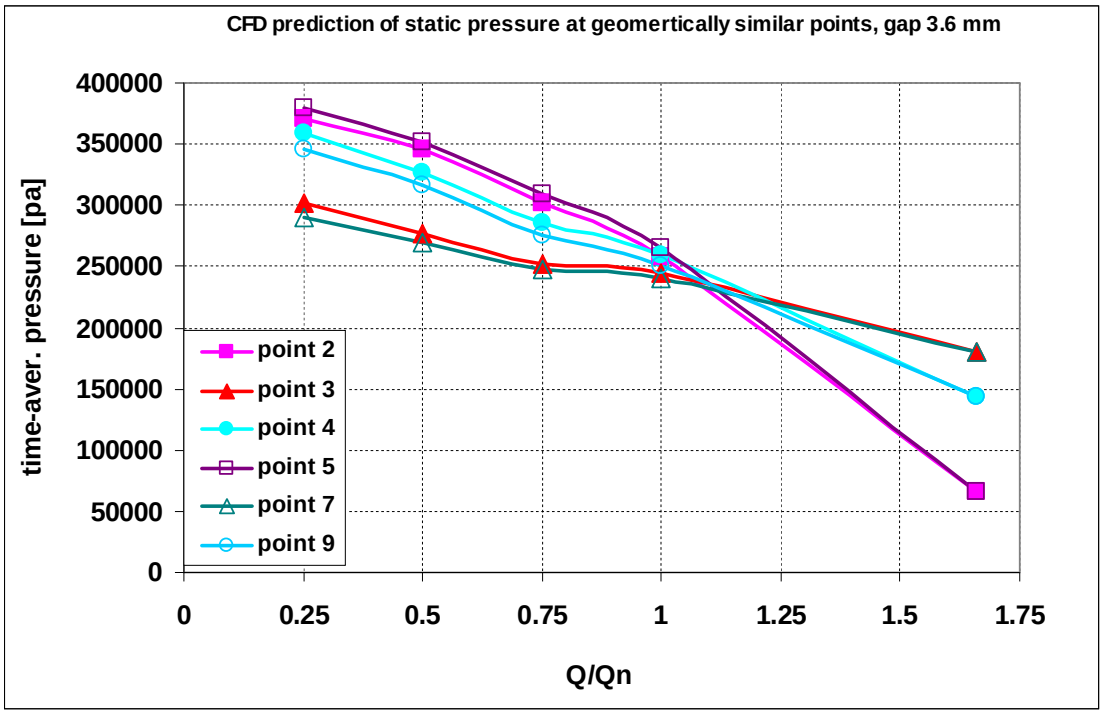

Figure 4.17 Time-averaged pressures at geometrically similar points around the impeller, at different flow rates

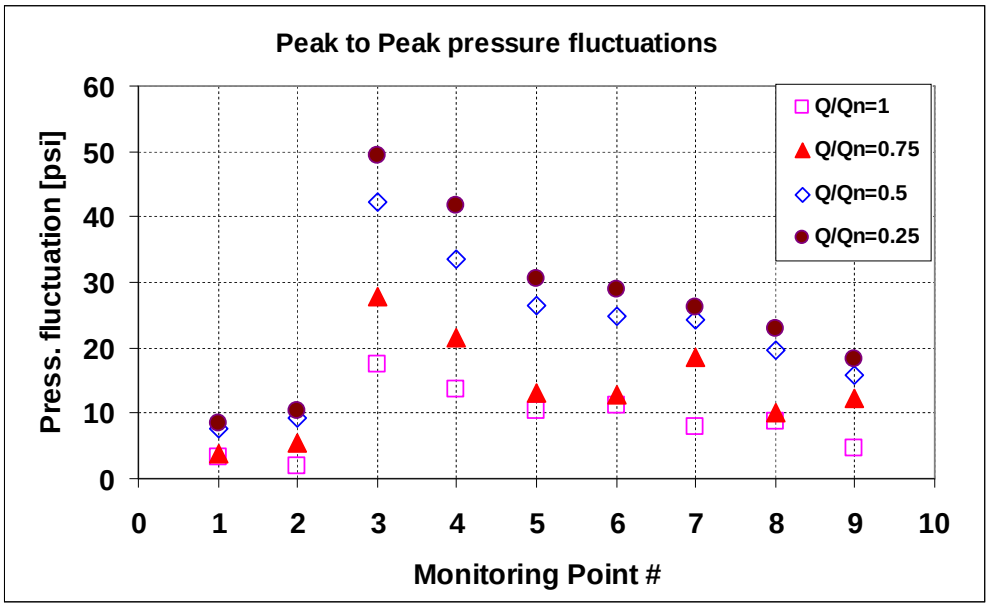

(a)

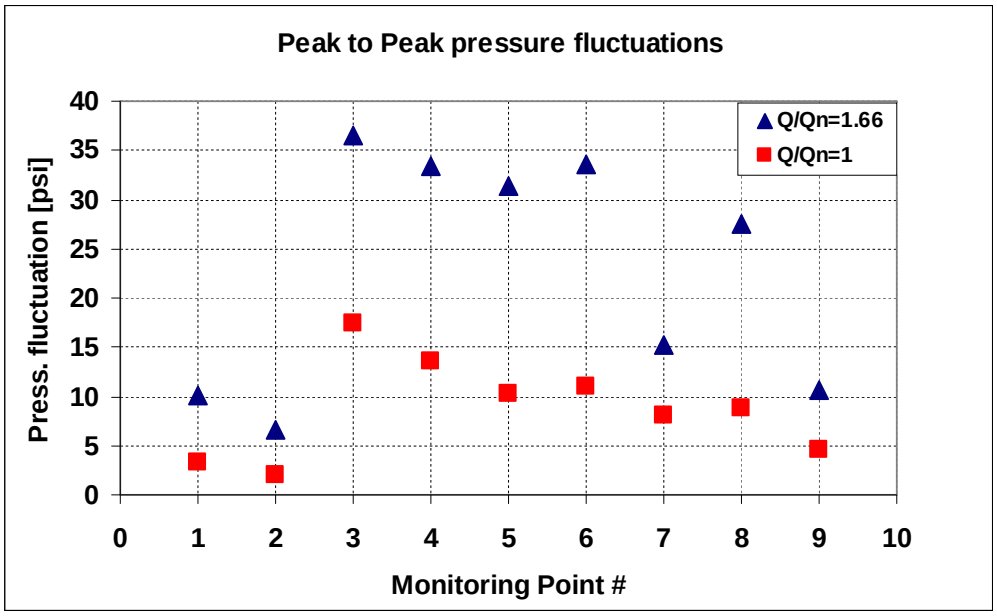

(b)

Figure 4.18 Peak-to-peak pressure fluctuations for the monitored locations at different flow rates

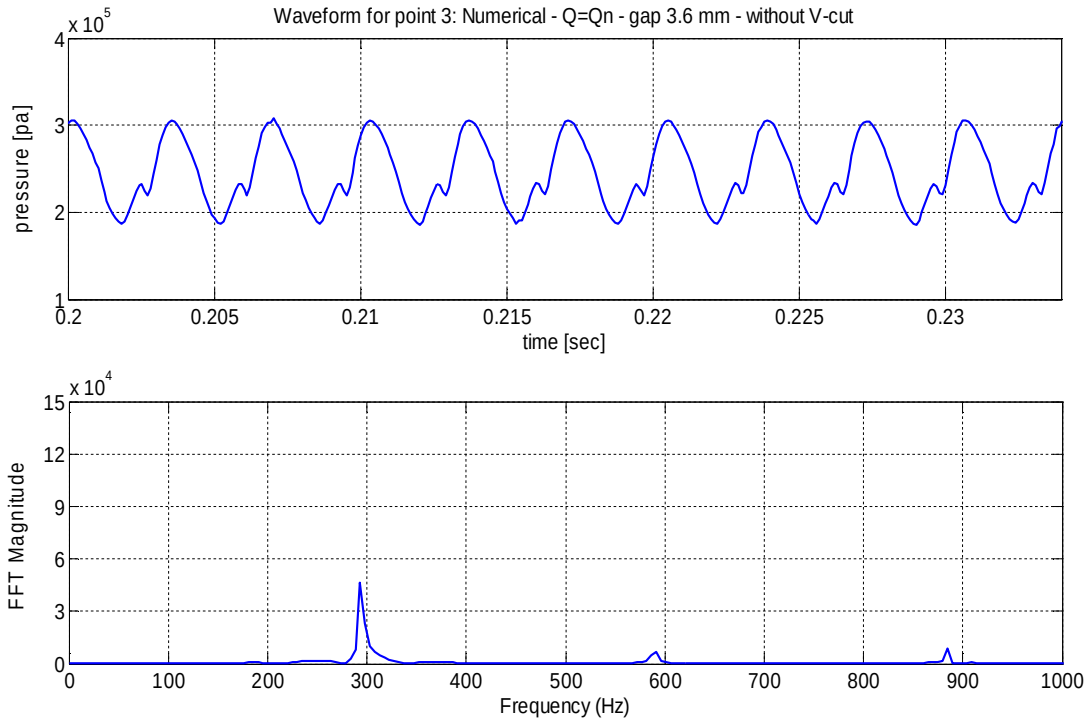
Waveform for point 3: Numerical - Q=Qn - gap 3.6 mm - without V-cut
x 10^5
pressure [pa]
time [sec]
x 10^4
FFT Magnitude
Frequency (Hz)

(a)

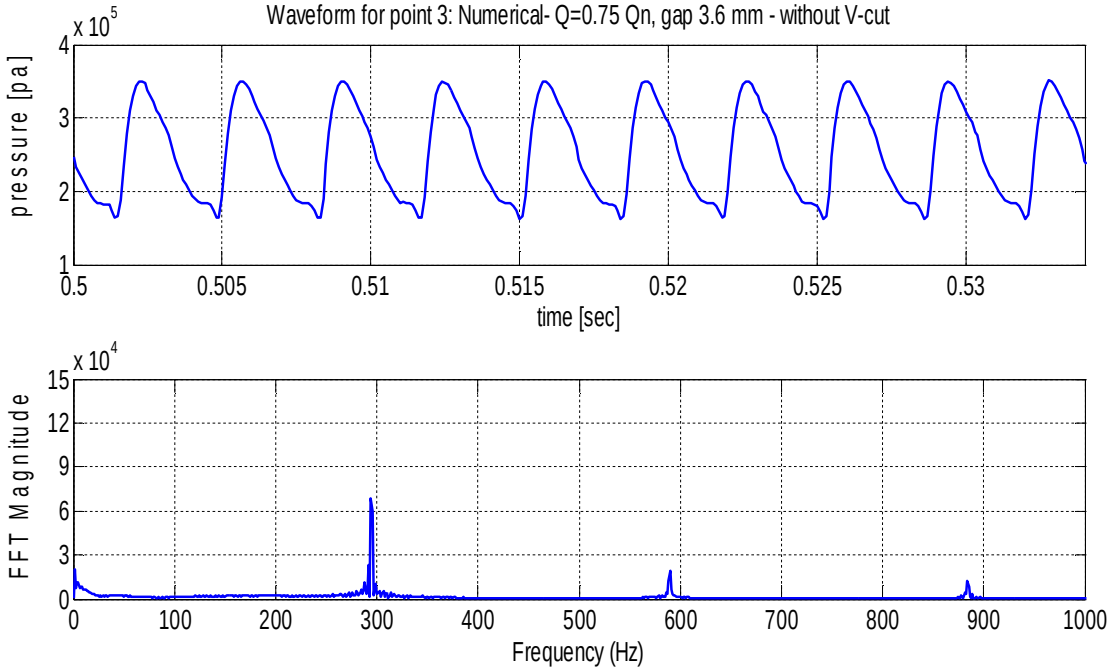
Waveform for point 3: Numerical- Q=0.75 Qn, gap 3.6 mm - without V-cut
x 10^5
pressure [pa]
time [sec]
x 10^4
FFT Magnitude
Frequency (Hz)

(b)

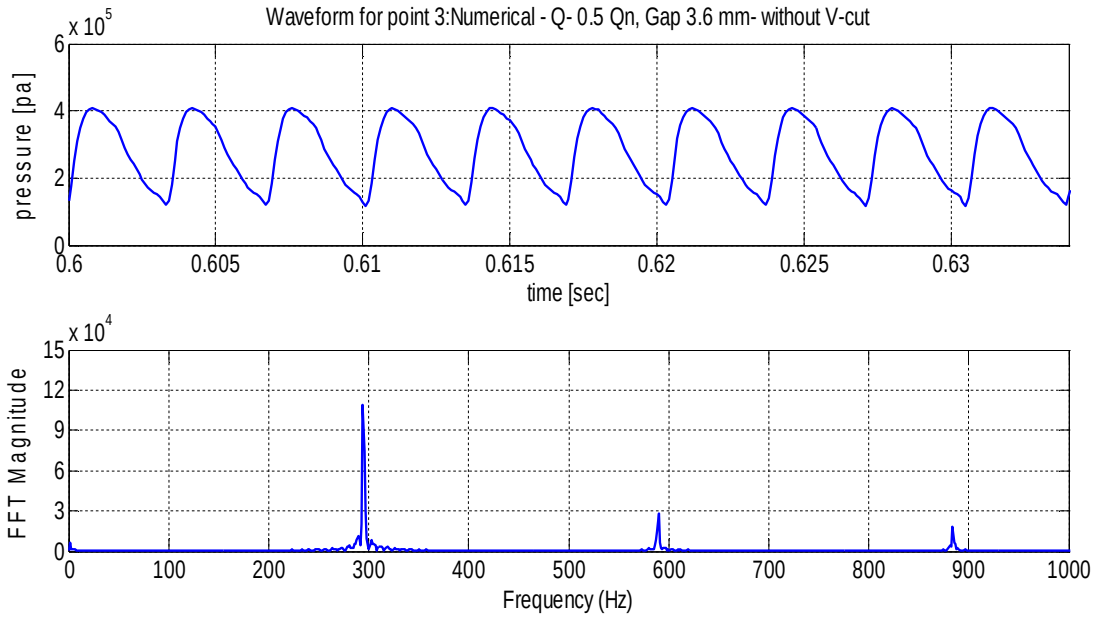
Waveform for point 3:Numerical - Q- 0.5 Qn, Gap 3.6 mm- without V-cut
x 10^5
pressure [pa]
time [sec]
x 10^4
FFT Magnitude
Frequency (Hz)

(c)

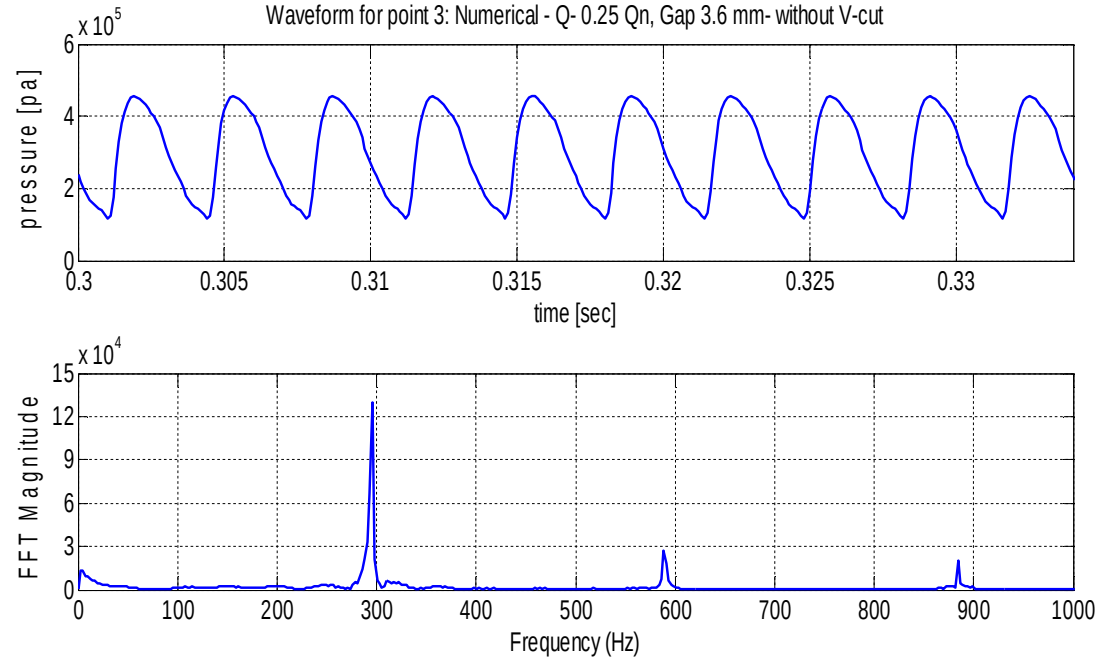
Waveform for point 3: Numerical - Q- 0.25 Qn, Gap 3.6 mm- without V-cut
x 10^5
pressure [pa]
time [sec]
x 10^4
FFT Magnitude
Frequency (Hz)

(d)

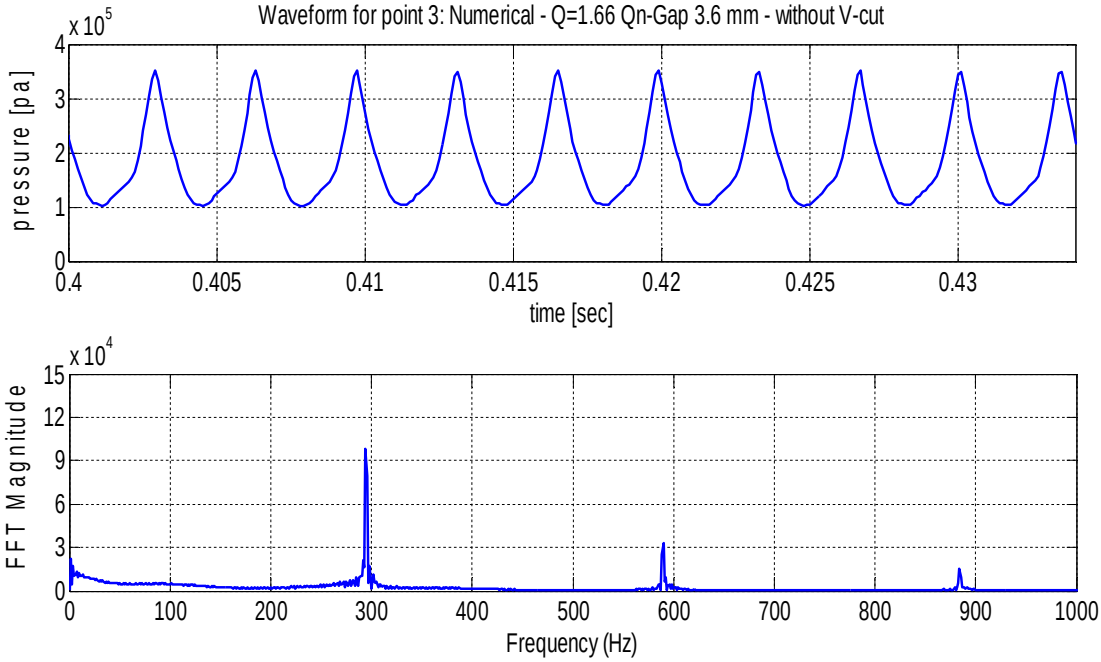

(e)

Figure 4.19 Effect of flow rate on unsteady pressure signal at point 3

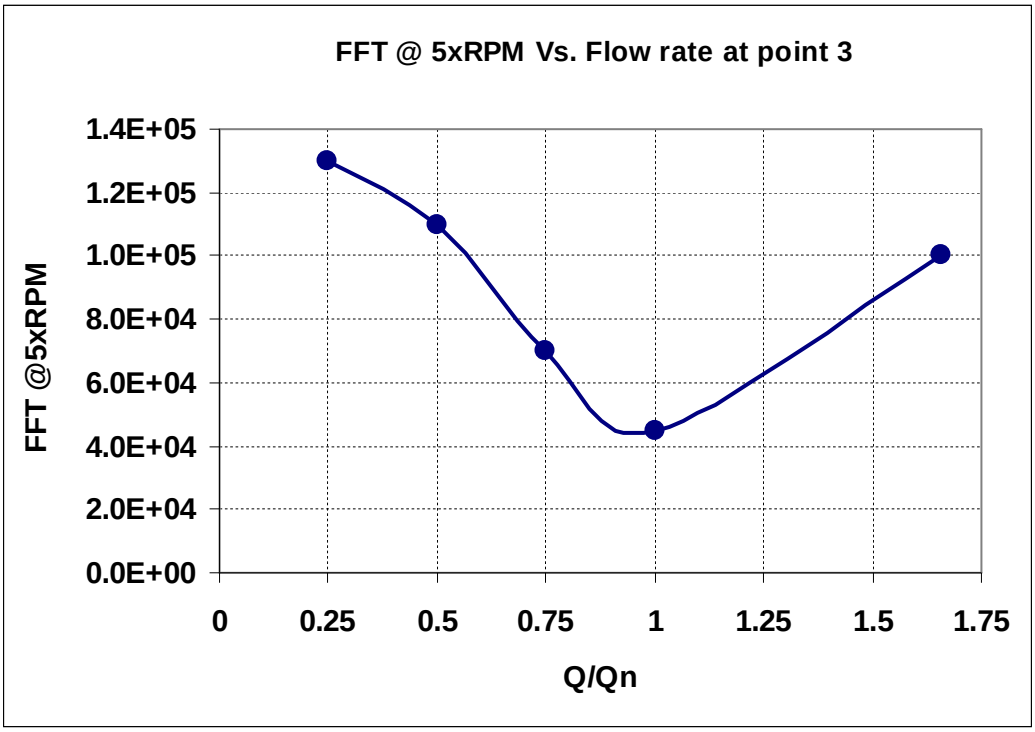

Figure 4.20 FFT peak magnitude of the 1st BPF at point 3 as a function of flow rate

The simulation also shows that the pressure fluctuations are affected by the location inside the pump. Thus, for a geometrically similar pair of locations, the fluctuations amplitudes and strengths are not equal. Figure 4.21 compares the time history and spectrum analysis of unsteady pressure at similar locations 3, 7 and 4, 9 at the design flow rate. Although similar locations have the same value of the time-averaged static pressure, they do not have the same values of fluctuations; even at the nominal flow rate. Figure 4.22 shows the effect of flow rate on pressure fluctuations at geometrically similar pairs of locations around the impeller. Minimum fluctuations were recorded at design flow rate. Similar pairs do not have the same pressure fluctuation amplitudes at all flow rates. Operating off-design increases the differences between the fluctuation amplitudes at similar location due to higher impeller-volute interaction.

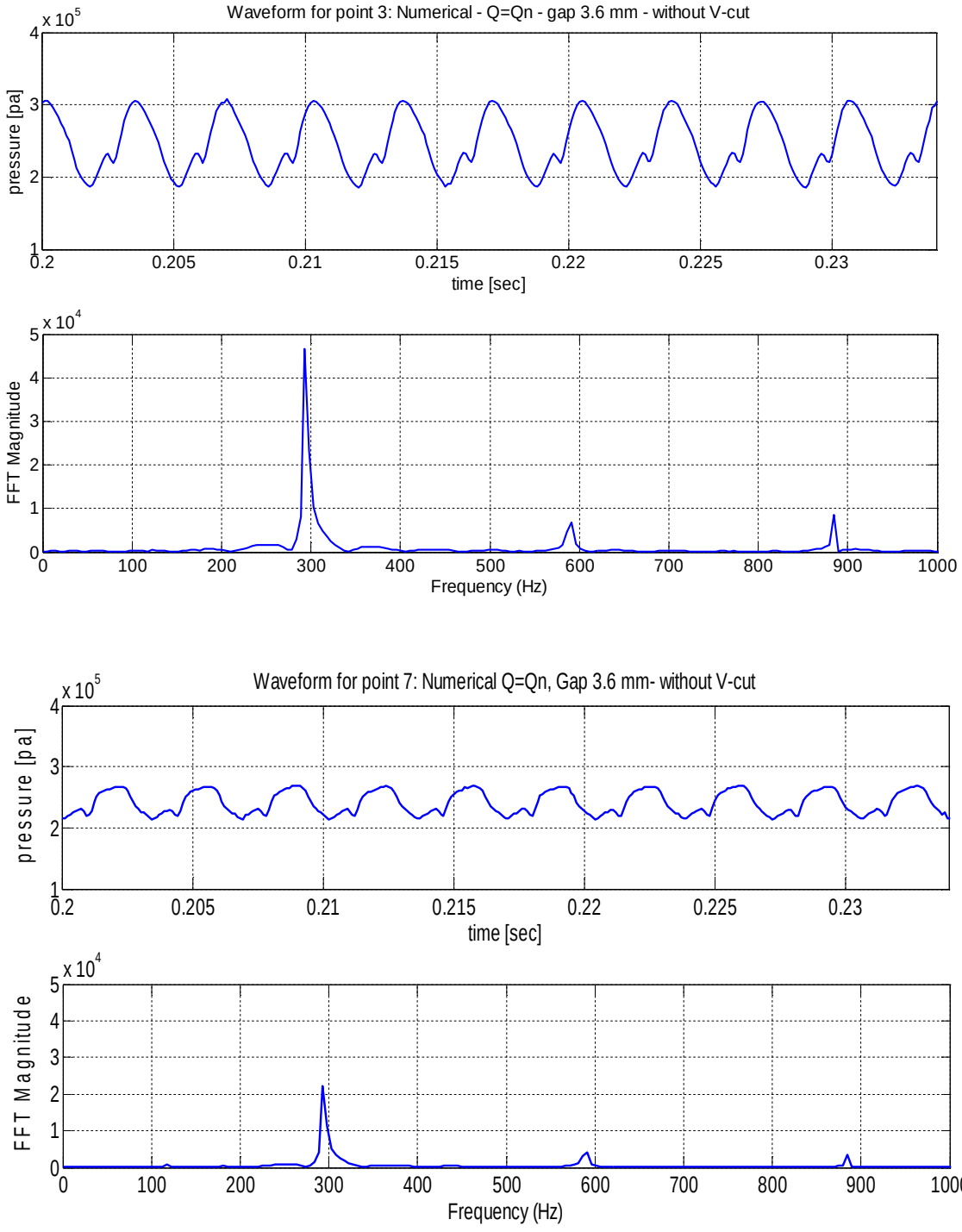

(a) Geometrically similar locations 3 and 7

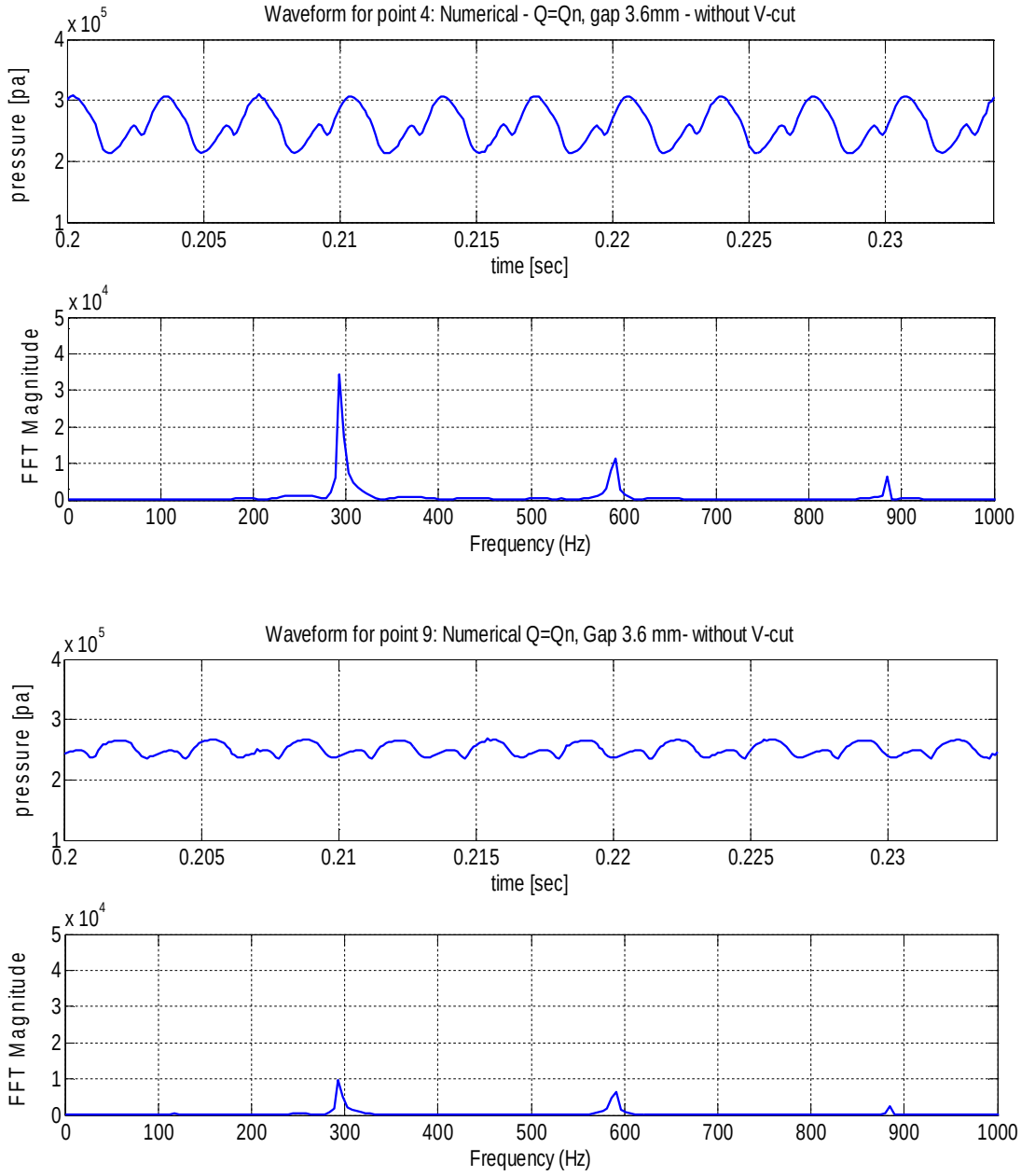

(b) Geometrically similar locations 4 and 9

Figure 4.21 Unsteady pressure signal at geometrically similar point, Q=Qn

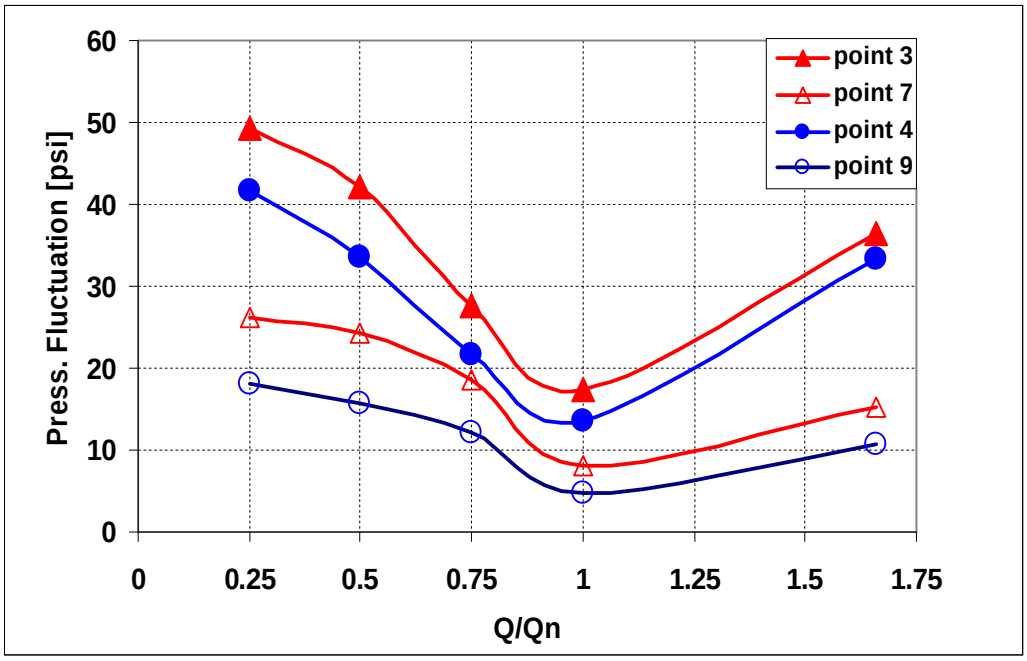

Figure 4.22 Peak-to-peak pressure fluctuations at geometrically similar pairs of locations around the impeller as a function of flow rate

4.4.2 EFFECT OF THE V-CUT

The effect of the V-cut design is to increase the effective radial gap between the impeller outer diameter and volute vanes. In a 2D model, we can not simulate the V-cut geometry itself but we can simulate its effect. In order to simulate the effect of the special V-cut at the impeller blade exit using a 2D model, the area of the V-shaped cut has been calculated and the impeller outer diameter was trimmed by an equivalent area as shown in Fig. 4.23. Monitoring locations are the same ones used for the previous case as mentioned in Table 4.2. The boundary conditions used for the simulation cases on the effect of the V-cut are listed in Table 4.3. Again these boundary conditions are based on the experimental operating conditions. Part load flow conditions are simulated for this geometry, namely; flow ratios (Q/Qn) of 1, 0.75, 0.5, and 0.25.

The simulations results for the V-cut case are compared to the original case of the impeller without the V-cut. A comparison between the two cases for the time-averaged static pressure distribution inside the pump is shown in Fig. 4.24 at different flow rates. In general, the differences in the pressure distributions are considered small (max 10% at some points). Figure 4.25 compares the pressure fluctuations for the two cases. The V-cut design has a significant favorable effect on the fluctuations especially at reduced flow rates. As an illustration, Fig. 4.26 focuses on point 3, the location of the highest fluctuation at reduced flow rates. It shows clearly that the V-cut is very effective in reducing the pressure fluctuations, particularly at low flow rates.

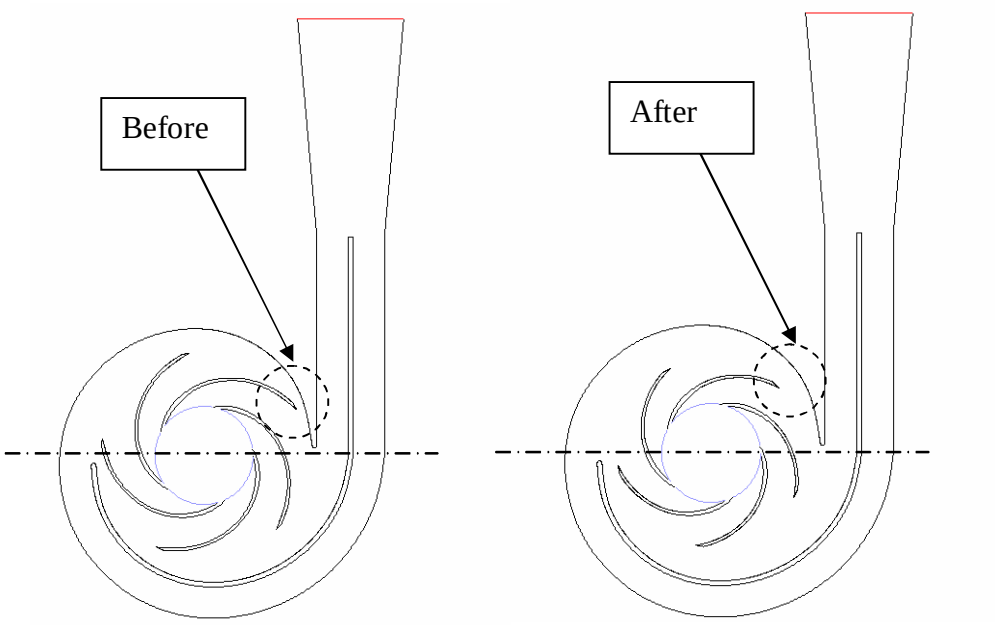

(a) Impeller without V-cut

(b) Simulation of the effect of V-cut (smaller impeller diameter)

Figure 4.23 Simulations of impeller geometries

Table 4.3 Boundary conditions used for simulating the V-cut effect: Experimental boundary conditions

Q/Qn	Velocity inlet [m/s]	Pressure outlet [pa]
1	3.2	270,000
0.75	2.4	320,000
0.5	1.6	360,000
0.25	0.8	377,000

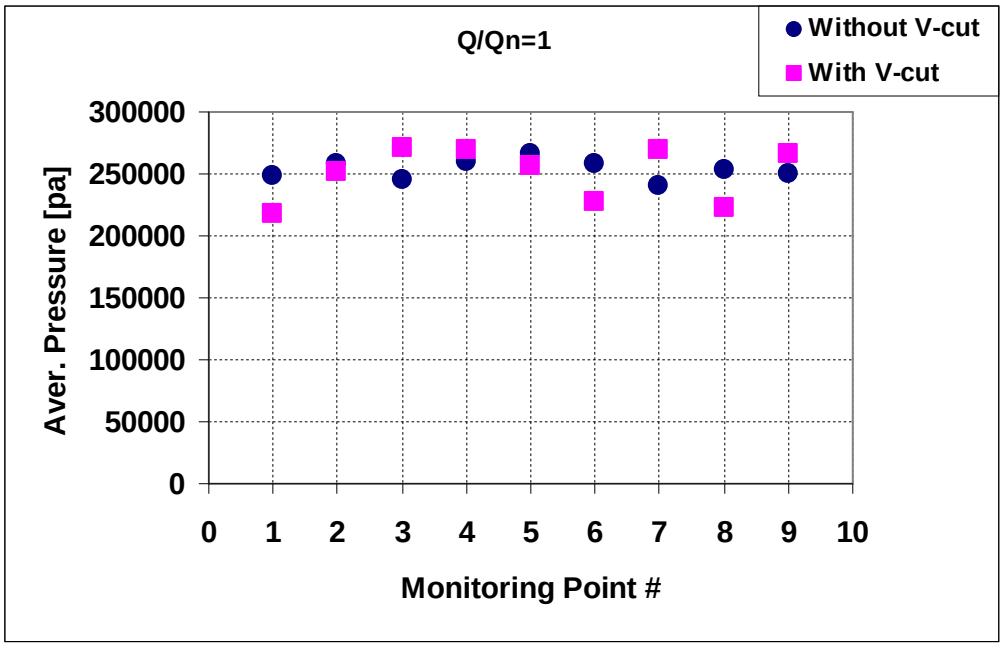
Q/Qn=1
Without V-cut
With V-cut
Aver. Pressure [pa]
300000
250000
200000
150000
100000
50000
0
0 1 2 3 4 5 6 7 8 9 10
Monitoring Point #

(a)

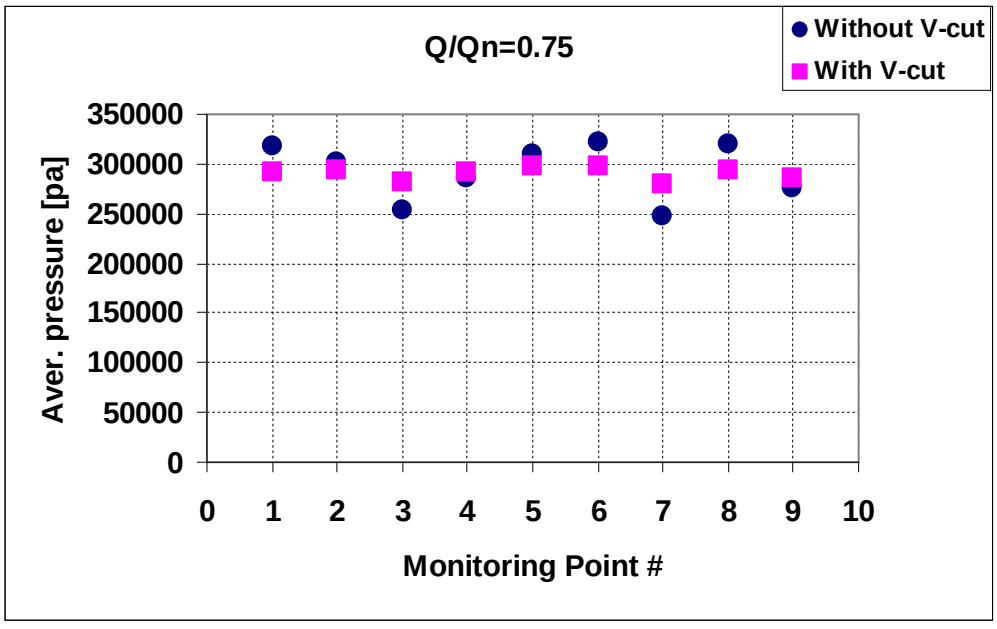
Q/Qn=0.75
Without V-cut
With V-cut
Aver. pressure [pa]
350000
300000
250000
200000
150000
100000
50000
0
0 1 2 3 4 5 6 7 8 9 10
Monitoring Point #

(b)

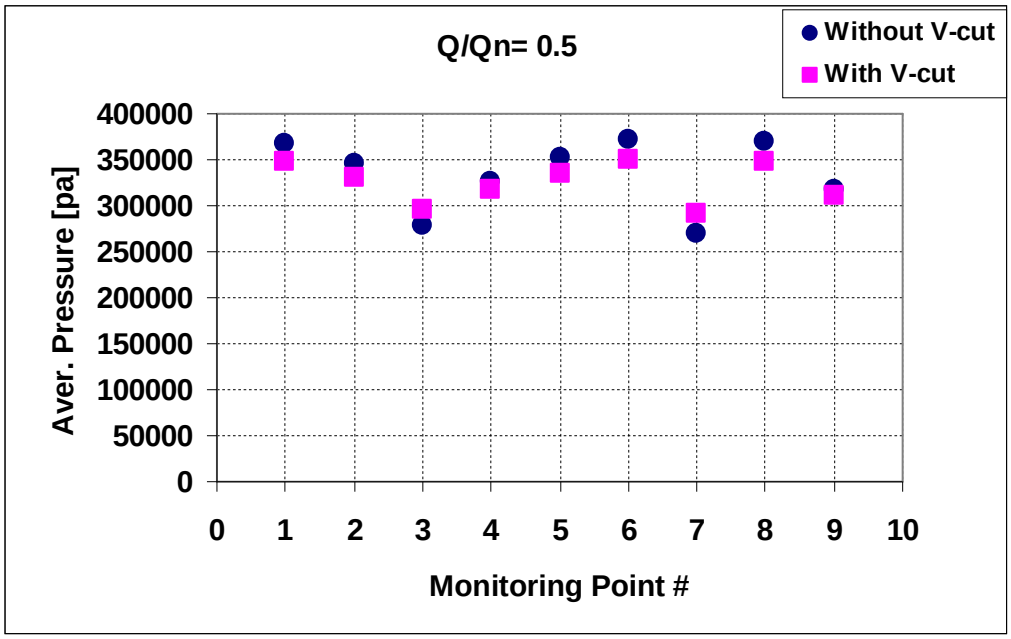

(c)

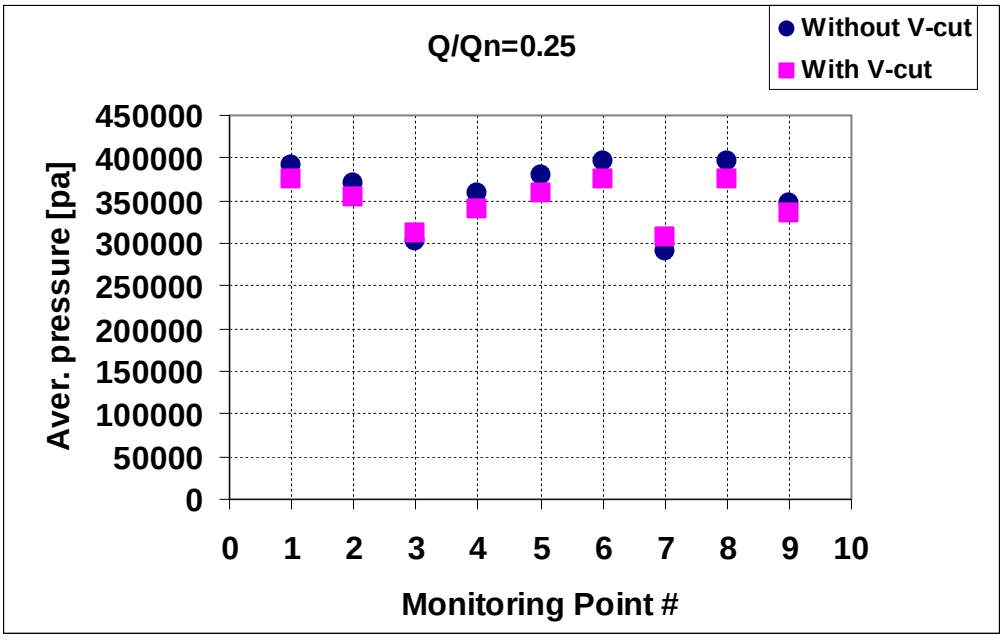

(d)

Figure 4.24 Effect of V-cut on time-averaged pressure distribution

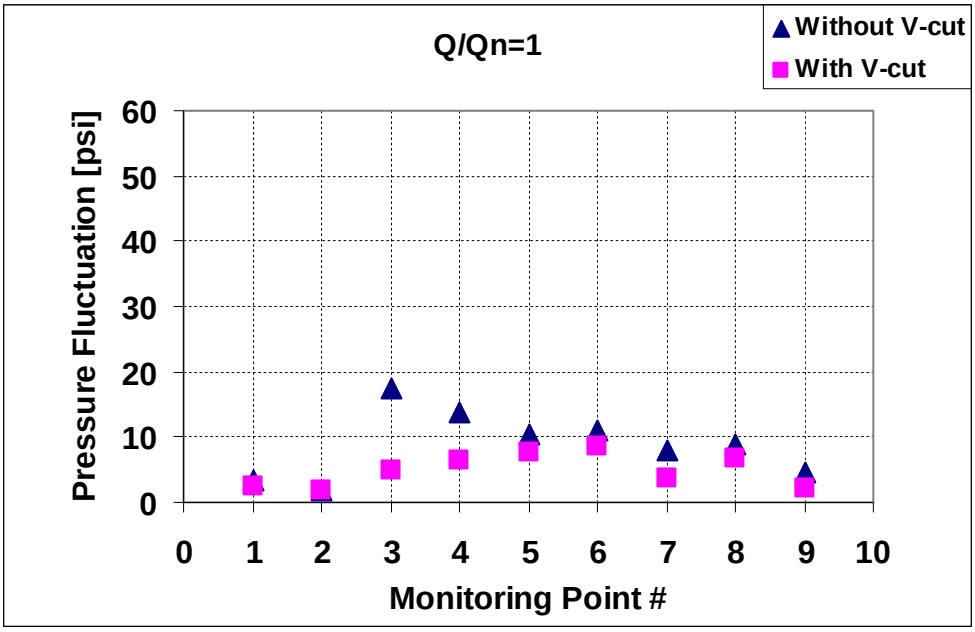
Q/Qn=1
Without V-cut
With V-cut
Pressure Fluctuation [psi]
60
50
40
30
20
10
0
0 1 2 3 4 5 6 7 8 9 10
Monitoring Point #

(a)

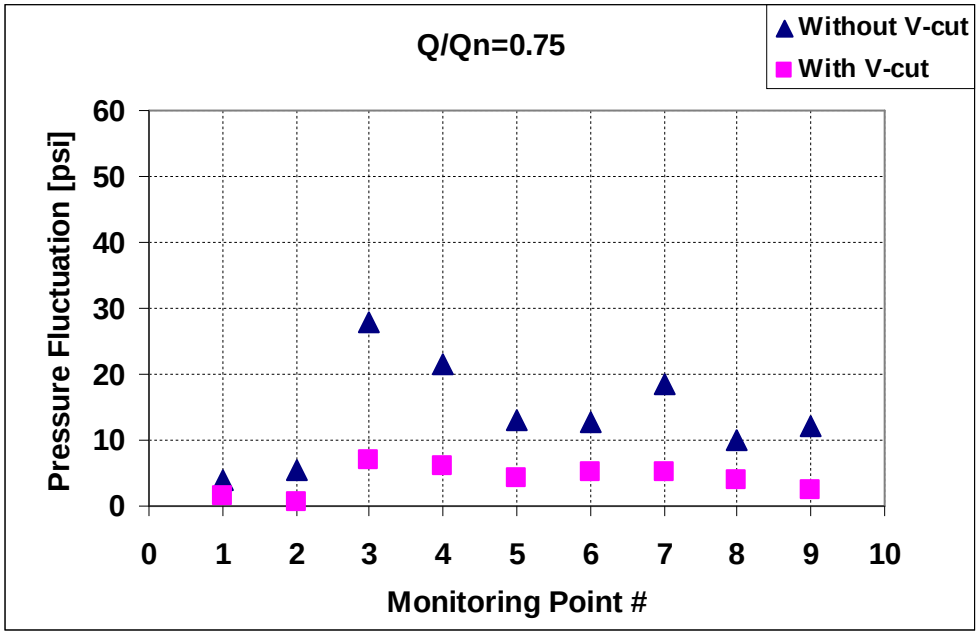
Q/Qn=0.75
Without V-cut
With V-cut
Pressure Fluctuation [psi]
60
50
40
30
20
10
0
0 1 2 3 4 5 6 7 8 9 10
Monitoring Point #

(b)

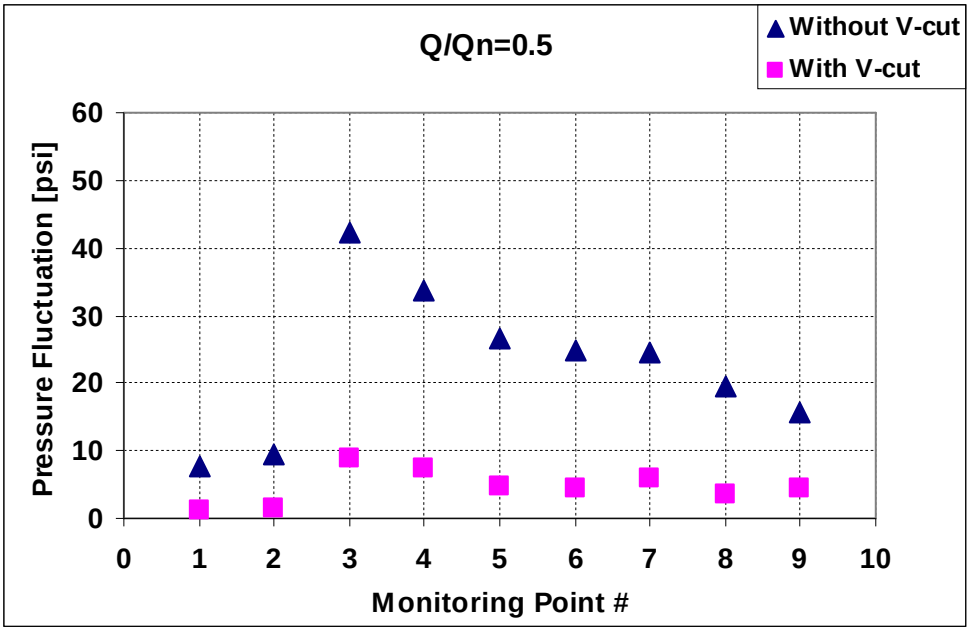

(c)

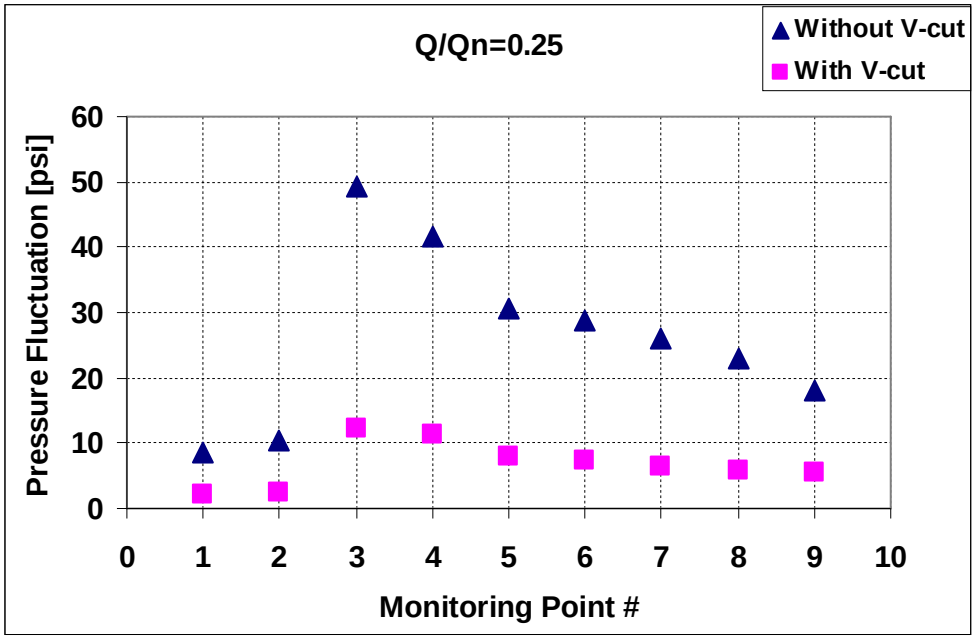

(d)

Figure 4.25 Effect of V-cut on pressure fluctuations at different flow rates

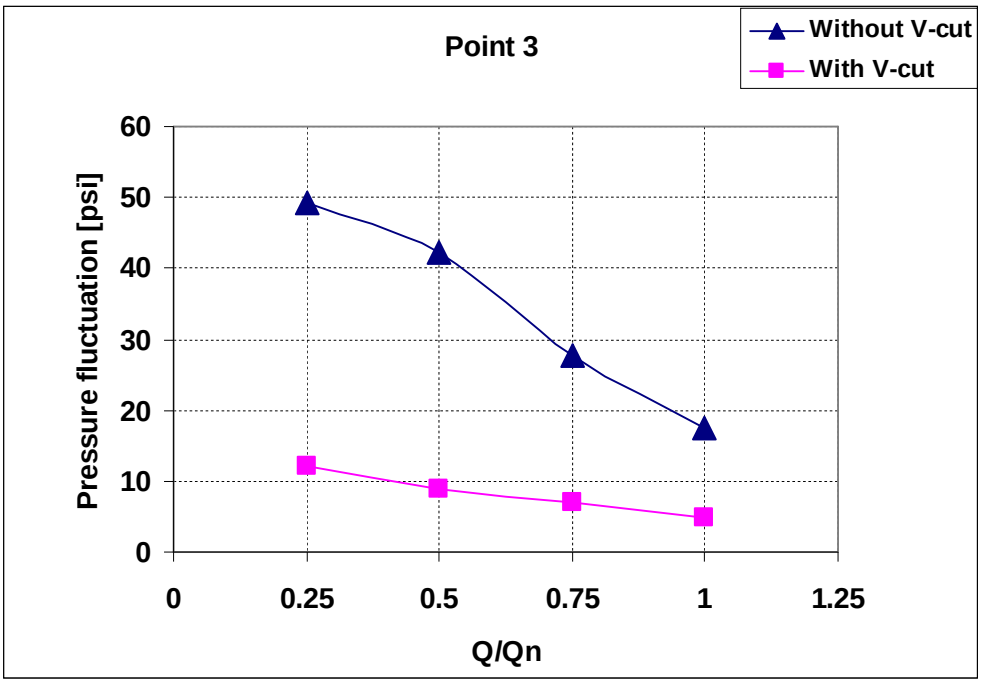

(a)

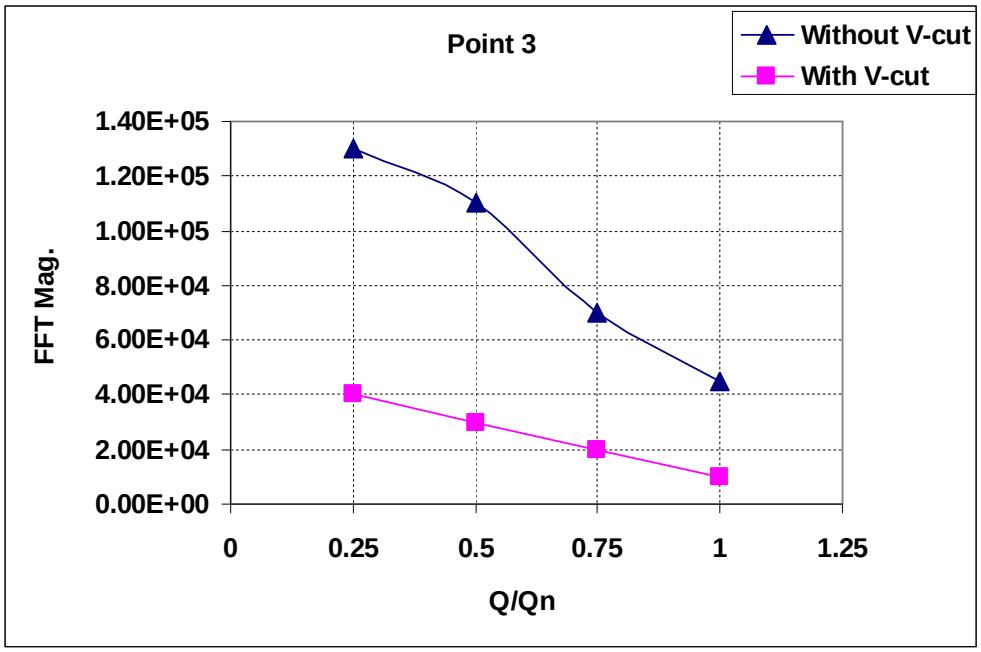

(b)

Figure 4.26 Effect of V-cut on pressure fluctuation and FFT magnitude at point 3 at reduced flow rates

4.4.3 EFFECT OF RADIAL GAP BETWEEN IMPELLER AND VOLUTE TONGUES

Numerical simulations were carried out to study the effect the minimum radial gap between the impeller outer diameter and the volute tongues. Two limiting cases are examined: (1) Reducing this gap by extending the volute tongues (along the same curvature) to reach a gap of 2 mm. (2) Increasing the gap by cutting back the volute tongues to reach a gap of 7 mm. The geometry of the 2 mm gap compared to the original gap design of 3.6 mm is shown in Fig. 4.27 for the impeller without the V-cut effect. The simulation results for this gap at points 3 and 4 are shown in Fig. 4.28 for the time-averaged static pressure and Fig. 4.29 for the pressure fluctuations (peak-to-peak). Decreasing the gap produces higher pressure fluctuations than the original design at off-design operating conditions. This conclusion is in agreement with the experimental results. Hence, smaller gaps are not recommended in general for this pump design. They produce stronger impeller-volute interaction resulting in higher pressure pulsation inside the pump and higher pump vibration.

For the second case, this gap is increased by cutting back the volute tongues (from the leading edges) to reach a 7 mm gap. This gap increase is expected to reduce the pressure fluctuations and pump vibration as measured experimentally. This gap was investigated numerically considering the two impeller blade types: the V-cut and without V-cut at blade as shown in Fig. 4.30. The boundary conditions for the two cases are listed in Tables 4.4 and 4.5. Comparisons for the pressure distributions and pressure fluctuations inside the pump between the gap of 7 mm and the original gap of 3.6 mm are shown in Figs. 4.31 and 4.32 respectively. The 7 mm gap had reduced the pressure fluctuations inside the pump by 20 to 60%, depending on location and flow

rate. This is considered to be a great achievement considering the small percentage in the pressure drop inside the pump at reduced flow rates (about 5%).

Combining the 7 mm gap with the effect of the V-cut design increases the uniformity of static pressure inside the pump as shown in Fig. 4.33. The pressure fluctuations are further reduced by the same amount (from 20 to 60% depending on location and flow rate) compared to the case of impeller without the V-cut as shown in Fig. 4.34. This behavior is in a good agreement with experimental results.

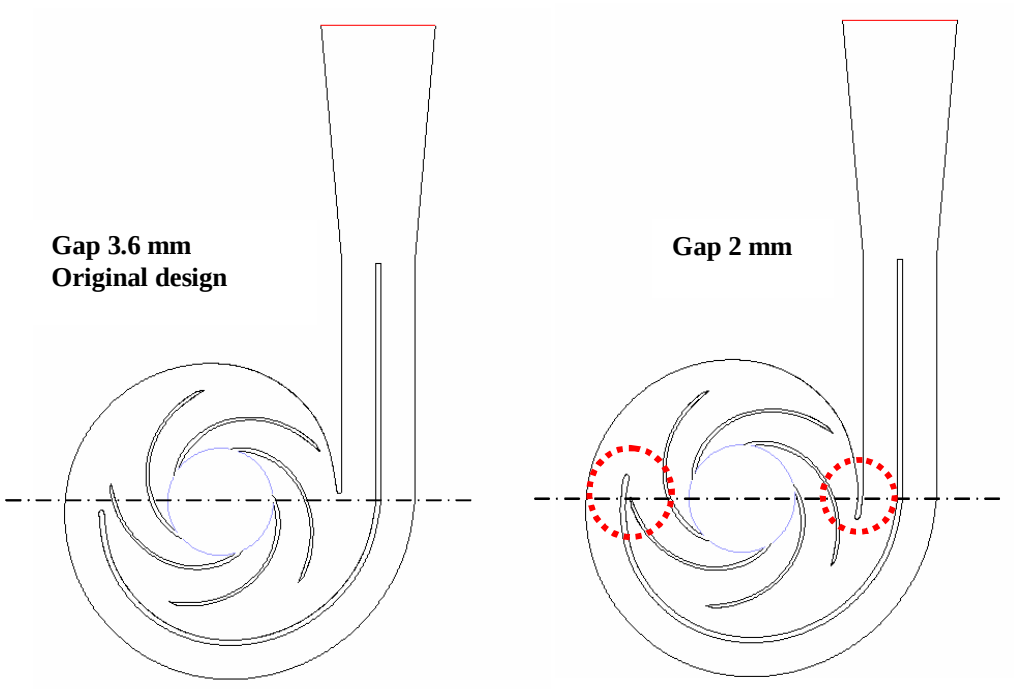

Figure 4.27 Extending the volute tongues to reach a gap of 2 mm

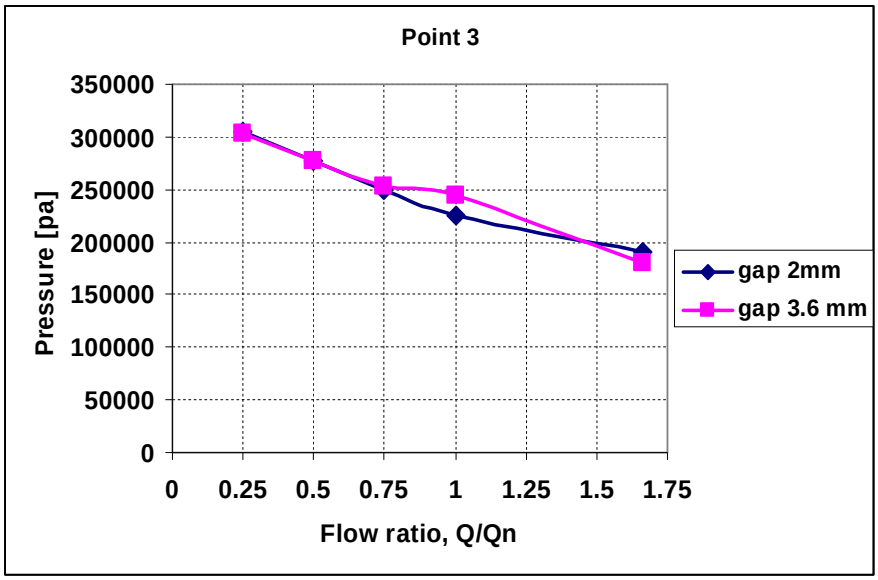

(a)

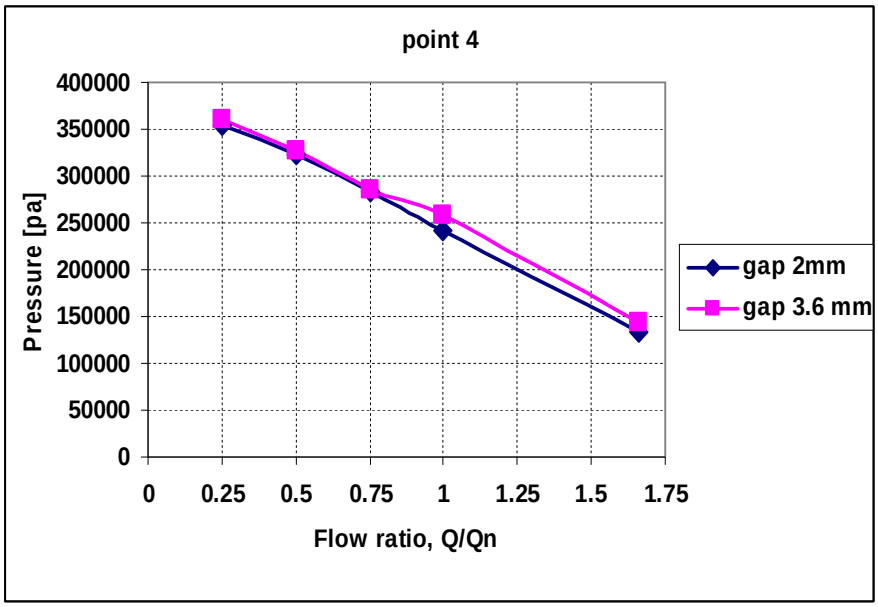

(b)

Figure 4.28 Effect of reducing the gap from 3.6 to 2 mm on time-averaged static pressures at points 3 and 4

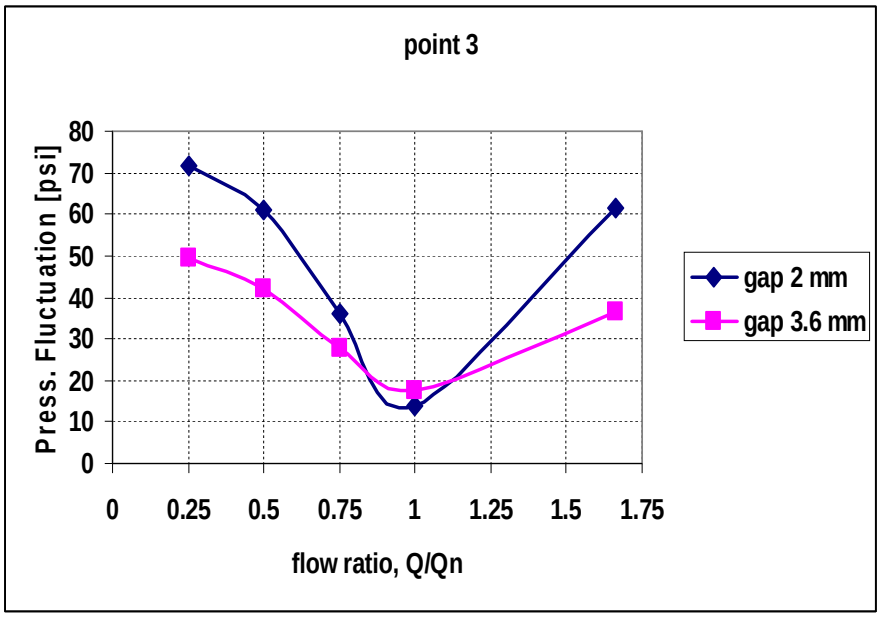

(a)

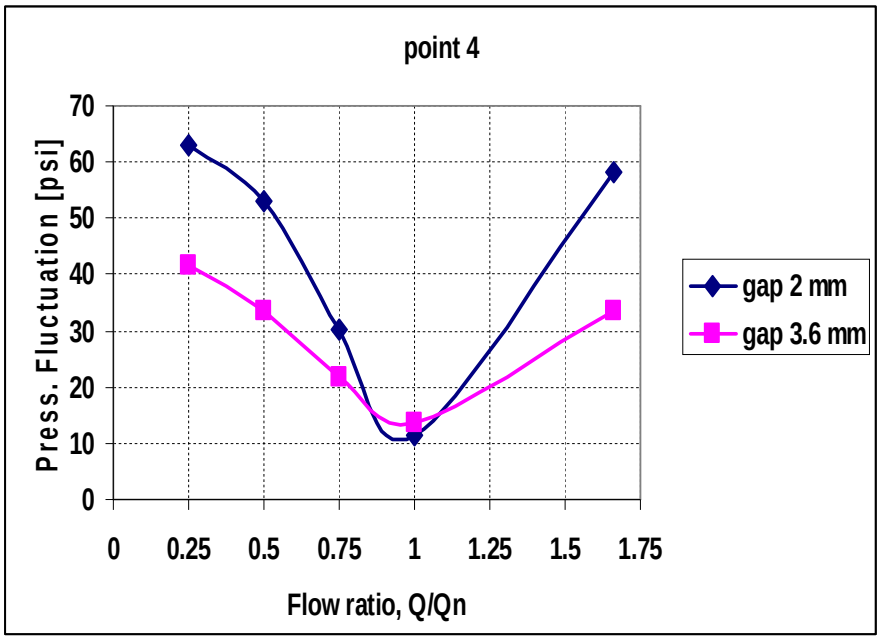

(b)

Figure 4.29 Effect of reducing the gap from 3.6 to 2 mm on pressure fluctuations at points 3 and 4

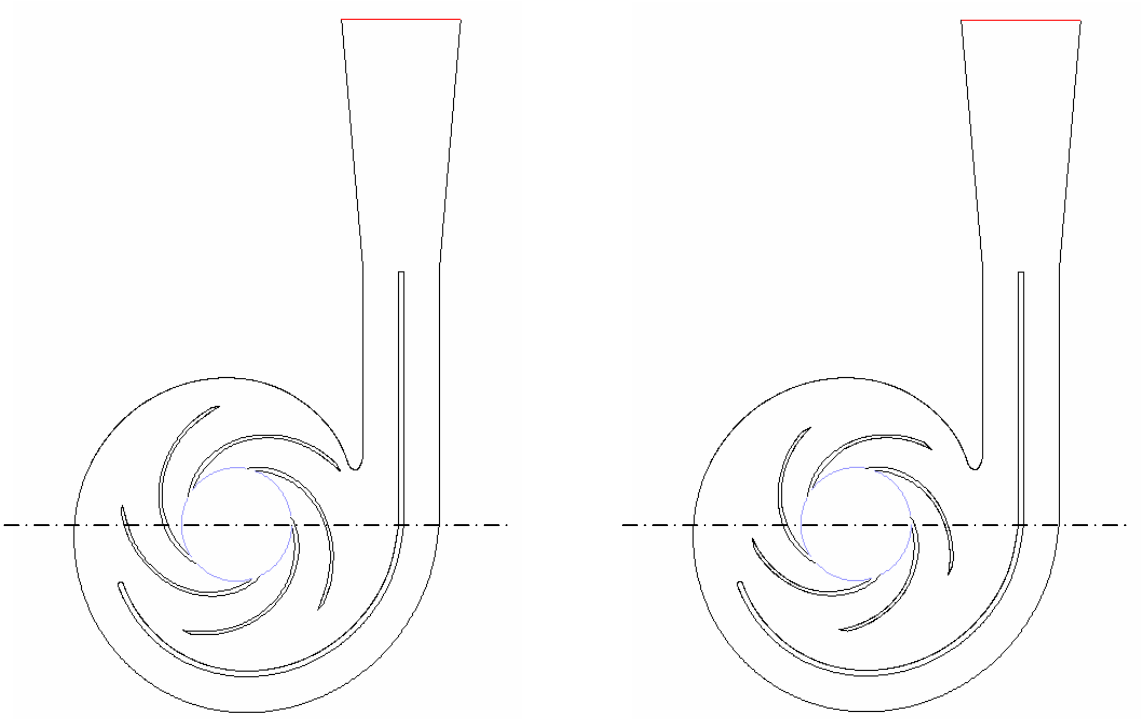

(a) Impeller without V-cut

(b) Simulation of the effect of V-cut (smaller impeller diameter)

Figure 4.30 Radial gap of 7 mm without V-cut and with the effect of V-cut

Table 4.4 Boundary conditions for 7 mm gap: Without V-cut

Boundary Conditions: speed 3540 rpm, Without V-cut at blade exit: gap 7 mm		
Q/Qn	Velocity inlet [m/s]	Pressure outlet [pa]
1	3.2	300,000
0.75	2.4	345,000
0.5	1.6	380,000
0.25	0.8	395,000

Table 4.5 Boundary conditions for 7 mm gap: the V-cut effect

Boundary Conditions: speed 3540 rpm, V-cut at blade exit: gap 7 mm		
Q/Qn	Velocity inlet [m/s]	Pressure outlet [pa]
1	3.2	270,000
0.75	2.4	322,000
0.5	1.6	360,000
0.25	0.8	380,000

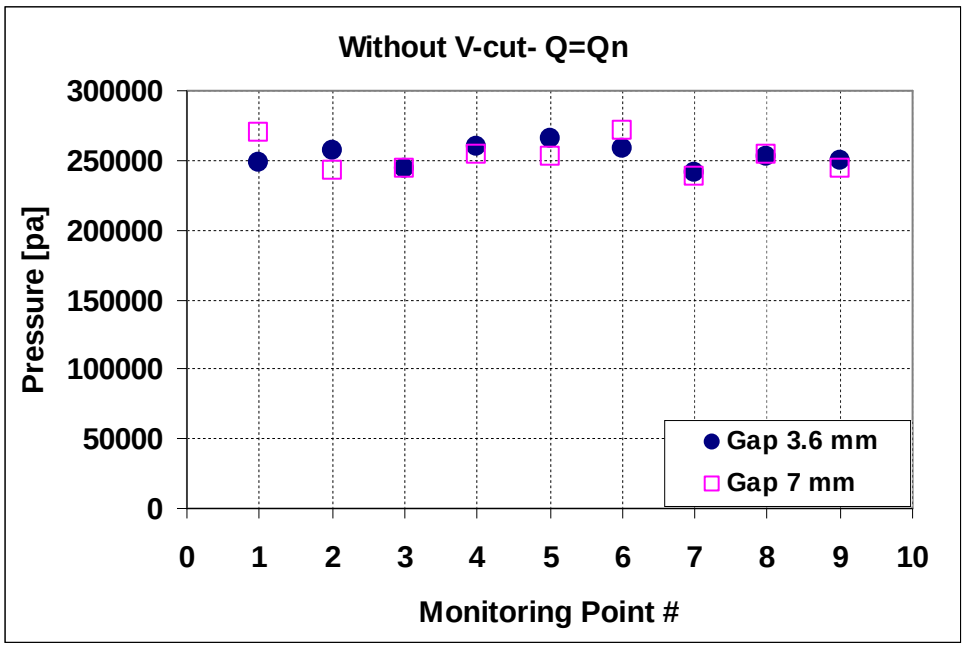
Without V-cut- Q=Qn
Pressure [pa]
300000
250000
200000
150000
100000
50000
0
0 1 2 3 4 5 6 7 8 9 10
Monitoring Point #
Gap 3.6 mm
Gap 7 mm

(a)

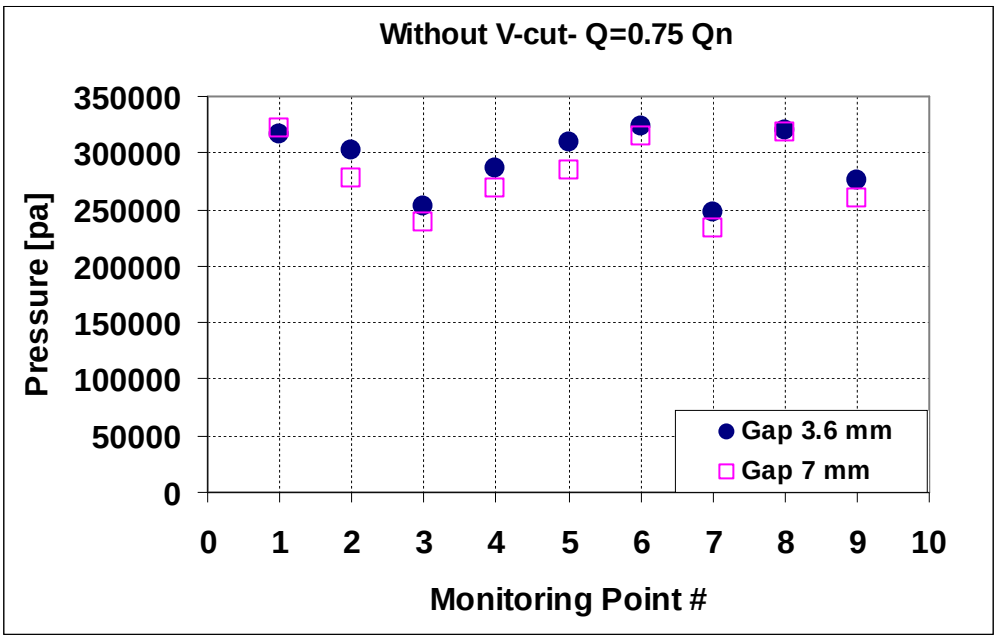
Without V-cut- Q=0.75 Qn
Pressure [pa]
350000
300000
250000
200000
150000
100000
50000
0
0 1 2 3 4 5 6 7 8 9 10
Monitoring Point #
Gap 3.6 mm
Gap 7 mm

(b)

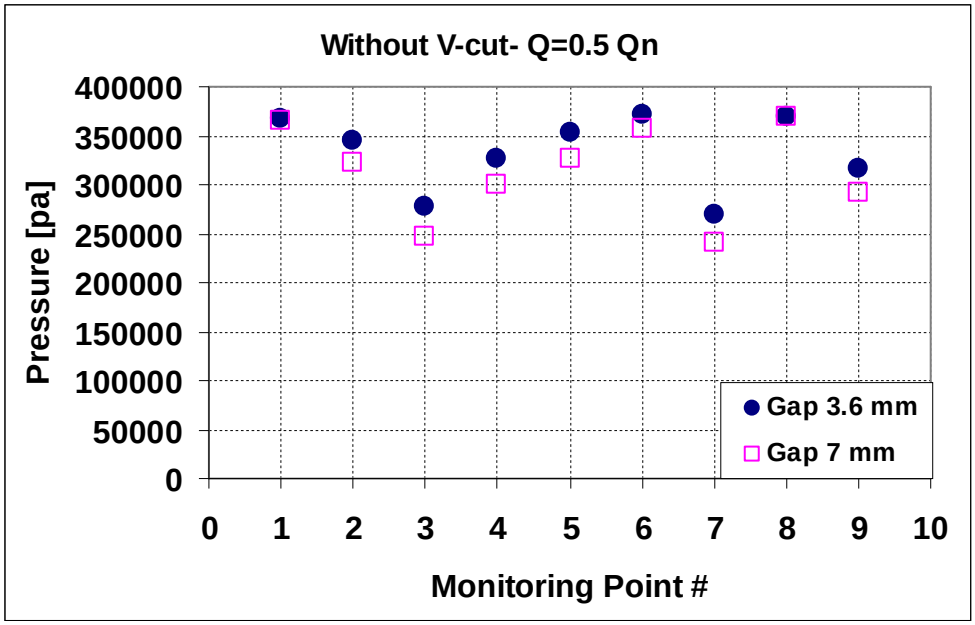

(c)

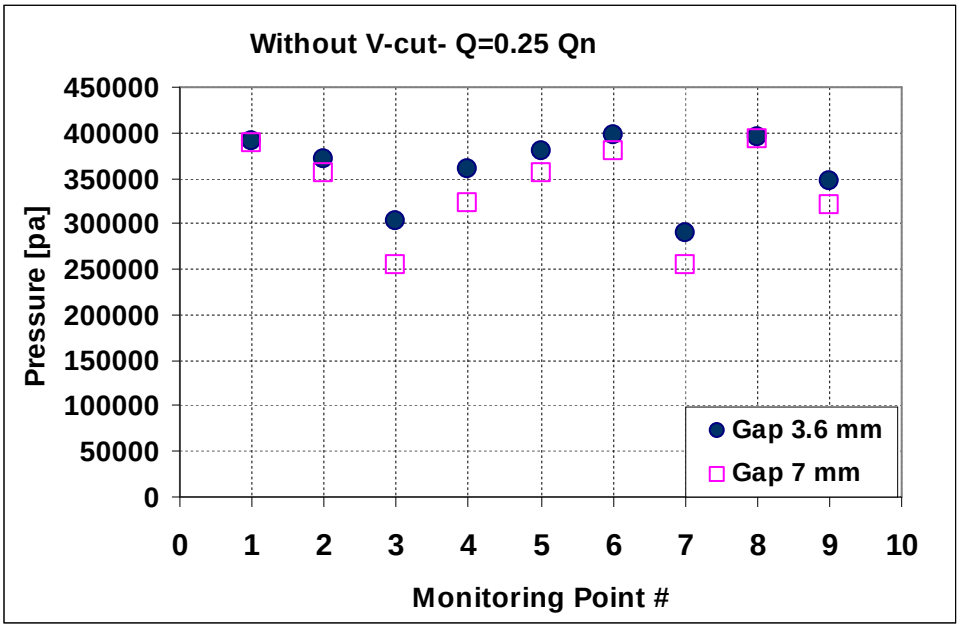

(d)

Figure 4.31 Effect of 7 mm gap on pressure distribution inside the pump compared to the original 3.6 mm gap

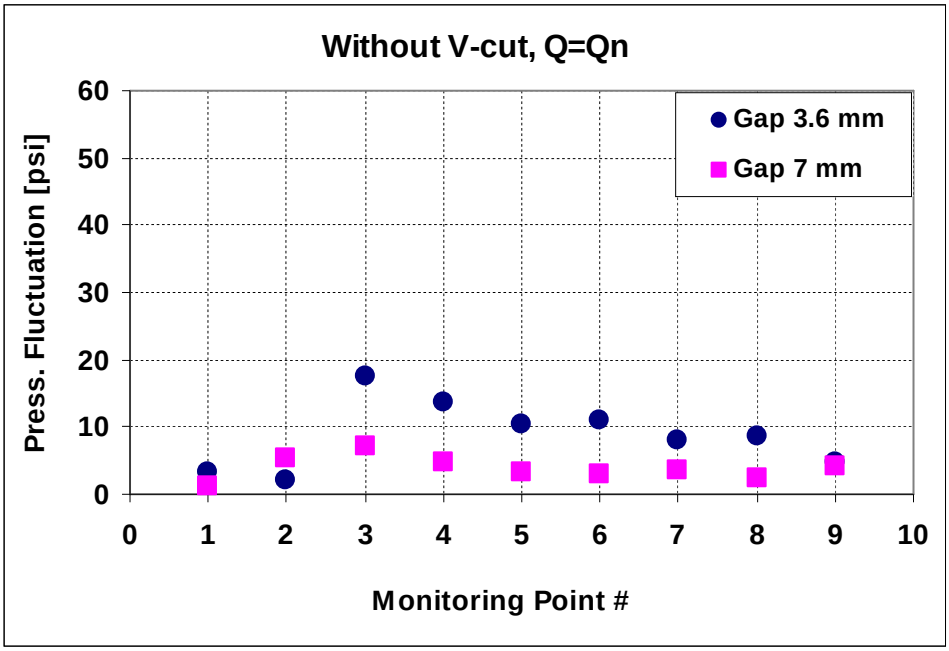
Without V-cut, Q=Qn
Press. Fluctuation [psi]
Monitoring Point #
Gap 3.6 mm
Gap 7 mm
0
10
20
30
40
50
60
0
1
2
3
4
5
6
7
8
9
10

(a)

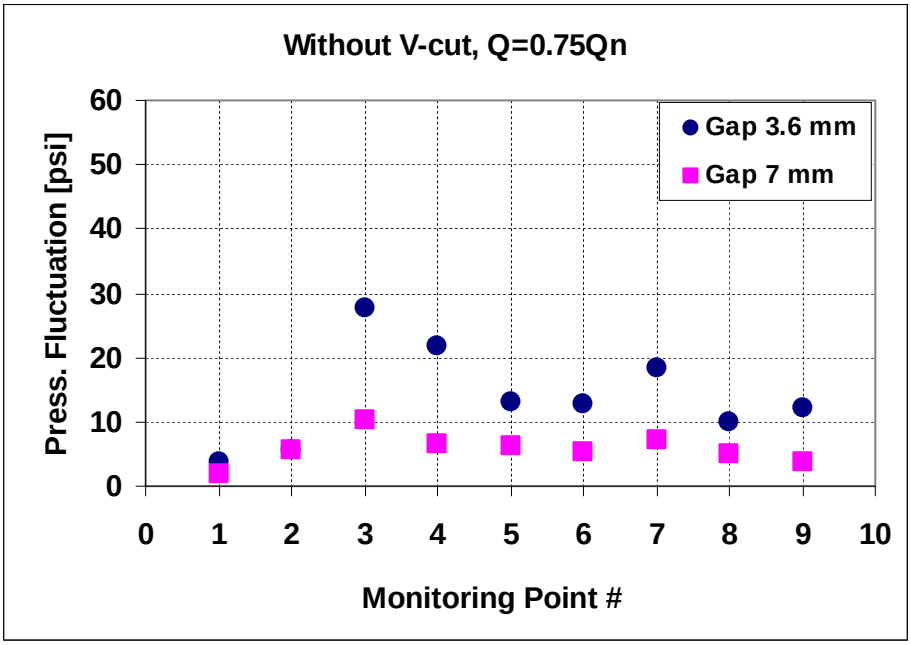
Without V-cut, Q=0.75Qn
Press. Fluctuation [psi]
Monitoring Point #
Gap 3.6 mm
Gap 7 mm
0
10
20
30
40
50
60
0
1
2
3
4
5
6
7
8
9
10

(b)

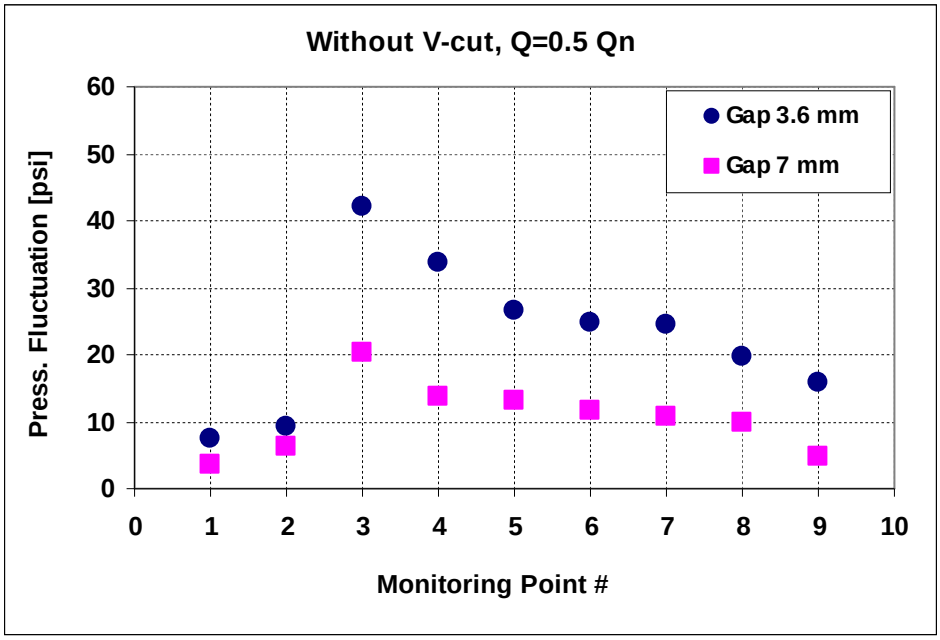

(c)

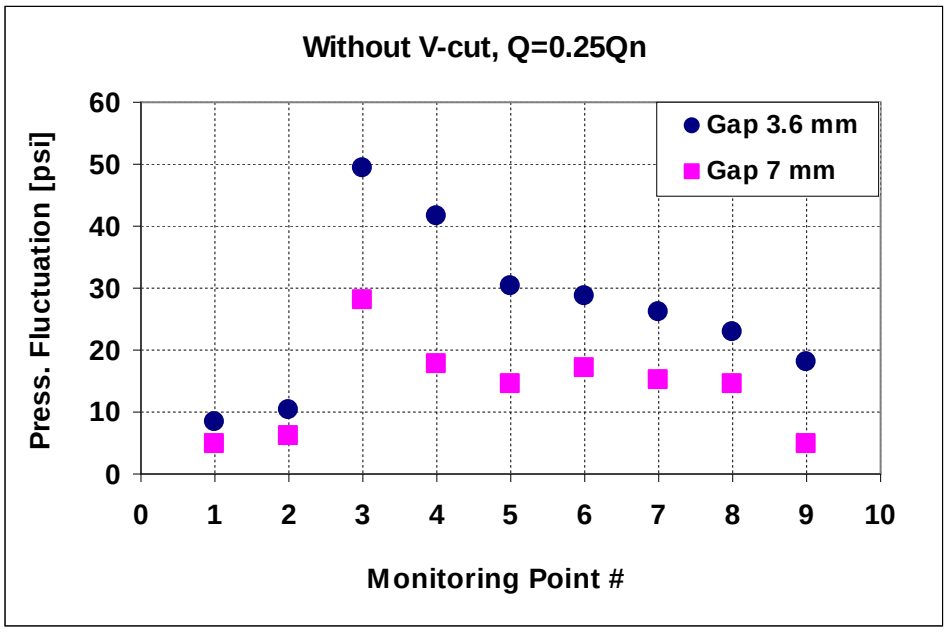

(d)

Figure 4.32 Effect of 7 mm gap on pressure fluctuations inside the pump compared to the original 3.6 mm gap

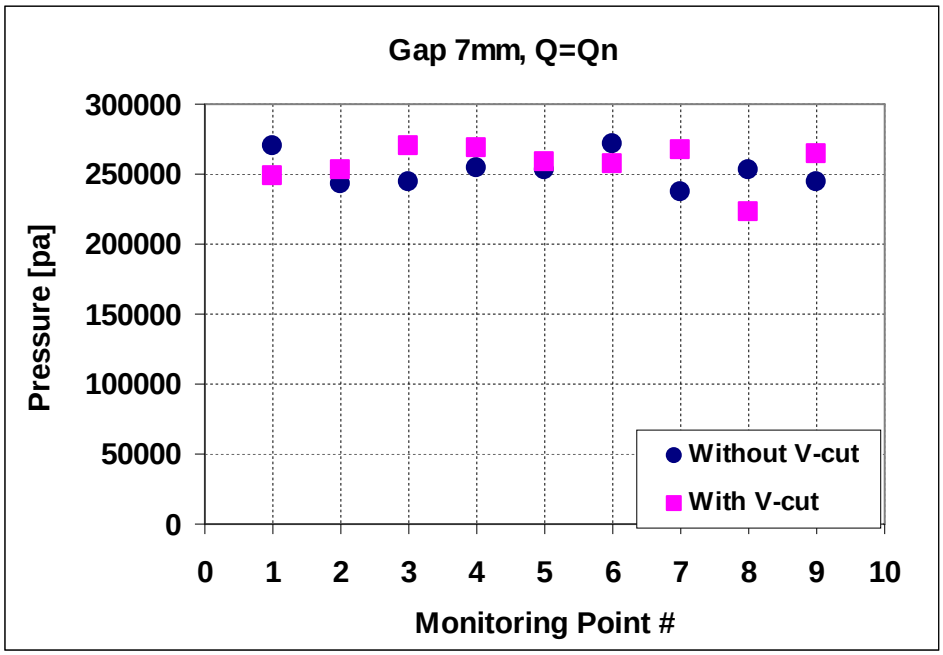
Gap 7mm, Q=Qn
Pressure [pa]
300000
250000
200000
150000
100000
50000
0
0 1 2 3 4 5 6 7 8 9 10
Monitoring Point #
Without V-cut
With V-cut

(a)

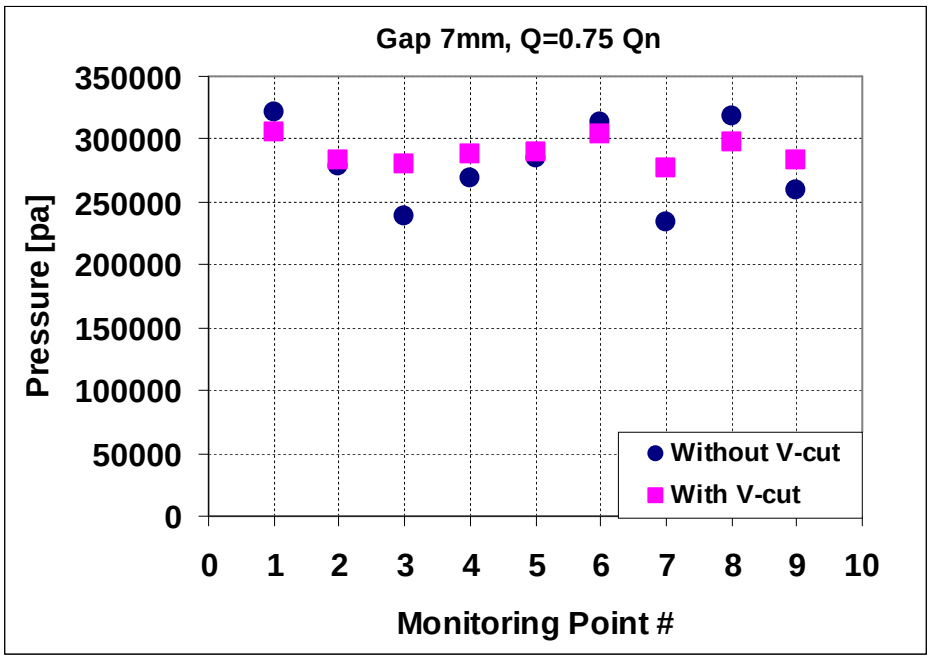
Gap 7mm, Q=0.75 Qn
Pressure [pa]
350000
300000
250000
200000
150000
100000
50000
0
0 1 2 3 4 5 6 7 8 9 10
Monitoring Point #
Without V-cut
With V-cut

(b)

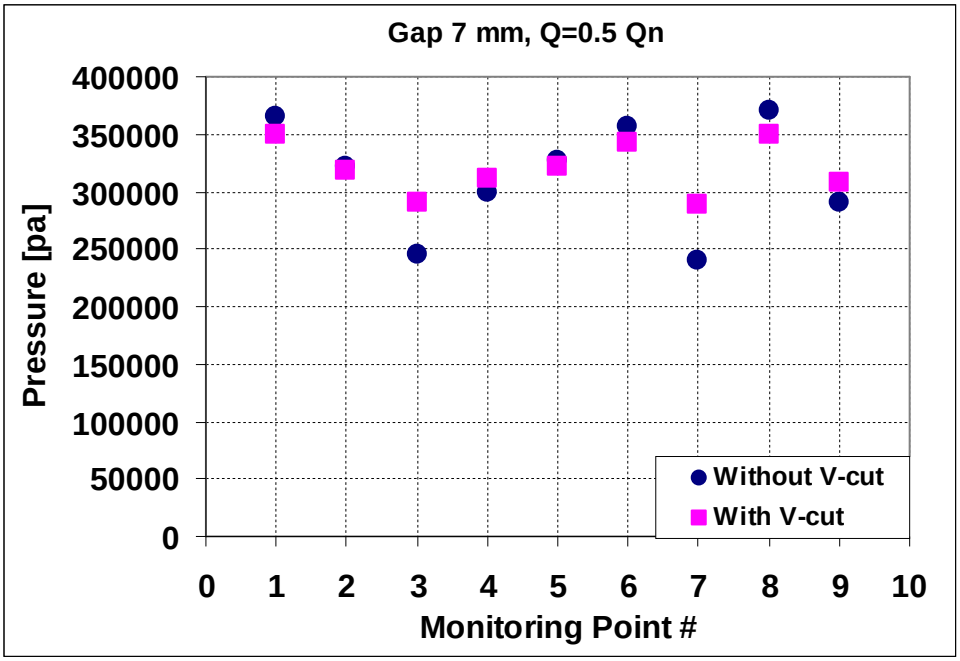

(c)

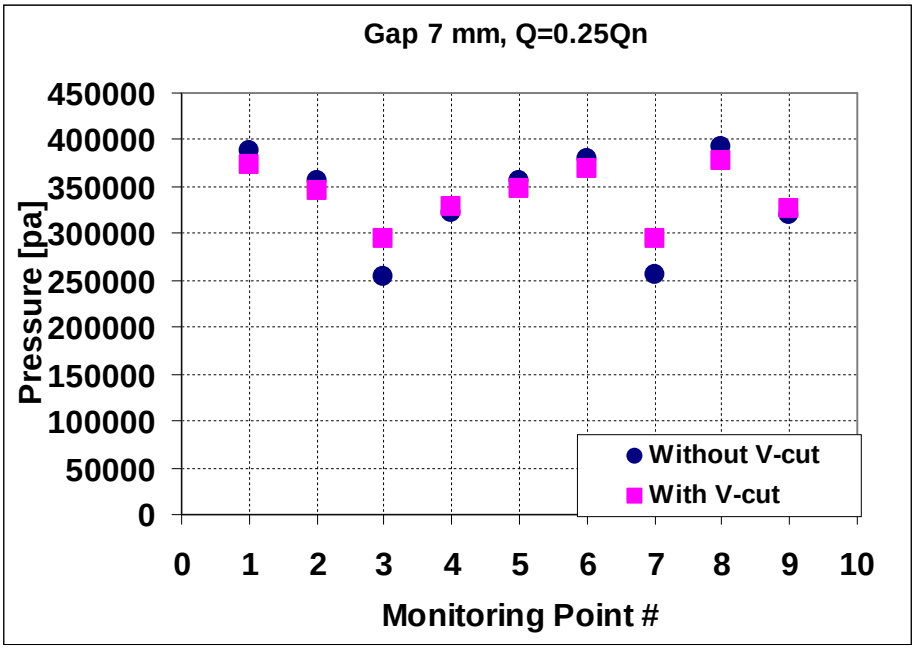

(d)

Figure 4.33 Gap 7 mm: Effect of V-cut on static pressure inside the pump

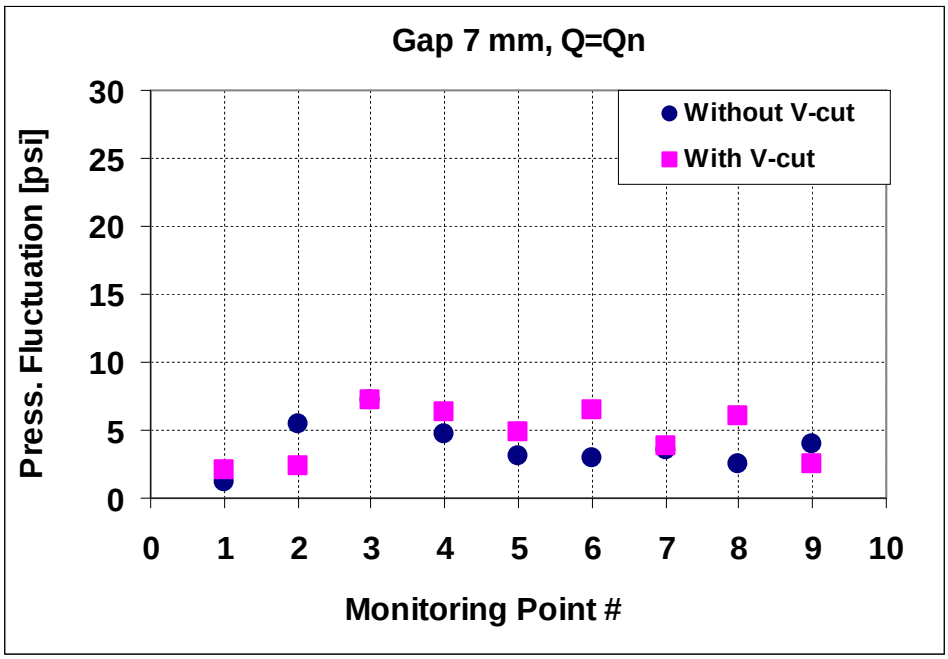
Gap 7 mm, Q=Qn
Press. Fluctuation [psi]
Monitoring Point #
Without V-cut
With V-cut
0
5
10
15
20
25
30
0
1
2
3
4
5
6
7
8
9
10

(a)

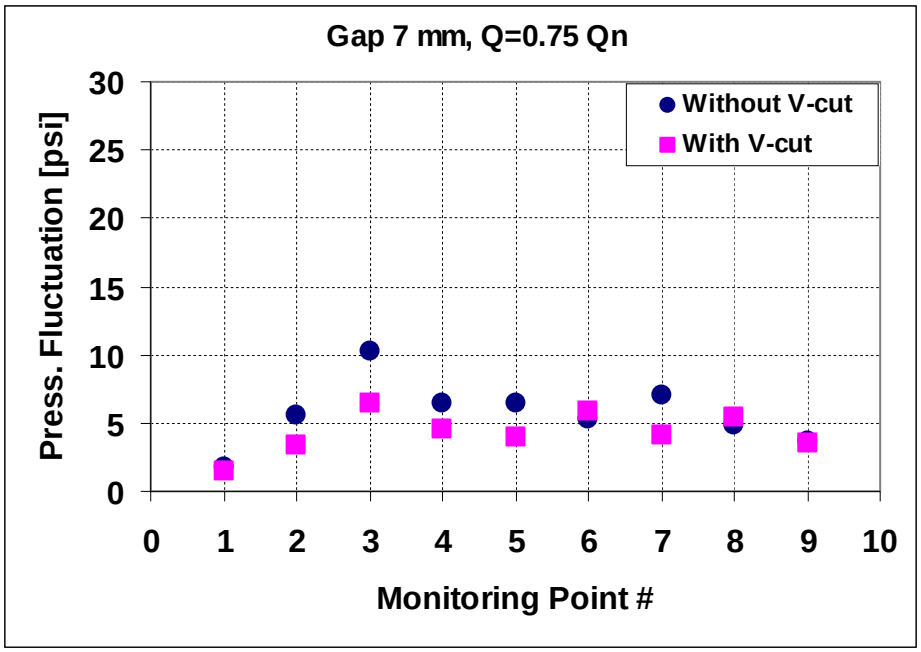
Gap 7 mm, Q=0.75 Qn
Press. Fluctuation [psi]
Monitoring Point #
Without V-cut
With V-cut
0
5
10
15
20
25
30
0
1
2
3
4
5
6
7
8
9
10

(b)

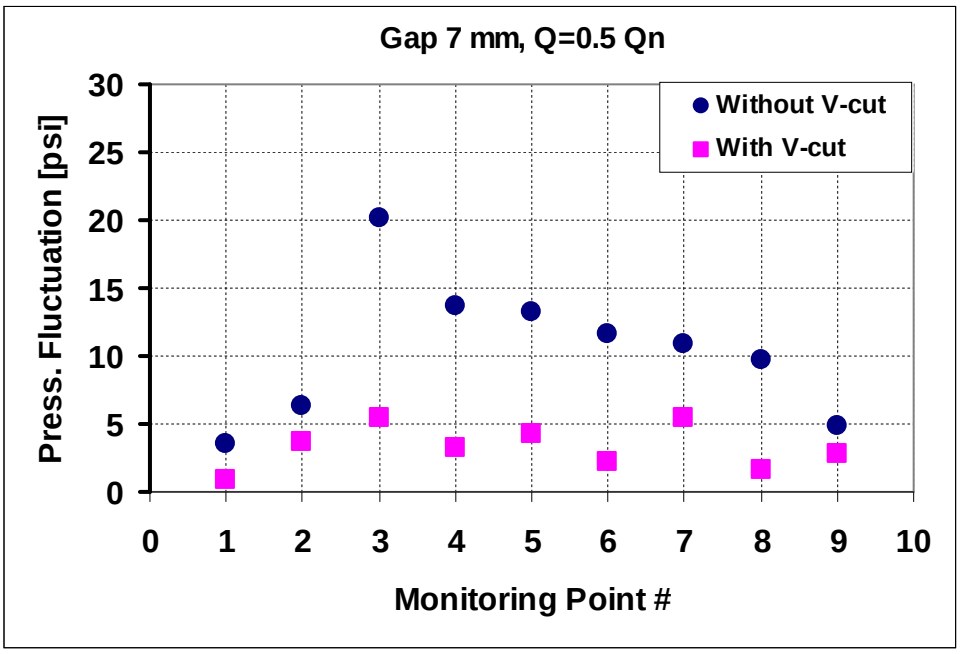

(c)

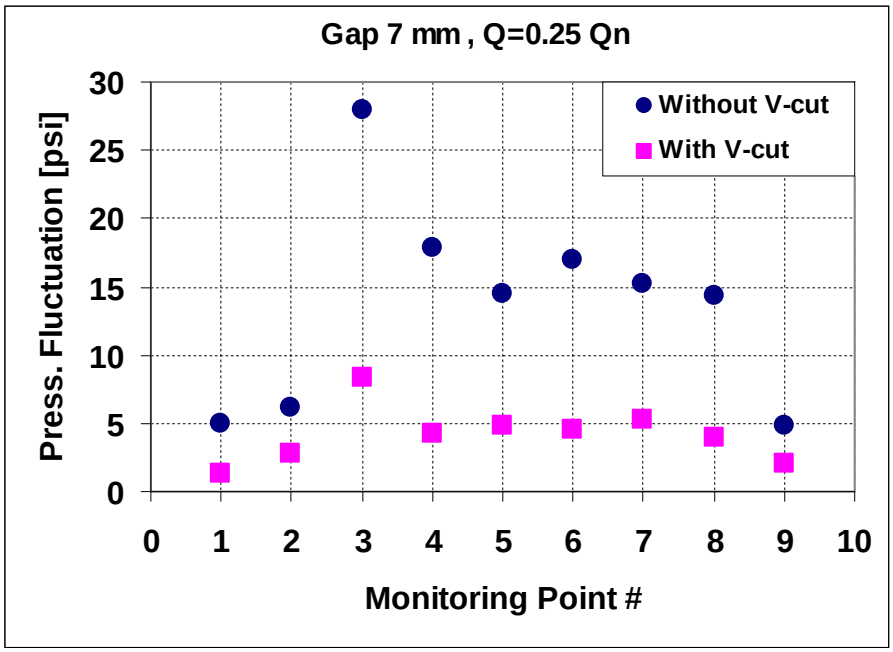

(d)

Figure 4.34 Gap 7 mm: Effect of V-cut on pressure fluctuations inside the pump

4.5 VALIDATION OF CFD RESULTS

This section assesses the validity of using the 2D unsteady CFD simulations in pumps. The previously presented results for the impeller without V-cut at blade, impeller with V-cut, gap of 7 mm are compared for the time-averaged static pressure distributions and the unsteady pressure fluctuations. The CFD predicted pump head is compared with the experimentally measured head in Fig. 4.35. The 2D simulations over-estimated the pump head (by about 30% for Qn). This over-estimation is due to the shortage of the 2D model to simulate the flow at impeller inlet resulting in very low pressure prediction at impeller inlet and the differences in accounting for velocity in simulation and experiments for head calculations.

Figures 4.36 to 4.43 give comprehensive comparisons between the numerical solutions and experimental measurements at different flow rates. The numerical results for time-averaged static pressure distribution inside the pump are in excellent agreement with experimental measurements at or close to the best efficiency flow rate. Small differences between numerical and experimental results were found at low flow rates especially when the effect of V-cut is implemented (max of 10% at some locations). This is an important conclusion which means that the pressure distribution inside the pump has actually a 2D behavior and is constant in the axial direction inside the pump. Thus measuring the pressure near the volute walls (as we did in experiments) is most probably equivalent to measuring it at the central plane of the impeller. The situation is different for the amplitudes of the pressure fluctuations. Although the numerical simulations results for the pressure fluctuations provided a qualitatively equivalent

behavior to experimental measurement for all locations under different flow rates, the 2D CFD models over-predicted the amplitudes of pressure fluctuations; especially at low flow rates for the impeller without V-cut. The 2D numerical simulations gave *closer* results to experimental ones for the larger gap of 7 mm with the effect of the V-cut. However, it is still higher than the experimental results. This means that the unsteady pressure fluctuations are location dependent in 3D space. The 2D model simulates the flow at the impeller central cross section. In the experimental testing, the pressure fluctuations are damped close to the wall where the transducers are located. Besides, the leakage effect is not modeled by the 2D model. A 3D simulation is needed for accurate prediction of the unsteady pressure magnitudes.

As a final conclusion, the 2D simulation using sliding mesh technique can predict the pressure distribution inside the pump with acceptable accuracy. It can also predict the effect of changing the flow rate and pump geometry. The frequencies of pressure fluctuations are captured. However, the magnitude of fluctuations can not be predicted accurately by the 2D models. It is believed that a 3D simulation is needed to predict the amplitudes of pressure fluctuations accurately with better simulation for pump inlet.

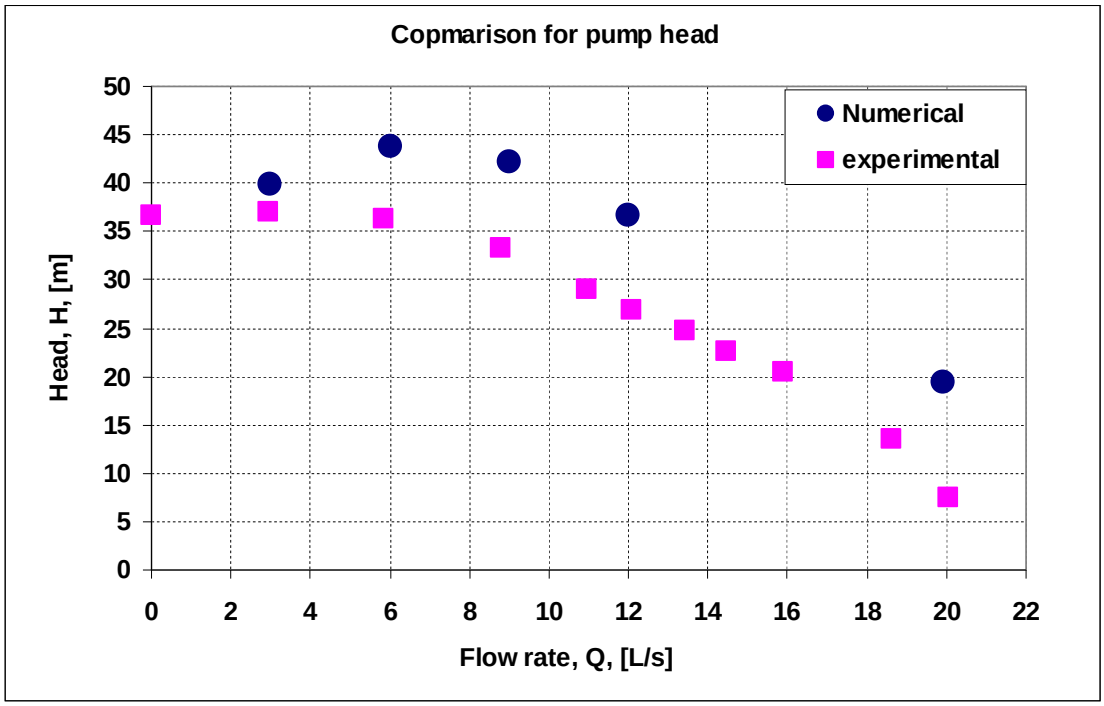

Figure 4.35 Comparison between the CFD prediction of pump head and experimental measurements

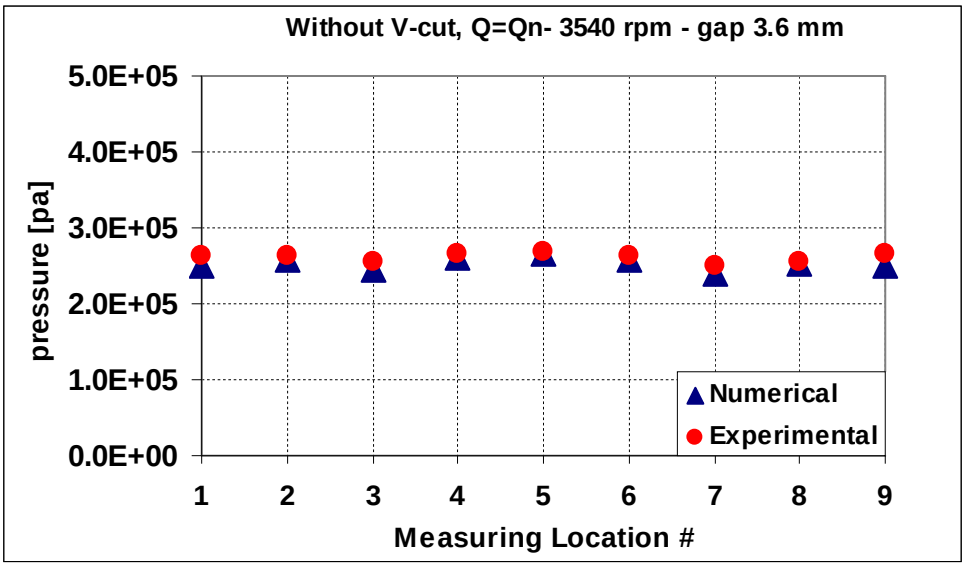
Without V-cut, Q=Qn- 3540 rpm - gap 3.6 mm
5.0E+05
4.0E+05
3.0E+05
2.0E+05
1.0E+05
0.0E+00
pressure [pa]
1
2
3
4
5
6
7
8
9
Measuring Location #
Numerical
Experimental

(a)

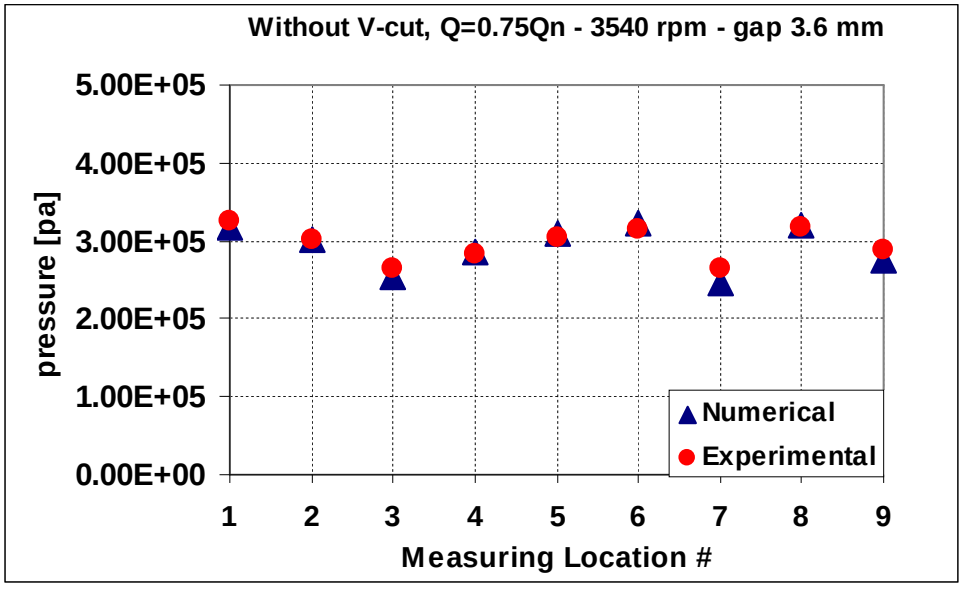
Without V-cut, Q=0.75Qn - 3540 rpm - gap 3.6 mm
5.00E+05
4.00E+05
3.00E+05
2.00E+05
1.00E+05
0.00E+00
pressure [pa]
1
2
3
4
5
6
7
8
9
Measuring Location #
Numerical
Experimental

(b)

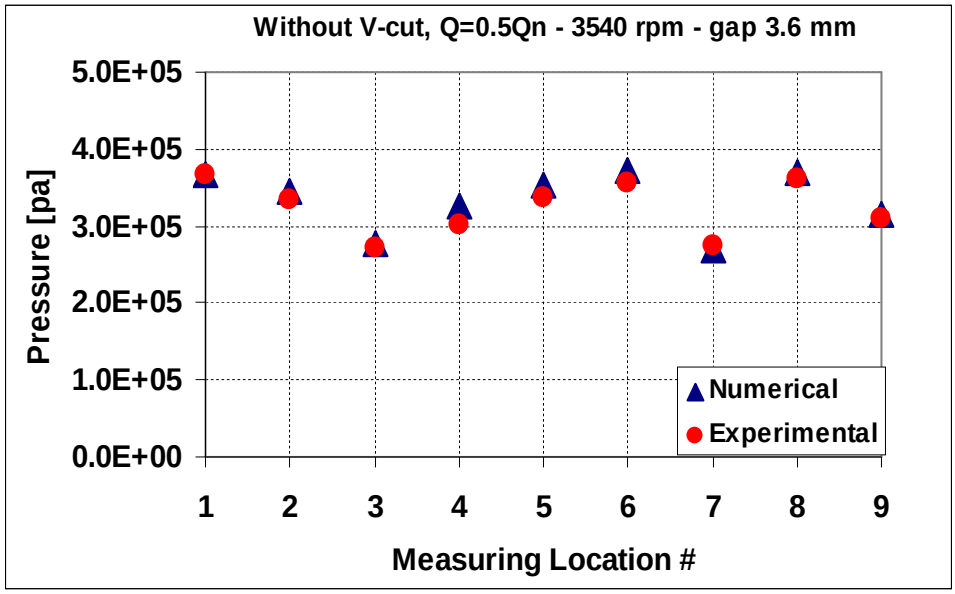

(c)

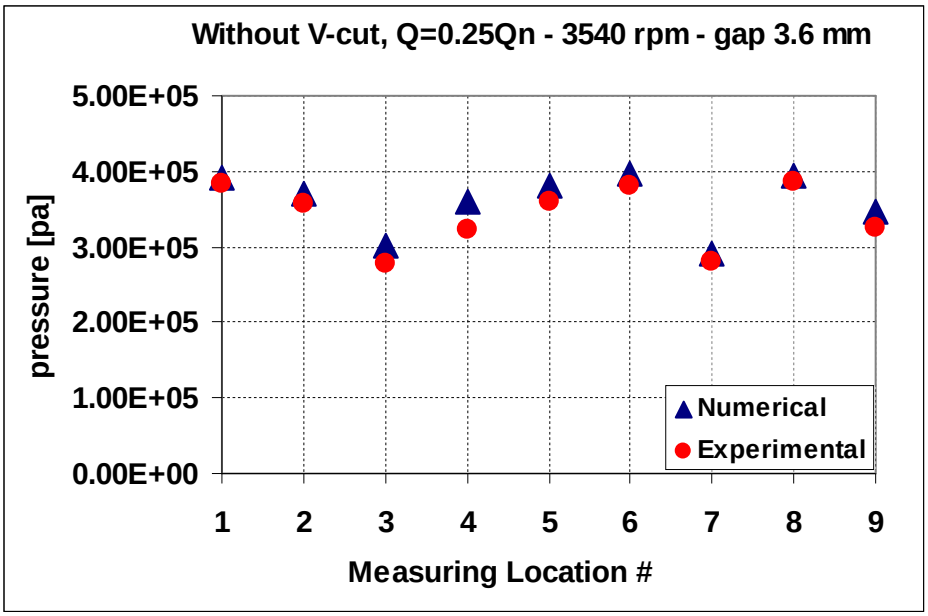

(d)

Figure 4.36 Effect of flow rate on time-averaged pressure distribution: experimental vs numerical for impeller without V-cut, gap 3.6 mm

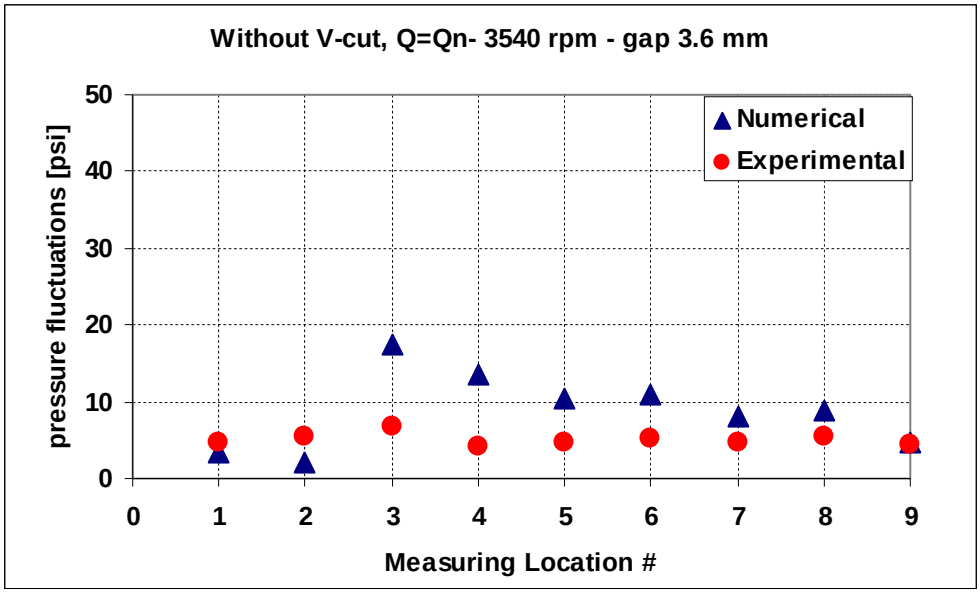
Without V-cut, Q=Qn- 3540 rpm - gap 3.6 mm
pressure fluctuations [psi]
50
40
30
20
10
0
0
1
2
3
4
5
6
7
8
9
Measuring Location #
Numerical
Experimental

(a)

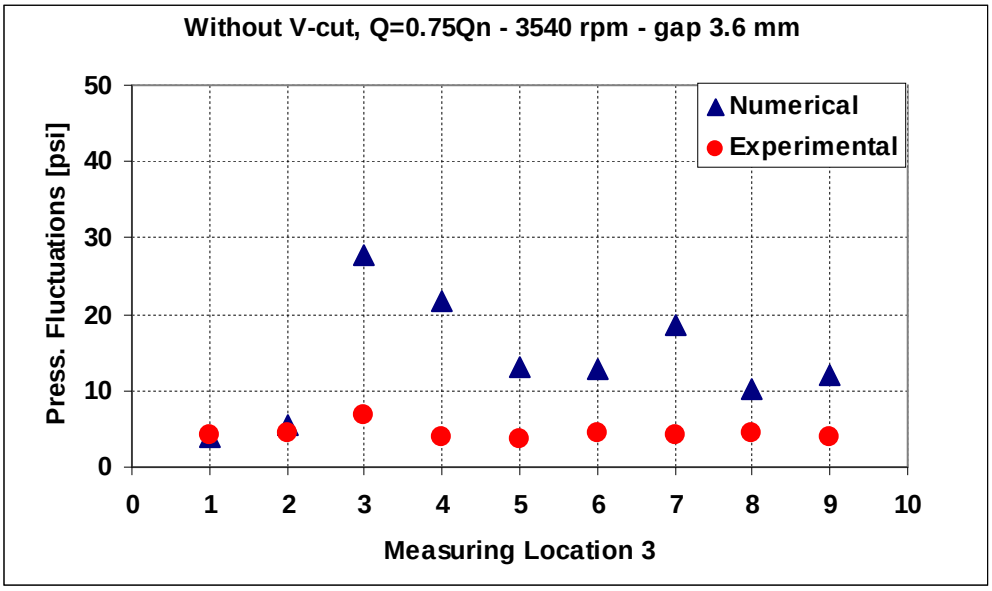
Without V-cut, Q=0.75Qn - 3540 rpm - gap 3.6 mm
Press. Fluctuations [psi]
50
40
30
20
10
0
0
1
2
3
4
5
6
7
8
9
10
Measuring Location 3
Numerical
Experimental

(b)

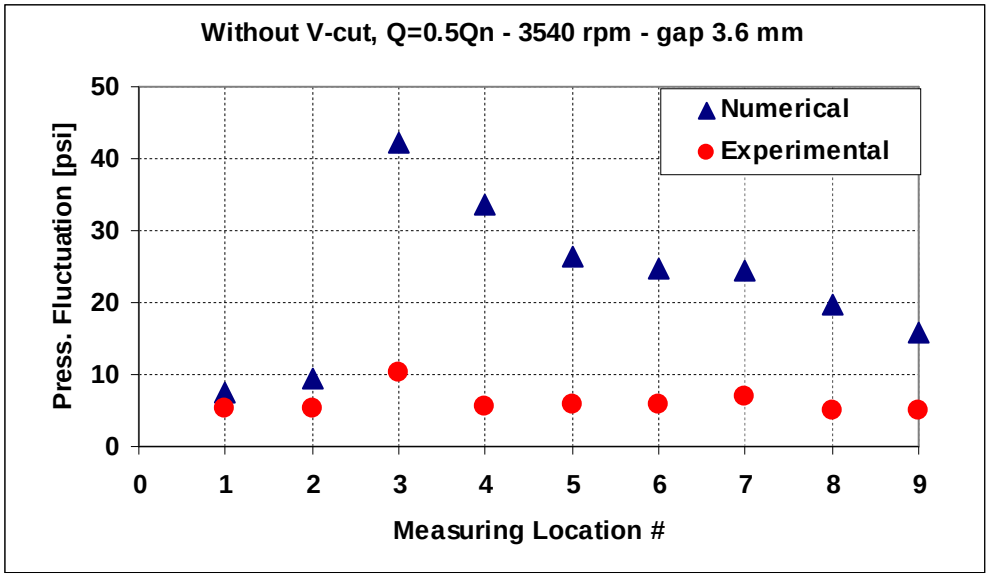

(c)

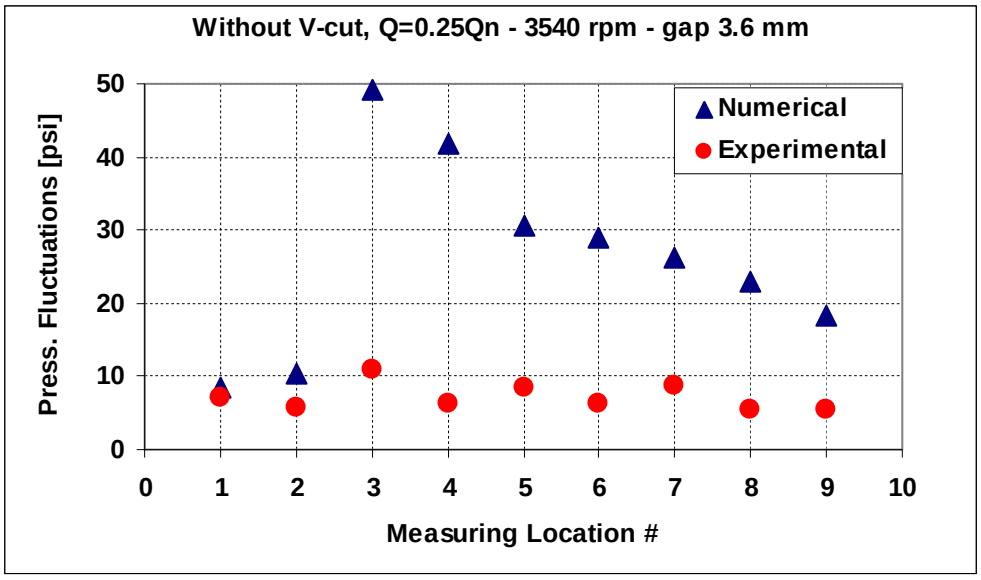

(d)

Figure 4.37 Effect of flow rate on pressure fluctuations: experimental vs numerical for impeller without V-cut, gap 3.6 mm

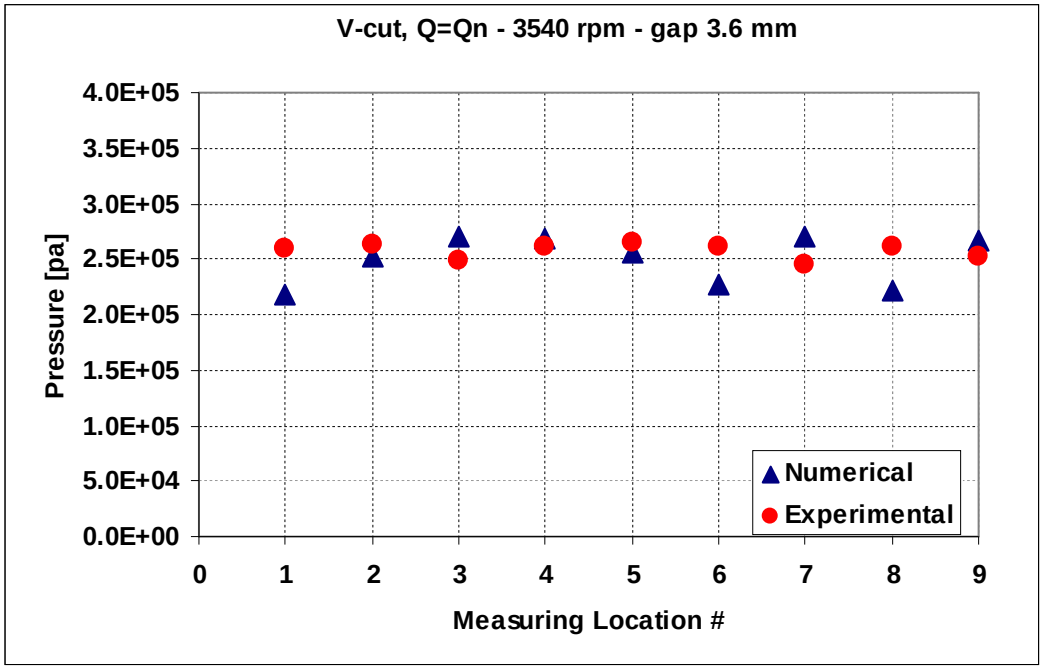
V-cut, Q=Qn - 3540 rpm - gap 3.6 mm
Pressure [pa]
4.0E+05
3.5E+05
3.0E+05
2.5E+05
2.0E+05
1.5E+05
1.0E+05
5.0E+04
0.0E+00
0
1
2
3
4
5
6
7
8
9
Measuring Location #
Numerical
Experimental

(a)

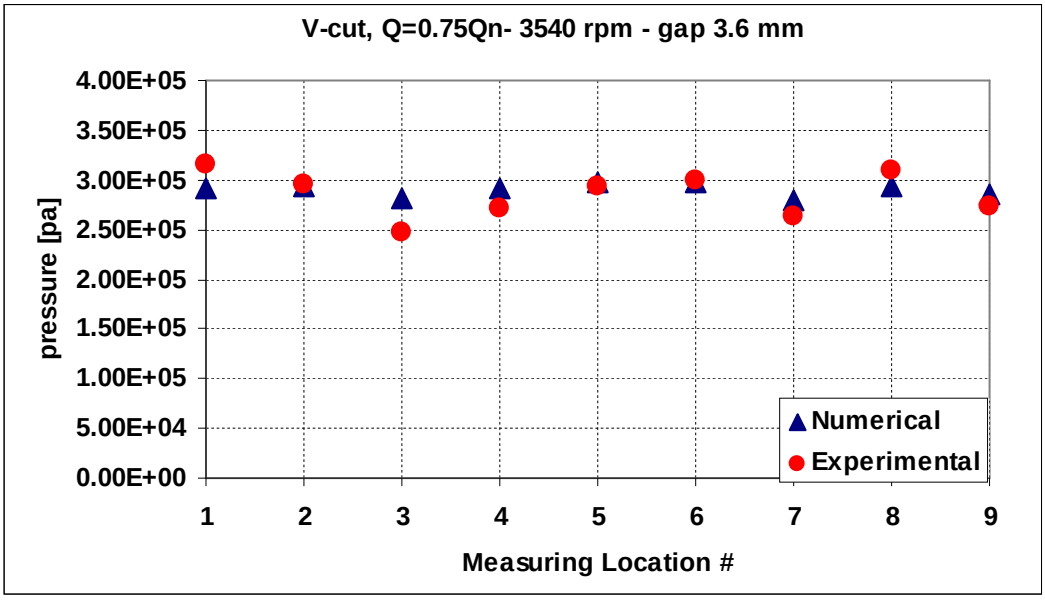
V-cut, Q=0.75Qn- 3540 rpm - gap 3.6 mm
pressure [pa]
4.00E+05
3.50E+05
3.00E+05
2.50E+05
2.00E+05
1.50E+05
1.00E+05
5.00E+04
0.00E+00
1
2
3
4
5
6
7
8
9
Measuring Location #
Numerical
Experimental

(b)

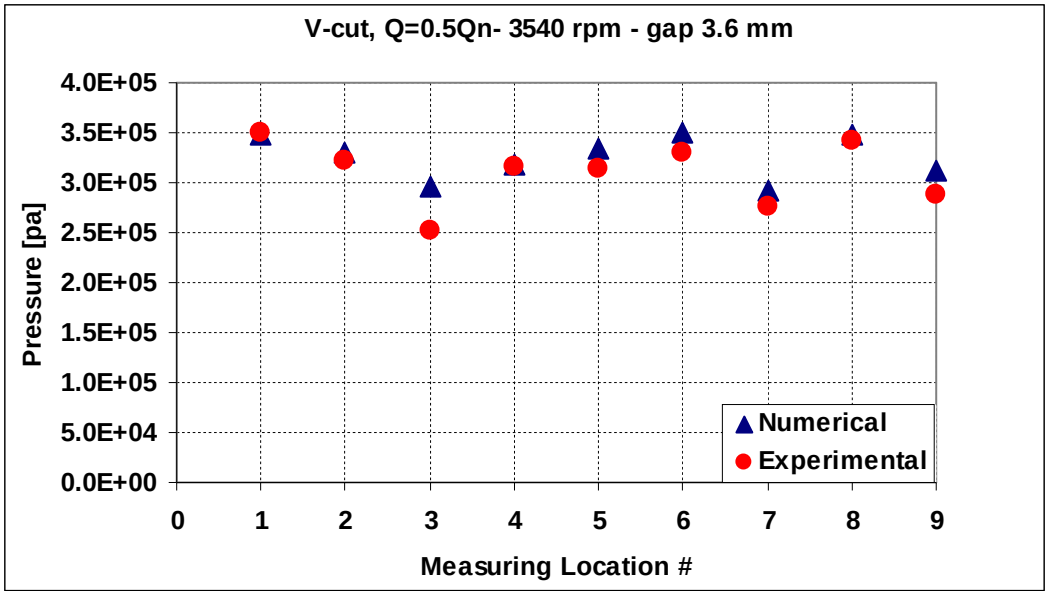

(c)

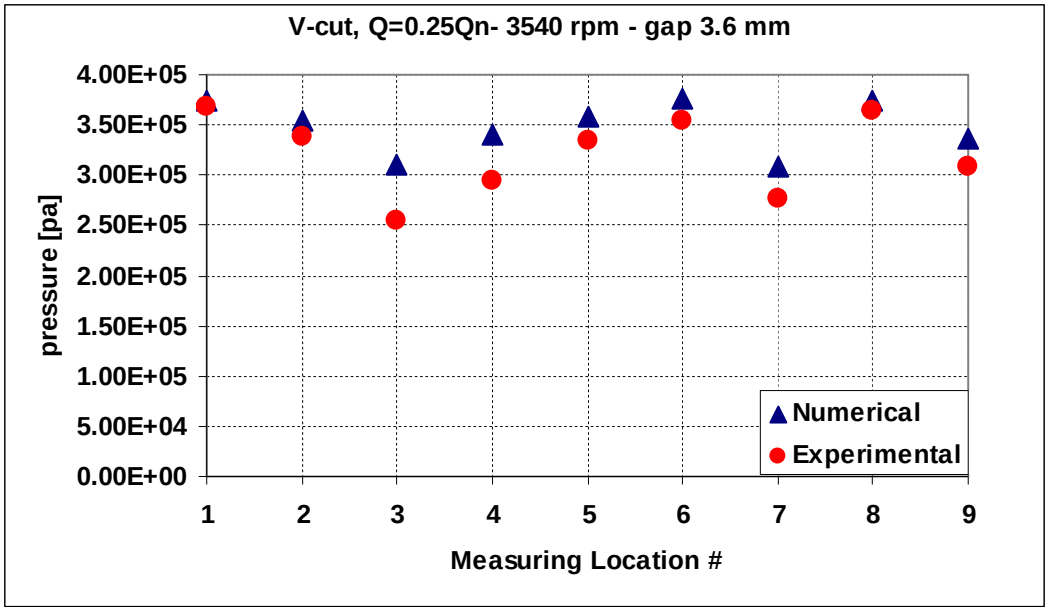

(d)

Figure 4.38 Effect of flow rate on time-averaged pressure distribution: experimental vs numerical for impeller with V-cut blade, gap 3.6 mm

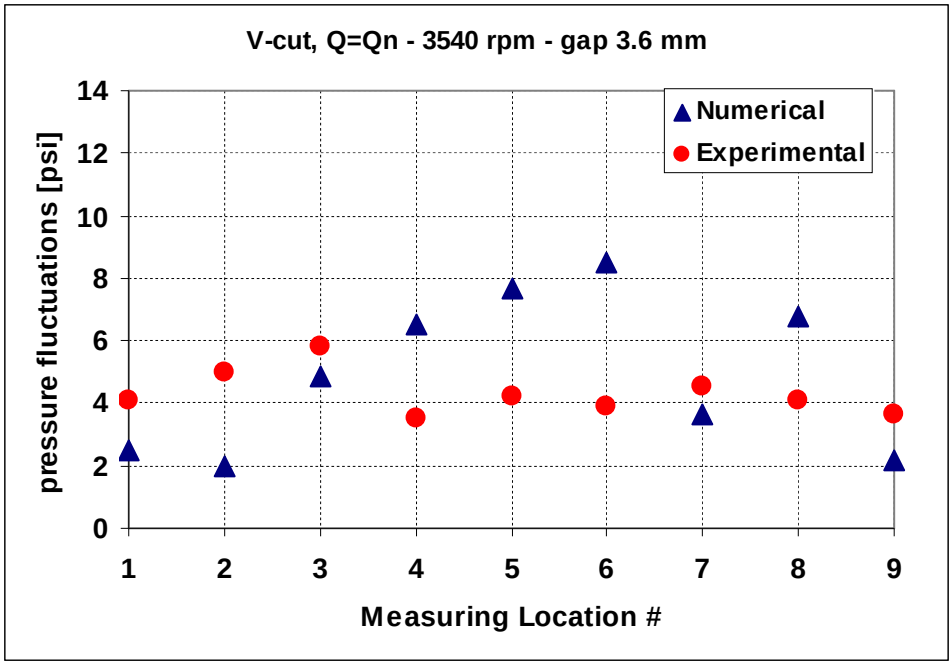
V-cut, Q=Qn - 3540 rpm - gap 3.6 mm
pressure fluctuations [psi]
Numerical
Experimental
0
2
4
6
8
10
12
14
1
2
3
4
5
6
7
8
9
Measuring Location #

(a)

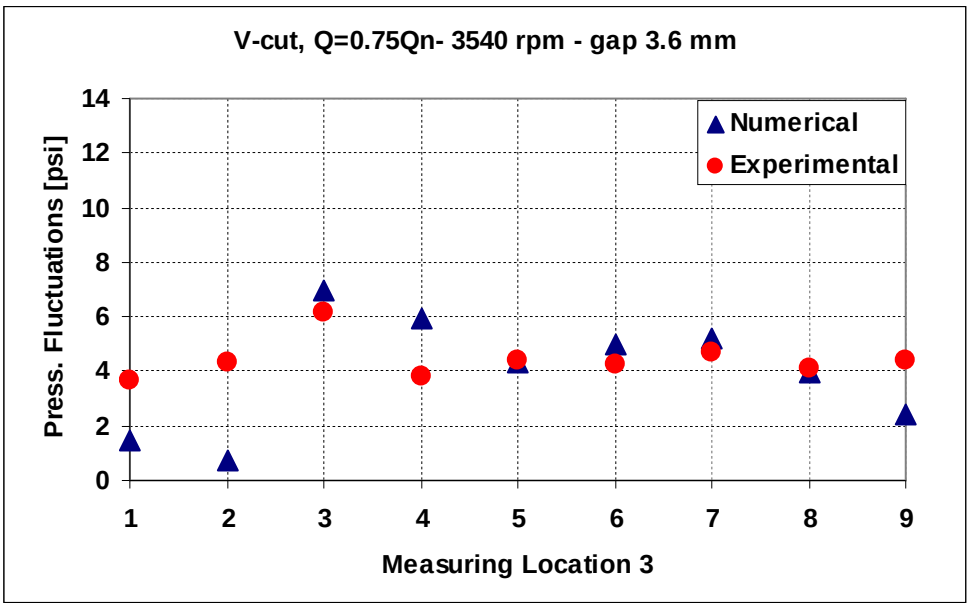
V-cut, Q=0.75Qn- 3540 rpm - gap 3.6 mm
Press. Fluctuations [psi]
Numerical
Experimental
0
2
4
6
8
10
12
14
1
2
3
4
5
6
7
8
9
Measuring Location 3

(b)

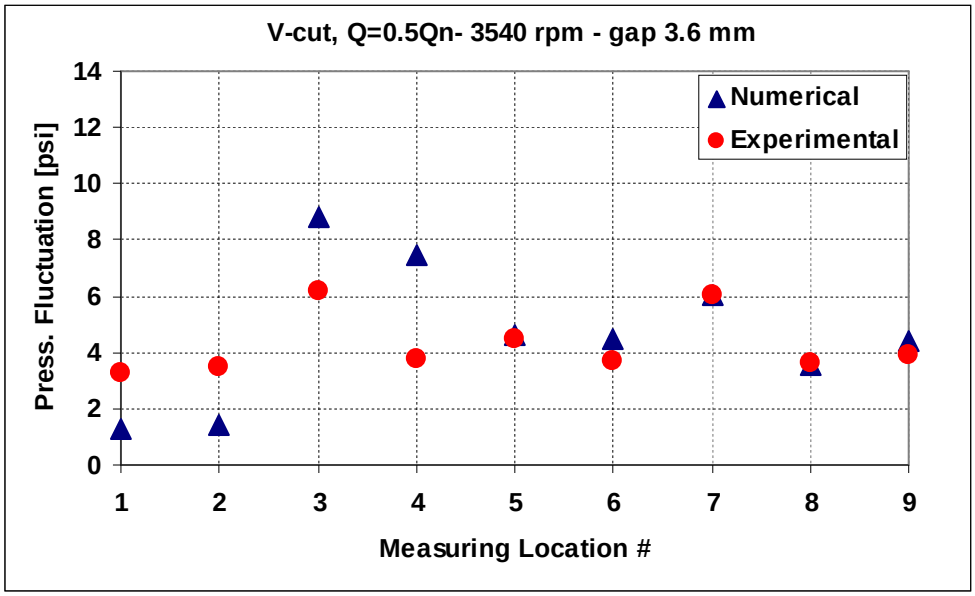

(c)

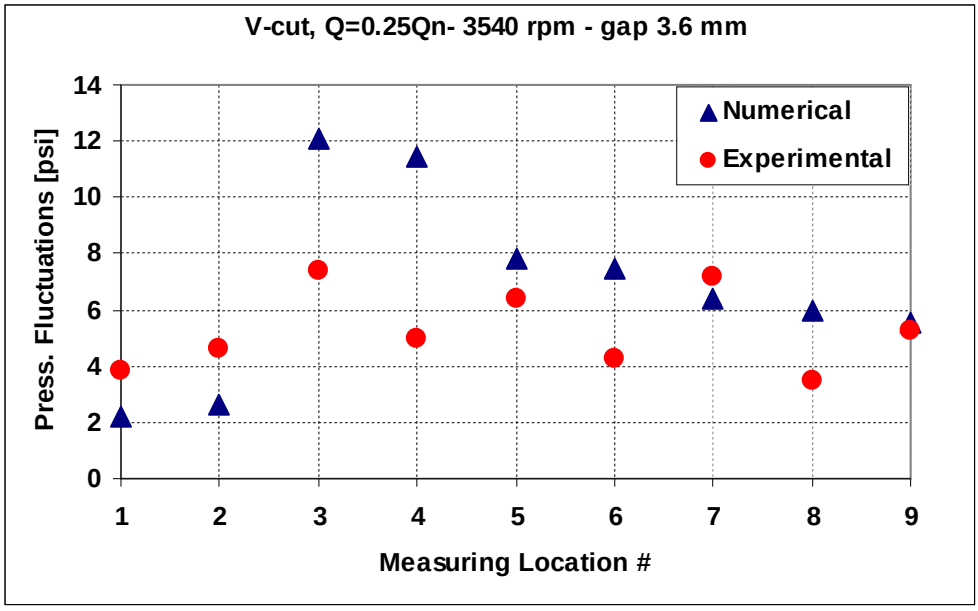

(d)

Figure 4.39 Effect of flow rate on pressure fluctuations: experimental vs numerical for impeller with V-cut blade, gap 3.6 mm

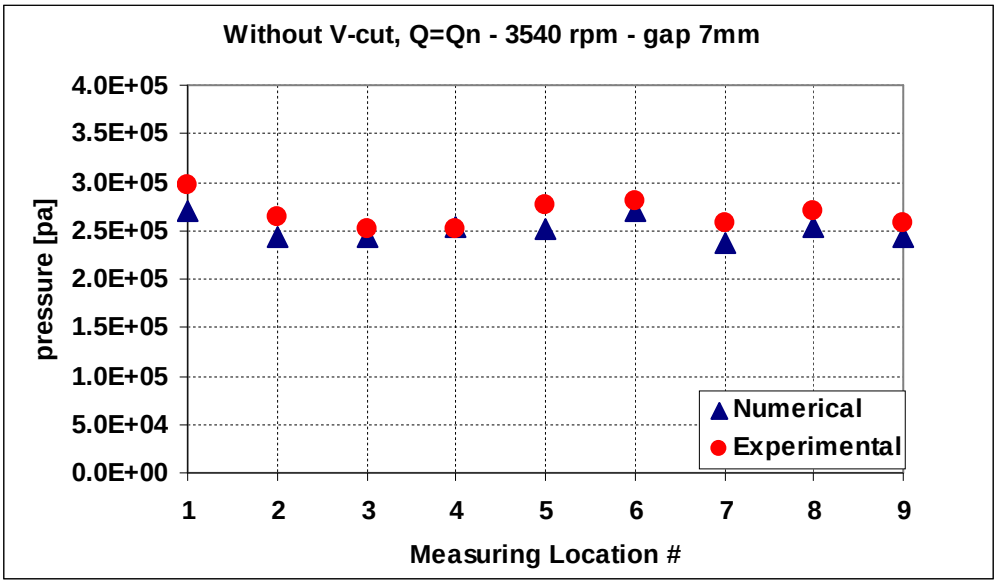
Without V-cut, Q=Qn - 3540 rpm - gap 7mm
pressure [pa]
4.0E+05
3.5E+05
3.0E+05
2.5E+05
2.0E+05
1.5E+05
1.0E+05
5.0E+04
0.0E+00
1
2
3
4
5
6
7
8
9
Measuring Location #
Numerical
Experimental

(a)

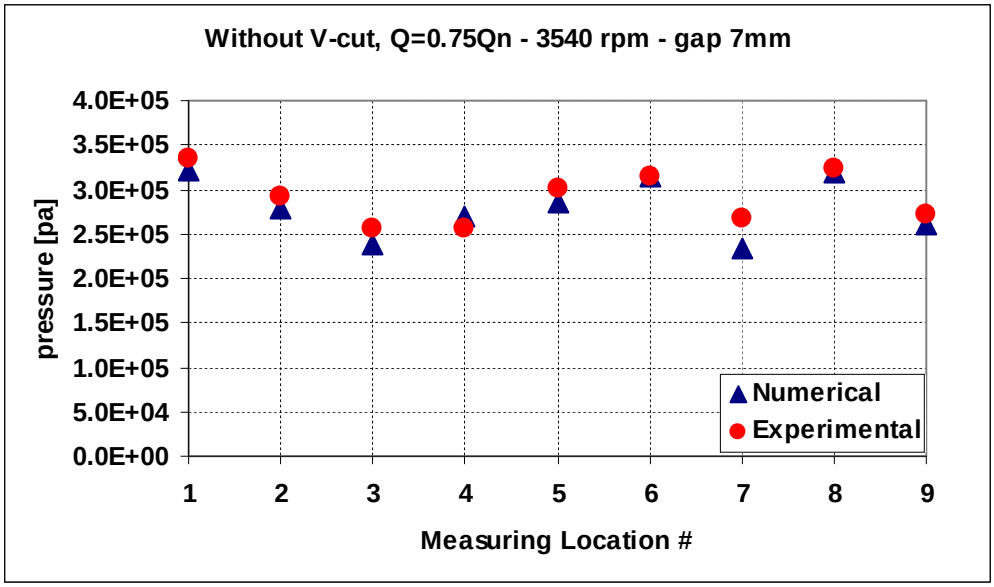
Without V-cut, Q=0.75Qn - 3540 rpm - gap 7mm
pressure [pa]
4.0E+05
3.5E+05
3.0E+05
2.5E+05
2.0E+05
1.5E+05
1.0E+05
5.0E+04
0.0E+00
1
2
3
4
5
6
7
8
9
Measuring Location #
Numerical
Experimental

(b)

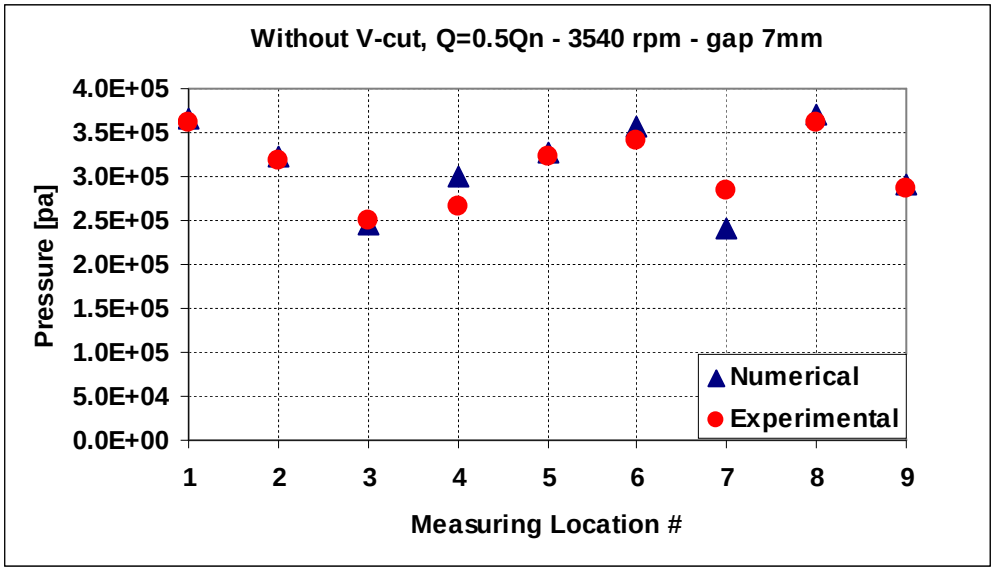

(c)

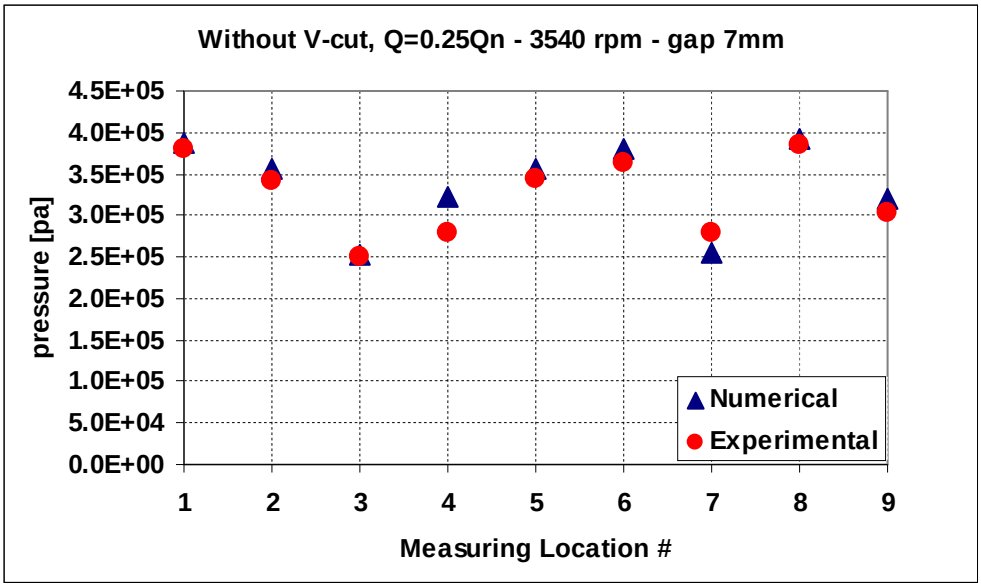

(d)

Figure 4.40 Effect of flow rate on pressure distribution: experimental vs numerical for impeller without V-cut, gap 7 mm

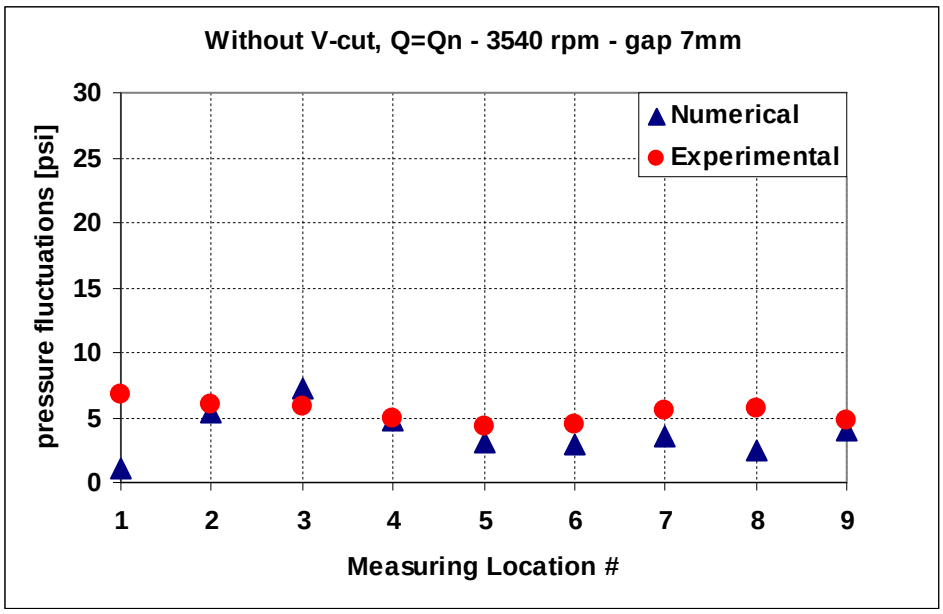
Without V-cut, Q=Qn - 3540 rpm - gap 7mm
pressure fluctuations [psi]
30
25
20
15
10
5
0
1
2
3
4
5
6
7
8
9
Measuring Location #
Numerical
Experimental

(a)

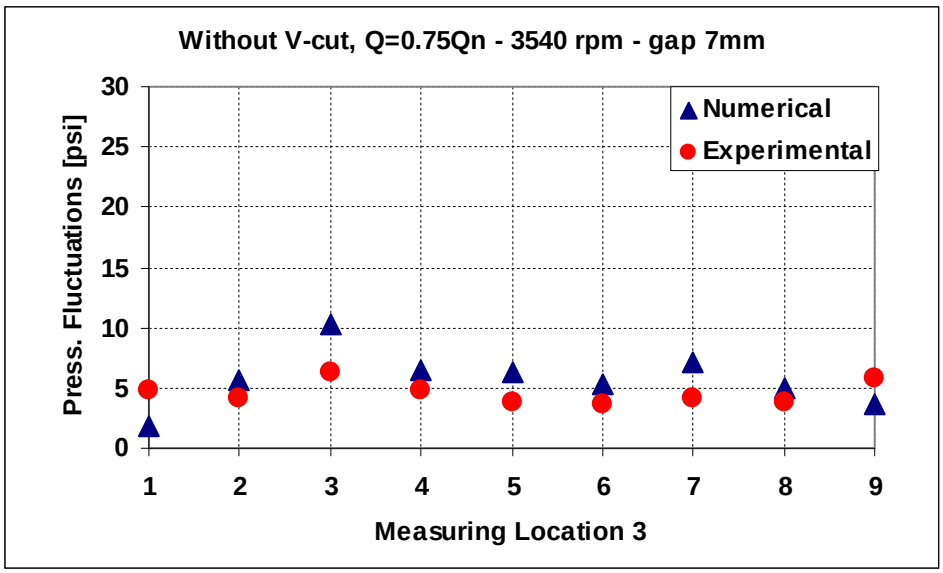
Without V-cut, Q=0.75Qn - 3540 rpm - gap 7mm
Press. Fluctuations [psi]
30
25
20
15
10
5
0
1
2
3
4
5
6
7
8
9
Measuring Location 3
Numerical
Experimental

(b)

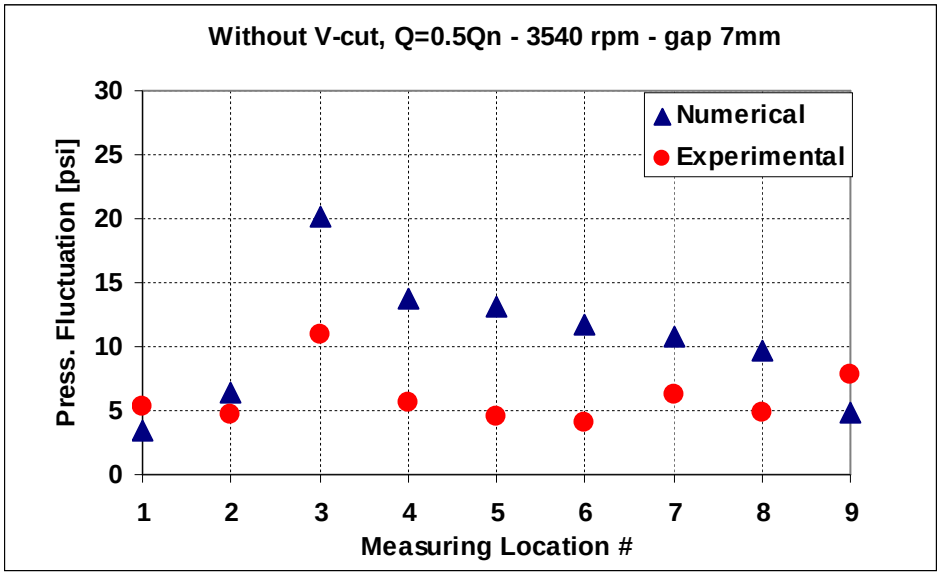

(c)

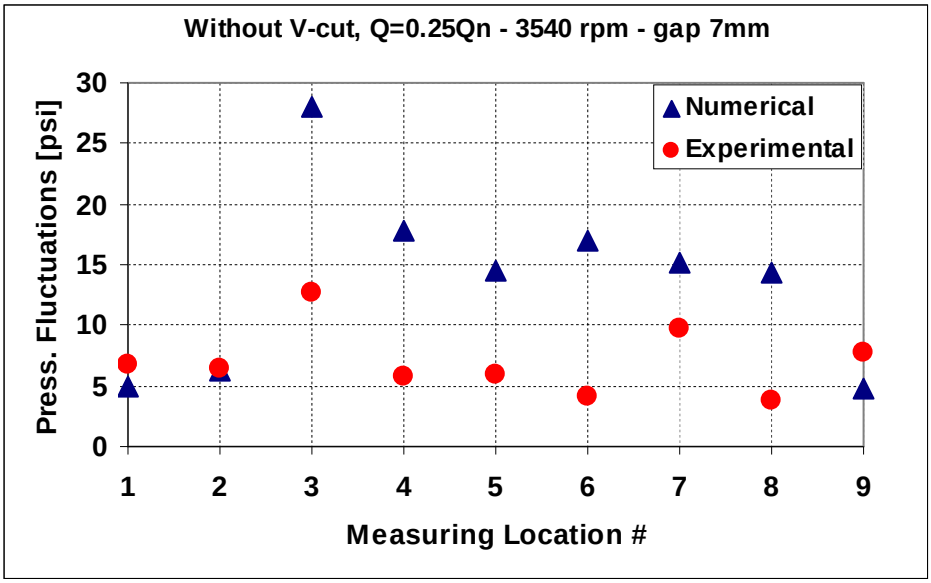

(d)

Figure 4.41 Effect of flow rate on pressure fluctuations: experimental vs numerical for impeller without V-cut, gap 7 mm

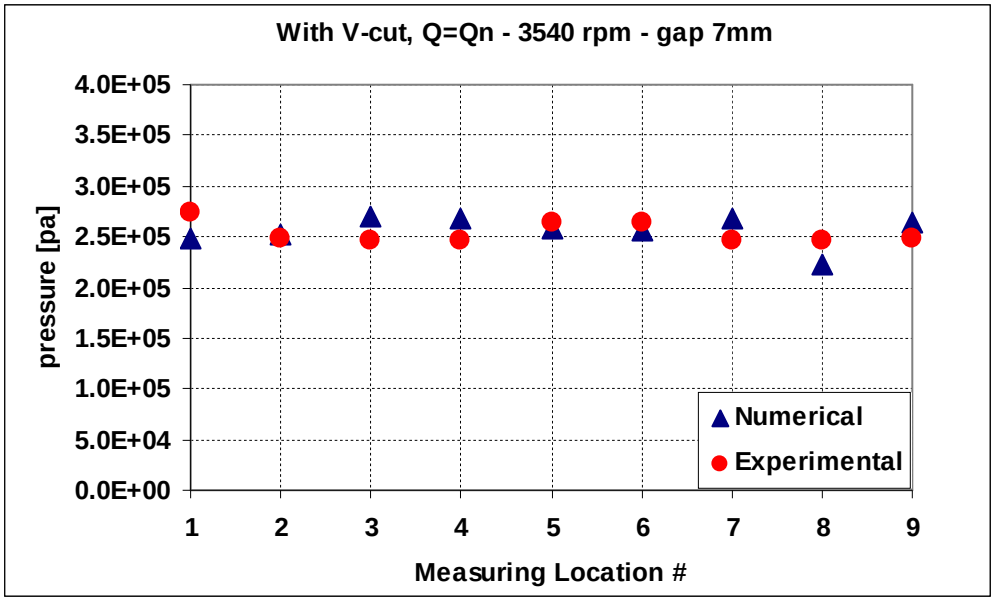
With V-cut, Q=Qn - 3540 rpm - gap 7mm
pressure [pa]
4.0E+05
3.5E+05
3.0E+05
2.5E+05
2.0E+05
1.5E+05
1.0E+05
5.0E+04
0.0E+00
1
2
3
4
5
6
7
8
9
Measuring Location #
Numerical
Experimental

(a)

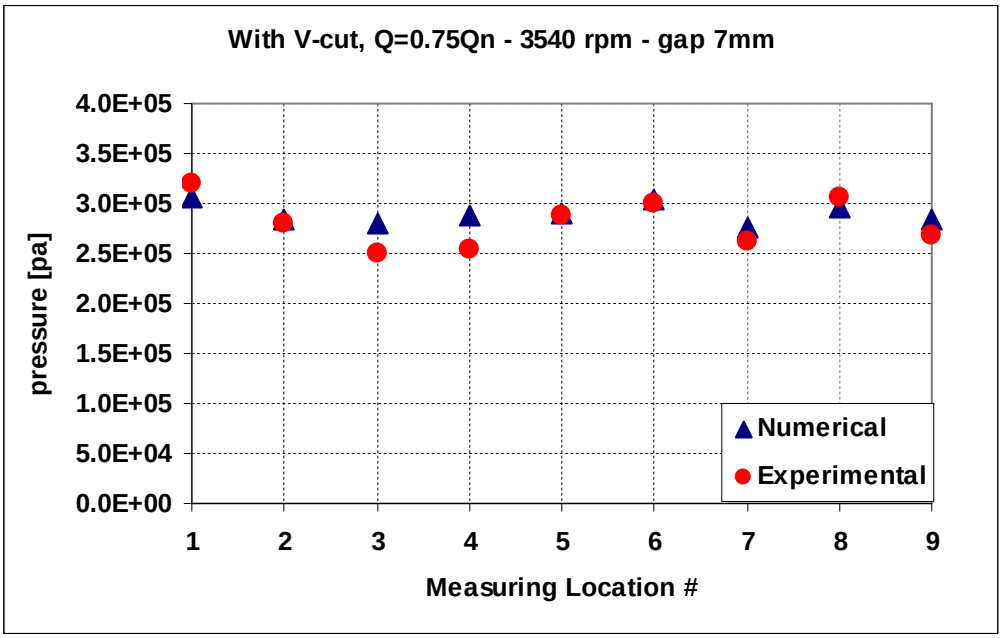
With V-cut, Q=0.75Qn - 3540 rpm - gap 7mm
pressure [pa]
4.0E+05
3.5E+05
3.0E+05
2.5E+05
2.0E+05
1.5E+05
1.0E+05
5.0E+04
0.0E+00
1
2
3
4
5
6
7
8
9
Measuring Location #
Numerical
Experimental

(b)

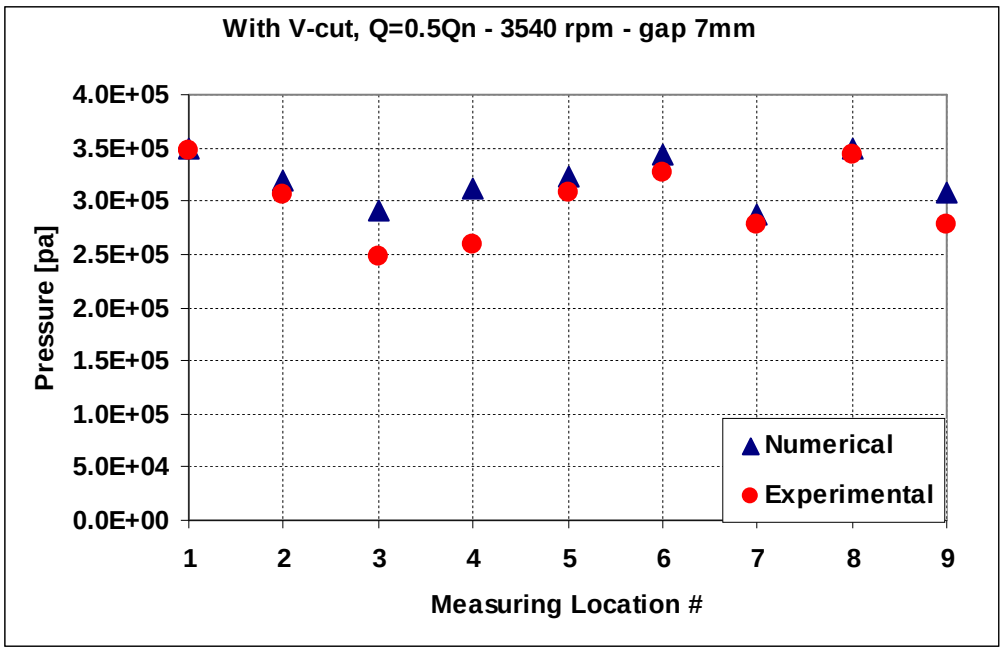

(c)

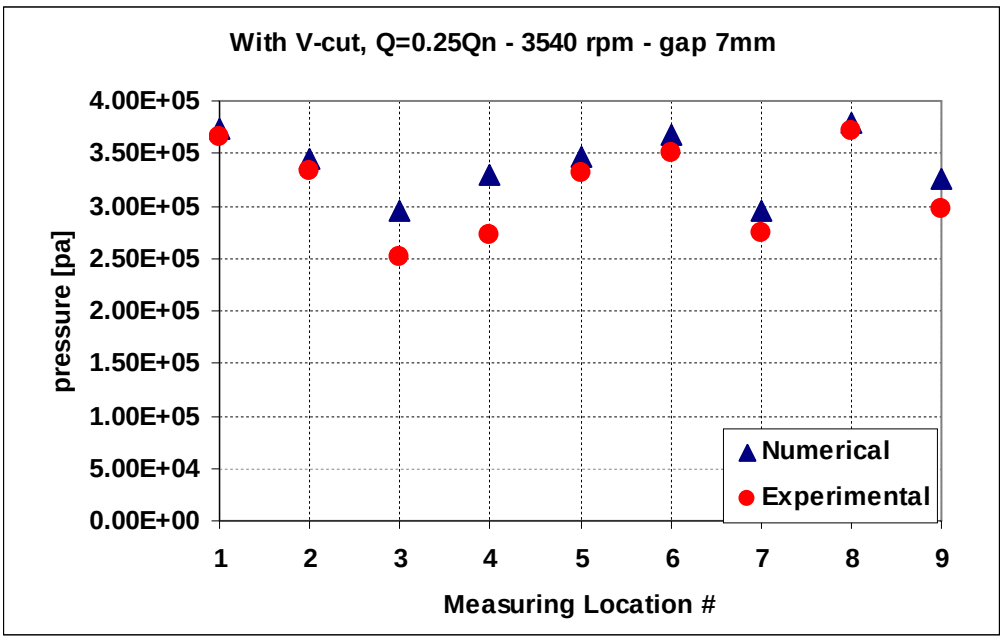

(d)

Figure 4.42 Effect of flow rate on pressure distribution: experimental vs numerical for impeller with V-cut blade, gap 7 mm

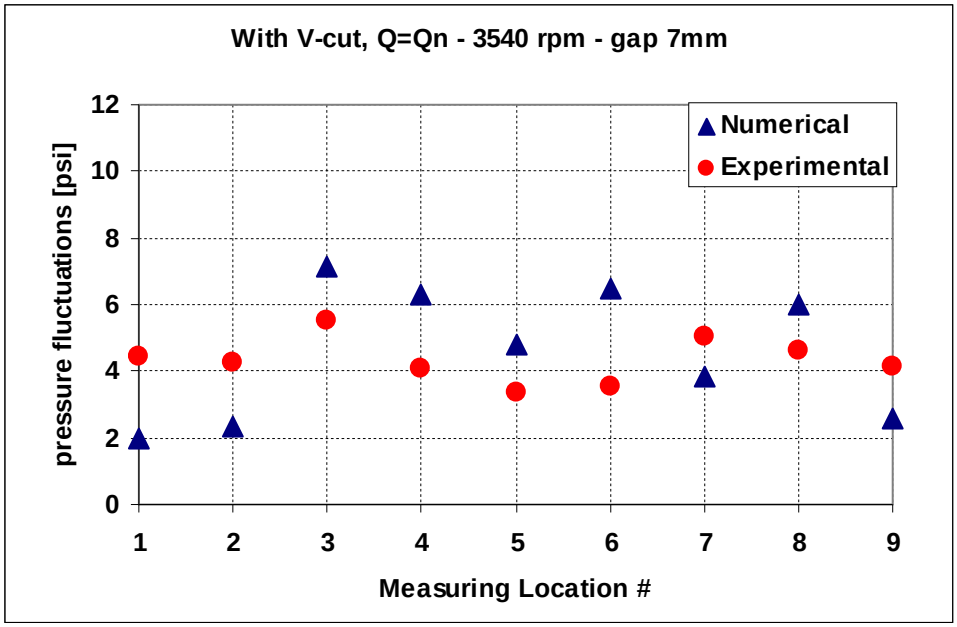
With V-cut, Q=Qn - 3540 rpm - gap 7mm
pressure fluctuations [psi]
Numerical
Experimental
0
2
4
6
8
10
12
1
2
3
4
5
6
7
8
9
Measuring Location #

(a)

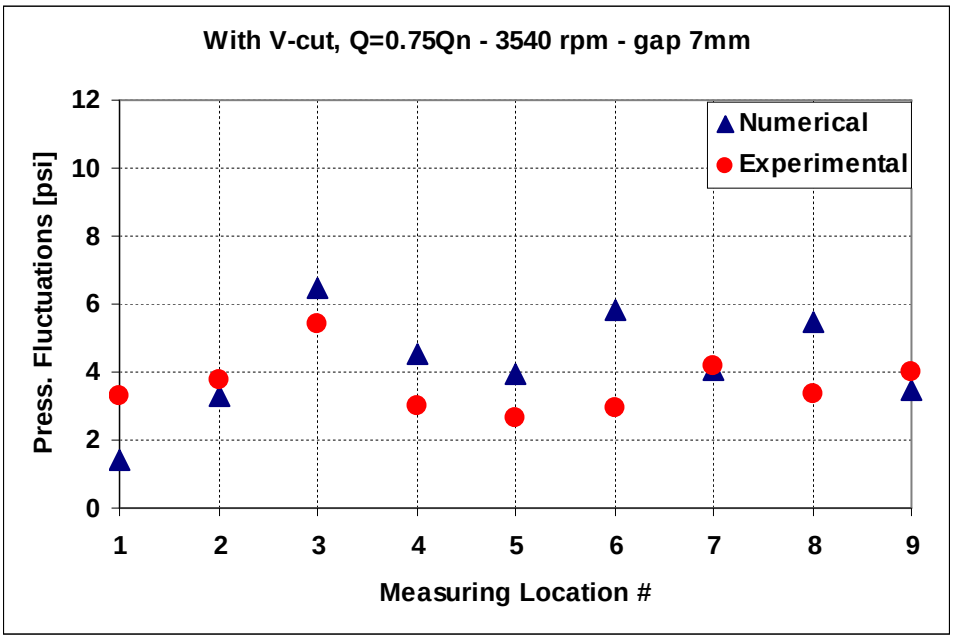
With V-cut, Q=0.75Qn - 3540 rpm - gap 7mm
Press. Fluctuations [psi]
Numerical
Experimental
0
2
4
6
8
10
12
1
2
3
4
5
6
7
8
9
Measuring Location #

(b)

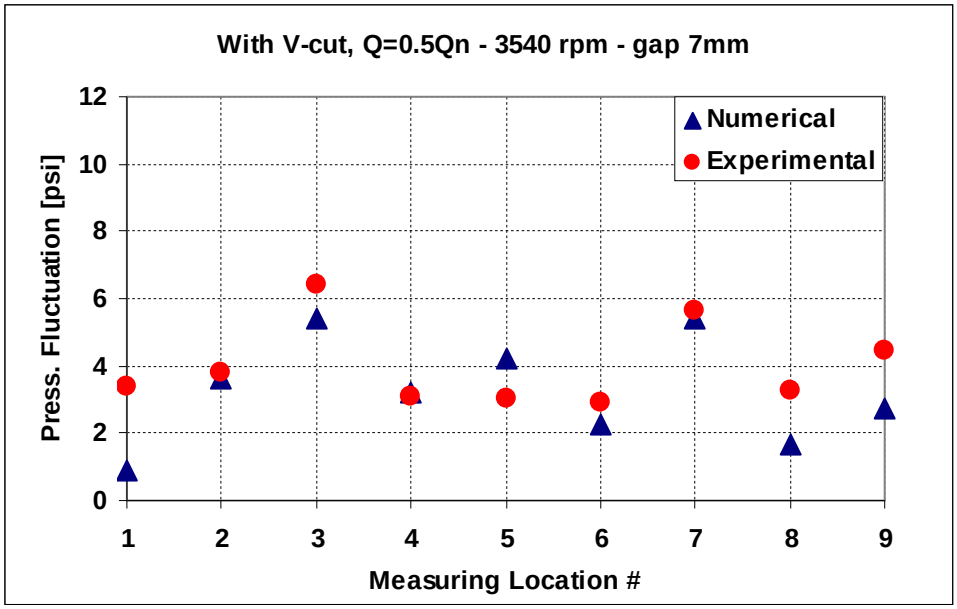

(c)

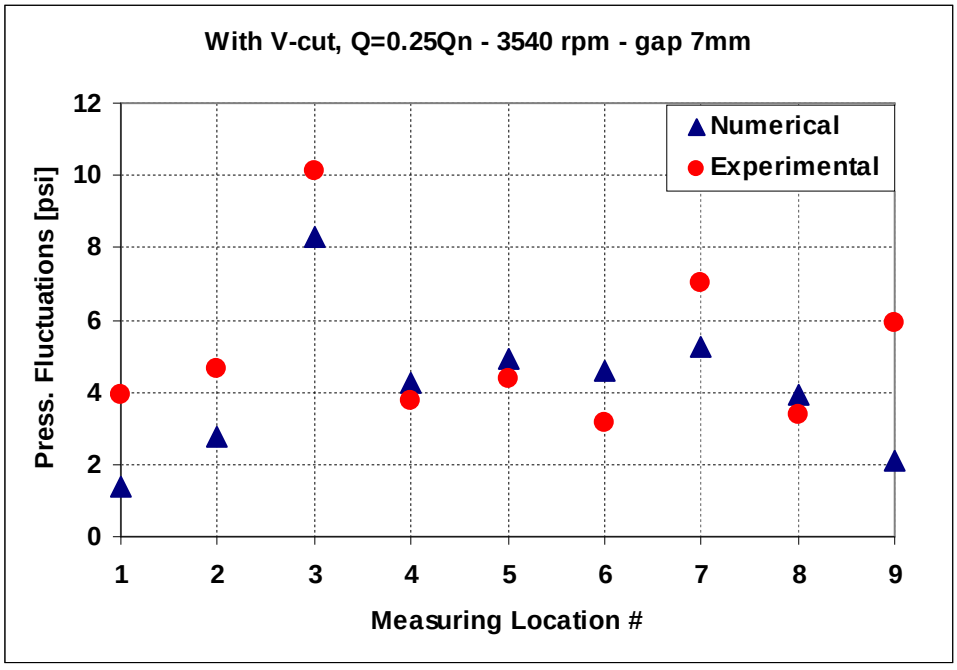

(d)

Figure 4.43 Effect of flow rate on pressure fluctuations: experimental vs numerical for impeller with V-cut blade, gap 7 mm

CHAPTER 5

CONCLUSIONS AND RECOMMENDATIONS

The problem of high vibration levels at the blade passing frequencies of the main boiler feed pump at SEC power generation plant has been investigated. The investigations consist of experimental testing on a model pump and 2D CFD simulations to study the effect of operating and design variables. The vibration has been found to be flow-induced due to the high interaction between the impeller rotating blades and the volute splitters. The effect of the operating and design variables on the internal unsteady pressure field, vibration of pump casing, and performance was studied. Detailed uncertainty analysis was performed for the instrumentation of the test loop in order to assess the effect of each design modification on performance. A scaled model single stage pump was produced by reverse engineering of the actual boiler feed pump components. As a validation of the test loop, the deviation between the measured pump head and capacity, at best efficiency point, and the similitude calculations is less than 4%.

The special design of V-cut at the impeller blades of the actual pump was studied experimentally for performance, pressure fluctuation, and pump vibration. The V-cut reduces the pump vibration. However, vibration levels of the actual boiler feed pump still above the acceptable limits even with the existence of the V-cut. In order to find an applicable solution to minimize the problem of the high flow-induced vibration of

the present pump, different radial gaps between the impeller and volute vanes were tested experimentally by cutting back the volute tongues. Also, two-dimensional CFD simulations were conducted using the sliding mesh technique and were validated by the experimental results at different operating conditions and for different geometrical designs.

The following conclusions can be made based on the experimental and numerical results:

1. The high pressure fluctuations and pump vibrations are primarily caused by the strong interaction between the impeller blades and volute splitters as manifested by maximum pressure pulsations close to the interaction regions at volute tongues. Both V-cut design and impeller-volute gap increase have been shown to reduce this interaction and hence pump vibration.
2. The main frequency of the internal pressure pulsations and the pump vibration is the first blade passing frequency (5xRPM). Higher harmonics (2^{nd} and 3^{rd} BPF) have smaller magnitudes compared to the 1^{st} BPF.
3. The amplitudes of the pressure fluctuations and their energies, at the 1^{st} BPF, are minimum at the rated flow rate and increase at off-design operating conditions.
4. Pressure fluctuations are not uniform inside the pump, even at the design flow rate where the static pressure is uniform. These fluctuations depend on the location relative to the interactions zone and the operating flow rate.
5. The design of V-cut at impeller blade exits reduces the pump vibration level while maintaining almost the same performance at the nominal flow rate. It is more effective in reducing the fluctuations inside the volute and the pump

vibration level at off-design flow rates but with a negative effect on the pump head (from 5 to 8% head loss).

6. The original gap design of 3.6 mm (2.5% of the impeller diameter) was found to be the most suitable gap for performance over a wide range of flow rates. Combining the V-cut design with the gap of 7 mm (5% of the impeller diameter) is found to be suitable solution which minimizes vibration levels for the present pump at a wide range of flow rates.
7. Cutting back 30 mm from the leading edges of volute vanes of the model pump was required to achieve a gap of 5% of the impeller diameter. This gap reduced the pump vibration by about 50% on average depending on flow rate. For the pump with V-cut and gap of 7 mm, the reduction in the amplitudes of pressure fluctuations and pump vibration was achieved at the expense of 5% loss in pump head and 1.6% in efficiency for the rated capacity.
8. The 2D simulations using the sliding mesh technique can predict the pressure distribution inside the pump with good accuracy (< 5%). However, accuracy of prediction of total pump head is poor. Also, it can predict the effect of variable flow rate and pump geometry on pressure distribution. It provides a qualitatively equivalent behavior to experimental measurement, under different flow rates.
9. The 2D models over-predict the amplitudes of pressure fluctuations. Possible reason is that the model can not simulate the internal leakage inside the pump and the damping of the fluctuations at the volute walls where the experimental measurements were taken.

10. The unsteady pressure fluctuations are location dependent and a 3D simulation model is needed to improve the prediction of the fluctuations magnitudes.

Future work

As an extension of the work presented in this dissertation, the following experimental and numerical activities are recommended.

1. Test the effect of measuring axial location of pressure fluctuations measurements. The V-cut design provides a maximum effective gap at the central plane of the impeller. If measured at the central plane of the impeller, the fluctuation amplitudes are expected to much higher than the values measured at the volute cover at wall.
2. Test the effect of trimming the impeller to produce an equivalent effective gap to the V-cut and check its effect on pump performance and vibration.
3. Try different shapes of cuts at blade exit.
4. Conduct 3D simulations.

Appendix

Uncertainty analysis

In detailed uncertainty analysis, one should consider all the elemental sources of bais and precision errors for each variable. The propagation analysis of these errors gives the uncertainty in the final result.

Consider result, r , to be function of many measured variables, x_i

$$r = r(x_1, x_2, x_3, ..., x_n) \tag{A-1}$$

then

$$U_r = \sqrt{B_r{}^2 + P_r{}^2} \tag{A-2}$$

Where U_r is the uncertainty in the result and B_r, P_r are the bias and precision limit for the result, respectively, calculated from bias and precision limits of the measured variables as

$$B_r = \left[\sum \left(\frac{\partial r}{\partial x_j} B_j \right)^2 \right]^{\frac{1}{2}} \tag{A-3}$$

$$P_r = \left[\sum \left(\frac{\partial r}{\partial x_j} P_j \right)^2 \right]^{\frac{1}{2}} \tag{A-4}$$

For each measured variable, J, the propagation of elemental source of error should be considered such that

$$B_J = \left[\sum_{k=1}^{m} (B_J)_k^{\,2}\right]^{\frac{1}{2}} \quad \text{and} \quad P_J = \left[\sum_{k=1}^{m} (P_J)_k^{\,2}\right]^{\frac{1}{2}} \tag{A-5}$$

The error sources will include the instrumentation errors, readout errors, rest errors, calibration errors, and unsteadiness errors. Any correlations between errors should be considered.

Pump Head:

$$H = \frac{p_d - p_s}{\gamma} + \frac{V_d^{\,2} - V_s^{\,2}}{2g} + \Delta z \tag{A-6}$$

Orifice flow rate:

$$Q = C_d \frac{A_2}{\sqrt{1-(A_2/A_1)^2}} \sqrt{\frac{2\Delta p}{\rho}} \tag{A-7}$$

Pump efficiency:

$$\eta = \frac{\gamma Q H}{\sqrt{3} * V * I * PF * \eta_{motor}} \tag{A-8}$$

Instruments accuracy:

The pressures $p_d \,\&\, p_s$ are measured by a pressure transducer with mV output which has an accuracy of 0.25% of full scale. The full scale output is 100 mV and thus the accuracy using this sensor is 0.25 mV. The pressure transducer is excited by a 10 V DC power supply with accuracy of 10 mV.

The velocity at both pump suction and delivery sides are calculated from the flow rate. The flow rate is mainly depends on the measurement of the pressure drop across the orifice which is measured by a mercury manometer. The power supplied to the pump is measured by measurements of the current and the voltage after the frequency inverter.

The pump power factor is 0.92 and the motor efficiency is 0.85. Water density is 994 kg/m^3 and the orifice discharge coefficient is 0.618.

Following the above method, the data reduction equations (DRE) for the results may be simplified as

$$H = H(P_d, P_s, \rho, g, \Delta z, \Delta h_{orifice}) \tag{A-9}$$

$$Q = Q(C_d, A_1, A_2, \rho, \Delta h_{orifice}) \tag{A-10}$$

$$\eta = \eta(P_d, P_s, \Delta h_{orifice}, volt, amp, \rho, g) \tag{A-11}$$

where,

$$P_d = 6000 * mV_d \tag{A-12}$$

$$P_s = 6000 * mV_s \tag{A-13}$$

$$V_d = Q / A_d \text{, and } V_s = Q / A_s \tag{A-14}$$

Estimated errors:

B: Bias error

P: Precision error

1) Static pressure transducer for $p_d \& p_s$

Source of error	Value [mV]
Sensor precision	P=0.25
Power supply	P=0.1
Unsteadiness	P=0.1
readout	P=0.01
Calibration	B=0.1

2) Orifice pressure drop

Source of error	Value [inch Hg]
Readout	P=0.02
Unsteadiness	P=0.05
reset	P=0.05

3) Voltage

Source of error	Value [Volt]
Readout	P=0.05
unsteadiness	P=0.5

4) Ampere

Source of error	Value [A]
Readout	P=0.1
unsteadiness	P=0.1

$$P_{static,mV} = [0.25^2 + 0.1^2 + 0.1^2 + 0.01^2]^{1/2} = 0.287 \text{ mV}$$

$$B_{static,mV} = 0.1 \text{ mV}$$

$$P_{\Delta H_{Orifice}} = [0.02^2 + 0.05^2 + 0.05^2]^{1/2} = 0.073 \text{ Inch Hg}$$

$$P_{Volt} = [0.5^2 + 0.05^2]^{1/2} = 0.5025 \text{ Volt}$$

$$P_{amp} = [0.1^2 + 0.1^2]^{1/2} = 0.1414 \text{ Amp}$$

Numerical example for the uncertainty calculations

Values in this example are taken at the best efficiency point for the impeller without V-cut at blade exit at 3540 rpm.

For the pump head, the functional equation is written as:

$$H = H(mV_d, mV_s, \rho, g, \Delta z, \Delta h_{orifice}, C_d, A_1, A_2, A_d, A_s) \qquad \text{(A-15)}$$

Constant values

ro = 994 [kg/m3]

g = 9.81 [m2/s]

As = 0.006969 [m2]

Ad = 0.004185263 [m2]

$A1_{or}$ = 0.006969 [m2]

dz = 0.5 [m]

C_d = 0.618

$A2_{or}$ = 0.00361 [m2]

Measured values

mvs = 5.755 [mV]

mvd = 48.3 [mV]

$dH_{orifice}$ = 3.4 [inch]

Head equation

$$Hp = (mvd - mvs)\cdot\frac{6000}{9.81\cdot 994} + \frac{\left[\dfrac{C_d\cdot A2_{or}\cdot 15.723\cdot\sqrt{dH_{orifice}\cdot 0.0254}}{\sqrt{1-\left(\dfrac{A2_{or}}{A1_{or}}\right)^2}}\right]^2}{2\cdot g\cdot(Ad^2 - As^2)} + dz$$

(A-16)

The bias limit is calculated by applying equation (3) to relation (12) considering the correlation between P_d and P_s

$$B_H = \left[\sum\left(\frac{\partial H}{\partial x_j}B_j\right)^2\right]^{\frac{1}{2}} + 2\frac{\partial H}{\partial mV_d}\frac{\partial H}{\partial mV_s}B_d B_s$$

$$= \left[\left(\frac{\partial H}{\partial mV_d}B_{mV_d}\right)^2 + \left(\frac{\partial H}{\partial mV_s}B_{mV_s}\right)^2 + 0 + 0 + 0 + ...\right]^{\frac{1}{2}} + 2\frac{\partial H}{\partial mV_d}\frac{\partial H}{\partial mV_s}B_d B_s$$

$$= \left[(0.6153(0.1))^2 + (-0.6153(0.1))^2\right]^{\frac{1}{2}} + 2(0.6153)(-0.6153)(0.1)(0.1)$$

$$= 0.0794\,m$$

Equation (5) is now applied to relation (12) to find the precision limit in the pump head.

$$P_H = \left[\left(\frac{\partial H}{\partial mV_d} P_{mV_d} \right)^2 + \left(\frac{\partial H}{\partial mV_s} P_{mV_s} \right)^2 + \left(\frac{\partial H}{\partial \Delta H_{orifice}} P_{\Delta H_{orifice}} \right)^2 + \left(\frac{\partial H}{\partial C_d} P_{C_d} \right)^2 + ... \right]^{\frac{1}{2}}$$

$$= 0.2498 \ m$$

The uncertainty limit in the pump head is calculated using equation (2)

$$U_H = \sqrt{B_H{}^2 + P_H{}^2} = 0.264 \text{ [m]}$$

Head = 26.95 ±0.2657 [m]

Similarly,

Flow rate = 0.01207 ±0.0001771 [m3/s], and

Efficiency = 0.5514 ±0.01071

From the above calculations:

1) Uncertainty of flow rate at best efficiency point is 1.467 %

2) Uncertainty of pump head at best efficiency point is 0.987 %

3) Uncertainty of pump efficiency at best efficiency point is 1.94 %.

REFERENCES

1. Baun, D. O. and Flack R. D., Effect of Volute Design and Number of Impeller Blades on Lateral Impeller Forces and Hydraulic Performance, *International Journal of Rotating Machinery*, 9(2): 145-152, 2003.
2. Breugehmans, F. and Sen, M., Pre-Rotation And Fluid Recirculation In The Suction Pipe Of Centrifugal Pump, Proc. 11th Int. Pump Symp., Texas A&M Univ., 165-180,1982.
3. Guo, S. and Maruta Y., Experimental Investigation on Pressure Fluctuations and Vibration of The Impeller in a Centrifugal Pump With Vaned Diffusers, *JSME International Journal*, series B, Vol. 48, No. 1, 2005.
4. Franke G., Fisher R., Powell C., Seidel U., Koutnik J., On Pressure Mode Shapes Arising from Rotor/Stator Interaction, Sound and Vibration, pp 14-18, March 2005.
5. Rodrigues, C., Egusquiza, E., Santos I., Frequencies in the vibration induced by rotor stator interaction in a centrifugal pump turbine, J Fluids Eng Trans ASME, Vol. 129, n 11, pp 1428-1435, Nov 2007.
6. Koji K., Mitsukiyo M., Eiji A., Velocity distribution in the impeller passages of centrifugal pump, Bulletin of JSME, Vol.28, N0. 243, Sep 1985.
7. Srivastav, O. P., Pandu K. R., and Gupta K., Effect of Radial Gap Between Impeller and Diffuser on Vibration and Noise in a Centrifugal Pump, *IE(I) Journal- MC*, Vol. 84, April 2003.

8. Makay E., Cooper P., Sloteman D. P., Gibson R., Investigation of Pressure Pulsations Arising From Impeller Diffuser Interaction in a Large Centrifugal Pump, Proceedings: Rotating machinery conference and Exposition, ASME, Vol. 1, 1993.
9. Atkins K. and Tison J., Solving Pulsation Induced Vibration Problem in Centrifugal Pumps, *Pumps And Systems Magazine*, January 1993.
10. Gonzalez J. and Santolaria C., Unsteady Flow Structure and Global Variables in a Centrifugal Pump, *Journal Of Fluid Engineering, Transactions Of The ASME*, September 2006, Vol. 128, 937-946.
11. Gonzalez J., Fernandez J., Santolaria C., and Blanco E., Numerical Simulation of the Dynamic Effects Due to Impeller-Volute Interaction in a Centrifugal pump, *Journal Of Fluid Engineering, Transactions Of The Asme*, June 2002, Vol. 124, 348-355.
12. Zhang M. and Tsukamoto H., Unsteady hydrodynamic Forces Due to Rotor-Stator Interaction on a Diffuser pump with Identical Number of Vanes on the Impeller and Diffuser, *Journal Of Fluid Engineering, Transactions Of The ASME*, July 2005, Vol. 127, 743-751.
13. Wang H. and Tsukamoto H., Experimental and Numerical Study of Unsteady Flow in A Diffuser Pump At Off Design Conditions, *Journal of Fluid Engineering, Transactions of the ASME*, September 2003, Vol. 125, 767-773.
14. Shojaee M., Boyaghchi F., Studies On The Influence Of Various Blade Outlet Angles In Centrifugal Pump When Handling Viscous Fluids, *American Journal of Applied Science, 4 (9): pp 718-724, 2007.*

15. *LI* X. H., Zhang S., Zhu B., Hu Q., The study of the k-ε Turbulence model for numerical simulation of centrifugal pump, *IEEE*, 2006.

16. http://www.cornellpump.com/documents/dv.htm

17. Lobanoff Val S. and Ross R., Centrifugal Pumps Design & Application, *Gulf Publishing Company,* 1985.

18. Bmnnen C.E., Franz R., and Arndt N., Rotor/Stator Unsteady Pressure Interaction , *Proc. 3rd Conf. on Advanced Earth-to-Orbit Propulsion Technology*, Huntsville, AL, NASA Conference Publication (CP-3012). NASA, Washington, DC, pp. 240-253, 1988.

19. FLUENT 6.1 User's Guide, 2003.

20. Cudina M., Detection of Cavitation Phenomenon in a Centrifugal Pump Using Audible Sound, *Mechanical Systems And Signal Processing*, 2003, 17(6), pp 1335-1347.

21. Muggli F. A., Wiss D., Eisele K., Zhang Z., Casey M. V., and Galpin P., Unsteady Flow In The Vaned Diffuser of Medium Specific Speed Pump, *ASME*, 1996.

22. Guo, S. and Okamoto, H., An Experimental Study on The Fluid Forces Induced By Rotor-Stator Interaction in a Centrifugal Pump, *International Journal Of Rotating Machinery*, 9(2): 133-144, 2003

23. Hergt P. and Stark J., Flow Patterns Causing Instabilities in the Performance Curve of Centrifugal Pumps with Vaned Diffusers, *Proceeding Of The Second International Pump Symposium*, Texas A&M Univ, p 67-75, 1985.

24. Wang D. J., Wang H. J., Tsai Z. D., Water Induced Vibration in The NSRRC, *Proceeding Of 2005 Particle Accelerator Conference*, Knoxville, Tennessee, pp 1102-1104, 2005.
25. Stoffel B. and Weib K., Experimental Investigation on Part Load Flow Phenomena in Centrifugal Pumps, *World Pumps,* October 1994.
26. Sinha M., Pin-Arbasi A., and Katz J., On The Onset and Development of Rotating Stall within a Vaned Diffuser of a Centrifugal Pump, *ASME/JSME Fluid Engineering Division Summer Meeting*, 2000.
27. Choi J. S., McLaughlin D. K., and Thompson D. E., Experiments on The Unsteady Flow Field And Noise Generation In A Centrifugal Pump Impeller, *Journal Of Sound And Vibration* 263, 2003, 493-514.
28. Qin W. and Tsukamoto H., Theoretical Study of Pressure Fluctuations Downstream of Diffuser Pump Impeller- Part 1: Fundamental Analysis on Rotor-Stator Interaction, *Journal Of Fluid Engineering*, September 1997, Vol. 119, pp. 647-652.
29. Qin W. and Tsukamoto H., Theoretical Study of Pressure Fluctuations Downstream of Diffuser Pump Impeller- Part 2: Effect of Volute, Flow Rate and Radial Gap, *Journal Of Fluid Engineering,* September 1997, Vol. 119, pp. 653-658.
30. Kaupert K. and Staubli T., The Unsteady Pressure Field in a High Specific Speed Centrifugal Pump Impeller-Part I: Influence of the Volute, *Journal Of Fluid Engineering*, September 1999, Vol. 121, pp. 621-626.
31. Kaupert K. and Staubli T., The Unsteady Pressure Field in a High Specific Speed Centrifugal Pump Impeller-Part II: Transient Hysteresis in the

Characteristic, *Journal Of Fluid Engineering*, September 1999, Vol. 121, pp. 627-632.

32. El Hajem M., Akhras A., Champagen J. Y. and Morel R., Rotor-Stator Interaction In A Centrifugal Pump Equipped With A Vaned Diffuser, *Proc Instn Mech Engrs,* Vol. 215 part A, 2001.
33. Gonzalez J., Parronda J., Santolaria C., and Blanco E., Steady And Unsteady Radial Forces For A Centrifugal Pump With Impeller To Tongue Gap Variation, *Journal Of Fluid Engineering, Transactions Of The ASME,* September 2006, Vol. 128, 937-946.
34. Sinha M., Pinarbasi A., Katz J., The Flow Structure During Onset And Developed States Of Rotating Stall Within A Vaned Diffuser Of A Centrifugal Pump, *Journal Of Fluid Engineering, Transactions Of The ASME*, September 2001, Vol. 123, 490-499.
35. Spence R., Amaral-Teixeira J., A CFD Parametric Study of Geometrical Variations on The Pressure Pulsations and Performance Characteristics of A Centrifugal Pump, *Computers & Fluids,* Vol. 38, pp 1243–1257, 2009.
36. Shin Y., Kim K., Blade-to-Blade Flow at Centrifugal Impeller Exit Under Rotating Stall, *JSME,* Series B, Vol. 46, No.1, PP 154-162, 2003.
37. Arndt, N., Acosta, A. J., Brennen, C. E., and Caughey, T. K., Unsteady Diffuser Vane Pressure and Impeller Wake Measurements in a Centrifugal Pump, *Int Proceedings of the Eighth Conference on Fluid Machinery,* Akadémiai Kiadó, Budapest, Hungary, pp. 49-56, 1987.

38. Rzentkowski G. and Zbroja S., Experimental Characterization Of Centrifugal Pumps As An Acoustic Source At The Blade-Passing Frequency, *Journal of Fluids and Structures*, Vol. 14, pp 529-558, 2000.

39. Grapsas V., Anagostopoulos J., Papantonis D., Hydrodynamic Design of Radial Flow Pump Impeller by Surface Parameterization, *1st Inter'l Conference on Experiments/Process/System Modeling/Simulation/Optimization*, Athens, 6-9 July, 2005.

40. Japikse D., Marscher W. D., and Furst R. B., Centrifugal Pump Design and Performance, *Concepts ETI, Inc.*, 1997.

41. Igor J. Karassik, Centrifugal Pump Clinic, *Marcel Dekker*, Inc., 1981.

42. Steven Anderson, Don't Forget Double Volute Pumps, *Pumps & Systems*, June 2004.

43. Spence, R. and Amaral, J., Investigation Into Pressure Pulsation In A Centrifugal Pump Using Numerical Methods Supported By Industrial Tests, *Computers & Fluids*, 2007.

44. Hodkiewicz M. R. and Norton M. P., The Effect Of Change In Flow Rate On The Vibration Of Double-Suction Centrifugal Pumps, *Proc Instn Mech Engrs, Vol. 216 part E: Process Mechanical Engineering*, 2002.

45. Roman W. Motriuk and Douglas P. Harvey, Root Cause Investigation of the Centrifugal Compressor Pulsation/Vibration Problems, *AD-Vol.53-2, Fluid-Structure Interaction, Aeroelasticity, Flow-Induced Vibration and Noise, Volume II, ASME*, 1997.

46. Miguel A., Farid B., Smaine K., Frank K., Robert R., Numerical Modelization Of The Flow In Centrifugal Pumps: Volute Influence In Velocity And Pressure Fields, International *Journal Of Rotating Machinery*, 2005:3, 244-255.
47. Akira G. and Mehrdad Z., Hydrodynamic Design of Pump Diffuser Using Inverse Design Method and CFD, *Journal of Fluid Engineering*, June 2002, Vol. 124.
48. Shoji H. and Ohashi H., Lateral Fluid Forces on Whirling Centrifugal Impeller (1st Report: Theory), *Journal of Fluid Engineering*, Transactions of the ASME, June 1987, Vol. 109.
49. Guleren K. M. and Pinarbasi A., Numerical Simulation of the Stalled flow within a Vaned Centrifugal Pump, *Proc Instn Mech Engrs, Vol. 218 part C: J. Mechanical Engineering Science, 2004.*
50. Patella R., Longatte F., Kueny L., Croba D., Numerical Analysis of Unsteady Flow in a Centrifugal Pump, ASME, Fluid Machinery, Vol. 222, p 41, 1995.
51. Sinha M., Katz J., Meneveau C., Qualitative Visualization Of The Flow In A Centrifugal Pump With Diffuser Vanes-II: Addressing Passage-Averaged And Large-Eddy Simulation Modeling Issues In Turbomachinery Flows, *Journal of Fluid Engineering*, Transactions of the ASME, Vol. 122, March 2000.
52. Cheah K., Lee T., Winoto S., Zhao Z., Numerical Flow Simulation in a Centrifugal Pump at Design and Off-design Conditions, *Inter'l Journal of Rotating Machinery*, 2007.
53. Majidi K., Numerical Study of Unsteady Flow in A Centrifugal Pump, *ASME J. Turbomachinery*, Vol. 127, No. 2, April 2005.

54. Moor J. and Palazzolo A., Rotordyanmics Force Prediction Of Whirling Centrifugal Impeller Shroud Passages Using Computational Fluid Dynamic Techniques, *ASME J. Eng. Gas Turbines Power*, Vol. 123, No. 4, Oct. 2001.

55. Wang H. and Tsukamoto H., Fundamental Analysis on Rotor-Stator Interaction in a Diffuser Pump by Vortex Method, *ASME J. Fluid Eng.* Vol. 123, No. 4, December 2001.

56. Parrondo J., Gonzalez J., Perez J., Fernandez J., A Comparison Between The F_{BP} Pressure Fluctuation Data In The Volute of A Centrifugal Pump And The Predictions From Simple Acoustical Model, *Proceeding of The Hydraulic Machinery And Systems, 21st IAHR Symposium,* Lausanne, September 9-12, 2002.

57. Friedrichs J.and Kosyna G., Unsteady PIV Flow Field Analysis Of A Centrifugal Pump Impeller Under Rotating Cavitation, *fifth international symposium on cavitation*, Osaka, Japan, November 2003.

58. Ronal L. Eshleman, Basic Machinery Vibrations, *VIPress, Incorporated, 1999.*

59. Christopher E. Brennen, Hydrodynamics of Pumps, Concepts ETI, Inc and Oxford University Press, 1994.

60. Mackay R., Shaft Deflection Part one: the Cause, *Pumps & Systems*, Nov. 2004.

VITAE

Personal Data

Name : ***Atia Esmaeil Atia Khalifa***
Date of birth : *01 /10 /1975*
Nationality : *Egyptian*
Marital Status : *Married*

Contact Information

Tel. No. : +20 48 3462444 (Egypt)
E-Mail : attia@kfupm.edu.sa and at_es@hotmail.com

Employment:

- ***Demonstrator**, Mechanical Power Eng. Department, Faculty of Engineering, Menoufiya University, Shebin El-Kom, Egypt, from Sept. 1999 – present.*
- ***Teaching Assistant**, Mechanical Engineering Department, College of Engineering, King Saud University, from Sept. 2001- May 2005 (Master degree).*
- ***Lecturer-B**, Mechanical Engineering Department, College of Engineering, King Fahd University, from Sept. 2005- Sept. 2009 (Ph.D degree).*

Education

Degree	Department &Specialization	GPA	University	Year of Graduation
PhD	Mechanical Engineering	3.95 / 4	KFUPM, Dhahran, KSA	2009
M.Sc.	Mechanical Engineering	4.91 / 5	KSU, Riyadh KSA	2005
B.Sc.	Mechanical Power Engineering	79 %	Menoufia Univ. Egypt	1998

Title of M. Sc. Thesis: *"Aeroelastic Behavior Study of Finite Wings Using 3-D Unsteady Model", King Saud University, Riyadh, Saudi Arabia, May 2005.*

Areas of Research Interest

- Fluid Mechanics
- Internal combustion engines and emissions
- Aerodynamics & Aerospace
- Fluid-Structure Interaction
- Pumping machinery
- CFD Simulation and Modeling
- Heat Transfer